University of Technology, Sydney
Faculty of Engineering and Information Technology

The Effect of Connection Flexibility on the Seismic Performance of Industrial Racking Systems

by

Ahmad Firouzianhaji

PhD Thesis

January 2016

CERTIFICATE OF ORIGINAL AUTHORSHIP

I certify that the work in this thesis has not previously been submitted for a degree nor has it been submitted as part of requirements for a degree except as fully acknowledged within the text.

I also certify that the thesis has been written by me. Any help that I have received in my research work and the preparation of the thesis itself has been acknowledged. In addition, I certify that all information sources and literature used are indicated in the thesis.

Signature of Student:

Date: 11 Jun 2015

Acknowledgment

I wish to express my deepest gratitude to my supervisors, Dr. Ali Saleh and Prof. Bijan Samali for their continuous support throughout my Ph.D study and research, for their patience, motivation, enthusiasm, and immense knowledge. There was absolutely no way I could have completed my PhD without your guidance and support from day one.

I am also grateful to my colleagues in the Engineering Department of DEXION Australia Pty Ltd., specially Mr. Peter Geoghegan and Mr. Lawrence Mok for sharing their expertise, immense knowledge and valuable guidance and encouragement extended to me.

Also, I would like to appreciate contribution of DEXION Australia Pty Ltd., in providing partial financial support on this project and providing their previous experimental test results.

I take this opportunity to express gratitude to all of the Department faculty members for their help and support.

I would like to offer my special thanks to my wife for being so supportive and my only family member in Australia.

Last but not the least, my Mom and Dad for their continues support and prayers. Also to my younger brother who has always given me positive energy to continue, not give up.

Table of Contents:

Table of Figures:

List of Tables:

NOTATION

The following symbols are used through the thesis unless notified otherwise:

A_{brace}	Cross section area of bracing members
$A^{*}_{bracing\ member}$	Modified cross section area of the bracing member
$A_{bracing\ member}$	Cross section area of the bracing member
A_d	Cross sectional area of the bracing members
C	Damping matrix, or;
	Number of storey levels
D	Upright width, or;
	Nominal diameter of bolt
D_{EqCyc}	First yield rotation on the moment-rotation backbone
E	Elasticity modulus
F_1	Vertical force applied by Jack 1
F_2	Horizontal force at pin above upright
f_a, f_b	The calculated frequencies at a response amplitude of '$1/\sqrt{2}$' of the peak response amplitude
$f_b(\theta)$	Moment rotation function of base plate connections
$f_c(\theta)$	Moment rotation function of beam to upright connections
f_n	Forcing frequency at resonance and
f_o	First yield force in the push over curve
F_{ult}	Upright – hook interaction
f_y	The force at which the structure starts to yield (yield strength)
H	Beam spacing , or;
	Storey height
I	Second moment of inertia of the upright member about an axis perpendicular to the upright frame
I_b	Second moment of area of the beam, or;
	Moment of inertia of bolt section

K	Stiffness matrix, or;
	Stiffness of a SDOF system
k	A factor depending on the position of the loads
$k_{1YEqCyc\ Initial}$	Stiffness of the equivalent moment rotation backbone
K_{avg}	Average stiffness of the moment rotation curve
$K_{bearing}$	Bearing stiffness
K_{bolt}	Stiffness of the bolts in the bracing connection
K_i	Initial Stiffness
K_{joint}	Stiffness of the bracing connection in vertical direction
K'_{joint}	The joint stiffness in the direction of the bracing member
K_{member}	Stiffness of the bracing member
K^*_{member}	Equivalent stiffness of the bracing members
K_s	Initial secant stiffness
K_{shear}	Stiffness of the shear frame excluding base plates
$K_{shear\ total}$	Stiffness of the shear frame including base plates
K_{uplift}	Stiffness of the base plate connection under uplift forces
L	Vertical distance from the load point to the connector's free edge, or;
	Distance between pin above upright and bottom of the base plate, or;
	The total height of the upright frame
L_b	Distance between upright flanges, or;
	Length of the beam
	Total mass of a SDOF system, or;
	Moment in the beam to upright connection
$\bar{m}$	Non-dimensional moment
$\bar{m}_u$	Non-dimensional ultimate moment
M	Mass matrix, or;
	Moment in the beam to upright connections
M_{1Y}	First yield point on the moment-rotation backbone
M_b	Base plate moment

M_{BU}	Ultimate moment of the beam end connector
M_{CU}	Ultimate moment of the beam
M_i	The effective or modal mass for mode i
m_j	Lumped mass at degree of freedom j
M_{max}	Maximum allowable moment of the base plate
M_p	Plastic moment of the base plate
$M_{p,b}$	Plastic moment of the beam
M_{ult}	Base plate moment, including second order effects
M_u	Ultimate moment
$M_{max-ups}$	Maximum moment in first storey uprights
M_y	Yield moment
N^*	Design value of the vertical action on the frame
N	Number of beams at every levels
N_b	Number of base plate connections
N_{brace}	Number of bracing members in tension
N_{brc}	Number of bracing members in the upright frame
N_c	Number of beam to upright connection
N_{cr}	Elastic critical load
P	Pallet load distributed at every beam
p_{cr}	Maximum allowable load at every beam level
P_E	External work in the down aisle direction
R	Seismic Reduction Factor
$S_{j,ini}$	The initial stiffness of the connection
S_p	Factor for redundancy of structure
S_{ti}	Transverse shear stiffness of an upright frame
T	Fundamental period of structure
t_b	Brace member thickness
t_c	Connector's thickness
t_u	Upright member thickness
U	Total displacement response of a MDOF structure, or; Internal work in the down aisle frame
U_E	External energy in the base plate assembly
U_I	Internal energy in the base plate assembly

u_m	Ultimate deformation of the system in the push over curve
u_o	First yield displacement
$\ddot{u}_g$	Ground acceleration
u_y	The displacement at which the structure starts to yield (yield displacement)
$V_{base\ shar}$	Seismic base shear in the structure
V_e	Elastic base shear at the maximum monitored displacement of the top beam level
V_{max}	Inelastic base shear at the maximum monitored displacement of the top beam level
W	The total potential energy of the system
$Y_n(t)$	Time varying displacement function
α	Parameters for developing hysteresis curves, or;
	Imperfection (out of plumb), or;
	Seismic intensity factor, or;
	The angle between the frame bracing member and the direction perpendicular to the upright
β	Reduction factor for the cross section area of the bracing members, or;
	Parameters for developing hysteresis curves
δ_1 to δ_4	Displacements at positions 1 to 4, respectively
δ_{ci}	Maximum allowable rotation of the connection
δ_{Fail}	Final point on the moment-rotation backbone
δ_L	Horizontal deflection at the bottom of the storey
δ_U	Horizontal deflection at the top of the storey
Δ_e	Equivalent elastic response displacement
$\Delta_{e,top}$	Top storey elastic displacement
$\Delta_{p,top}$	Inelastic top level displacement
Δ_s	Stability displacement limit
ζ	Damping ratio
η	Parameters for developing hysteresis curves

θ	Drift of the down aisle frame excluding imperfection
θ_1.	Maximum first storey inter-storey drift ratio,
θ_b	Relative rotation of base plate connection
$\theta_{b,p}$	The value of θ_b at failure.
θ_D	The minimum required rotation of the connector to allow a Plastic mechanism to occur
$\theta_{top\ storey}$	Maximum top storey drift ration
θ_u	Ultimate rotation of the beam to upright connections
θ_{ult}	Ultimate rotation of the base plate connectionn
θ_y	Yield rotation
λ	The factor to convert the multi degree of freedom model to the equivalent single degree of freedom model
μ	Ductility of structure
σ	Normal stress
σ_{ult}	Maximum stress at upright-hook interaction
τ	Shear stress
Φ	Dynamic Mode shape matrix, or; Frame imperfection
$\overline{\emptyset}$	Non-dimensional rotation
$\emptyset_b$	The angle between horizontal and diagonal braces
Φ_b	The angle between horizontal and diagonal braces
$\Phi_{i,j}$	Relative deformed shape displacement for mode i at degree of freedom j
Φ_{max}	Largest value of the sway index
Φ_n	Time-independent vector of the system's n^{th} mode shape and
$\Phi\mu$,R_μ , q	Ductility of structure
γ	The angle between brace member and the horizontal direction
φ	Sway rotation equal to 0.02 Rad, or; Total drift of the down aisle frame including imperfection
Ω	Over Strength Factor

Abstract

Industrial racking systems are load bearing structures for the warehouse storage of goods. They are normally fabricated and assembled from cold-formed perforated open thin-walled vertical members and can be 4 meters to 40 meters high. To resist lateral actions such as seismic loads, racking structures rely typically on flexible boltless beam to upright connections along the storage aisles and braced frames in the transverse cross-aisle direction. Compared to their self weight, industrial racks carry very heavy pallet loads as opposed to other conventional structures. High slenderness ratio, heavy pallet loads, connection flexibility and low degree of redundancy make rack structures very different from conventional steel structures. Therefore, in the racking industry special analysis and design codes are adopted which require specific experimental tests to determine the performance of the key structural components. However the current standards do not give sufficient guidance for seismic design. This PhD research investigates both numerically and experimentally the effect of different connections on the performance of industrial racking systems. The research focus is on three critical connections: (a) Beam-upright connection; (b) Floor connection (Base-plate connection); and (c) Bolted brace connection. Courtesy of Dexion Australia, part of the research was based on test results conducted on their racking components. More than 70 beam to upright connection tests including monotonic and cyclic tests, 15 base plate tests under combined axial and bending loads and 4 full cross aisle shear frame tests were studied. FE models were then developed and verified against the test results. Further FE analyses revealed the behaviour of the aforementioned local connections under monotonic and cyclic actions and as a result simple theoretical models were proposed. After deep investigations on the performance of different connections of a typical rack structure, more than 20 full scaled shake table tests were conducted to reveal the dynamic features of a rack structure and one full scaled static cyclic push over test was performed to evaluate the system deterioration under cyclic actions. Both dynamic and static full scaled tests were accurately modeled using the proposed beam to upright connection model. A new performance based seismic analysis approach was proposed at the end of the thesis which showed much more accurate results compared to the seismic analysis approach in the current racking codes and specifications.

1. CHAPTER 1: INTRODUCTION, LITERATURE REVIEW AND RESEARCH SIGNIFICANCE

1.1 Background

The process of moving the manufactured products from the producer to the end user needs highly engineered industrial storage rack facilities. “Racking systems are load bearing structures for the storage and retrieval of goods in warehouses. The goods to be stored are generally on pallets or in box-containers. Racking is constructed from steel components including upright frames, beams and decking. Special beam to column (upright) connections and bracing systems are utilized, in order to achieve a three dimensional steel structure with ‘aisles’ to enable order pickers, industrial trucks or stacker cranes to reach the storage positions” (EN 15512, 2009, p. 7)

The benefit of racking structures is that they allow comparatively efficient use of floor space combined with direct access to every item in the store. They range from small 4 meter high racks used in personal garages to 45 meter high storage racks. As the significant cost of the rack structures comes from material tonnage, industrial racks are normally framed structures fabricated from cold-formed sections and relative to their self weight (dead load or permanent action) carry very high pallet loads (live load or imposed action) compared to other typical civil engineering structures. A typical frame with different connections is shown in Figure 1.1. Relative to their footprint, racking frames can be very tall making them slender when heights exceed 30m. Racking systems sometimes also need to support the perimeter structures which are exposed to heavy wind loads (Cladded Rack systems). Due to their slenderness, controlling sway deformation is an important factor in the design of industrial racks and hence special attention must be given to factors such as ‘upright slenderness’, ‘bracing connections’, ‘beam to upright connections’ and ‘base plates connections’ (Figure 1.1, a to c respectively). Flexibly connected beam to upright frame is used along the aisle (down aisle direction) while typically braced frame is used as structural system in transverse direction (cross aisle direction). Heavy pallet loads, very flexible frame and lack of enough redundancy make rack structures vulnerable to seismic motions.

Due to their peculiarities in comparison with conventional steel construction, special analysis and design rules are adopted in the racking industry such as EN 15512 (2009), RMI (2008) and AS 4084 (2012). According to the most recent design specifications for steel storage rack structures the design and analysis of the structures should be supported by specific experimental tests to evaluate the performance of the key parameters like: beam and upright capacity, beam end connector's capacity and ductility, upright frame flexibility, looseness, base plate connections behaviour, etc. Generally beams are boxed or "C" cross sections which are connected to thin walled open uprights by using a very fast installation mechanism provided by boltless connections. Such boltless semi-rigid connections are referred to as beam-end-connectors and consist of angled end plates welded to each end of beams with interlocking arrangements to join with perforated uprights. Boltless beam to upright connections can have a great influence on the performance of these structures.

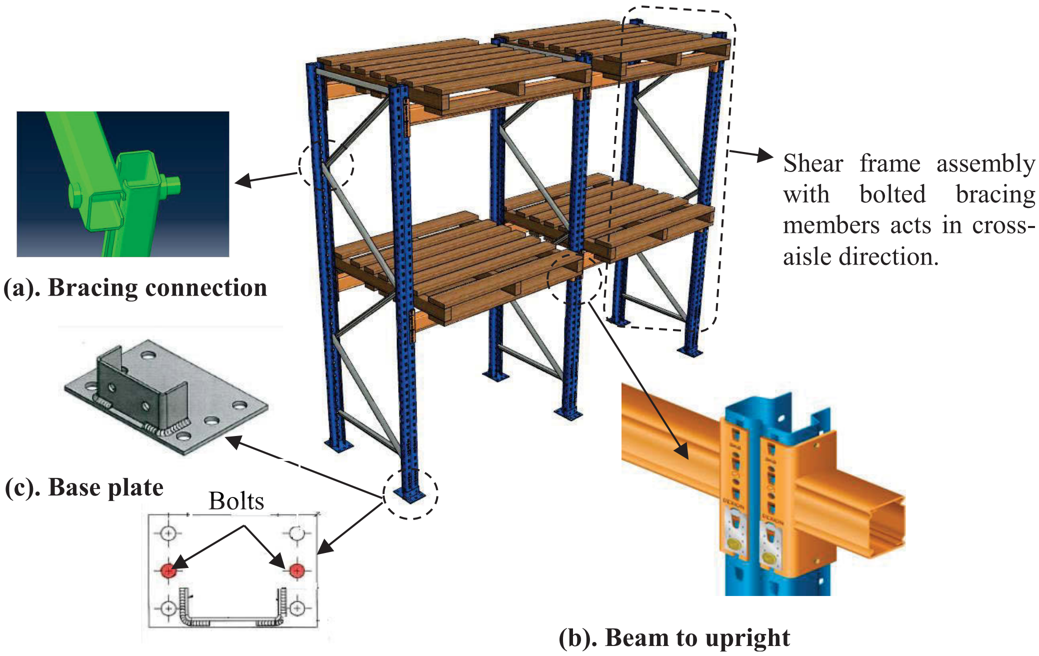

Figure 1.1. A typical low rise rack structure.

Few hooks are the main parts that are expected to transfer the loads from beams to uprights. These connections are categorized as semi-rigid connections and hence the stiffness and performance of racking system depends upon the efficiency of the beam end connectors. The behaviour of pallet rack structures under load is largely governed by sway so that an understanding of the moment-rotation characteristics of the beam to upright connection is important (Prabha, Marimutho, Saravanan & Jayachandran, 2010). In the cross aisle directions uprights are connected together by cold formed lipped C-shaped bracing members that are bolted to the uprights in their ends. Cross aisle braced frames are also known as upright frames and have depths from 800 mm to 2500 mm. In down aisle direction, rack systems can be unbraced or braced in the back (spine bracing). Using spine bracing members in down aisle frames significantly increase the stiffness of the racks in their down aisle direction, however, it limits the accessibility to the racks by blocking one side. Horizontal bracing (plan bracing) is also needed at each pallet level to link to two braced and unbraced sides of the rack. (See Figure 1.2)

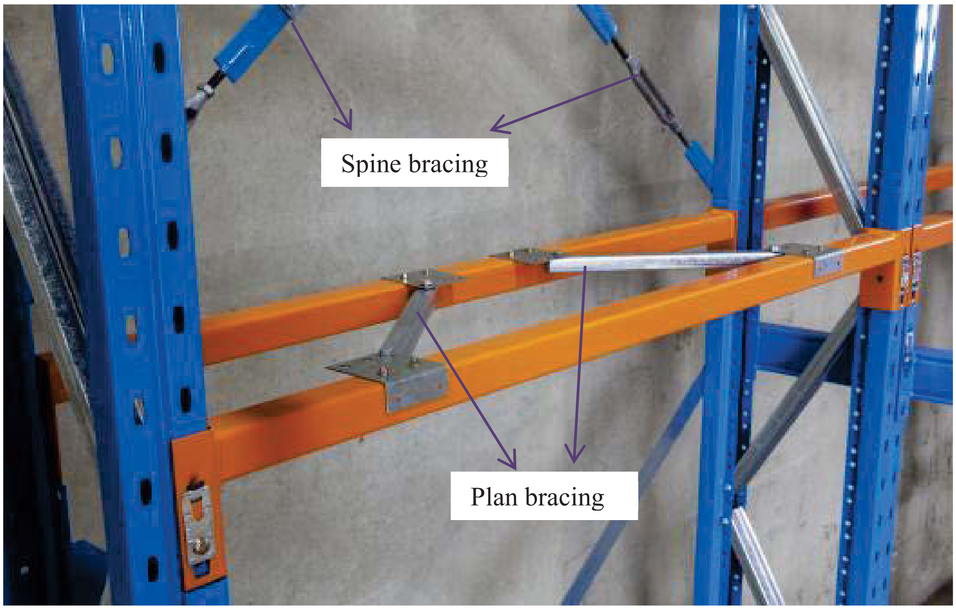

Figure 1.2. Spine bracing and Plan bracing

Uprights, beams, beam end connectors and frame bracing members are produced from strips of steel through a number of different operations such as coiling or uncoiling, bending, piercing and forming which may cause residual stress in the sections that can affect their load carrying capacity.

Many types of storage pallet racks with different functionalities are available, each appropriate for specific usage. Every type of rack system has its own advantages and disadvantages.

Some of the most common storage rack systems used in industry are outlined below:

1. Regular selective pallet racks

Regular selective pallet racking is the best solution for the warehouses where there is a need for direct access to all the pallets. This system is quite adjustable and provides with the possibility of accommodating different pallet sizes at different beam spacing. This system can be compatible with different handling equipment. Figure 1.3 shows a typical selective rack system.

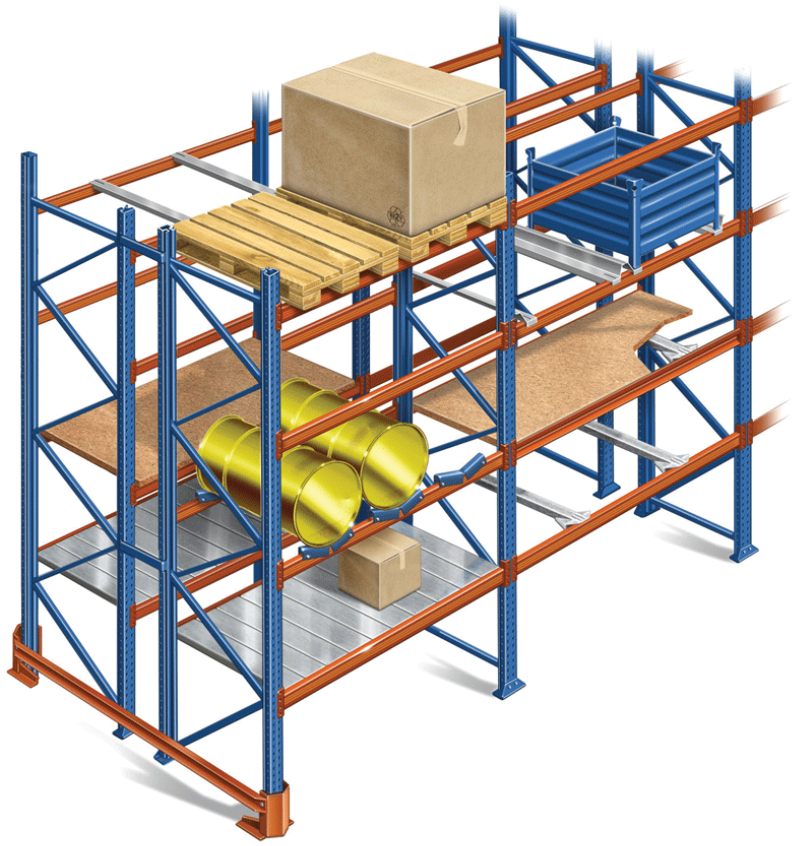

Figure 1.3. Regular selective rack system

2. Double deep pallet racks

Double deep pallet racking provides four pallets deep in double entry rack.

Increasing storage density, this system decreases the accessibility of rack to 50% comparing to regular selective racks. Lower ratio of steel weight to pallet weight is an advantage of this system. (a) Cross aisle direction (b) Down aisle direction

Figure 1.4 shows a typical double deep pallet rack system.

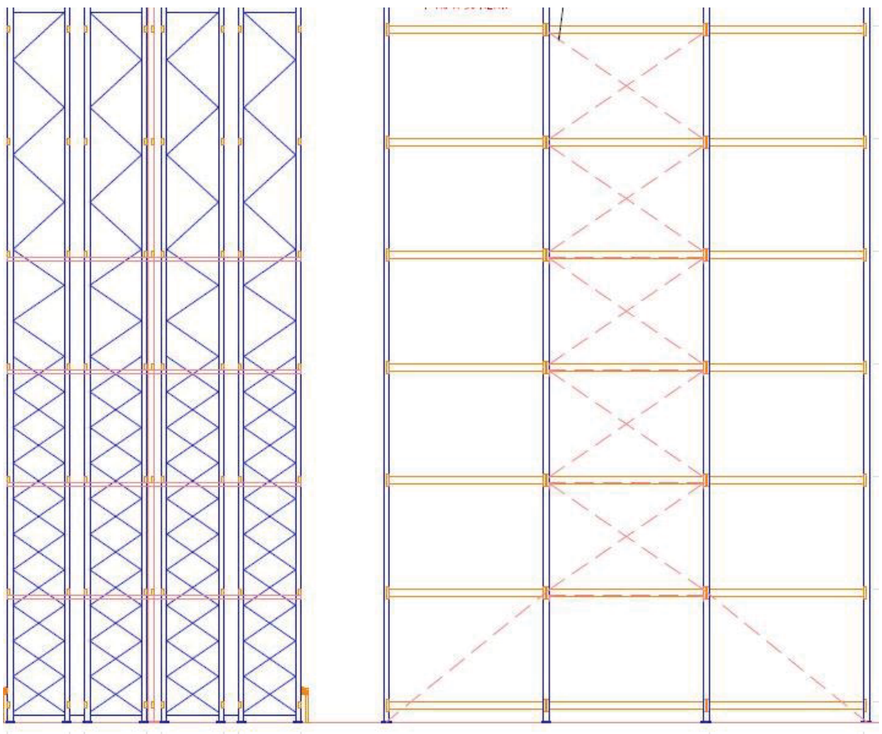

(a) Cross aisle direction (b) Down aisle direction

Figure 1.4. Double deep selective rack system

3. Drive-in rack

This system allows forklift to drive directly through the lane of the bays.

Figure 1.5 shows a typical Drive-in rack system.

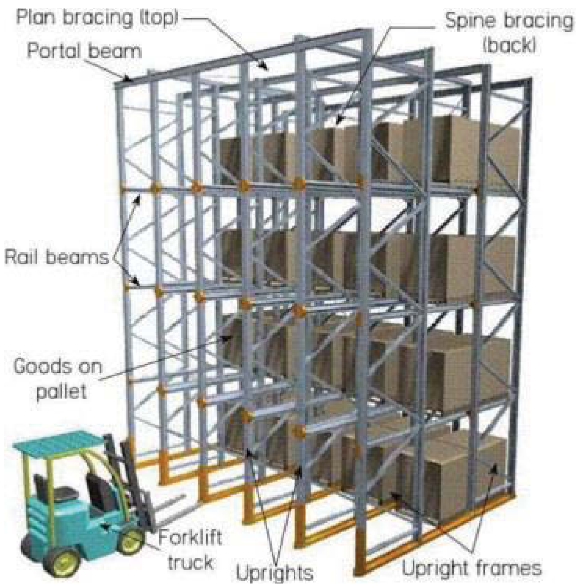

Figure 1.5. Drive-in rack system (Gilbert, 2010, p. 3)

4. Cantilever Racks (Tree Racks)

In cantilever racks the pallets are stored on top of very strong cantilever arms. Figure 1.6 shows a typical cantilever rack system.

Figure 1.6. Cantilever rack system

1.2 Literature Review

In this part an overall review of the most relevant, influential and significant papers and research reports are briefly presented and then more details are discussed in the main chapters of this thesis as required.

1.2.1 Racking Design Codes and Specifications

Rack Manufacturer Institute specification, RMI (2012) is the American code for design of steel storage racks in North-America. This code provides the components test procedures as well as Static/Seismic design specifications. RMI (2012) superseded the RMI (2008) and RMI (1997). The seismic design procedure in RMI (1997) was inspired by the Uniform Building Code of America UBC (1997) while the next versions of RMI (2008) and RMI (2012) are in line with the International Building Code (IBC, 2006). Federal Emergency Management Agency (FEMA 460, 2005) also provided a design guide particularly for seismic design of steel storage racks located in areas accessible to the public.

In Europe, steel storage racks are designed based on the European Standard EN 15512 (2009) and in Australia racking systems are designed based on Australian Standard AS 4084 (2012) which is primarily based on EN 15512 (2009). The latest European standard (EN 15512, 2009) superseded the Federation Europeenne de la Manutention, FEM (1998), while Australian Standard AS 4084 (2012) superseded the AS 4084 (1993) which was inspired by the American racking code of RMI (1997).

However, none of the above latest versions of European and Australian Specifications address the seismic design of rack structures like RMI specification. The only European specification for seismic design of rack structures is Federation Europeenne de la Manutention (FEM 10.2.08, 2010). Like Australia, many other countries across the globe even those located in high seismic risk regions do not have their local seismic codes and hence refer to either RMI (2012) or FEM 10.2.08 (2010) for seismic design. More details of seismic design procedures are explained in Chapter 7.

According to all the above codes, design of rack structures and specifications rely primarily on experimental tests on the main components of rack structures such as beams, uprights, upright frames and different connections.

1.2.2 Behaviour of Beam to Upright Connections

Compared with literature available for the analysis and design of conventional steel construction, relatively little has been published on different types of beam end connectors used in the racking systems and especially their performance under earthquake actions. Most literature presenting the behavior of typical beam end connectors used in rack structures are published after 2000, while a few experimental investigations are reported before that. Lack of sufficient design rules and the need of such structures in seismic regions forced engineers to experimentally investigate the behaviour of beam end connectors. One of the earliest investigations in determining the parameters governing an efficient beam end connector design is presented by Markezi, Beale and Godley (1997). They investigated the behaviour of different classes and products of commercially available beam end connectors by presenting the associated moment rotation diagrams. He then concluded that increasing the number of tabs leads to increase in the stiffness and the strength of the beam end connector. Changing the profile of the upright to increase its stiffness, increases the stiffness of beam end connector. Increasing the number of contact planes between the beam end connector and upright increases the stiffness of the connection. Bernuzzi and Castiglioni (2001) presented a paper on an experimental analysis aimed at investigating the behaviour of beam to upright connections under cyclic reversal loads. They investigated important parameters such as "moment drop at the load reversal point in the hysteresis curves" and "degradation of the energy dissipation capabilities over the number of cycles". They highlighted the urgency of a more accurate seismic design philosophy. Baldassino and Bernuzzi (2000) presented a paper which consists of a numerical study on the response of pallet racks commonly used in Europe. The influence of beam to upright connection modelling on the overall frame response was then investigated by the authors. They concluded that the behavior of steel storage pallet racks depend on the behavior of the beam to upright connections. Beam to upright connection flexibility was also evaluated by Prabha, Marimuthu, Saravanan and Jayachandran (2010). They conducted experimental tests on commercially available pallet rack connections and by varying the most influencing parameters a parametric study was performed followed by a 3D finite element analysis utilizing ABAQUS software. They also tried to use Fry-Morris empirical model (Fry & Morris, 1975) to present the nonlinear behaviour of beam to upright connections based on curve fitting method. However, they didn't propose a simplified analytical model to obtain the stiffness of the beam to upright connections. An experimental and numerical investigation was carried out to determine the flexibility of beam-to-upright connectors used in thin walled cold-formed steel pallet racking systems by Bajoria and Talikoti (2006). They aimed to modify the conventional cantilever test method. For this reason they used double cantilever method and verified the results by conducting a full scale frame test. A 3D non-linear finite element analysis was then carried out using ANSYS software. A theoretical and experimental investigation of pallet rack structures under sway was carried out by Abdel-Jaber, Beale and Godley (2005). For this reason, single storey portal frames were tested with different percentages of side loads and free to sway. They also analyzed the effect of semi rigidity of the connections on the frame sway and a comparison was made between the different methods of presenting the beam to upright connections stiffness. Aguirre (2005) presented a paper in which the behaviour of rack structures under static and cyclic load is investigated. The failure mode of boltless connections was explained and the performance of the hooks in beam end connectors was investigated. The importance of considering the nonlinear behaviour of the connections for design was emphasized.

Godley (1997) investigated the required ductility of beam end connectors to allow plastic design of the beams. He proposed the minimum required rotation, θ_D, of the connector to allow a plastic mechanism to occur, should be calculated as follows:

For unbraced racks: $$\theta_D = \frac{L_b}{6EI_b}\left(2M_{CU} - M_{BU}\right) \quad (1\text{-}1)$$

For Braced racks: $$\theta_D = \varphi + \frac{L_b}{6EI_b}\left(2M_{CU} - M_{BU}\right) \quad (1\text{-}2)$$

where;

L_b : Length of the beam

E : Elasticity modulus

I_b : Second moment of inertia of the beam

M_{CU} : Ultimate moment of the beam

M_{BU} : Ultimate moment of the beam end connector

φ : Sway rotation equal to 0.02 Rad

Beam end connectors should be able to rotate more than θ_D before failure, to be sufficiently ductile to allow plastic design of the beams.

As an example, a 2.5 meter long '95-50 Box beam' with a moment capacity of 5.78 kN.m should have a connecter with rotational capacity of 0.021 for braced and 0.041 for unbraced systems to allow plastic design. (Moment capacity of the beam end connectors are taken as 2.4 kN.m)

Experimental tests and numerical analyses proved that beam end connectors usually undergo large inelastic rotations exceeding 0.2 rad compared to building moment-resisting connections having inelastic rotation capacity in the range of 0.04 rad for special moment-resisting frame systems (Filiatrault, Higgins & Wanitkurkul, 2006, Saleh, 2012, Firouzianhaji, Saleh & Samali, 2012). However, it should not be concluded that most of the racking connections show satisfactory degree of ductility because of the following two reasons:

1. Although they allow large rotations, they might be performing like hinged connections.
2. The entire rack system may lose its stiffness and become unstable at rotations smaller than θ_D.

Both effects have been investigated in this thesis.

Structural beam to column connection behaviour is one of the most important factor on performance of the whole system under different actions. Structural connections are usually considered as fully hinged or fully rigid but in reality the behaviour is different and most of the connections behave between these two absolute extremes leading to so called Semi-Rigid connection. (Chen & Lui, 1991)

Moment-Rotation curves best represent the behaviour and performance of the connections. Generally, moment rotation curves include two parts. The first part represents the elastic behaviour of the connection which is usually represented by an initial stiffness and the second part shows the behaviour of the connection when the material starts to yield. Commercial beam end connectors are considered as semi-rigid connections while Baldassino and Bernuzzi (2000), on the basis of an extensive experimental analysis, remarked that joints should be, in most cases, modelled as hinges, if classified in accordance with Euro Code 3 (EN 1993-1-8, 2005) criteria. Hence, because of the high slenderness of the members, second order effects influence remarkably the frame performance.

There are several approaches available to predict the moment rotation behaviour of structural connections for various connections. The models may be classified as Empirical, Analytical and Numerical approaches. A comprehensive review on the modelling of joint behaviour in steel frames is reported by Diaz, Marti, Victoria and Querin (2011).

In empirical modelling, a mathematical equation will be proposed based on curve fitting method. Different geometrical and mechanical parameters should be investigated by a large number of experimental tests or finite element simulations. Each parameter is then included in the empirical formulation by different methods such as Linear, Bi-Linear, Power formulations, Polynomial formulations, etc. The Fry and Morris (1975) model and Krishnamurthy (1978) model are the most popular empirical models that are proposed for different configuration of end-plate steel structures. These approaches were used in several studies to represent the behaviour of connections in steel frames. In racking structures, as was mentioned earlier, Fry and Morris model was used by Prabha et al. (2010) to evaluate the beam end connectors flexibility in rack structure design.

Analytical models use basic analytical concepts such as shell and plate theories, energy method, compatibility and equilibrium relations to obtain the rotational stiffness and the ultimate moment and rotations. “Briefly described, the method consists of modelling a joint as an assembly of extensional springs and rigid links, whereby the springs represent a specific part of a joint that, dependent on the type of loading, make an identified contribution to one or more of its structural properties” (Mofid, Mohammadi & McCabe, 2005, p. 450). Chen and his colleagues were pioneers of predicting the behaviour of steel joints from the geometrical and mechanical (Diaz et al., 2011, Kishi and Chen, 1987, Chen, Kishi, Natsuoka & Nomachi, 1988). However, no analytical model has been developed so far to predict the moment rotation behaviour of the boltless beam – upright connections used in rack structures. Chapter 2 of this thesis; therefore, presents an analytical model of the boltless beam to upright connections.

Numerical simulations have become more widely used among engineers and researchers after the emergence of high powered computers because of many reasons:

1. Lack of sufficient experimental results encouraged engineers to look for a more cost effective method.
2. Finite element analysis reveals local effects which may be difficult to be presented analytically or may not be visible in experiments.
3. FE simulation provides a powerful and cost effective tool to conduct extensive parametric studies.

The final results represent the complicated interactions between the elements of the model. Material and geometrical nonlinearities can be taken into account to better represent the model behaviour, although it may make the model computationally expensive. Nevertheless, using finite element software packages needs a good knowledge of finite element theories since unrealistic assumptions when employing FE analyses can significantly impact the accuracy of the results.

Several FE analyses were carried out to model various structural connections and undertake extensive parametric studies (Diaz et al., 2011).

1.2.3 Base Plate Connections

Rack structures are connected to the concrete floors via base plate connections consisting of two parts of base plate and up-stand bracket(s). As shown in Figure 1.7, uprights are bolted to the up-stand bracket by 2 to 4 bolts and the base plates are again connected to the floor by 2 to 4 bolts. Upright forces transfer to the up-stand brackets and finally to the floor via anchor bolts. Obviously, different anchoring arrangements cause different base plate behaviour (i.e. stiffness and strength).

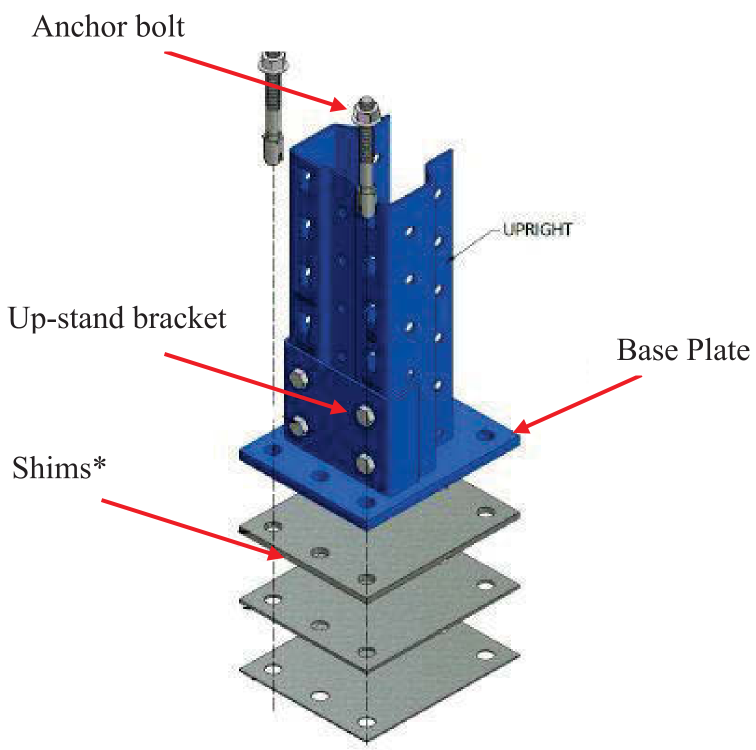

* Shims may be used under the base plate to maintain the plumbness of the storage rack (RMI, 2012)

Figure 1.7. Base plate assembly (DEXION Installation Manual, DEXION AUSTRALIA Pty Ltd.)

Base plate connection characteristics, like stiffness and moment capacity, are important parameters in design of a rack structure. Current most popular international specifications of RMI (2012) and EN 15512 (2009) use different approaches to determine the connection stiffness. RMI (2012) uses an empirical equation considering only the elastic deformation of the concrete floor under the base plate but not the base plate connection itself. However, the base plates should have higher rotational capacity than the rotational capacity of beam - upright connections. Otherwise, the base plate connections act like hinged connections.

The EN 15512 (2009) recommends experimental testing to determine the stiffness and strength of the base plate connections for a reasonable range of axial compression loads. However, the proposed test set up, according to the EN 15512 (2009), has some practical and technical issues that were addressed by Gilbert and Rasmussen (2011) and then the Australian racking specification, AS 4084 (2012), updated the test set up procedure based on the work of Gilbert and Rasmussen (2011). Chapter 3 of this thesis presents another modified test set up procedure for base plate connections.

The effect of axial compression force on the baehaviour of the base plate connections were investigated experimentally and numerically by Godley and Beale (2007), Gilbert and Rasmussen (2011), Saleh (2012) and Firouzianhaji, Sale and Samali (2014). Godley and Beale (2007) and Gilbert (2010) found that the stiffness of base plate connections is very sensitive to the axial compression force in the upright but the moment rotation curves seem to never drop and hence large rotational capacity was observed for the base plate connections. Chapter 3 of this thesis presents a method to define a rotational limit for the base plate connections based on stability analysis.

Godley and Beale (2007) also developed a very simple theoretical model based on yield line theory. His model was improved in this research and is presented in Chapter 3 of this thesis.

Beale and Godley (2002) showed that increasing the base plate stiffness above a certain level does not change the capacity of rack structures and the base plate connections can be treated as fixed (rigid) connections. However, the cyclic behaviour of base plate connections has not been seriously investigated so far. Chapter 3 of this thesis presents a numerical investigation of the cyclic behaviour of base plate connections.

1.2.4 Stability analysis of the rack structures in their down aisle direction

Connection behaviour in rack structures plays a significant role in global stability of rack structures. “The essential analytical requirement for the consideration of down-aisle stability is a suitable second-order elastic analysis for a large plane frame with semi-rigid joints” (Davies, 1992, p. 418)

A simple 2D model of an un-braced down aisle frame is shown in Figure 1.8.

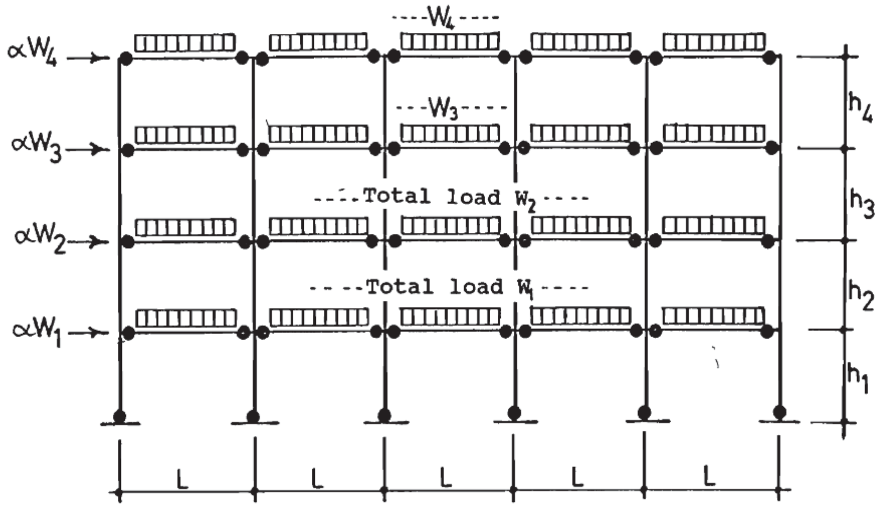

Figure 1.8. 2D analytical model of a down aisle frame (Davies, 1992, p. 417)

Stark and Tilburgs (1979) proposed a simple model for down aisle stability analysis (See Figure 1.9)

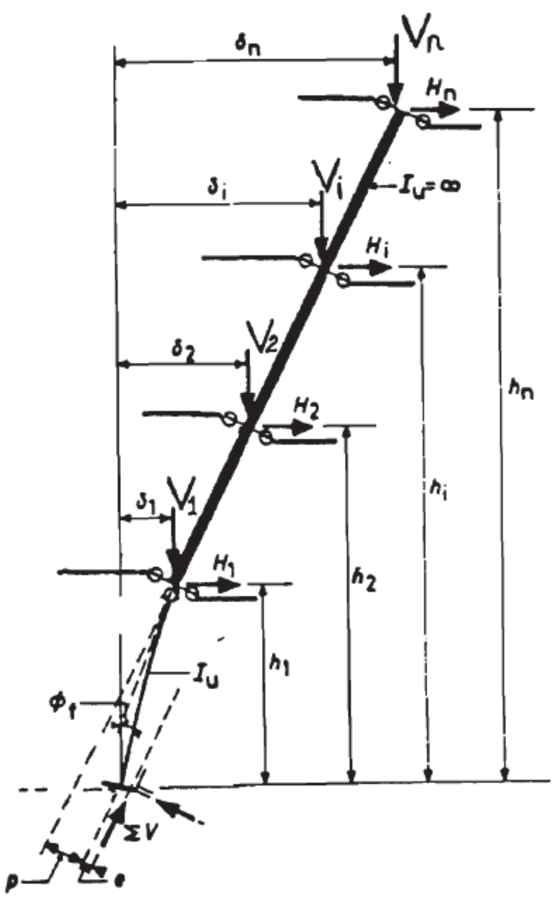

Figure 1.9. Analytical model of a down aisle frame proposed by Stark and Tilburgs (1979) (Davies, 1992, p. 418)

However, this basic method is based on simplified assumptions which are outlined below:

1. It is based on a single internal upright, regardless of the number of bays.
2. It only allows for column flexibility below the level of the first beam and the remainder of the column is treated as rigid.
3. Base plate bahaviour is included by using “eccentricity method” in the model. For this reason the vertical reaction is offset by an amount “*e*”.
4. Second order effect is considered in the analysis.

Later, Davies (1980) described a general exact procedure for determining the elastic critical load of plane frames with flexible joints. He mathematically modelled the entire un-braced frame by using matrix analysis.

Lewis (1991) produced a simple design approach to work out the critical pallet load of an unbraced down aisle frame using energy method. The assumptions he made for the stability analysis were:

(a) Uprights were pinned at the base
(b) Pallet loads at each levels were the same
(c) Flexural deformation of uprights and beams were negligible
(d) The height between storey levels are the same

Davies (1992) improved the down aisle frame model based on the work of Horne (1975).
He described a simplified model for determination of sway behaviour of slender pallet racks with semi-rigid connections (See Figure 1.10). An estimation of the elastic critical load and bending moment distribution were also described.

Feng, Godley and Beale (1993) and Feng (1994) developed a single column model incorporating the semi rigidity of the connections and flexural deformation of the upright which can be used for determination of frame’s buckling load.

Godley, Beale and Feng (2000) developed a theoretical method for analysis and design of unbraced down aisle pallet rack structures. The proposed method accounts for multi bay frames with variable number of stories, semi rigid base plates and beam to upright connection. The simplified model is shown schematically in Figure 1.11.

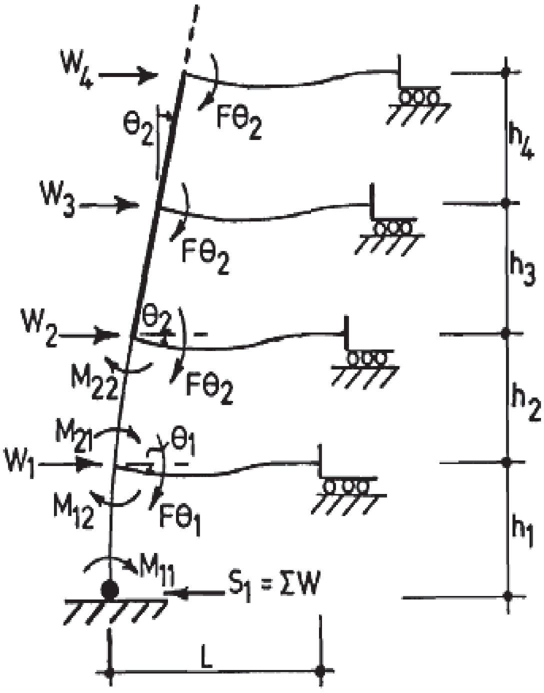

Figure 1.10. Analytical model of a down aisle frame proposed by Davies (Davies, 1992, p. 423)

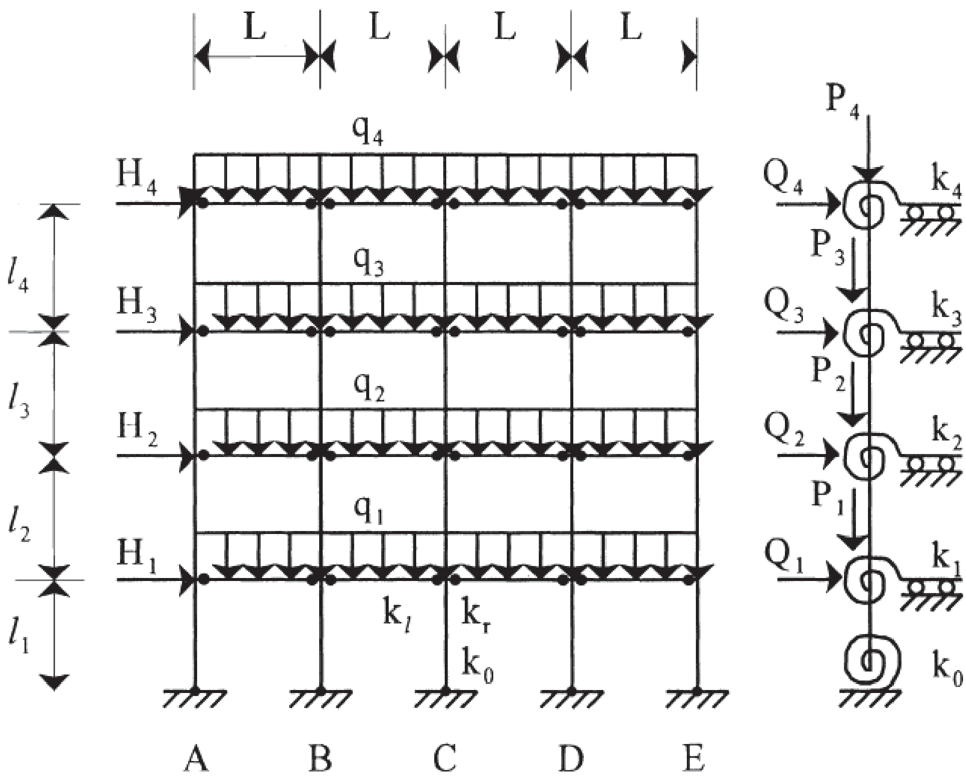

Figure 1.11. Analytical model of a down aisle frame proposed by Godley et al. (2000) (p. 397)

The proposed method was later improved to consider the effect of splices in spliced down aisle frames.

The RMI (2012) specification states in clause 6.3.1:

"For the portion of the column between the bottom beam and the floor as well as between the beam levels, the effective length factor K shall be taken as 1.7 or as otherwise determined by an analysis properly accounting for the member stiffnesses, the semi-rigid nature of the beam to column connections and the partial fixity of the base, allowing for average load reduction, as applicable." (RMI, 2012, p. 22)

"The effective length factor for pallet racks, stacker racks, and movable-shelf racks is "K = 1" provided that all such racks have diagonal bracing in the vertical plane and that such racks have either a rigid and fixed top shelf, or diagonal bracing in the horizontal plane of the top fixed shelf." This approach can be potentially unsafe, however, exact analyses show that values of K, well in excess of 1.7, are not uncommon (Davis, 1992, p. 419).

As the stiffness of the semi-rigid joints reduces, the effective length of the uprights in the down-aisle direction of a rack structure increases. The effective length factors of 1.0 for a braced frame and 1.7 for an un-braced frame underestimate the flexural-torsional buckling stress. (Teh, Hancock and Clarke, 2004)
Australian Standard, AS 4084 (2012) defines the elastic critical ratio of the vertical load (*Ncr/N**) for buckling in a sway mode which will be determined from equation 1.3:

$$N_{cr} / N^{*} = \Phi / \Phi_{max} \qquad (1\text{-}3)$$

where
N^* : Design value of the vertical action on the frame
Φ : Frame imperfection
Φ_{max}: Largest value of the sway index

$$\Phi_{max} = \frac{\delta_U - \delta_L}{H}$$

where
δ_U : Horizontal deflection at the top of the storey
δ_L : Horizontal deflection at the bottom of the storey

H : Story height

Teh et al. (2004) studied the three dimensional frame buckling behaviour of high rise double deep selective racks by developing a 2D model which can give a reliable estimation of elastic flexural – torsional buckling stresses of the upright columns.

Beam to upright connections are modelled as rotational springs in all the stability analysis methods described above. However, all proposed models only consider the un-braced down aisle frames. To close this gap, the stability analysis of the braced and un-braced down aisle frames under seismic actions has been published by the author (Firouzianhaji, Saleh & Samali, 2014).

1.2.5 Upright frame analysis

Braced frame systems are typically used in cross aisle direction of rack structures. C-shaped bracing members are usually bolted to upright flanges to implement a hinge joint as shown in Figure 1.1. There may be one or two bracing members to be connected to the upright flanges (X & V[1] bracing systems) to obtain different stiffness in cross aisle direction.

The transverse shear stiffness of an upright frame (shear frame) impacts the fundamental period of vibration, stability and load carrying capacity of a rack structure in the braced cross aisle frame. Due to its importance in design, experimental tests are used to establish the real stiffness of upright frames. Australian standard AS 4084 (2012) and European norm, EN 15512 (2009) propose a test set up to obtain the shear stiffness of the upright frame and allow the use of experimental value in stability analysis of a full frame. As it is practically not feasible to conduct experimental tests on braced frames of high rise rack structures, an accurate analytical method to evaluate the performance of rack structures in cross aisle directions becomes necessary. However, no analytical approach has been proposed so far.

[1] Such systems are not very popular as the performance of the system is almost unknown. A finite element analysis can discover the behaviour of eccentric bracing under seismic actions. FEM 2011 allows using such systems with greater seismic ductility factor but required that the dissipation capability of the dissipative zones to be proved.

Racking design standard RMI (2012) allow the use of Timoshenko and Gere (1961)'s shear formula to determine the shear stiffness of braced frames.
Also, Timoshenko and Gere (1961)'s equations are used for the stability analysis of the braced frames:

$$P_{cr} = \frac{\pi^2 EI}{k^2 L^2} \frac{1}{1 + \frac{\pi^2 I}{k^2 L^2 A_d sin\emptyset \cos^2 \emptyset_b}} \tag{1-4}$$

where A_d is the cross sectional area of bracing members, E is the elasticity modulus, I is the moment of inertia of the upright member about an axis perpendicular to the upright frame, k is a factor depending on the position of the loads, L is the total height of the upright frame and $\emptyset_b$ is the angle between horizontal and diagonal braces. In that method, it is assumed that the shear deformation of an upright frame is solely due to axial deformation of the bracing members and that a fully hinged joint is implemented at both ends of every bracing member.

In pallet racking design codes, the flexibility of bolted joints is not considered, however, in modelling, codes allow an equivalent reduction of the modulus of elasticity or cross sectional area of bracing members. The effect of different bracing patterns and different height to width ratios of the diagonal bracing members were experimentally and numerically investigated by Rao, Beale and Godley (2004) and Sajja, Beale and Godley (2006 and 2008). They also concluded that the Timoshenko and Gere (1961) equation (Equation 1.3) significantly overestimates the shear stiffness of the upright frame.

Sangle, Bajoria and Talicotti (2011) described in a paper a three dimensional finite element modelling and buckling analysis of a single 2D and 3D upright frame of conventional pallet racking system. They remarked that 3D modelling of the rack structures is necessary to find the buckling loads. It was concluded that the elastic buckling loads obtained from the equations proposed in the current design codes are usually conservative compared to the 3D FE analysis results. Their findings highlighted the need for a thorough investigation of the behavior of the cross aisle frames. They also investigated the effect of stiffening of the open upright sections on the overall stability of the entire frame which can increase the capacity of the upright frames. Gilbert, Rassmussen, Baldassino, Cudini and Rovere (2012) also developed 2-D numerical models in ABAQUS and calibrated their model by experimental test results. They calculated a factor to reduce the cross sectional areas of the bracing members. However, their calculated factor is only appropriate for the conditions of their experiment. Godley and Beale (2008) experimentally investigated the effect of looseness on the stiffness and the load bearing capacity of the upright frames. They recommended that the effect of looseness should be considered as the initial out of plump of the frame for analysis and design of the rack structures.

Chapter 4 of this thesis investigates the behaviour of upright frames and presents a theoretical method of calculation of shear stiffness of an upright frame.

In addition, few full frame static and dynamic experimental tests have also been reported in the literature and are thoroughly discussed in Chapters 5, 6 and 7.

1.3 Objective and Scope

The wide usage of rack structures in countries with high earthquake risk, like New Zealand and many Asian countries, and the lack of adequate specifications and codes for their seismic design, underline the importance of much needed research in this area. This project was motivated by previous observations of rack failures due to the recent New Zealand earthquakes that have further highlighted the effect of connections which play a significant role in transferring the load to different parts of the system. Actual examples of rack collapse have been discussed in Chapter 5 in detail.

Due to the non-linear response characteristics of racking components, including the connections, analysis methods that can reliably predict the behaviour of racking structures are not practical in commercial applications. Current design methods, therefore, rely primarily on test results of individual racking components for the modelling and analysis of the entire racking system. However, in some cases, especially for seismic design, test results and analysis assumptions may not always be consistent and, therefore, a better understanding of the component behaviour and its effect on the entire racking system is required in order to develop more accurate and practical analyses of the global system. Such models will enable developing and incorporating design recommendations and rules specific for seismic conditions that would enrich the existing codes in the future.

In general the main objective of this PhD project is to investigate the 3D behaviour of cold form steel storage rack structures through component tests as well as full scale experimental tests and numerical models. For this reason the following steps have been defined:

- Developing practical modelling approaches for the boltless beam to upright connections, which can be employed in finite element simulations, that consist primarily of beam elements and special purpose connection models that take both the monotonic as well as the cyclic / hysteretic connection behaviours into account.

- Investigating the behaviour of base plate connections under monotonic and cyclic loads.

- Investigating the stiffness of shear frames (braced frames) and their connections and proposing analytical model to calculate the frame stiffness.

- Conducting full scaled Shake Table tests and Cyclic Push Over tests and reporting the dynamic characteristics of the racks as well as the structural deformed shape under seismic motions.

- Proposing an accurate simulation method of the dynamic tests by using a commercial Finite Element software package.

- Proposing a more accurate displacement based seismic analysis approach.

1.4 Methodology

This research involves both experimental and numerical investigations of the behaviour of such non-traditional structures under monotonic as well as seismic actions with particular focus on the performance of three important connections:

(a) Beam-upright connection, also referred to later as Beam-End Connector (BEC);
(b) Floor connection, also referred to later as Base-Plate Connector (BPC);
(c) Bolted brace connection.

The influence of those connections on the behaviour of rack structures will be considered.

1.4.1 Structural testing and Numerical investigations

Courtesy of Dexion Australia, part of the research will be based on a large number of test results conducted on their racking components[2] (Saleh, 2012). The tests were carried out in order to establish the structural performance of different racking components such as failure modes, strength and ductility of base plate and beam to upright connections as well as shear frame assemblies that contain bolted brace connections.

To complement the existing tests which involved only monotonic loading, additional tests including tests with cyclic loading, applied to beam-upright connections, have been conducted during the first phase of this research. Test results provide the most realistic response of connections and will, therefore, be used to better understand the connections' behaviour. They will be used to verify and guide the development of practical connection models for use in numerical simulations. While FE can be a relatively reliable tool to simulate the connection, such complex FE models are not practical for modelling a complete storage rack which contains a large number of

[2] Saleh, A. (2012), Bending Tests on Beam End Connectors - Components manufactured in China and Australia, Report prepared on behalf of AccessUTS Pty. Ltd. For Dexion Australia. Project 201100070.

Saleh, A. (2012), Base Plate Tests – Components manufactured in China. Report prepared on behalf of AccessUTS Pty. Ltd for Dexion Australia. Project: 2011000170.

Saleh, A. (2012), Shear Stiffness of Upright Frames tests - Components manufactured in Australia Report prepared on Behalf of AccessUTS Pty. Ltd. for Dexion Australia. Project 2011000170.

connections. As one of the main objectives of this research, it is intended that connection models will be developed that are capable of simulating the important components of rack structures. For this reason all test results not only will be investigated to understand practical issues and failure modes, but are very important to verify the simple models (Theoretical and Numerical) which were developed in the second stage of this project. In this stage Abaqus software was used among many different finite element software packages due to author's familiarity with that software.

The following finite element models have been prepared and validated against experimental component test results. Details of these models, which were prepared using the Abaqus and Sap2000 software programs, are presented in Chapters 2-4.

(a) FE models of boltless beam-upright connections subjected to both monotonic and cyclic loading have been prepared and analyzed. The models are used to obtain moment-rotation curves of the connections and to assess their strength, flexibility and ductility. Details of these FE models and the results of the connection behaviours under monotonic and cyclic loadings will be discussed in chapter two.

(b) FE models of base-plate connections subjected to combined actions of compression and bending have been developed and analyzed for a range of axial compression loads and different floor bolting arrangements. FE results are presented and discussed in Chapter 3.

(c) FE models of a bolted brace connection have been prepared in order to determine both the flexibility and load carrying capacity of the connection and the effect of connecting the bracing members in a "front-to-front" and a "back-to-back" configuration. Using these models, the proposed strategy for developing practical analyses approaches, which is central to this research, is examined by comparing the FE and experimental results. Furthermore, a formula was derived for estimating the effective shear stiffness of a bolted bracing member when it is assembled in a typical shear frame. Derivation of the formula and its application are discussed in Chapter 4.

Understanding the behaviour and performance of each component under both cyclic and monotonic actions will underpin the development of simple mathematical models that can be easily incorporated in single degree of freedom link elements that are readily available in most commercial FE programs. These models will provide a practical tool for designers to prepare realistic FE models of complete rack structures.

Furthermore, to validate numerical models developed as part of this research, an extensive shake table test and cyclic push over test program on a full scale racking frame has been conducted to evaluate the effects of ductility, strength and stiffness of connections and to check the adequacy of existing analysis methods. Experimental dynamic tests also revealed other phenomena like damping and pallet sliding on the beams which are not easy to understand or model by FE models.

FE models of a complete racking frame have then been developed using the Sap2000 software. These models used simple beam type elements and incorporated the simplified connection models developed separately as part of this research. The accuracy and validity of the full frame modelling approach was verified by comparing the FE results with the results obtained from the shake table tests. The proposed modelling approach including the simplified connection models was fine-tuned to achieve a higher level of accuracy in simulating the seismic response of an entire racking frame.

1.5 Outline

This PhD thesis has been structured as below:

1. Chapter one presents the Introduction, Literature review and Objectives of this thesis.

2. Chapter two presents details of the Experimental, Numerical and Analytical investigations on the behaviour of the boltless beam to upright connections under both monotonic and cyclic loads. Numerical and Analytical models

were developed in that chapter and were verified against the experimental component test results.

3. Chapter three explains the behaviour of the base plate connections, both experimentally and numerically. Failure moment, ultimate rotations and stiffness of different base plate connections with different anchoring conditions were investigated. Numerical simulation of the behaviour of the base plate connection under cyclic loads is also presented in Chapter 3.

4. Chapter four of this thesis presents the Experimental and Numerical investigations of the full assembly of a shear frame. A simplified mathematical model was also developed to determine the stiffness of the shear frame using particular bracing connections.

5. Details of the full scale dynamic shake table test set up and the test results are presented in Chapter 5.

6. Chapter 6 presents the Finite Element simulation of the full rack frame. Steps of FE modelling procedure and the effect of beam to upright connection models were investigated thoroughly. Response of a typical 4-storey rack structure under different earthquake records such as 1940 El Centro and 1994 Northridge was first investigated and then Finite Element model was developed to simulate the shake table test conditions.

7. Chapter 7 explains the details of the cyclic push over test set up and the applied loading protocol. The behaviour of a full rack frame under cyclic action is presented and the cyclic test results are compared with the dynamic test results of Chapter 5. A displacement based seismic design of rack structure is also proposed and presented in this chapter.

8. Conclusions and recommendations for further research and investigations are presented in chapter 8.

1.6 Publications

The following published papers and research reports are based on this PhD program.

1.6.1 Technical papers

1. Firouzianhaji, A., Saleh, A. & Samali, B. (2013). Finite element modeling of a beam-column connection in industrial storage racking structures. *Proceedings of the 22nd Australasian Conference on the Mechanics of Structures and Materials*, *ACSM 22* (pp 813-818). Sydney, Australia: CRC Press.

2. Firouzianhaji, A., Saleh, A., & Samali. B. (2014). *Non-Linear Analysis of base Plate Connections used in Industrial Pallet rack Structures.* Paper presented at the Australasian Structural Engineering Conference, Auckland, New Zealand.

3. Firouzianhaji, A., Saleh, A., & Samali, B. (2014). Stability Analysis of steel storage rack structures. *Proceedings of the 23rd Australasian Conference on the Mechanics of Structures and Materials (ACMSM23)* (pp 583-588). Byron Bay, Australia.

4. Firouzianhaji, A., Saleh, A., & Samali, B. (2015). *Non-Linear Behaviour of Boltless Beam to Upright Connections in Cold Formed Steel Storage Racks*. Paper presented at the International Conference on Advances in Steel Structures (ICASS'2015), Lisbon, Portugal,

5. Firouzianhaji, A., Saleh, A., & Samali, B. Analysis of boltless beam-upright racking connections under cyclic loading. *Thin walled structures journal*. (under preparation)

6. Firouzianhaji, A., Saleh, A., & Samali, B. Seismic analysis of steel storage rack structures with boltless beam to upright connection. *Thin walled structures journal*. (under preparation)

7. Firouzianhaji, A., Saleh, A., & Samali, B. Analysis of base plate connections used in cold formed rack structures. *Journal of Constructional steel research*. (under preparation)

2. CHAPTER 2: MODELLING OF BEAM TO UPRIGHT CONNECTIONS

2.1 Introduction

As indicated earlier, the design and analysis of industrial storage racks typically relies on test results to determine the performance of the key structural components such as strength and stiffness of beam to upright connections. As shown in Figure 2.1 in a typical beam to upright connection used in rack industry, beams are welded to a L-shaped connector angle with a number of hooks that are designed to be engaged to the upright perforations. Such a simple and fast installation process is one of the reasons that these kinds of connections are becoming more and more popular in rack industry.

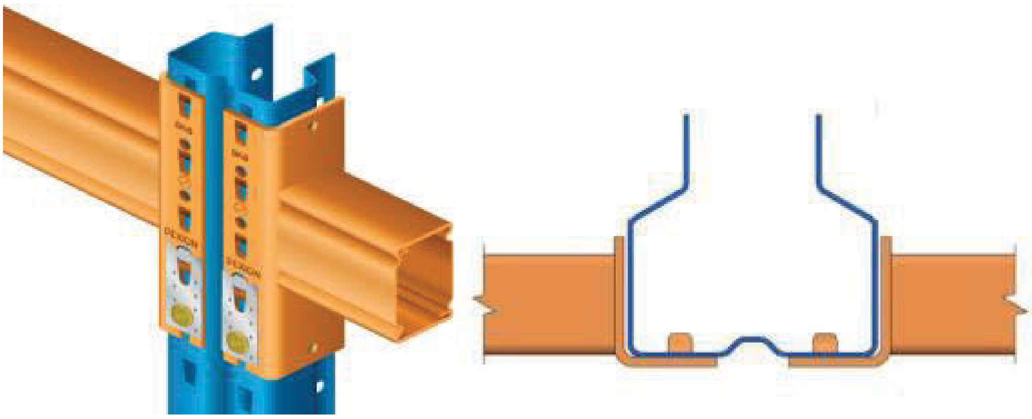

Figure 2.1. Typical beam to upright connections using boltless beam end connectors(DEXION Pty Ltd.)

However, the simple installation process is not the only difference that these kinds of connections have with conventional steel building connections. The non-linear response of hooked connections is also remarkably different:

"At large rotations, the inelastic rotation capacity of the of beam-to-upright connectors is significant and for some connections can exceed 0.20 rad compared to building moment-resisting connections having inelastic rotation capacity in the range of 0.04 rad for special moment-resisting frame systems." (Filiatrault et al., 2006, p.

162) Although the connections are capable to undergo large rotations, due to their slenderness the entire rack frames usually lose their stability at smaller drifts and become unstable before the connections reach their ultimate capacity.

The lower rotational stiffness of beam to upright connections is another distinctive feature of the hooked connections. The rotational stiffness of beam to upright connections is an important parameter in specifying the performance and stability of the rack structures under vertical and horizontal actions. Stiffness of the connections usually falls between the two extremes of rigid and hinged connections and hence needs to be properly defined in the analysis and design of steel racks.

Current racking design codes require that the stiffness and strength of the connections are derived from actual experimental tests. No rigorous analytical method has been presented so far to be used as an alternative to expensive experimental tests. Racking codes and specifications such as AS 4084 (2012) and BS EN 15512 (2009) simplify the non-linear moment – rotation curves by a linear model. As shown in Figure 2.2, by adopting the equal energy principle, the corresponding linear stiffness value is defined as the slope of the line that encloses equal areas (A1, A2) below and above the experimental curve.

However, codes provide flexibility to the engineers to specify the stiffness values:
"Any value of the design load or moment may be chosen less than or equal to the allowable maximum in order to optimize the possibly conflicting requirements for stiffness and strength. Thus, by reducing the design strength, a greater design stiffness may be achieved." (AS 4084, 2012, p. 70)

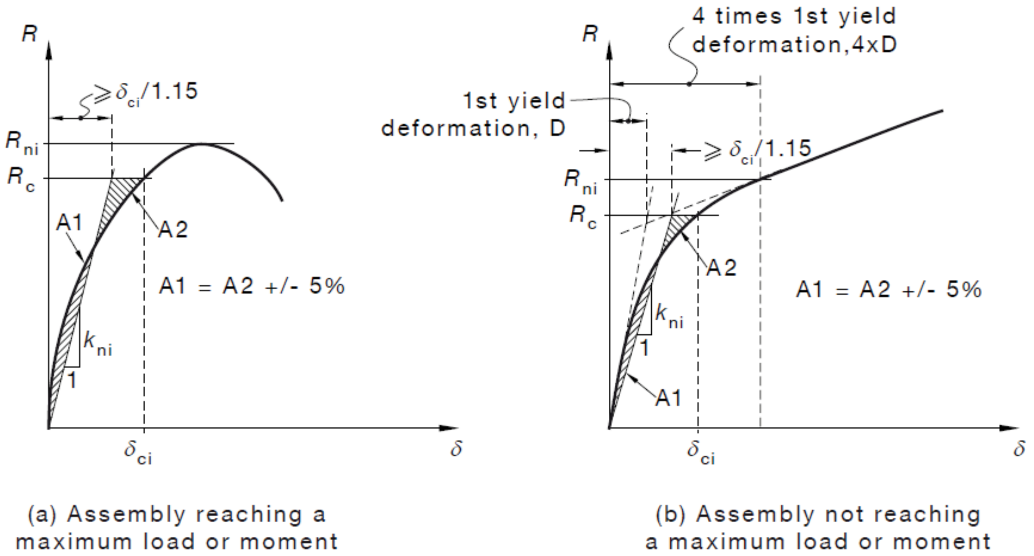

Figure 2.2: AS4084:2012 Figure 7.2.2.2, explaining method to determine the rotational stiffness of beam to upright connections (AS 4087, 2012, p. 70)

Obviously the presented method of obtaining rotational stiffness and strength of the connections that is based on the monotonic moment rotation curves, is fully dependant on actual experimental tests that are expensive and time consuming. This highlights the importance of parametric and analytical investigations of the moment rotation behaviour of beam to upright connections.

This chapter presents the behaviour of beam to upright connections in two parts. The first part investigates the monotonic response of the connections while the second part focuses on the behaviour of the connections subjected to cyclic loads to discover their cyclic and hysteretic features.

Firstly, based on monotonic tests on beam end connectors with different box beam cross sections, the effects of key parameters such as beam/upright dimensions on the moment- rotation behaviour of the connections were investigated. Finite Element models were then developed to simulate the monotonic tests and afterwards an analytical approach was used to calculate the ultimate and yield moment of the connections under monotonic loads.

In the second part of this chapter, the cyclic test results are presented and a suitable method of obtaining rotational stiffness and ultimate moment of the connections is proposed. Unlike the current methods, this method considers the effect of cyclic features and is indeed more suitable for seismic design.

2.2 Monotonic behaviour of beam to upright connections

2.2.1 Experimental investigations

Before commencement of this study a set of 108 bending tests on Beam End Connectors (BEC) were carried out at the University of Technology, Sydney and the results were available to start this study. The purpose of the BEC tests was to determine the moment-rotation curve under monotonic loading in the pre- and post ultimate region and to derive the initial stiffness of the connection. A typical moment-rotation curve and a schematic test rig are shown in Figure 2.3 (a & b).

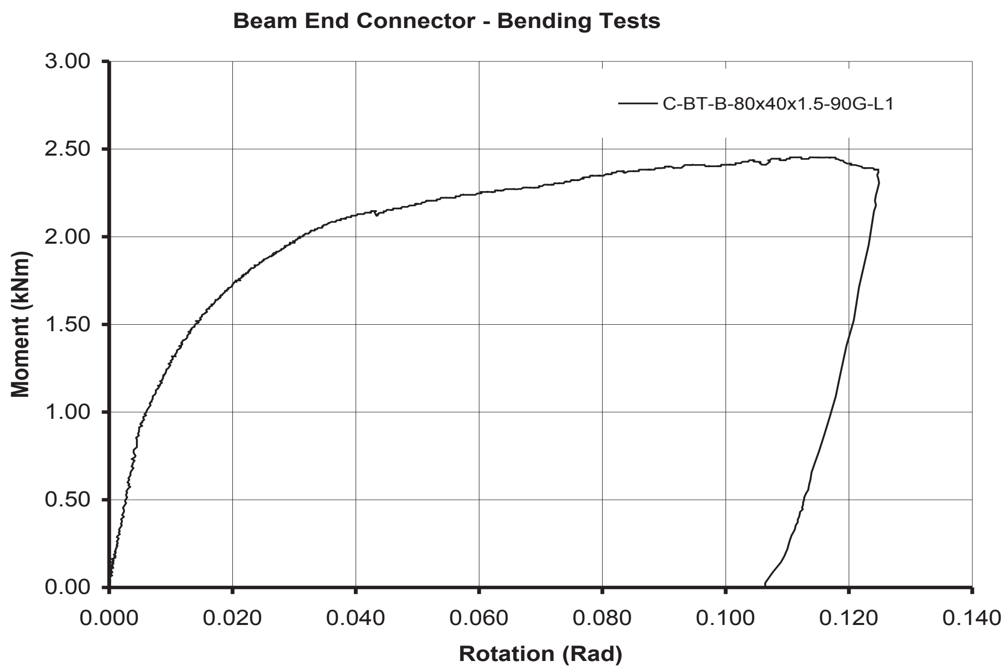

Figure 2.3 (a)

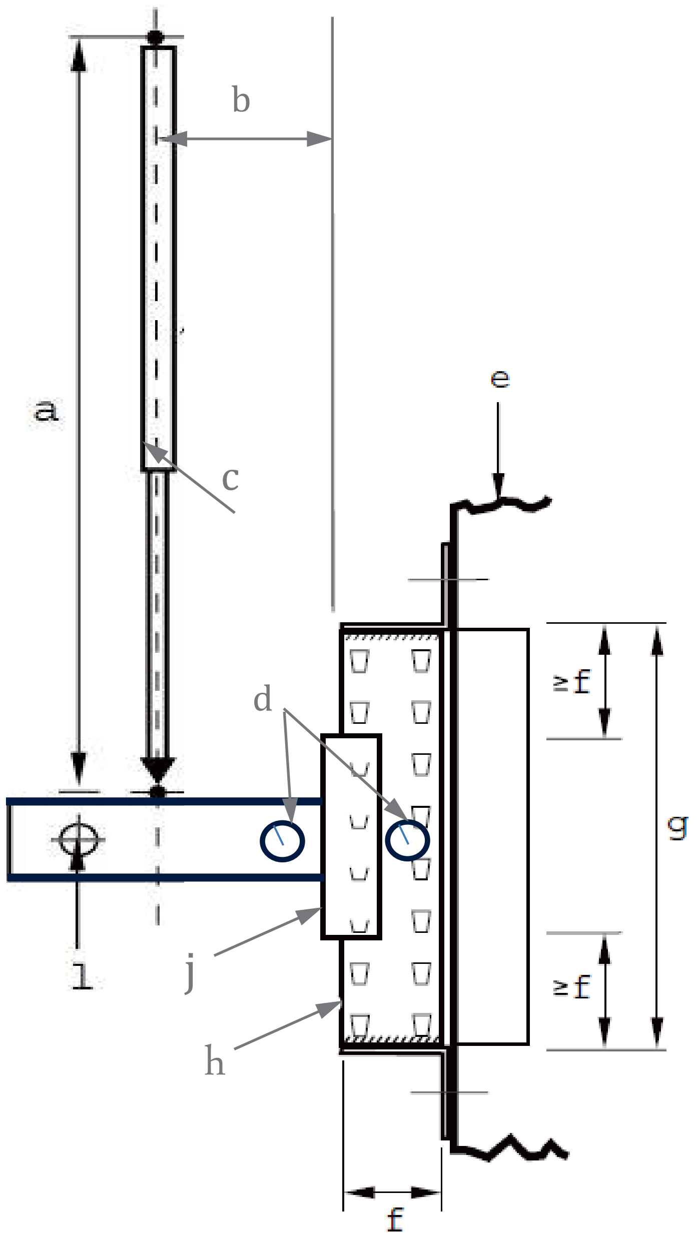

a ≥ 750mm
b 400mm
c load jack
d measuring devices (Inclinometers)
e test rig structure
f upright face width
g length of test specimen
h Stub Column
j beam end connector
l lateral restraint allowing vertical deflection

Figure 2.3 (b)

Figure 2.3 a and b: Moment-Rotation curve and experimental test set up

Also, at the start of this PhD program 60 additional monotonic tests were conducted based on the test arrangement described in EN 15512 (2009) and the test rig depicted in Figure 2.3. During the test, the beam was loaded by means of a hydraulic jack at a distance b=400 mm from the face of the upright. The jack was pinned at both ends to allow free in-plane rotation and had a length between connecting pins greater than a=750mm. During the test the jack load was applied slowly until a further load increase was no longer possible. As shown in Figure 2.4, a load cell was used to record the applied force, while two inclinometers attached to the beam and the upright were used to record their individual rotations and to enable the relative rotation between beam end and upright to be determined. For each test, the cantilever moment at the face of the upright was computed and the corresponding moment versus rotation curve was plotted. Moment-rotation curves enable the semi-rigidity of the connections to be investigated.

At the conclusion of the monotonic tests, a further 7 tests were conducted in order to investigate the behaviour of bolt-less beam end connectors under cyclic loading. The tests highlighted the urgent need to study the effect of cyclic loading on the connection ductility, which is critical for seismic design. This is because of significant deterioration of the connection that was observed from cyclic test results which was not addressed in the current methods of obtaining stiffness and strength of the connections for seismic design. Details of cyclic test results are presented in section 2.3.1.

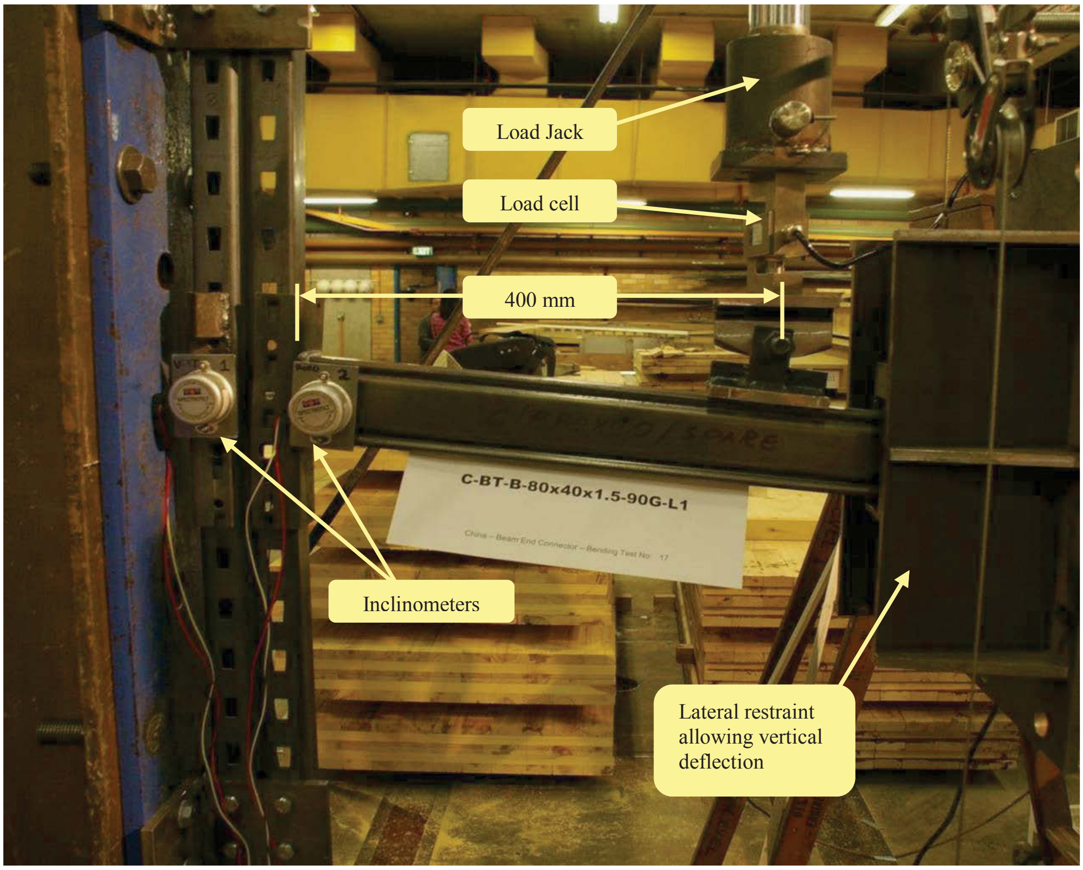

Figure 2.4. Test rig of beam end connector bending test with a specimen during testing

2.2.1.1 Test Observations

Typical failure modes of the connection were primarily by bending of the connector plate and severe deformation of the upper hooks mostly on the tension side. A detailed list of the failure modes can be found in Appendix A.

Since the connection relies primarily on the hooks to transfer the applied moment between beam and upright, damage of the hooks greatly reduces the strength and stiffness of the connection. As the load is applied, failure of the connection occurs gradually starting typically with the outer most hooks and progressing toward the centre of the connection with damage to the hooks next in line until complete loss of connection strength. In some specimens the connector plates were found to tear off close to the hooks at the end of the connector. Typical examples of failure modes observed are shown in Figure 2.5 and Figure 2.6, the uprights were not visibly damaged by bending but local damage in the form of indentation or tearing at the perforations of the uprights coinciding with the location of the top and bottom hooks.

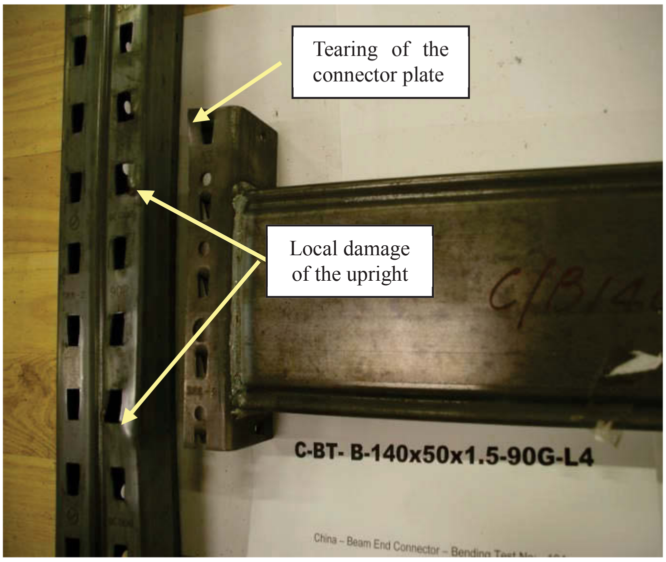

Figure 2.5: Typical failure modes observed in beam end connector and upright

Figure 2.6: Typical failure modes in different beam end connectors. Top left: tearing at hook near top of connector. Bottom left: bending of connector hooks cutting into upright slots. Right: Bending of connector plate

2.2.1.2 Beam-End Connector (BEC) test results

The results for BEC tests were further analyzed in order to study the effect of beam depth and upright stiffness and the ultimate strength and stiffness of the connections.

The recorded test data for each connection was used to determine the ultimate strength and stiffness to present the connection response in form of a moment-rotation curve. A typical moment-rotation curve is shown in Figure 2.7.

It can be observed that while the overall connection response is non-linear, the first part of the curve is relatively linear, which enables an initial stiffness to be established approximately. The nonlinear part begins when materials start yielding followed by a peak in strength and then failure.

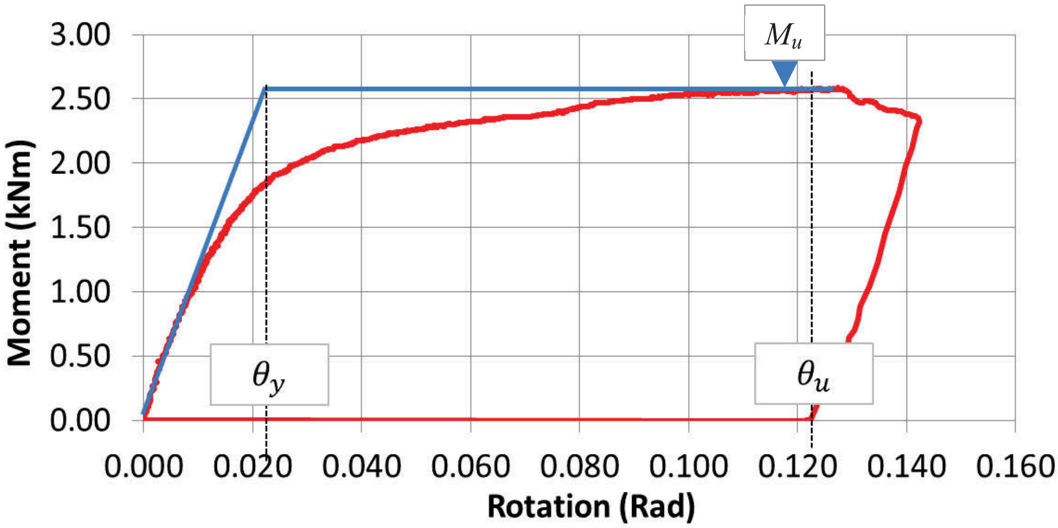

Figure 2.7: Typical moment rotation curve of the beam end connector test

The upright total rotation during the test was recorded and was found to be very small and hence the only significant source of deformation affecting the beam end connector's rotation were:

1. The hooks and their movement through the upright slots by indenting the upright metal or bending the hooks.
2. The deformation of the L-shaped connector.

Failure moments are presented in Table A.1. The initial stiffness was calculated from the slope of the secant line passing through two points, which were identified by visual inspection of the moment-rotation curve near zero loads.

A Non-dimensional form given in equations (2-1) and (2-2) was used to better compare the experimental results of different connection types and to establish the connection's semi-rigidity in accordance with the European norm EN 1993-1-8 (2005).

$$\overline{m} = \frac{M}{M_{p,b}} \quad \text{and} \quad \overline{m_u} = \frac{M_u}{M_{p,b}} \tag{2-1}$$

$$\overline{\emptyset} = \emptyset \frac{EI_b}{L_b M_{p\prime b}} \tag{2-2}$$

where in equations (2-1) and (2-2):

$\overline{m}$ is the non-dimensional moment, $\overline{m_u}$ is the non-dimensional ultimate moment, $\overline{\emptyset}$ is the non-dimensional rotation, M is the moment in the beam to uptight connection, M_u is the ultimate moment in the beam to uptight connection curve, $M_{p\prime b}$ is the plastic moment of the beam, E is Young's modulus, I_b is the second moment of area of the beam and $L_b$is the nominal length of the beam usually used in rack systems (assumed as 2400 mm in this study). The normalized results of the experiments are sketched in Figure 2.8, in comparison with the lower bound and upper bound, which according to EN 1993-1-8 (2005), are the set limits for fully hinged and fully rigid joints, respectively.

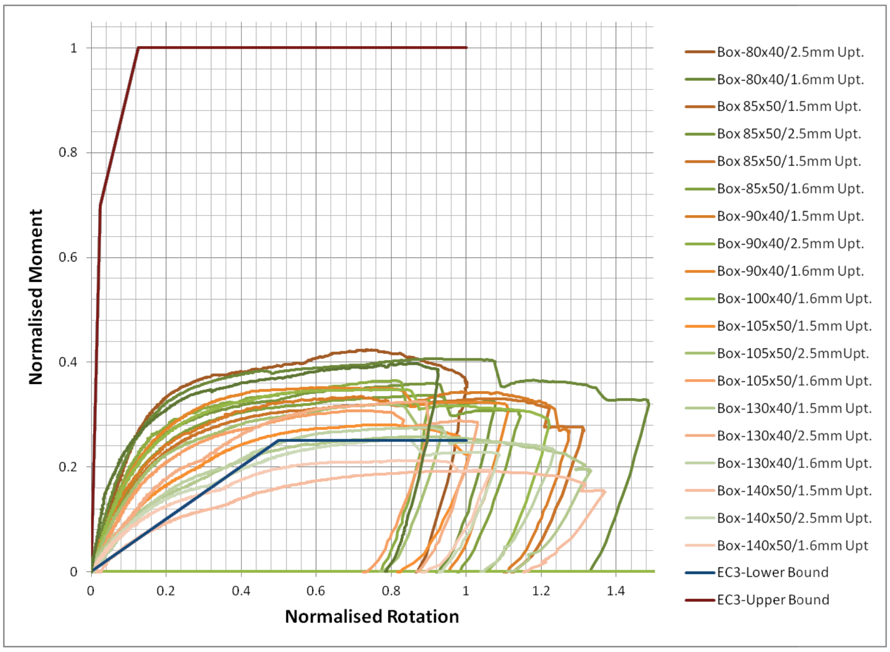

Figure 2.8: Normalized moment – rotation monotonic curves of 19 different beam to upright connection configurations

Normalized moment rotation curves in Figure 2.8 show that most beam end connections are semi-rigid and only a few (i.e. those with deeper beams) can be considered as pinned. Deeper beams have larger plastic moment '$M_{p,b}$' while on the other hand the beam end connector, which is responsible for resisting the applied moment '*M*' is identical for all the beams regardless of their depth. Therefore the non-dimensional ultimate moment '$\overline{m}_u$' of the connections with deeper beams, according to equation 1, drops significantly and falls into the category of hinged connections in Figure 2.8. As explained above, rigidity of the connection is a relative concept and depends on the section properties of the beam profile. It is therefore recommended to increase the number of hooks of the beam end connectors that are connected to deeper beams.

2.2.1.3 Parametric analysis

Experimental results were used to study the effects of the main parameters such as Beam depth and width as well as upright thickness.

2.2.1.3.1 Beam depth

The ultimate moment of 4 different connections with the same upright and the same beam width but different beam depth (BOX Beam 80 x 40, BOX Beam 90 x 40, BOX Beam 100 x 40, BOX Beam 130 x 40) were derived from the monotonic moment rotation curves and are shown in both actual and non-dimensional formats. Interestingly, the two curves show completely different trends. The ultimate moment slightly increases by increasing the beam depth while on the other hand the non-dimensional ultimate moment decreases. The amount of increase and decrease is shown in Figure 2.9 (a and b).

The reason that the non-dimensional moments of connections with deeper beams are smaller compared to the non-dimensional moment of other connections, as has been explained earlier in section 2.2.1.2, was the use of the same size connector for different beam depths tested in this study. It is expected that tests on similar type connectors by different manufacturers would yield a similar trend.

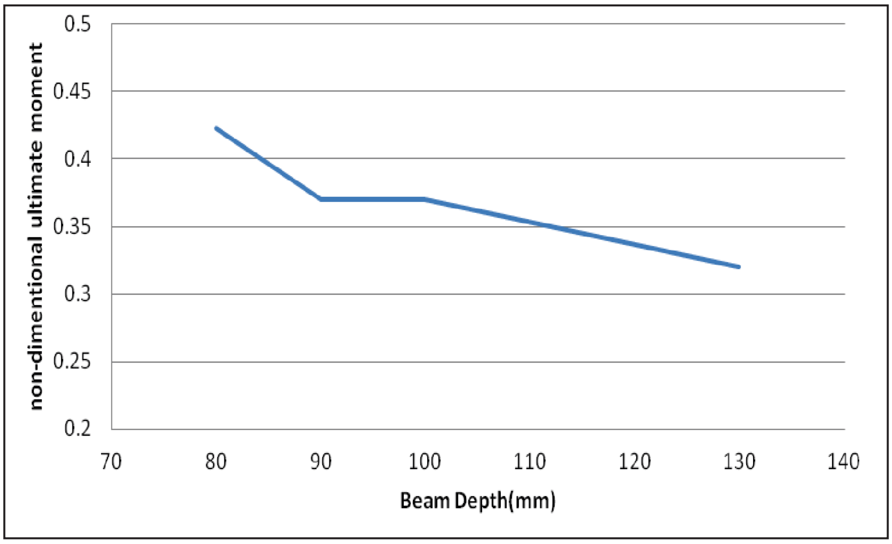

(a)

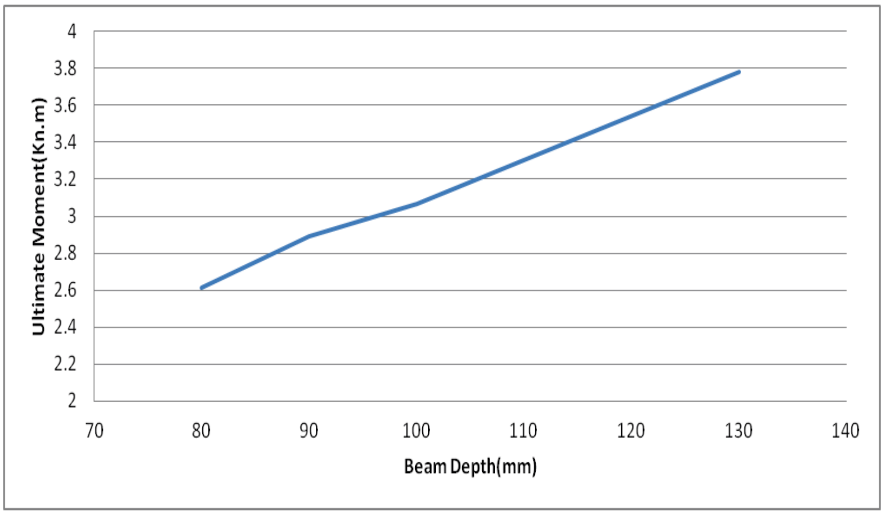

(b)

Figure 2.9: (a) Effect of beam depth on the non-dimensional ultimate moment; (b) Effect of beam depth on the ultimate moment

The initial stiffness, $S_{j,ini}$, of the connection is another parameter which is affected by the change in beam depth. (See Figure 2.10)

Figure 2.10: The effect of beam depth on non-dimensional initial stiffness

2.2.1.3.2 Upright thickness

The effect of upright thickness on the ultimate moment was also studied using the test results.

In this study, uprights have been categorized into two classes based on their thickness (2.5mm and 1.6mm). The ultimate moment increases slightly with increasing both the upright thickness as well as the initial stiffness (See Figure 2.11).

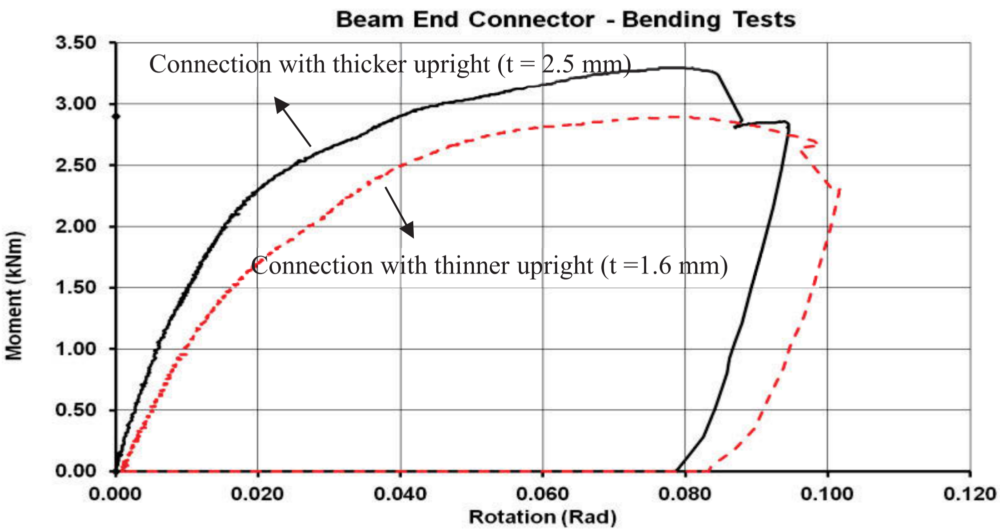

Figure 2.11: Different non-dimensional moment rotation curves for two different upright thicknesses

According to Table A.2, in some cases (connections with deeper beams) the moment rotation curves showed a slight transient increase (hump) in the slope in the nonlinear part of the curves which occurred between 70% - 85% of the ultimate moment. This can be attributed to the connector face coming into contact with the upright's flange as the load is applied and thereby closing the initial clearance which exists between the beam end connector and the upright (See Figure 2.12).

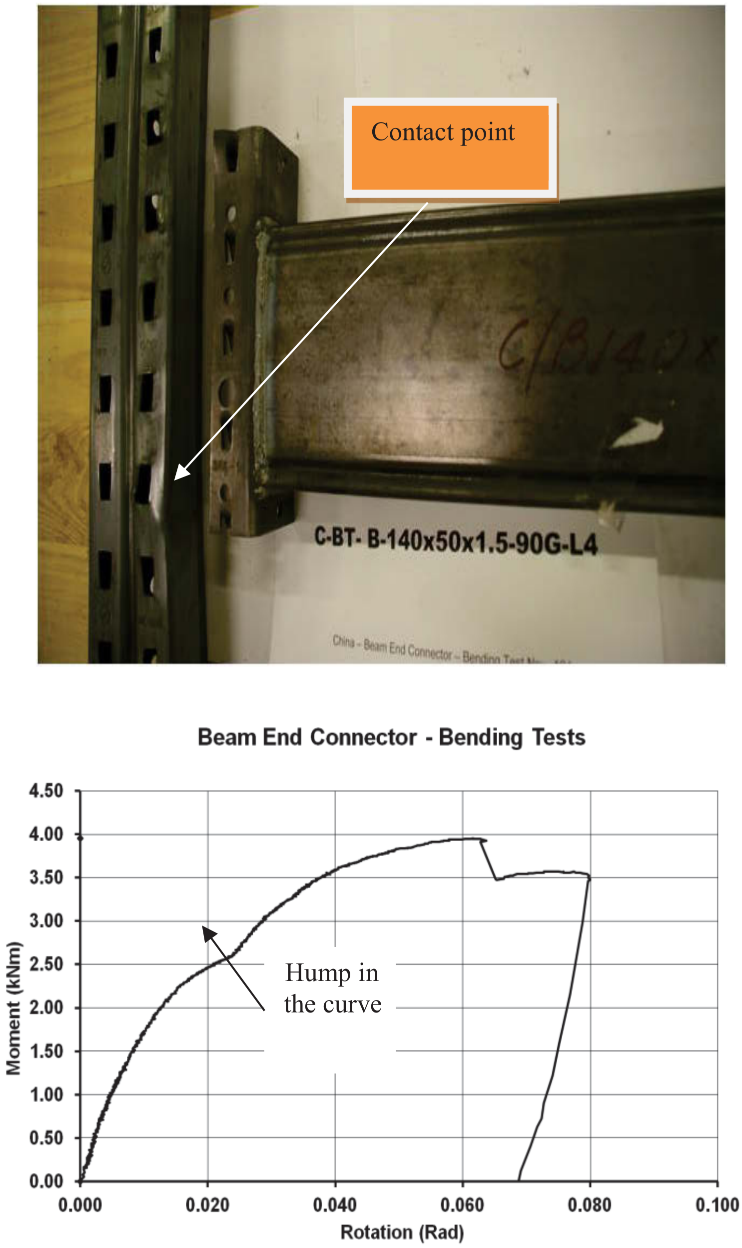

Figure 2.12: The slope discontinuity in the moment rotation curve due to contact of connector face to upright flange

2.2.1.3.3 *Ultimate and Yield Rotation (θ_u & θ_y)*

The ultimate and yield rotations of the connections were also derived from the idealized perfect elasto-plastic moment rotation curves and their values are shown in Figure 2.13 and Figure 2.14. The ultimate rotation was defined as the rotation corresponding to the ultimate moment. The yield rotation was the rotation at the interception point of the line tangent to the moment rotation curve at the origin and the horizontal line passing from the ultimate rotation point. (See Figure 2.7)

According to Figure 2.13 and Figure 2.14, the yield rotation 'θ_y' is almost the same in all the connections, with a standard deviation of 0.001 radians, regardless of the beam depth and the upright thickness. Therefore, an average value of 0.02 can be considered as a constant value indicating the yield rotation of the connections. Ultimate rotation 'θ_u' also shows fairly close values for 56 beam end connector bending tests with an average of 0.1 radians and standard deviation of 0.019 radians. Investigations reported by Prabha et al. (2010) and Markezi et al. (1997) also show 'θ_y' and 'θ_u'values of around 0.02 and 0.1 radians, respectively.

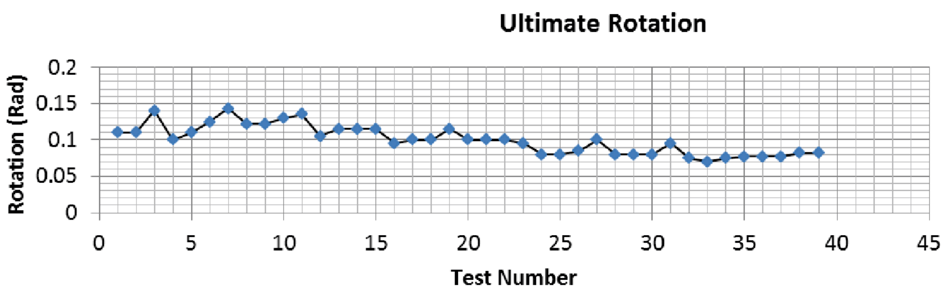

Figure 2.13: Amount of Ultimate rotations of the connections.

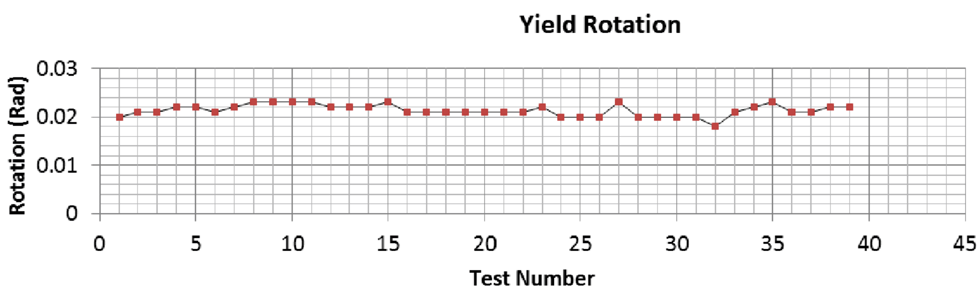

Figure 2.14: Amount of Yield rotations of the connections.

The relative constancy of the ultimate and yield rotations of different connections can be justified by the fact that similar beam end connectors are used in all the connections and connections basically starts to yield when the uppermost hook yields and therefore despite the differences in the beam/upright configurations, yield and ultimate rotations show relatively constant values.

2.2.2 Numerical Analysis of beam end connectors

Finite element analyses simulating the seismic response of structures containing geometric and material nonlinearities necessitate an iterative solution and can hence be time consuming and require substantial computer resources. It is, therefore, important to choose a finite element model which is both accurate and computationally efficient. Included in this report are finite element models; which were prepared to identify the effects of different modelling parameters on both the quality of results and the corresponding computational effort required to achieve the results. A typical FE model is shown in Figure 2.15. The effect of element types, model size and the inclusion and simulation of contact non-linearity were compared. Using the ABAQUS software (2011), all FE models were three dimensional and accounted for both material and geometric non-linearity. The material law of beam, upright and connector plate were modelled using the tri-linear stress-strain diagram of Figure 2.16 and the experimental values of Table 2-1. Hexahedral solid elements were used in the FE models and meshed with up to four solid elements through the metal thickness to better simulate flexural behaviour.

It is reported in literature that the 8-noded brick elements, if adopted in a fine enough mesh, provide better results for regions with high stress gradients than a coarse 20-noded brick elements mesh (Khodaie, Mohamadi-Shooreh, & Mofid, 2012). The element type used in the majority of models in this study was, therefore, the 8-noded linear brick element (C3D8R).

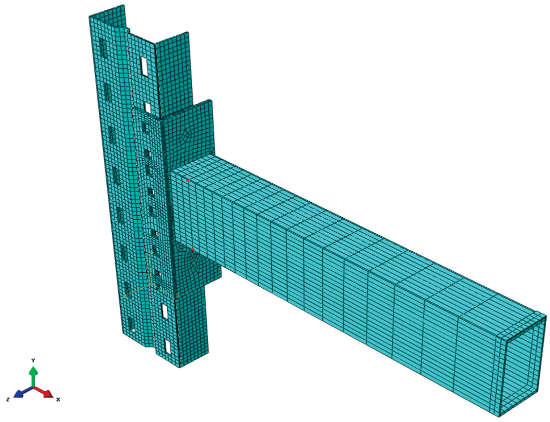

Figure 2.15 Typical Finite Element Model

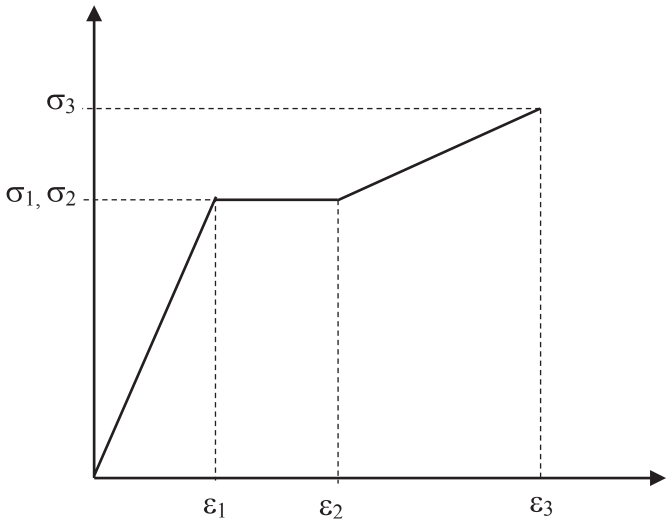

Figure 2.16 Typical three-linear stress strain diagram

The triangular shell element (S3R) was also used in two of the models. Different model sizes were considered in order to compare result accuracy and solution time. (See Table 2-2) As can be seen in Figure 2.17 and Figure 2.18, a finer FE mesh was used in areas where a high stress gradient was expected such as around the hooks and the weld location between beam and connector plate. In the FE model the upright was fully fixed at both ends in order to simulate the experimental setup. Special attention was given to the modelling of the contact areas that represent the interaction between the surfaces of hooks and column slots (See Figure 2.18). Geometric nonlinearities were accurately taken into account by defining proper interactions which allows separation of surfaces in the surface normal direction. An efficient simulation of the hooks creating a dent in the upright slots was then obtained as depicted in Figure 2.19. Preliminary FE models indicated that the best results were obtained from FE models with 3 elements through the thickness of the connector plate and 4 elements through the thickness of the hooks.

The non-linear solution of the FE model in which material, geometrical and contact nonlinearities were considered was obtained using a full Newton iterative procedure. The load was applied and increased incrementally and the moment at the face of upright was computed using a force lever arm of 400 mm. At each converged step, the corresponding rotation was established from the relative displacement of two nodes located near the connector plate at the top and bottom of the beam. The iterative solution was terminated in the following cases: (a) areas of excessive yielding in parts of the FE model were observed, typically near the upper connection hooks or; (b) the number of iterations became excessive. Either cases typically occurred at loads that coincided with the experimental failure loads[3].

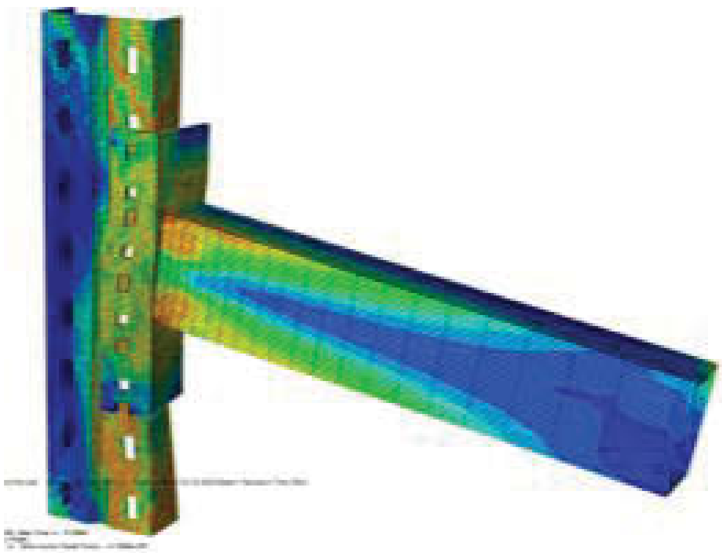

Figure 2.17: Deformed connection with Von- Mises stress contours

[3] A displacement control based analysis was later carried out and the accuracy of the results were verified

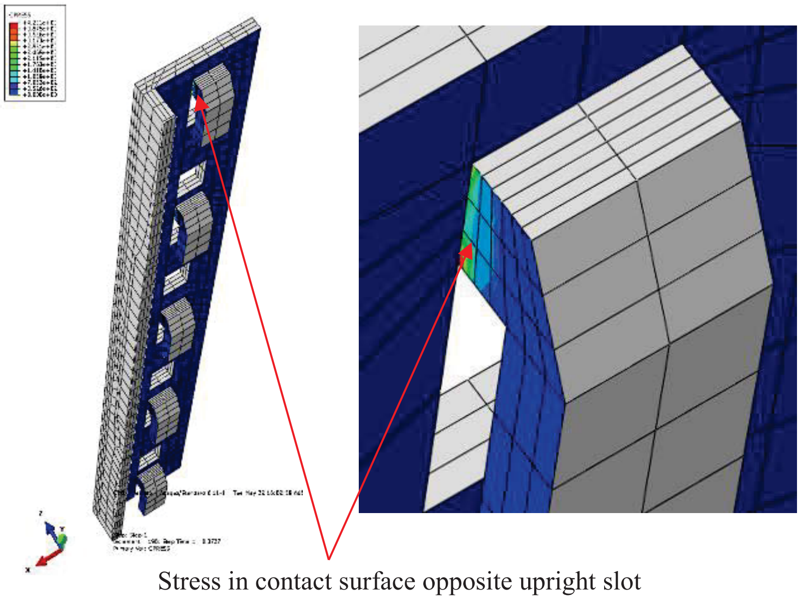

Figure 2.18 Connector plate hooks and contact areas

Table 2-1: Material properties

Component	Beam	Upright	Connector
ε_1 (%)	0.15	0.15	0.15
σ_1 (MP)	350	350	300
ε_2 (%)	3.15	3.15	3.15
σ_2 (MP)	350	350	300
ε_3 (%)	20	20	35
σ_3 (MP)	500	480	350

Table 2-2: Finite Element models

Model	***Element type***	***Total number of Elements***	***Total number of Nodes***	***Degrees of freedom per node***	***Analysis Time CPU (Sec.)***	***Moment at 0.1 rad (kN.m)***	***Error In Moment (%)***	***Error In Initial Stiffness (%)***
Experiment	---	---	---		---	*2.57*	---	---
A	*C3D8R*	*5536*	*10581*	*3*	*1015*	*2.88*	*10*	*8.8*
B	*C3D8R*	*10536*	*19115*	*3*	*2314*	*2.46*	*4*	*5.1*
C	*S3R*	*13767*	*9482*	*6*	*1525*	*2.77*	*7*	*15.7*

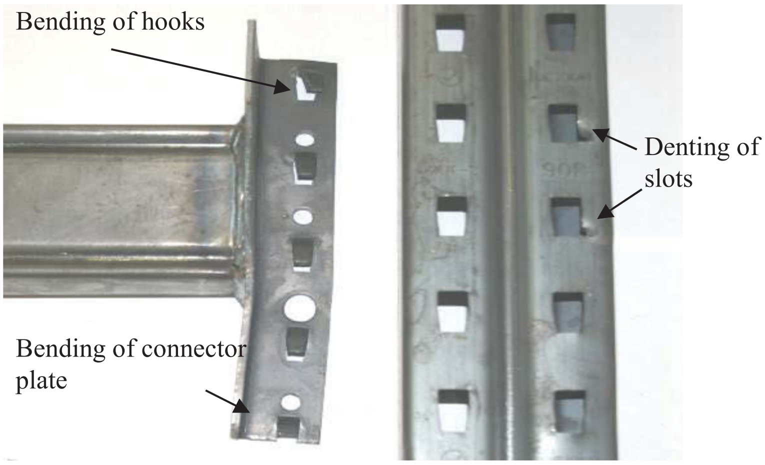

Figure 2.19: Typical plastic deformation of connection after test

2.2.2.1 Comparison of experimental and FEA results

Moment-rotation curves obtained from each of the FE models are compared with the experimental curves in Figure 2.20. It can be seen that the numerical and experimental curves are generally in good agreement up to approximately 80% of the failure moment.

A comparison of initial stiffness indicates that models A (with coarse mesh) and B (with fine mesh) deliver the best result with the difference being respectively 8.8% and 5.1% (see Table 2-2).

In this study, the weld geometry between the beam and connector plate was not modelled, which may partly explain the differences in the shape of moment-rotation curves in comparison with the experimental curves presented in Figure 2.20. Localized areas of stress concentration that exceeded the ultimate stress were observed in the FE models at the interface between beam and connector plate. It is hypothesized that redistribution of these stresses and corresponding strains was associated with a change in rotational stiffness.

By visual inspection of the experimental moment-rotation curves, the rotation of 0.1 rad was chosen as a basis to compare the moment values of FE models near the ultimate connection moment in Table 2-2 (see Figure 2.20).

The best results were obtained from the models with solid elements. It can be seen in Table 2-2 that in model B the difference in ultimate moment (at $\theta = 0.1$ rad) was 4% or less. Model with shell elements did not perform well and showed a stiffening of the moment-rotation curve after the experimental failure moment was reached. While the solution time of models A were the lowest, the accuracy was not satisfactory. The deformed shape obtained from FE model B and the corresponding Von-Mises stress contour plot is shown in Figure 2.17. Close inspection of the FE model revealed that yield stress was exceeded at the contact between upper hooks and upright slots. This is consistent with the denting of upright slots and bending of the hooks that were observed at the conclusion of the experiment (See Figure 2.19). Hooks are, therefore, a critical component in transferring the load between the beam and the upright and hence hook failure can lead to connection failure.

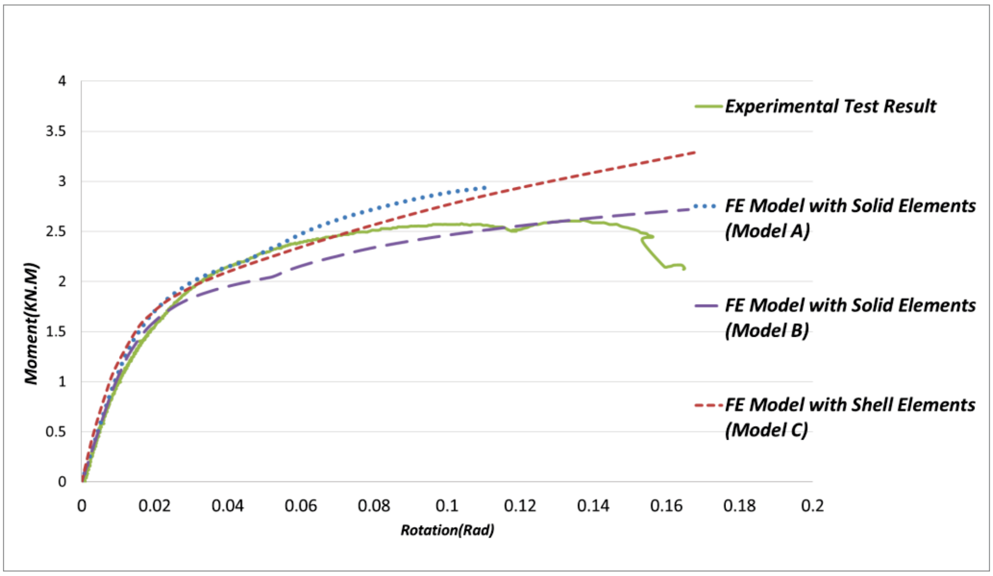

Figure 2.20: Test results against results of FE models with shell/Solid elements

In summary, the adequacy of three different Finite Element models of a typical beam end connection used in industrial racking, which were analysed using the Abaqus software was investigated by comparing the results against experimental moment-rotation curves. The differences between models were model size (coarse vs fine), the type of elements (solid vs shell). The FE models which incorporated the effects of contact-, geometric- and material non-linearity provided results that were generally in good agreement with the experiment especially up to approximately 80% of ultimate moments when the non-linear response was relatively low. Close inspection of the FE model revealed that yield stress was exceeded at the contact between hooks and upright slots.

The verified FE model explained above can provide more confidence to step forward and investigate other beam to upright connections and focus on key parameters like failure modes, ductility and flexibility of the connections. Figure 2.21 to Figure 2.23 Show FE analysis results for three different connections. Again very good agreement is observed in the first part of the curves for all the models to estimate the elastic stiffness of the connections.

FE models could also fairly predict the ultimate moment and rotation of the connections in all cases. Achieving a good correlation between the numerical and experimental results, as shown above for monotonic loading, was necessary if the same FE models were to be used to simulate the connection behaviour under cyclic loading. While under monotonic loading small errors may be acceptable, in models subjected to cyclic actions errors can accumulate as the number of cycles increases. Investigation of the beam to upright connection under cyclic loads is the subject of part 2.3.

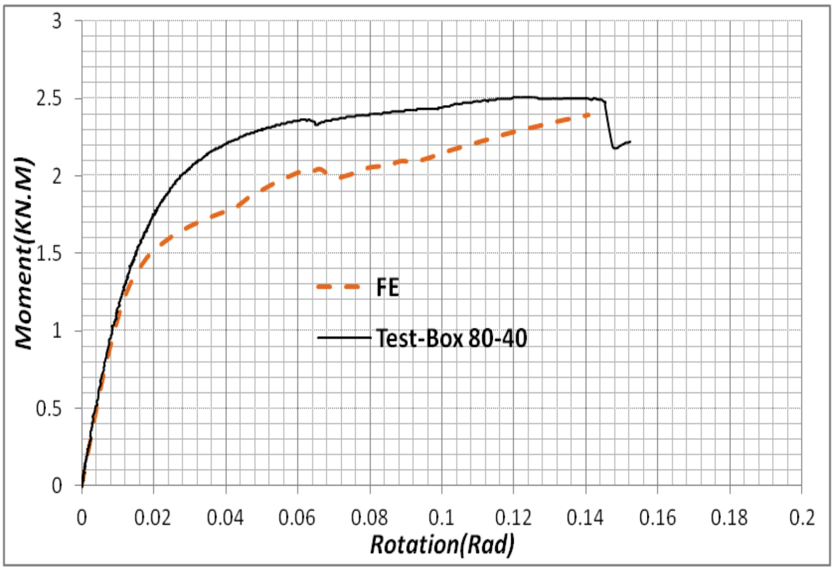

Figure 2.21: Box 80-40 FE Vs. Experiment

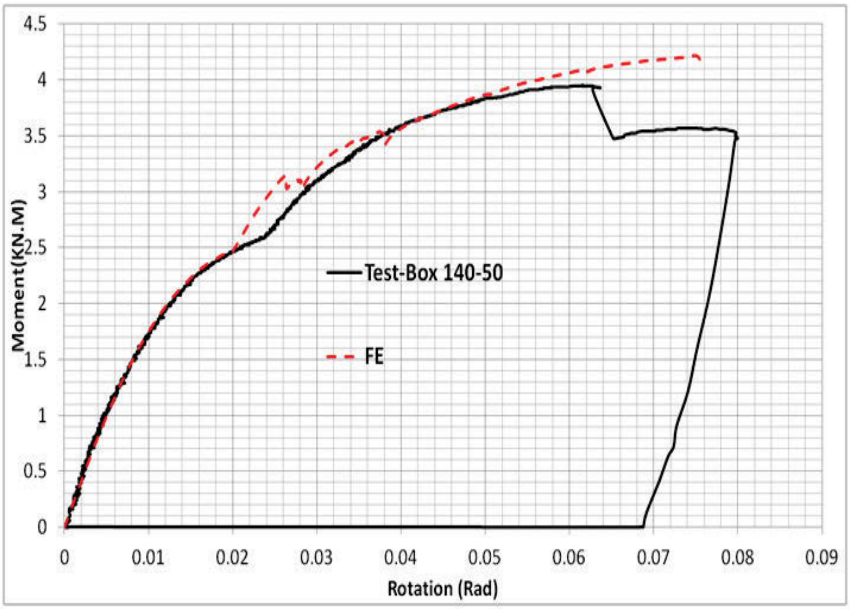

Figure 2.22: Box 140-50 FE Vs. Experiment

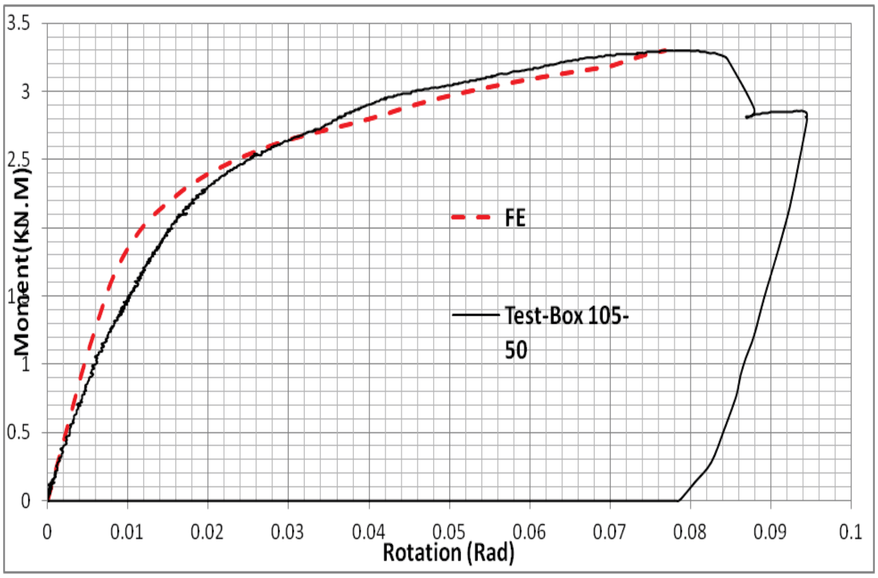

Figure 2.23: Box 105-50 FE Vs. Experiment

2.2.3 Analytical model

One of failure modes observed in the experimental tests as shown in Figure 2.24 is the tearing of the connector plate close to the upper hook. A bi-linear model was developed in order to approximate the moment rotation behaviour of the connections. The following assumptions are made:

1. The deformation of beam and upright are assumed to be negligibly small compared with the deformation caused by connector plate and hooks.

2. The effect of weld dimensions and strength is ignored (i.e. it is assumed that weld failure will not occur).

3. The behaviour of the beam, upright and connector is considered as Bi-Linear perfectly elastoplastic.

4. Yielding only takes place at the connector plate which is parallel to the upright web and hooks

To determine the ultimate moment of the connection for the above failure mode, the following assumptions were made[4]:

- The connector metal yields at line (A) and (B) in Figure 2.25. The concentrated force ‘F’ is used to model the upright – hook interaction. The maximum value of ‘F’ can be determined by calculating the combined shear and normal stresses at lines (A) and (B) (See Figure 2.25).
- The amount of stress values at lines (A) and (B) are assumed to be approximately the same.
- The values of stresses other than normal and shear stress in the direction of force ‘F’ are negligible at lines (A) and (B).

[4] These assumptions were made based on FE analysis results

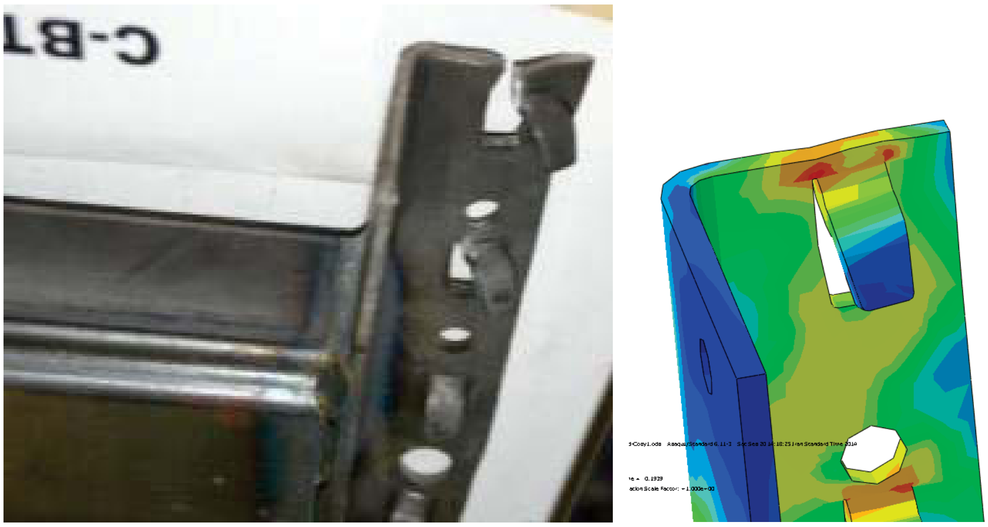

Figure 2.24: Hook failure; Test observation and FE Von-Mises stress contour

Using the above assumptions ‘Fult’ can be obtained from equation 2-3: (See Figure 2.25)

$$F_{ult} = F_{ult_A} + F_{ult_B} \cong 2F_{ult_A} = 2\sigma_{ult}\, t_c\, l \qquad (2\text{-}3)$$

When ‘t_c’ is the connector’s thickness and ‘l’ is the vertical distance from the load point to the connector’s free edge.

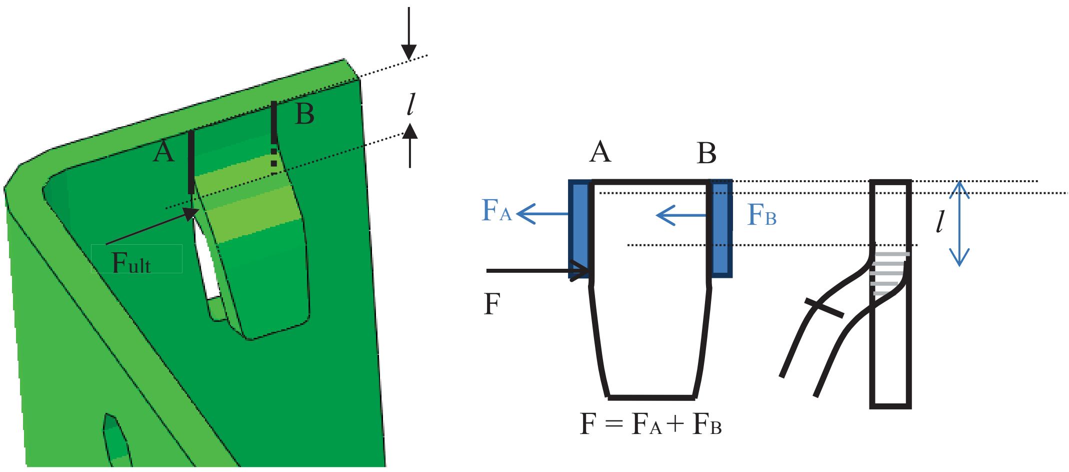

Figure 2.25: Geometrical dimensions

The contact force between hook and upright slot is represented by the concentrated force ‘F’ shown in Figure 2.25. Force ‘F’ is assumed to cause a state of plane stress in the connector section through lines ‘A’ and ‘B’ whereby the maximum value of ‘F’ is reached when the combined shear stress ‘τ’ and normal stress ‘σ’ cause full plastification at sections 'A' and 'B'.

For the given ratio, $\alpha = \frac{\tau}{\sigma}$, the Von Mises yield criterion may be expressed as:

$$\sigma_y = \sqrt{\sigma^2 + 3\tau^2} = \sigma\sqrt{1 + 3\alpha^2} \qquad (2\text{-}4)$$

FE analysis of the connector showed that only a relatively small variation in the value of 'α' takes place when the connector load is increased up to the ultimate load, whereby 'α' was in the range of 0.3 to 0.4. At the ultimate load, the normal stress acting on the connector section at 'A' and 'B' can be approximately equal to $\sigma\sqrt{1 + 3(0.3)^2} \leq \sigma_u \leq \sigma\sqrt{1 + 3(0.4)^2}$. The average value of equation (2-5) can be considered as a reasonable estimate of normal (and shear) stress:

$$\sigma_u = \sigma\sqrt{1 + 3(0.35)^2} = 1.169\,\sigma \;\; (or;\ \sigma = \frac{\sigma_u}{1.169}) \qquad (2\text{-}5)$$

By substituting equation (2-5) into equation (2-3), F_{ult} can be calculated:

$$F_{ult} = \left(2\left(\frac{\sigma_u}{1.169}\right) t_c\, l\right) = \left(\frac{2}{1.169}\right) \sigma_u\, t_c\, l_1 \qquad (2\text{-}6)$$

To calculate the moment capacity of the beam end connector the model presented below was used to approximately consider the effect of the number of hooks and their position in the connector angle (See Figure 2.26).

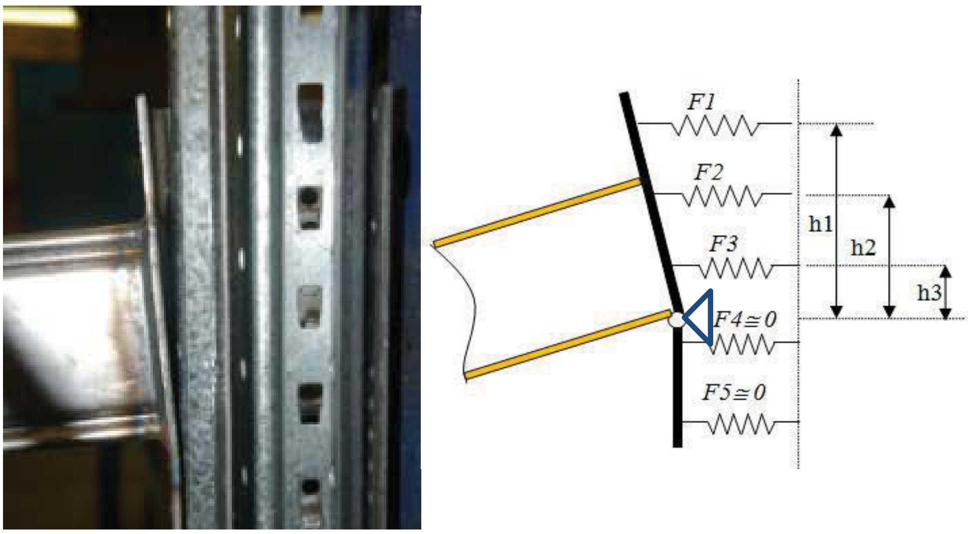

Figure 2.26: Analytical model of the connection using Component Method

In the above model the hooks are represented by translational springs and the centre of rotation of the beam was assumed to be close to the lower beam flange. The lower hooks are almost ineffective. This assumption was supported by test observations as shown in Figure 2.26.

The position of the beam relative to the hooks in the connector angle and the formation of a plastic hinge as shown by the circle in Figure 2.26 are important in calculating the moment capacity of the connection. The circular perforation in the connector at the location indicated in Figure 2.27 weakens the connector and attracts the plastic hinge to form near the bottom flange of the beam. Figure 2.26 shows the bending associated with this failure mechanism.

The ultimate moment (M) corresponding to this failure mode can be then calculated using the following analytical model:

$$M = F_1 h_1 + F_2 h_2 + F_3 h_3 + \left(\sigma_u\, t_c\, c_1 \left(w - \frac{c_1}{2}\right) - \sigma_u\, t_c \frac{c_2^2}{2}\right) \qquad (2\text{-}7)$$

where F_i values are the forces at the hooks located above the centre of rotation and h_i values are the vertical distances of the hooks to the centre of rotation (See Figure 2.26). 'σ_u' is the ultimate stress of the connector material and t_c is its thickness. Parameters 'c1', 'c2' and 'w' are illustrated in Figure 2.28.

Circular hole weakens the connector and leads to localization of the plastic hinge in this region.

Figure 2.27: Yielding of the metal near the hole leads to this failure mode

F_1 in equations 2-8 and 2-9 can be obtained using equation 2-6, and F_2 and F_3 can be calculated by a linear interpolation[5]:

$$F_2 = \frac{h_2}{h_1} F_1 \tag{2-8}$$

$$F_3 = \frac{h_3}{h_1} F_1 \tag{2-9}$$

Therefore;

$$M = F_1 \left(h_1 + \frac{h_2^2}{h_1} + \frac{h_3^2}{h_1}\right) + (\sigma_u\, t_c\, c_1 \left(w - \frac{c_1}{2}\right) - \sigma_u\, t_c \frac{c_2^2}{2})$$

$$= (\frac{2}{1.169}) \sigma_u\, t_c\, l_1 \left(h_1 + \frac{h_2^2}{h_1} + \frac{h_3^2}{h_1}\right) + (\sigma_u\, t_c\, c_1 \left(w - \frac{c_1}{2}\right) - \sigma_u\, t_c \frac{c_2^2}{2}) \tag{2-10}$$

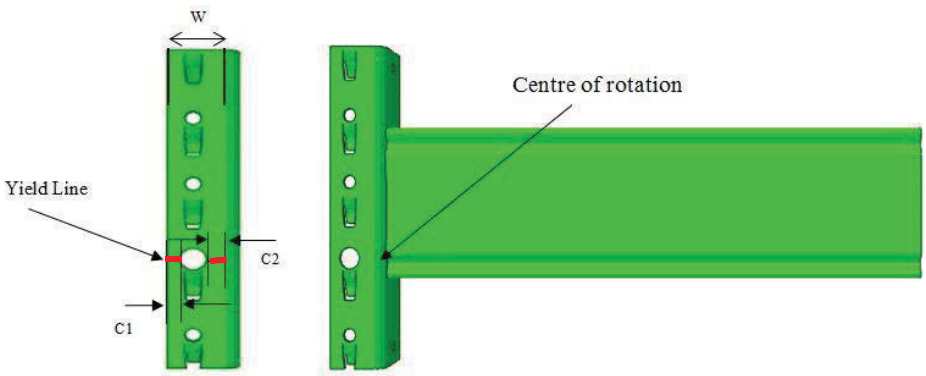

Figure 2.28: Geometric dimensions

2.2.3.1 Bi-Linear Moment Rotation curves

A theoretical bi-linear moment rotation curve can be established from the yield and ultimate moments derived earlier. Only two points on the curve are required; at yield (θ_y, M_y) and at ultimate (θ_u, M_u) (See Figure 2.29).

[5] The simplifying assumption of linear interpolation is conservative as it leads to a lower failure moment of the connections

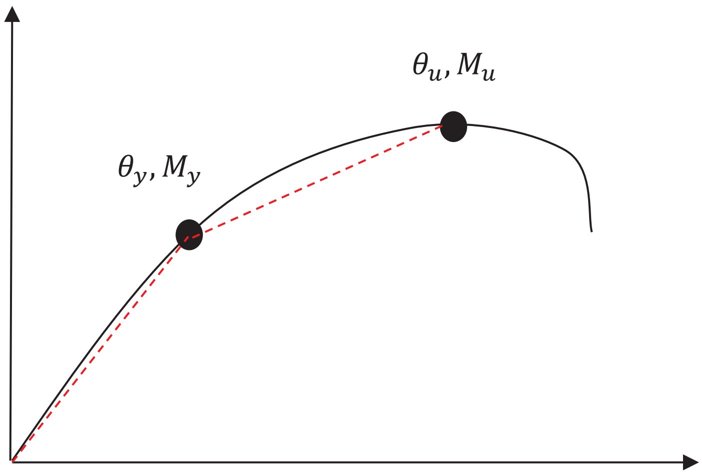

Figure 2.29: Simplified Bi-Linear Moment Rotation curve

Parameters θ_y, θ_u and M_u can be estimated according to section 2.2.1.3.3 and section 2.2.3 of this chapter. Mofid et al. (2005) proved that for the end plate structural steel connections with perfectly elasto-plastic material, the yielding moment of the connection , M_y, can be roughly evaluated from the ultimate moment:

$$M_y = 0.7\, M_u \tag{2-11}$$

By applying the same assumption of having perfectly elasto-plastic material for the beam end connector and upright, 'M_y' can be approximately calculated for the racking connections.

Examples of simplified moment-rotation curves are presented in Appendix B for 3 different connection types.

2.3 Behaviour of beam to upright connections under cyclic loads

Cyclic behaviour of beam to upright connections is very important in overall behaviour of the system under seismic actions. To the author's knowledge, there are no comprehensive seismic design rules available for rack structures, except FEM 10.2.08 (2011) and RMI (2012). AS 4084 (2012) and EN 15512 (2009) do not propose any cyclic test set up to evaluate the hysteresis moment rotation curve of the beam end connectors as they are only for static design.

This is because of very limited studies on the behaviour of racking components such as beam to upright connections. Therefore, all standards for pallet rack design still require experimental tests to assess the key structural components of racking systems such as beam to upright connections. The storage rack shall be designed for the total minimum lateral forces which are related to seismic performance, behaviour factor and fundamental period of rack structure. Alternatively, the seismic design may be performed using performance based method described in FEMA 460 (2005). However, FEMA 460 (2005) does not consider those high rise racks under severe seismic loads which require vertical and horizontal bracing to support down aisle frames.

American specifications developed by Rack Manufacturing Institute, RMI (2012) recommends response modification factors (i.e. seismic force reduction factor) of 6 and 4 for down aisle direction and cross aisle direction, respectively[6] followed by a ductility check (i.e. rotational capacity check) based on the corresponding reduction factor. This is regardless of the type and geometry of structural components like beam end connectors, uprights and base plates, and frame bracing patterns.

European design provisions in earthquake resisting design of structure, EN 1998-1-8 (2004) do not specifically apply to rack structures but they categorize structures into two structural ductility classes of low dissipative structural behaviour and dissipative structural behaviour. In dissipative structural behaviour the capability of parts of the structure (dissipative zones) to resist earthquake actions through inelastic behaviour is taken into account. When adopting the concept of dissipative structural behaviour, sufficient requirements may be fulfilled such as satisfactory rotation capacity that should be ensured under cyclic loading without significant degradation of strength and stiffness. Recommendations for the design of steel pallet racks under seismic conditions developed by "Federation Europeenne de la Manutention" FEM 10.2.08 (2010), also refers to European standard Euro Code 8 to define dissipative zones and the reduction factors (q-factors). Also a reduction factor related to pallet sliding friction is defined in FEM 10.2.08 (2010) while a less accurate estimate of sliding

[6] According to FEMA 460, selection of those values of R, are based on building structural systems and may not be appropriate for rack structural systems and connections

effect is proposed in RMI[7]. The proposed behaviour factors in FEM 10.2.08 (2010) are more accurate compared to RMI (2012). Referring to Euro Code 8, FEM 10.2.08 (2010) proposes behaviour factors "q factors" based on structural regularity criteria and energy dissipation capabilities which cannot be greater than 4.

Australian standard for steel storage racking design (AS 4084, 2012) refers to Australian standard for earthquake actions (AS 1170.4, 2007) which proposes a seismic force reduction factor of 3 for both directions ($\frac{\mu}{S_p} = 3$).

Due to the limited full frame pushover tests data reported in the literature, it has been generally observed that instability and plasticity of connections (beam end connectors and base plate) lead to total failure and collapse (See Figure 2.30). In some cases plastic hinges occurred in the uprights rather than in the beam end connectors. Therefore, it seems connections cannot be considered as dissipative zones where the energy associated with earthquakes cannot be dissipated by the connections properly (Castiglioni, Carydis, Negro, Calado, Degée, & Rosin, 2009). This statement is not in agreement with recommendations of building seismic safety council for the Federal Emergency Management Agency FEMA 460 (2005). Therefore, a special focus on the typical beam end connectors is needed to better understand the behaviour of the connections in seismic conditions.

As was stated earlier, it is believed that the performance and energy dissipation capability of the rack structures depend on the hysteresis behaviour of beam to upright connections. Hence, FEMA 460 (2005) recommends that the design curve of connection moment versus connection rotation shall be developed based on cyclic tests rather than monotonic tests to better consider the seismic behaviour of the connections. In particular, in rack structures, frame stability in down aisle direction is highly dependent on the hysteresis behaviour of beam to upright connections under cyclic loads. Therefore, for the frames to remain stable, the allowable gravity load on every pallet is required to be a function of hysteresis behaviour of connections and to consider the progressive deterioration of beam end connectors.

[7] A constant factor of 0.67 is defined in RMI 2011 to reduce the seismic mass and seismic weight when a linear relation is proposed in FEM 2011 which is a function of materials in contact and environment. The design spectrum modification factor due to sliding effect (ED1) should not be less than 0.4 or greater than 1.0

Figure 2.30. Plastic hinge in the Upright

2.3.1 Experimental investigations

A total of seven tests were carried out on beam end connectors comprising two different beam / upright configurations. In each configuration the left hand connectors were each subjected to four and three tests.

Based on the cantilever test set-up specified in AS 4084 (2012) (part 7.5.1.2), the test rig depicted in Figure 2.31 was used. During the test the jack load was controlled according to the pre-programmed displacement-time history of Figure 2.32. The displacement was applied slowly at a rate of 1 mm/s whereby the connection was cycled through increasing levels of displacement, three cycles to each increment, until failure occurred. The displacement amplitudes were applied in constant increments of 3 mm with very small initial amplitude of 3 mm. Hence, the sequence used in the test was 3 mm, 6 mm, 9 mm, 12 mm, up to failure.

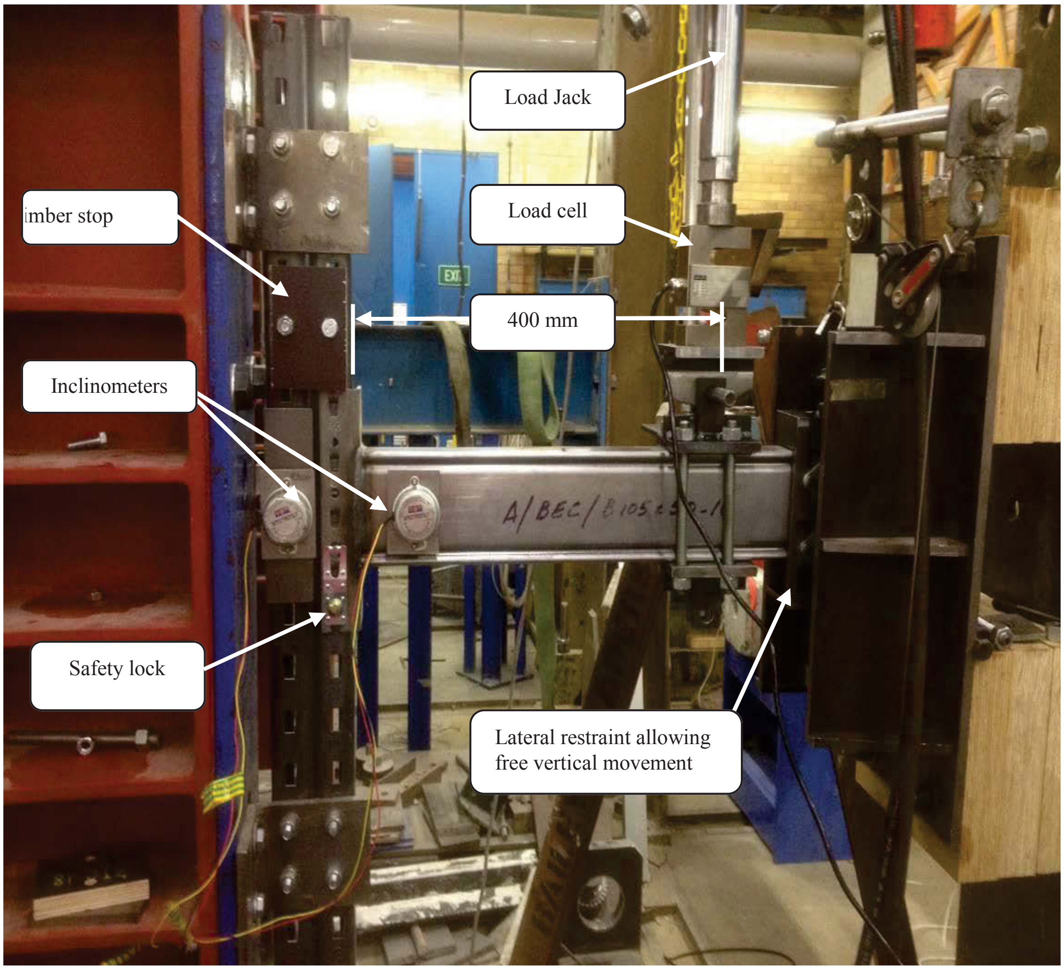

Figure 2.31. Test rig of beam end connector cyclic bending test with a specimen

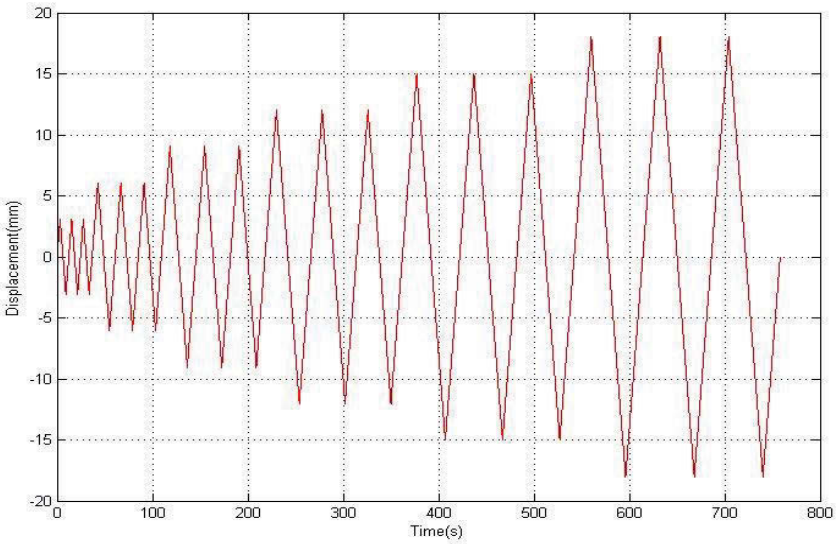

Figure 2.32. Displacement time history at load point of cyclic cantilever

2.3.1.1 Presentation of test data

For each test, the cantilever moment at the face of the upright was computed and the corresponding moment versus rotation curve was plotted. In all plots the relative rotation between beam and upright was used. Such a diagram is required to evaluate the stiffness, ductility, energy dissipation and stiffness degradation of beam end connectors. The closed curve of Figure 2.33 shows a moment-rotation curve of a single cycle and the area enclosed by the curve represents the inelastic energy absorption capability of the connection during that cycle. The curve in Figure 2.34 presents a summary of moment-rotation curves by taking the mean of the curve peaks in the 3rd cycles that are obtained in both positive and negative directions and consolidating them into one curve. This leads to the average curve presented in Figure 2.34, from which the equivalent connection stiffness can be established as the ratio of maximum moment and corresponding rotation.

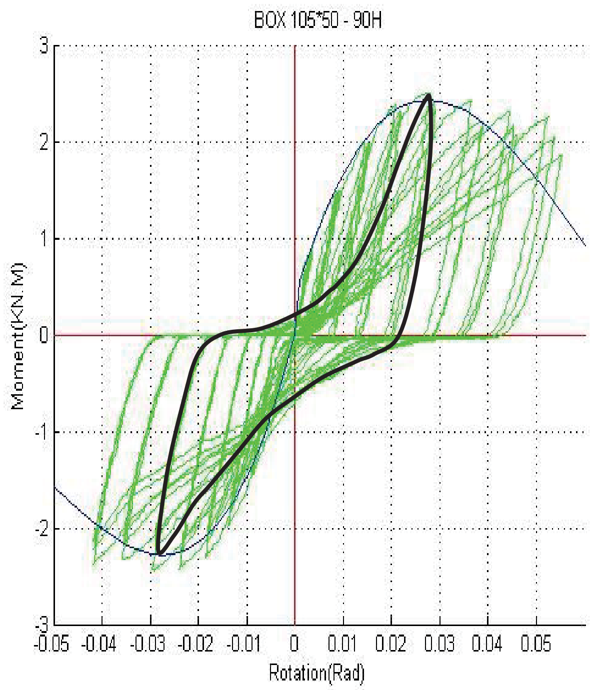

Figure 2.33. Hysteresis curve

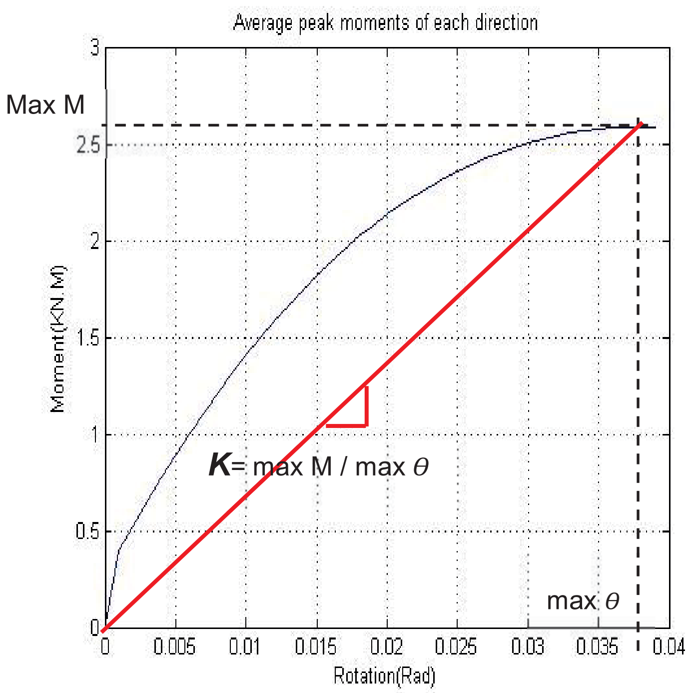

Figure 2.34. Typical Moment-Rotation curve of mean of the 3rd cycle peaks obtained in both directions

2.3.1.2 Test observations

Typical failure modes of the connections, as shown in Figure 2.35 and Figure 2.36, were primarily by tearing of the upright metal due to hook/upright interaction and deformation of the hooks for thinner and thicker upright, respectively. In some specimens the connector plates were found to tear off close to the hooks at the end of the connector. In tests where a thicker upright was used, the upright was generally not visibly damaged by bending or denting. However, local damage was usually observed in the form of small indentation at the perforations of the uprights typically coinciding with the location of the top and bottom hooks. In the second series of tests (thinner upright) damage to column slot by the connector hooks was visible. Therefore, the test was continued until complete failure of connection zone. (See Figure 2.35). The Moment-Rotation curves for the two tested specimens can be found in Figure 2.37 and Figure 2.38, while Table 2-3 provides a summary of the maximum moments and corresponding stiffness values of these connections. A moment rotation loop of a single cycle is shown for both connections in Figure 2.37 and Figure 2.38 enabling computation of the energy absorption capability of the two different connections to be carried out. Close inspection of the curves indicated a degradation of the connection behaviour after a few cycles in form of slippage (looseness) during load reversal of the order of ±0.03 rad. Such slippage, which was virtually not present in static looseness tests of similar connections (Saleh, 2012), can be detrimental in the case of seismic actions. It is noted that in the static looseness tests conducted in accordance with the Australian standard, the moment values were only 10% of the ultimate moment capacity of the connection.

The above observations are consistent with observations of other researchers. According to the available literature, an experimental analysis was carried out by Aguirre (2005) in which the cyclic behaviour of commercial beam end connectors were evaluated. A slippage of around 0.02 rad was observed after several cycles and energy absorption in the second cycle was dramatically lower than the first cycle and also a high stiffness degradation of the connection could be seen. Bernuzzi, Chesi and Parisi (2004) presented a paper in which the capability of energy dissipation and stiffness degradation of two different types of beam end connector under cyclic and monotonic loads with constant amplitude was described. Although the performance and ductility of beam end connectors under monotonic loads were satisfactory, a large slippage of around 0.04 rad was observed in the hysteresis moment rotation curves of connections.

Figure 2.35. Typical failure mode in the connections with thinner material which causes slippage and rigid motion in the connection

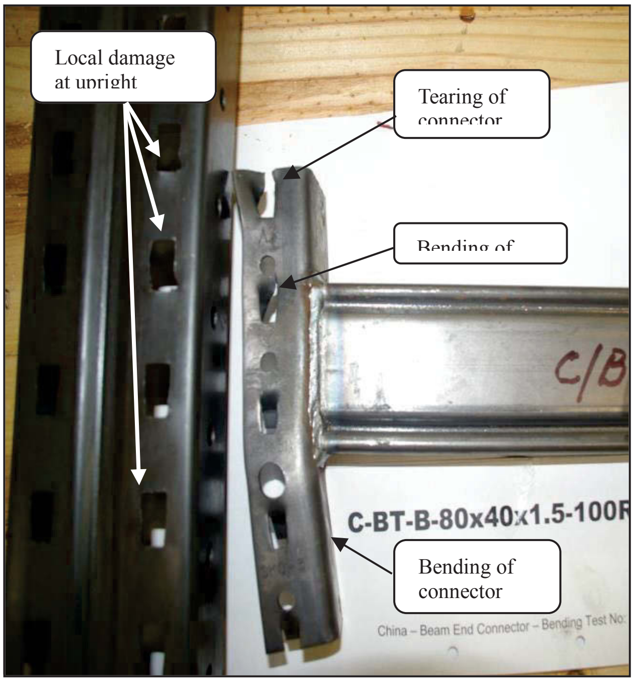

Figure 2.36. Typical failure mode in the connections with thicker material

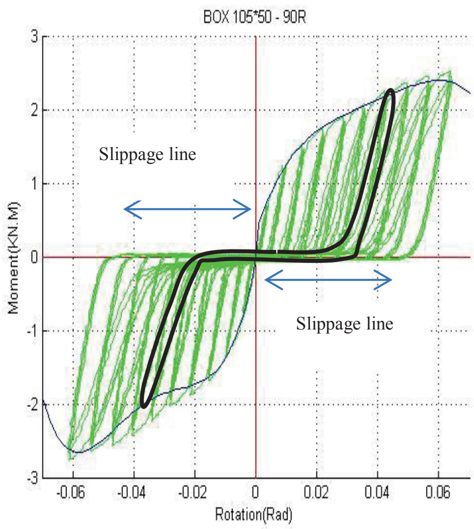

Figure 2.37. Hysteresis curve for thinner upright (1.6 mm)

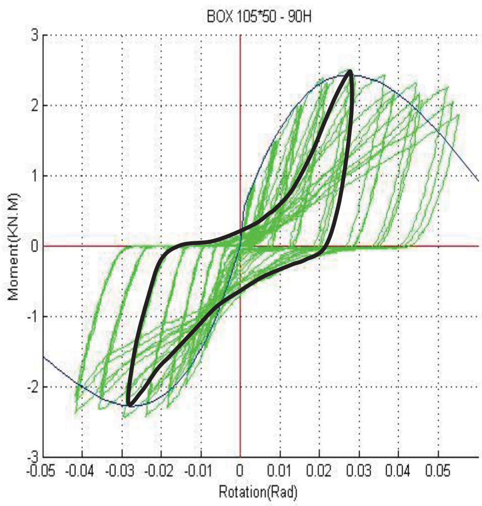

Figure 2.38. Hysteresis curve for thicker upright (2.5 mm)

2.3.2 Finite Element Analyses

To the best knowledge of the author there are no FE models reported in the literature to accurately simulate the entire cyclic response of beam to upright connections including post-yield (inelastic) range. Existing models could only predict one part of the non-linear moment rotation curve but not the entire curve.

For this reason and to be able to better understand the effect of different components and parameters that were the subject of investigation in section 2.2, under cyclic loads, a finite element model has been developed to predict the cyclic response of beam end connectors and the results were verified against cyclic test results as shown in Figure 2.39. Solid curves are the outputs of FE models while the dotted curves represent test results. The FE model used was the same as the model used to model the monotonic moment-rotation behaviour of the connection, except the load which was applied as a prescribed displacement at the tip of the beam with the same cyclic pattern used in the experiments.

A theoretical model was then developed, to be able to represent the cyclic behaviour of beam to upright connections without the need for a detailed FE model.

Table 2-3. Beam End Connector Cyclic Bending Test

Specimen Label	Maximum Moment [8][kNm]	Maximum Rotation [Rad]	Stiffness kc [kNm/rad]
Test 1. Thicker Upright	2.4	0.028	85.7
Test 2. Thinner Upright	2.5	0.06	41.6

[8] Maximum moment at the face of the upright obtained from the mean of curves of the 3rd cycle peaks in both (positive and negative). The moments were computed from the jack load F and the 0.4 m load point distance (M = 0.4F).

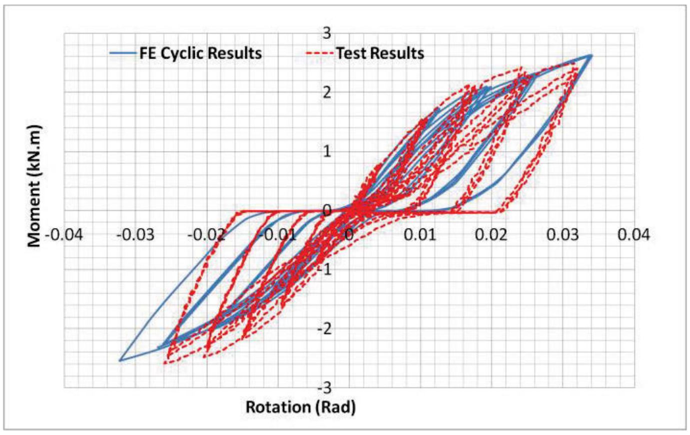

Figure 2.39.Hysteresis curve for ticker upright (2.5 mm) (Experimental results vs. FE result)

2.3.3 Simplified Hysteresis models

Although the finite element results of Figure 2.39 show acceptable agreement with the experimental test results, a more efficient method was developed in order to give a much faster and simpler model using one non-linear beam (link) element. For this reason different cyclic methods that are available in the literature were examined and the best and most reliable algorithm was used to model the hysteresis curves of the boltless beam to upright connections of rack structures[9]. Details of the investigations are presented in the following.

2.3.3.1 Overview of different Hysteresis Models

Hysteresis behaviour, in general, is specified by cycles of force-deformation (or moment-rotation) structural response under imposed cyclic actions. Hysteresis behaviours are usually presented in different levels such as for local components (Connections) and also for overall response of structures (Cyclic push over) (Taucer, Spacone, & Filippou, 1991).

To develop a non-linear hysteresis model, the most important and influential parameter is a ‘cyclic back bone’ that defines the boundaries in which the force – deformation (or moment - rotation) loops will excurse. Figure 2.40 shows a force – deformation back bone curve in both directions of negative and positive loading.

[9] A capstone research project was defined and supervised to cooperate with the author in this regard to come up with an appropriate cyclic model [2.28]

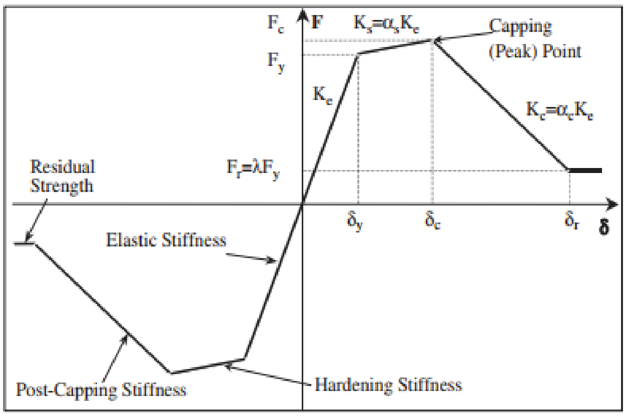

Figure 2.40: Backbone curve (Ibarra, Medina & Krawinkler, 2005, p. 1492)

Hysteresis models can also be capable of modelling the strength and stiffness deterioration if needed. Strength deteriorations can be directly derived from the back bone boundaries, however, the stiffness deterioration is dependent on the algorithm which is used to create the hysteresis curves. Takeda, Sozen and Nielsen (1970), Dowell, Seible and Wilson (1998) and most recently Ibarra, Medina and Krawinkler (2005) and Medina and Krawinkler (2004) proposed cyclic models that account for both strength and strength deterioration of the structural components under cyclic reversal loads.

Three cyclic models have been studied in this project and their results were matched with the experimental cyclic test results.

2.3.3.1.1 Cyclic Kinematic Model

The Kinematic model is the simplest hysteresis model available in most finite element software packages.

“Under the rules of kinematic hardening, plastic deformation in one direction ‘pulls’ the curve for the other direction along with it.” (Computers and Structures Inc., 2009) (See Figure 2.41)

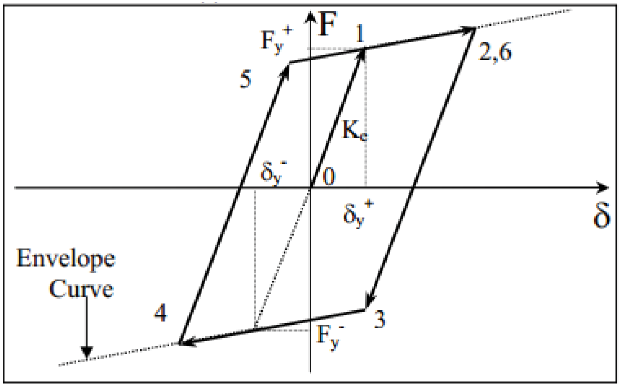

Figure 2.41. Kinematic Hysteretic Model (Medina & Krawinkler, 2003, p. 26)

2.3.3.1.2 Peak Oriented Model (Takeda Model)

"The peak-oriented model is characterized by reloading directed towards the previous maximum deformation reached; it is, therefore, able to model stiffness degradation." (Reyes, 2013, p. 50)

"When crossing the horizontal axis upon unloading, the curve follows a secant path to the backbone force deformation relationship for the opposite direction." (Computers and Structures Inc., 2009, p. 261) (See Figure 2.42 and Figure 2.43)

Peak – Oriented model is also known as Takeda model and like the Kinematic model is available in commercial software such as SAP 2000 software and does not require user interference to specify cyclic parameters.

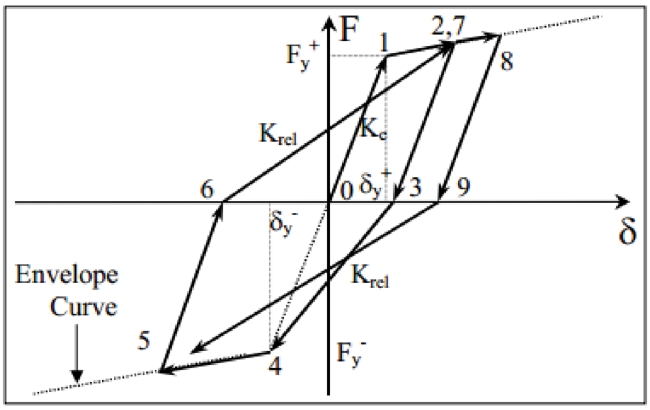

Figure 2.42: Takeda Hysteretic Model (Medina & Krawinkler 2003, p. 26)

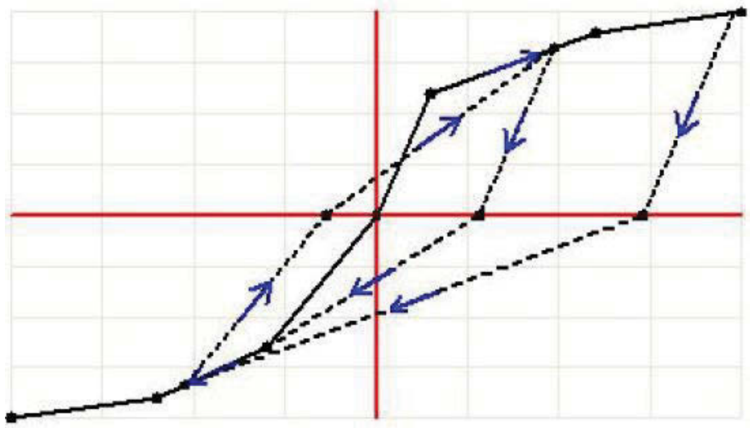

Figure 2.43: Takeda Model from SAP2000 User Manual(Computers and Structures Inc., 2009, p. 261)

2.3.3.1.3 Cyclic Pivot Model

The Pivot Hysteresis Model was first proposed by Dowel et al. (1998) to accurately model the non-linear hysteresis behaviour of reinforced concrete structures. The Pivot model is different with Takeda model only in generating the reloading path that is directed towards 'pivot points'.

"Unloading and reverse loading tend to be directed towards specific point, called pivot points." (Computers and Structures Inc., 2009, p. 261)

The Pivot hysteresis model is available in SAP 2000 software package and requires the input of different parameters of α, β and η to form the cyclic loops according to the algorithm explained by Dowel et al. (1998). Two α values form unloading path and two β values define the pivot points for reverse loading paths to be directed. Finally, η determines the amount of elastic slope degradation after plastic deformations. (Computers and Structures Inc., 2009)

Figure 2.44 schematically shows the algorithm of developing Pivot hysteresis model.

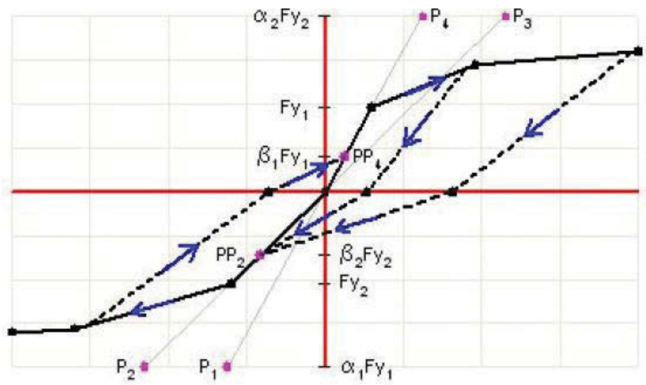

Figure 2.44: Pivot Model from SAP2000 User Manual. (Computers and Structures Inc., 2009, p. 262)

Parameters α, β and η are further explained and defined later in section 2.3.3.2.2. More details regarding the three parameters of α, β and η is well explained by Dowell et al. (1998).

2.3.3.2 Beam to upright boltless connection modelling

The hysteresis modelling of beam end connectors engaged to thicker uprights (2.5 mm) is presented in this part. Connections to thinner uprights (< 2mm), as was mentioned, do not show good performance under cyclic actions by demonstrating remarkable rigid movement (zero moment line) in the hysteresis loops which leads to accumulative drift of the overall frame after few consecutive load cycles[10]. As a recommendation, using thinner uprights for seismic applications is unsafe, even if strength wise they satisfy the provisions of Australian cold formed steel structural design standard (AS 4600, 2007). The reason for that is the *equivalent static method* is unable to consider the cyclic deterioration of the dissipative zones and consequently progressive drift of the system is overlooked since the structures are being designed based on their monotonic behaviour.

On the other hand, connectors engaged to thicker uprights (> 2mm) can be accurately modelled by the existing hysteresis models and in fact provide structures with good performance under seismic loads (See Chapters 5 and 6). Visual similarities of the hysteresis features of the presented beam to upright connection shown in Figure 2.45

[10] The reason is that the tearing length will be significantly long which cause a permanent damage to the system leading to sliding of the hooks within the tearing length. As a consequence a rigid motion will be observed as can be seen in Figure 2.37.

with the Pivot hysteresis model's algorithm, indicated that frame analysis software (such as SAP 2000), if they include the Pivot model algorithm, can analyze this connection to an acceptable level of confidence through a single beam element (link element).

To develop a hysteresis model, the first requirement is defining a boundary (or back bone) in which the force – deformation (moment - rotation) loops will circulate. By looking at the cyclic and monotonic response of the connection in a same system (Figure 2.45) one can clearly notice a reduction of the peak moment in the hysteresis curves in comparison with the monotonic curve. This phenomenon is called cyclic strength deterioration which indicates the difference between monotonic and cyclic back bone curves.

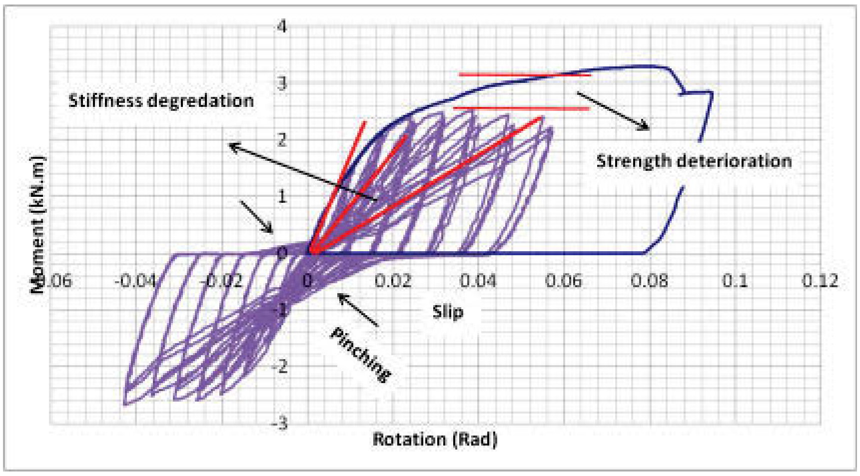

Figure 2.45: Beam-Upright Connection Hysteresis Feature

Both effects of strength deterioration and stiffness degradation in the moment – rotation hysteresis curves cannot be addressed by the monotonic curves. Therefore, the monotonic moment – rotation curves should not be used as a back bone in which the hysteresis loops are located. The best and most accurate method is to derive the back bone curve directly from the laboratory cyclic test results. However, this method needs cyclic testing in the lab which is very expensive and time consuming compared to the monotonic tests. Therefore, an equivalent method will be presented in this chapter to define a hysteresis back bone from monotonic moment – rotation curves which considers the strength deterioration. Proposed hysteresis backbone is used for both positive and negative moments as the cyclic test and FE results showed symmetry in positive and negative moments in the hysteresis curves. Similar observation was also shown by Aguirre (2005) and Rosin et al. (2009).

2.3.3.2.1 Proposed Method to Derive Equivalent Cyclic Backbone

The method is described in the following steps:

Step 1:

Find the point of effective first yield. This point is the interception between the line tangent to the monotonic moment – rotation curve at origin (zero moment) and a line representing the inelastic stiffness as shown in Figure 2.46.This point is called the "1^{st} yield point" corresponding to a rotation of D and a moment of M_{1Y}.

Step 2:

Let $k_{1YEqCyc} = 0.8 \times k_{1Y}$.

The *first point on the backbone* shall be defined by the moment M_{1Y} and the rotation "D_{EqCyc}" found by dividing M_{1Y} by $k_{1YEqCyc}$.

The factor of 0.8 is to convert the initial secant stiffness 'Ks' to the effective initial stiffness 'Ki'. Effective initial stiffness 'Ki' can also be calculated by taking a line which intersects the moment rotation curve and the yield moment line and divides them into two equal areas as shown in Figure 2.47.

However, according to AS 4084 (2012), the effective initial stiffness should not be greater than 0.88 times of the secant stiffness. By calculating the initial secant stiffness and effective initial stiffness of the connections from the experimental test results, a conversion factor of 0.75 to 0.85 was obtained. Therefore, the factor of 0.8 seems to be a reasonable value of obtaining the effective initial stiffness from the secant stiffness without calculating the equal areas enclosed by the moment rotation curve and the yield moment line.

Step 3:

Find the maximum allowable rotation 'δ_{ci}' corresponding to the connection's maximum design moment capacity 'M_c' as defined by AS 4084 (2012) Equation 7.2.2.1. The second point on the backbone shall be defined by the moment $M_{1Y}$and the rotation δ_{ci}.

<u>Step 4:</u>

The *third and final point on the backbone* is the failure point defined by zero moment and a rotation of "δ_{Fail}" = 1.1 x δ_{ci}.

Factor 1.1 is defined only to let the moment gradually drop from 'M_{1Y} 'to zero and hence not effect the hysteresis curve.

Note that this method defines the backbone to be rotationally symmetric about the origin for negative values; therefore, the negative arm of the backbone is found by simply taking negative values of the moments and rotations defined above.

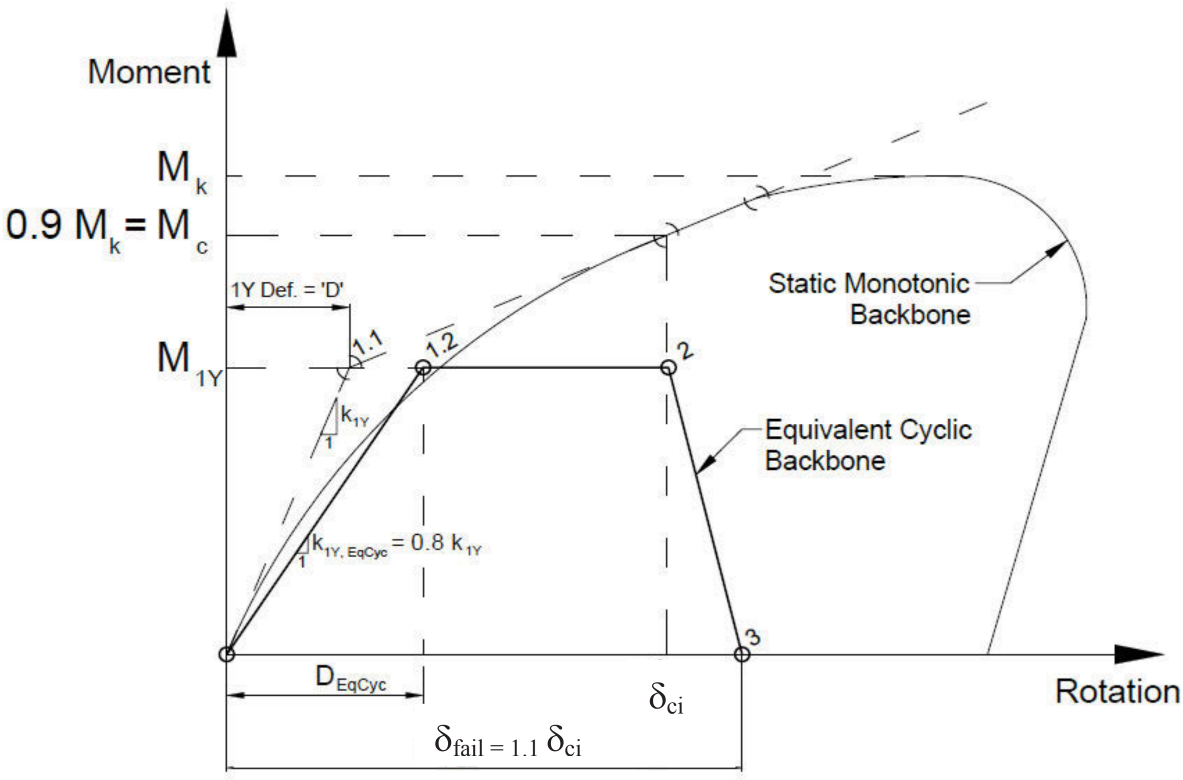

Figure 2.46: Proposed Equivalent Cyclic Backbone from Static Monotonic Test (Reyes, 2013, p. 59).

Figure 2.46 shows the difference between the monotonic moment – rotation curve and the proposed cyclic back bone and the reduction of the maximum moment due to cyclic strength deterioration.

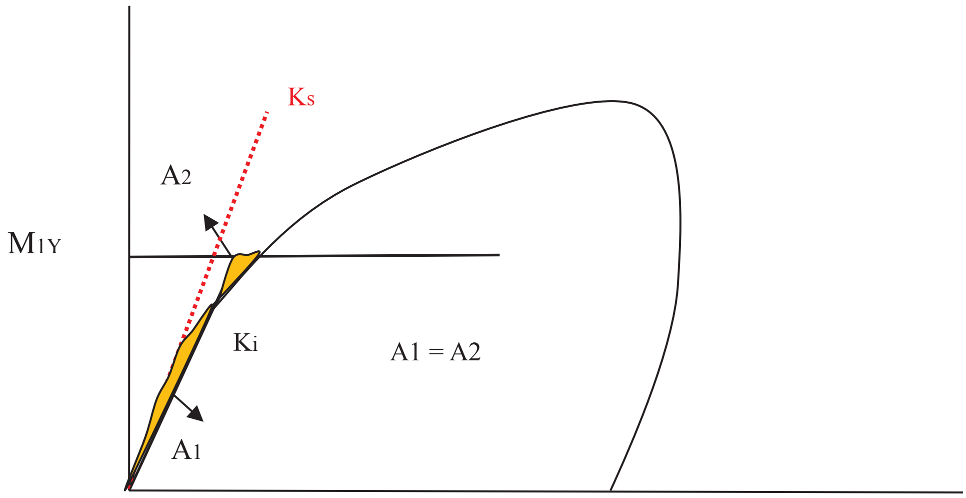

Figure 2.47: Initial and Secant stiffness

2.3.3.2.2 Connection cyclic test simulation

To assess the suitability and accuracy of the proposed cyclic back bone and also to develop an appropriate cyclic (hysteresis) model by a simple link element, different modelling options (algorithms) listed in Table 2-4 will be examined in this section. For this reason the beam upright connection test was simply modelled in SAP 2000 by only two elements of simulating beam and the connection link. (See Figure 2.48)

Figure 2.48: SAP2000 Beam-Upright Connection Cyclic Test Simulation (Reyes, 2013, p. 55)

The above model can be a much simpler and faster model in comparison to the FE model in ABAQUS and if an appropriate back bone curve is defined it can be used instead of running expensive experimental cyclic tests.

Table 2-4 Backbone-Hysteresis Models for Beam-Upright Connections.

Backbone	Hysteresis Model	Back bone Curve	Reference I.D.
Equivalent Cyclic	Kinematic	Equivalent Cyclic Back bone	EqCyc-KIN
Equivalent Cyclic	Takeda	Equivalent Cyclic Back bone	EqCyc-TAK
Equivalent Cyclic	Pivot	Equivalent Cyclic Back bone	EqCyc-PIV
Lab Cyclic	Pivot	Actual Cyclic Test Back bone	LabCyc-PIV

As discussed earlier in this chapter, unlike Kinematic and Takeda models, the pivot model needs user specification of hysteresis parameters as well as back bone envelop curve. To specify reliable values for the pivot model parameters a closer inspection of the hysteresis response of the connection is needed. Figure 2.45 shows that both pinching and slippage occur in the nonlinear hysteresis response of the connections. With reference to the Pivot model's algorithm, illustrated schematically in Figure 2.44 and reproduced in Figure 2.49, reloading part of the cyclic response is directed toward the 'pinching pivot point', which is set according to the β values.

Obviously '$\beta \neq 0$' models pinching and '$\beta = 0$' models slippage (See Figure 2.50). However, the pivot model is not capable to model both slippage and pinching in a particular case. The proposed model in this study considers 100% slippage by setting '$\beta_1 = \beta_2 = 0$' which is in fact more conservative than considering pinching in the hysteresis loops, since pinching leads to less area enclosed by the moment – rotation curves. The unloading path is also defined to return to zero moment line with a sharp slope (See Figure 2.51). Therefore, a reasonably large 'α' value is needed to be defined. Analysis results showed that '$\alpha_1 = \alpha_2 = 100$' satisfy this condition (See Figure 2.52 and Figure 2.53).

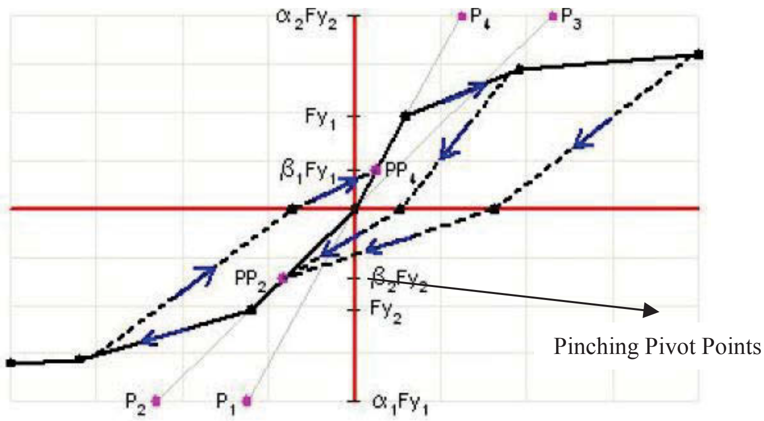

Figure 2.49: Pivot Model

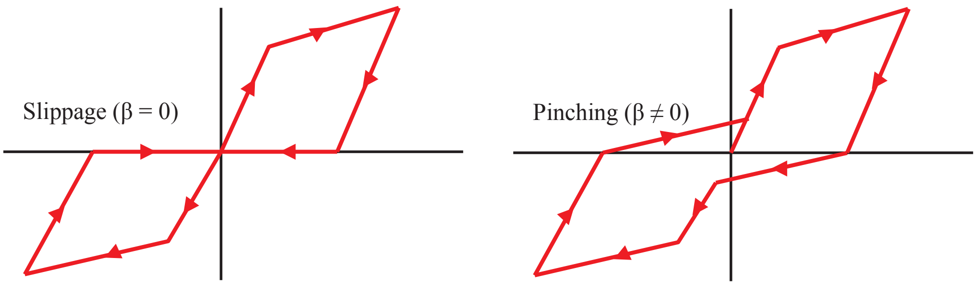

Figure 2.50: Slippage and Pinching effect can be modeled by defining appropriate 'β' value

The amount of degradation of elastic slopes after plastic deformation was also ignored (η = 0).

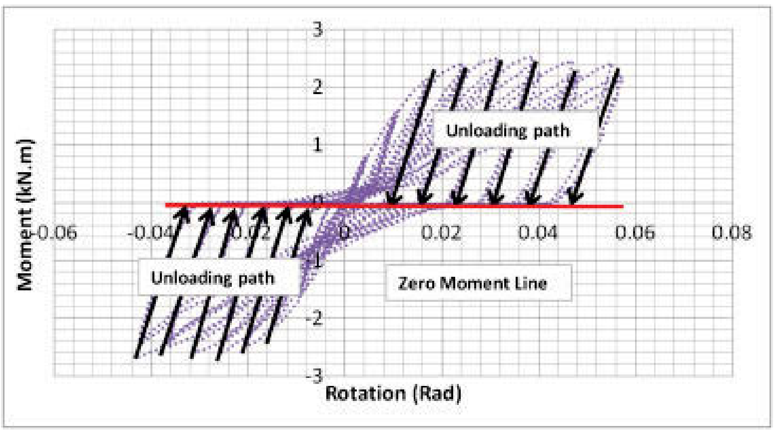

Figure 2.51: Hysteresis features of the beam – upright connection

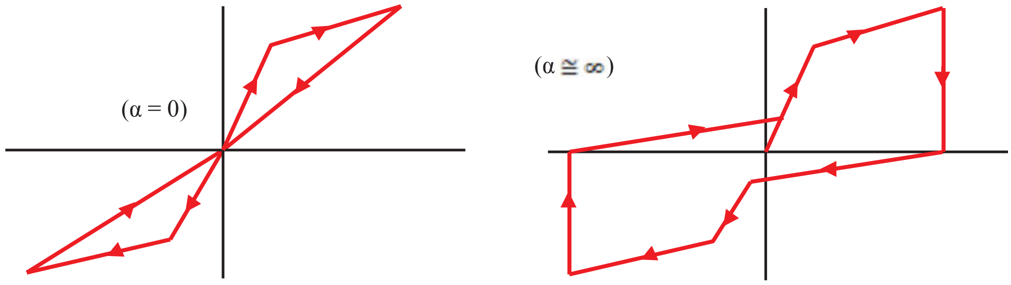

Figure 2.52: Two extreme cases of the unloading path for different values of (α)

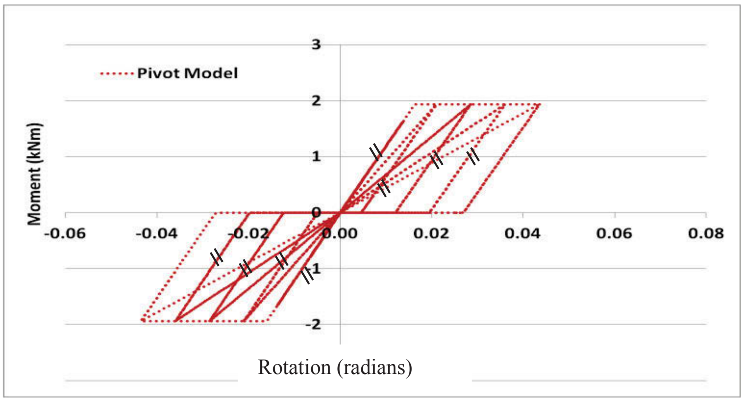

Figure 2.53: An example of Pivot Model (The parallel unloading paths is because the ‘η’ is assumed to be zero)

Therefore, Table 2-5 provides the suitable parameters for the proposed Pivot model.

Table 2-5. Calibrated Pivot Model Parameters for 'Type A' Beam-Upright Connections

Pivot Parameter	Adopted Value
α_1	100
α_2	100
β_1	0
β_2	0
η	0

As illustrated in Figure 2.54, two back bone curves and three different cyclic models are investigated in this study.

Figure 2.55 to Figure 2.58 show the experimental and numerical hysteresis curves of the connections using different cyclic back bones and different cyclic models.

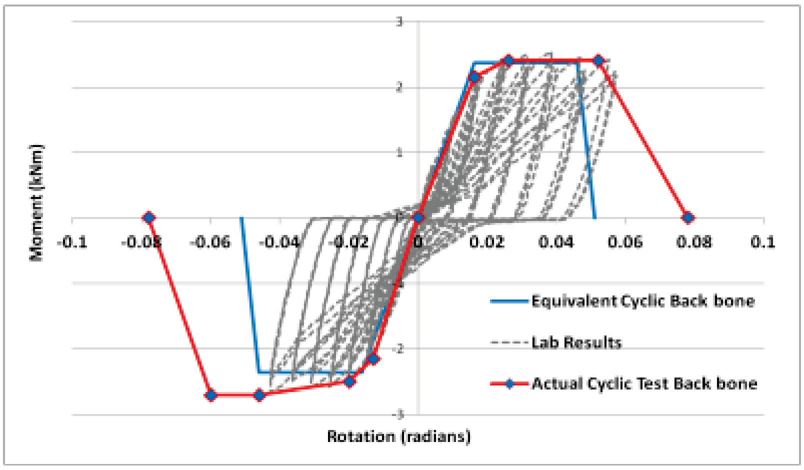

Figure 2.54. Beam – Upright connection back bones

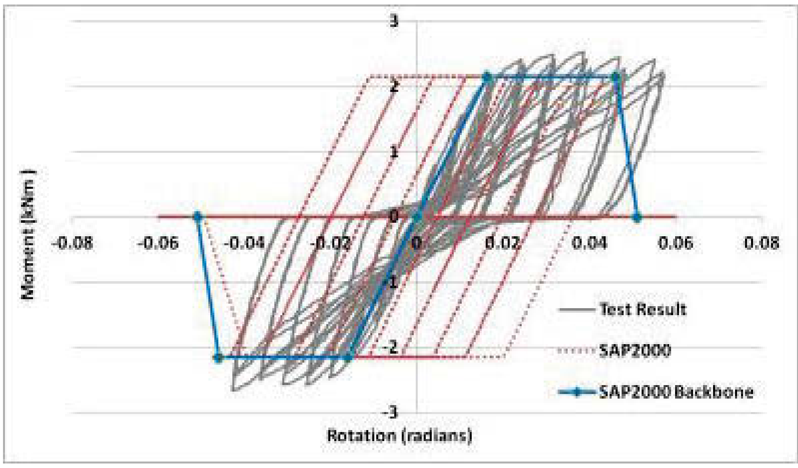

Figure 2.55 Experimental and Numerical Cyclic Test Comparison using EqCyc-KIN Link.

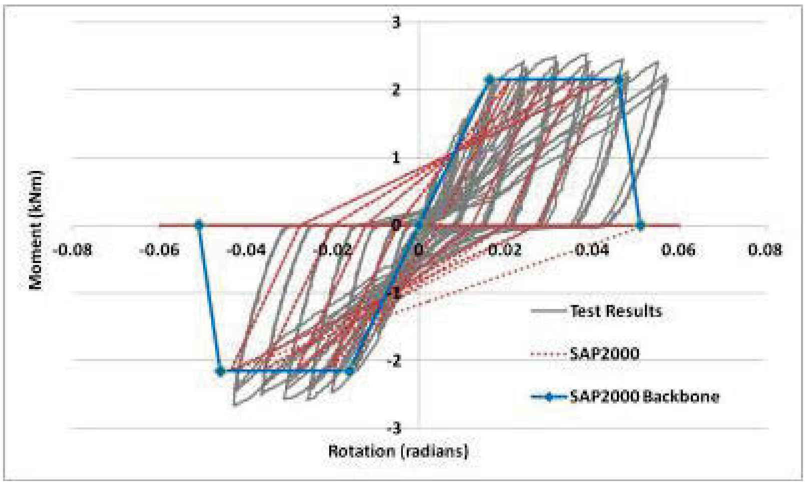

Figure 2.56. Experimental and Numerical Cyclic Test Comparison using EqCyc-TAK Link.

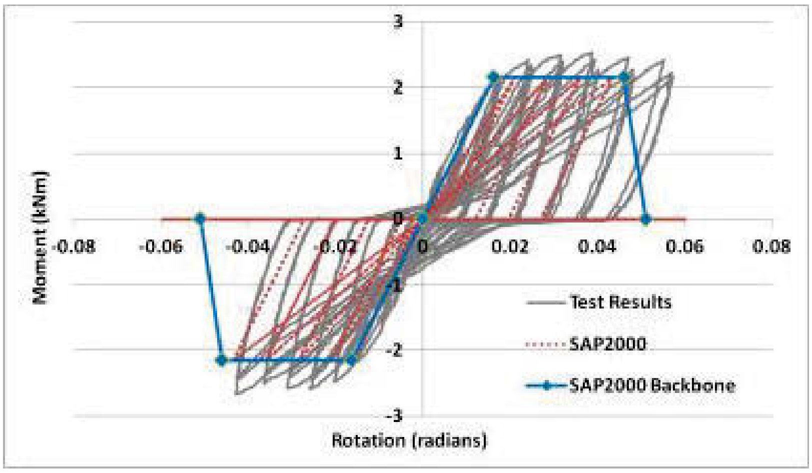

Figure 2.57. Experimental and Numerical Cyclic Test Comparison using EqCyc-PIV Link.

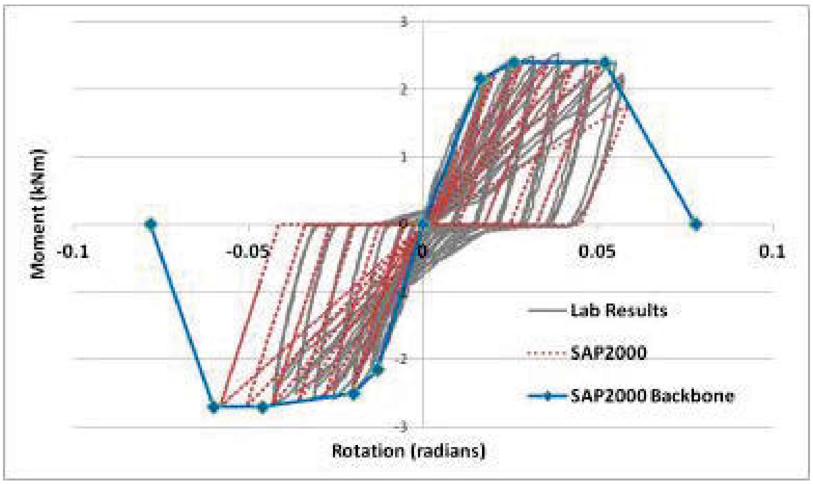

Figure 2.58. Experimental and Numerical Cyclic Test Comparison using LabCyc-PIV Link.

At first look at the above results, the Pivot hysteresis model presents the best cyclic model for the connection compared to the other cyclic models. However, cyclic response of the model using actual cyclic test back bone (LabCyc-PIV Link) provides better results compared to the model using the proposed Equivalent cyclic back bone (EqCyc-PIV Link). To have a more accurate comparison, energy dissipation curves were also drawn and shown in Figure 2.59. The energy dissipation curves were calculated via numerical integration of the moment – rotation response by calculating the area enclosed by the hysteresis curves[11].

[11] The energy dissipation calculation was done by Reyes (2013) through programming in Office Excel software package. As shown in the below Figures, the Energy absorption which can be calculated by measuring the area enclosed by the moment- rotation hysteresis curves via trapezoidal rule numerical integration. According to the below Figures, the Energy shows positive values (energy gain) until reaching a peak point on the moment-rotation curve and after that the amount of calculated energy shows a negative (energy loss) value which slightly reduces the amount of total energy. That's the reason that energy curves show a zigzag pattern.

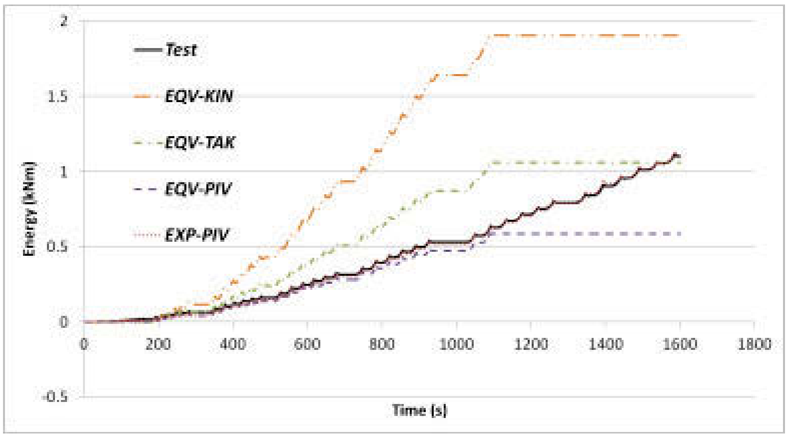

Figure 2.59. Connection Energy Dissipation Comparison.

According to Figure 2.59 the reasonable agreement between the numerical and experimental results for both (EQV-PIV) and (EXP-PIV) models proves the ability of the presented algorithm to perfectly model the hysteresis response of the connections.

It should be noted that the flat lines in the energy function of the (EQV-PIV) model represent the early failure[12] (moment drop) of the hysteresis loops. This is because the hysteresis loops are forced to circulate with a smaller back bone (e.g. boundary) compared to the actual cyclic test back bone with wider back bone. However, this drop occurred at such high rotations (> 0.03 Rad) where the entire frame may already have become globally unstable. Therefore, this method works well in a reasonable rotation range and can give accurate results close enough to the actual cyclic test results. The presented model needs to be also verified by more examples by modelling the experimental cyclic test. However, as experimental cyclic testing is time consuming and expensive, ABAQUS Finite Element software package was used

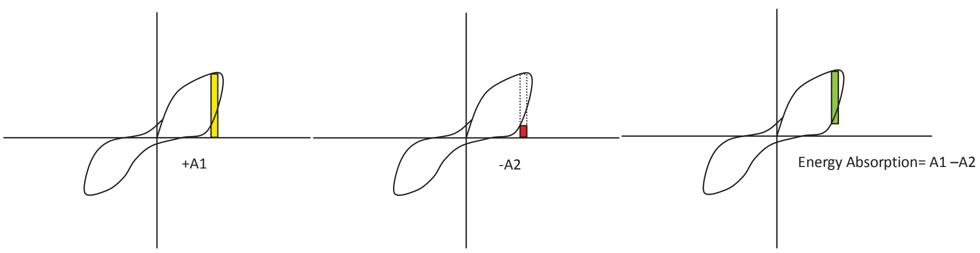

[12] It is considered as failure as the energy line is constant indicating that the connection can no longer absorb energy

to simulate cyclic tests. Finite element models were developed by making the same assumptions as explained earlier and the monotonic and cyclic curves of three extra beam to upright connections were derived. Following the proposed algorithm, the hysteresis curves were derived and are shown in Figure 2.60. The accuracy of the models were demonstrated by calculating the cumulative energy absorption function and measuring the area enclosed by hysteresis loops.

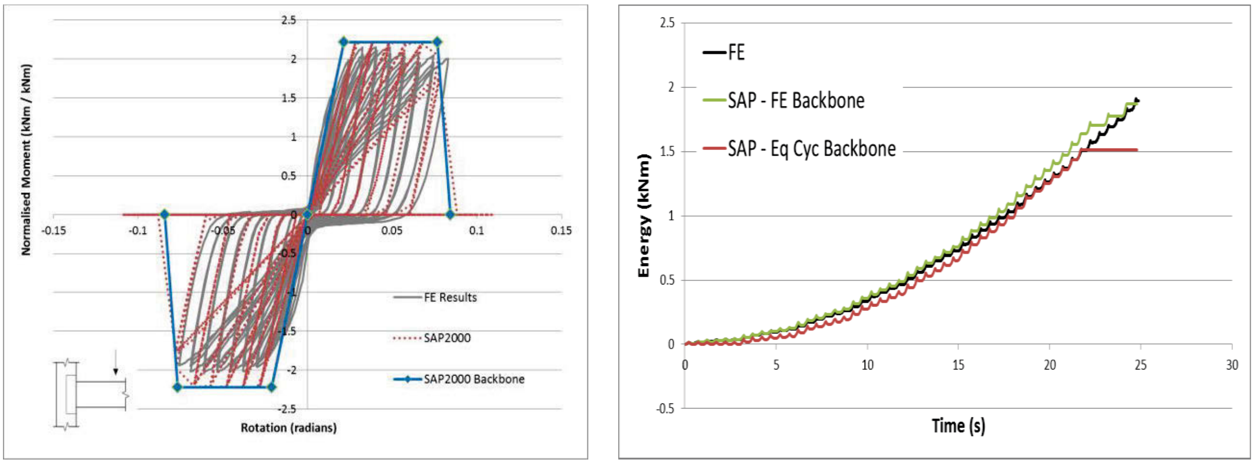

(a) (b)

Box 85-50, Upt 2.5 mm (a)FE Hysteresis loops vs. Pivot model hysteresis loops based on EQV.CYC back bone, (b) Energy dissipation comparison of FE results vs. EQV Pivot model

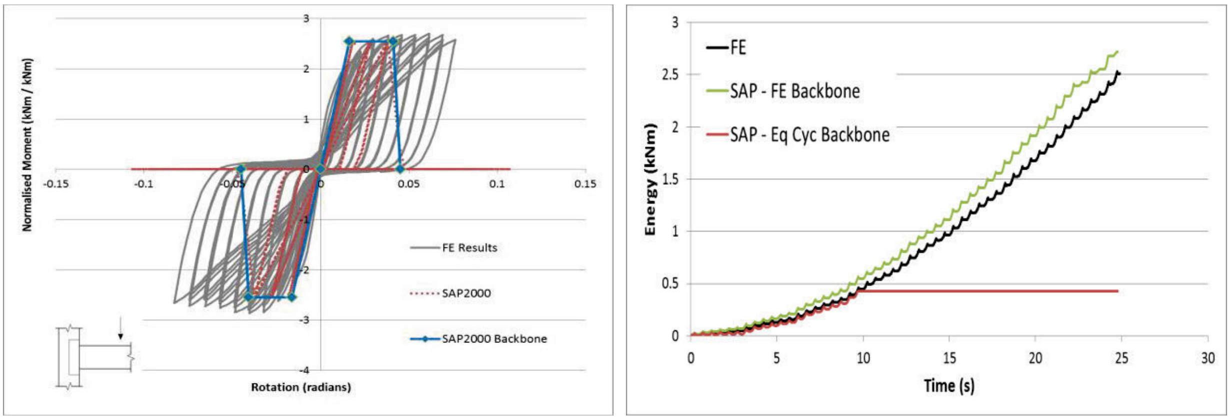

(a) (b)

Box 140-50, Upt 2.5 mm (a)FE Hysteresis loops vs. Pivot model hysteresis loops based on EQV.CYC back bone, (b) Energy dissipation comparison of FE results vs. EQV Pivot model

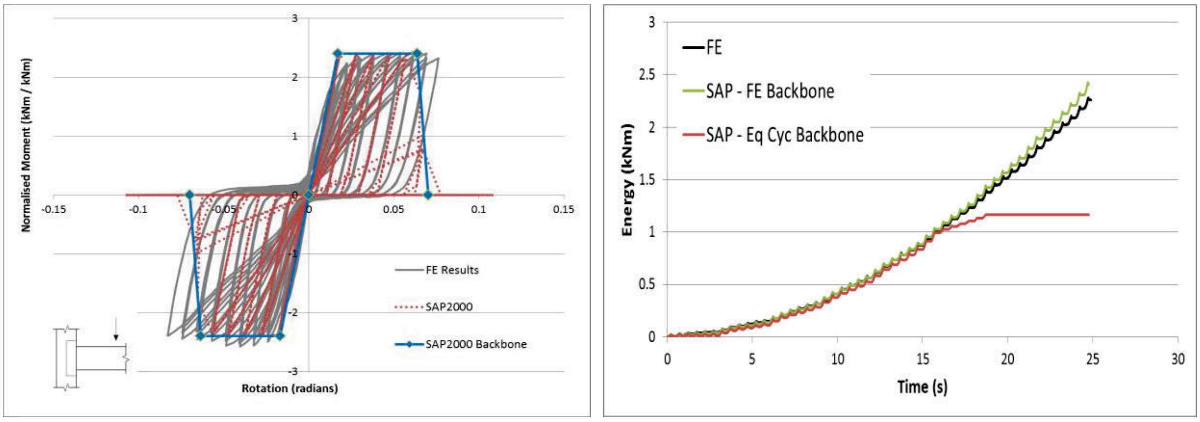

(a) (b)

Box 100-40, Upt 2.5 mm (a)FE Hysteresis loops vs. Pivot model hysteresis loops based on EQV.CYC back bone, (b) Energy dissipation comparison of FE results vs. EQV Pivot model

Figure 2.60: Comparison of hysteresis loops of different connections

2.4 Conclusions

This chapter presents the behaviour of typical boltless beam to upright connections used in rack industry. A large number of experimental tests were first conducted to establish a platform for further investigations. More than 60 Monotonic bending tests and 6 cyclic bending tests were performed and the failure modes were carefully investigated. Simplified methods were then used to model the behaviour of the connections with so called satisfactory accuracy. The purpose of the connection modelling is to give a better understanding of the behaviour of boltless connections and to provide a simpler tool than experimental testing to analyze the behaviour of those connections under monotonic as well as cyclic loads. As a consequence of analyzing the connections, the entire rack frames can be analyzed and designed more accurately.

This chapter is written in two separate parts relating to monotonic and cyclic analyses.

Parametric study was first conducted to discover the relations between the key parameters of the connections such as 'beam width, and 'upright thickness' and the ultimate moment and rotations of the connections. Also by normalizing the monotonic curves and presenting the curves between the two extreme cases of rigid and hinged connections, the semi rigid behaviour of the connections was shown.

Finite Element Models were also developed in this study to simulate both monotonic and cyclic test conditions. Finite element analysis gives researchers the ability to investigate the force flow and stress distribution into the connection components, and as a result, provides a better understanding of the connections behaviour.

Analytical models of connections were also developed based on mathematical equations to calculate the Ultimate and Yield Moment of the connections. These equations give the engineers the ability to design their connections without the need for experimental testing or FE modelling.

The second part of this chapter focuses on the cyclic behaiour of the connections which is most important for seismic analysis of rack structures. Experimental test results were first presented in this part and the influence of the upright thickness on the seismic performance of the connections was discussed. Also, important cyclic features of the connections such as stiffness degradation and strength deterioration which are generally known as ‘progressive cyclic damage’ were observed. As the cyclic testing is very expensive and time consuming, an *Analytical model* was used as an alternative to provide the hysteresis curves of the connections. Available cyclic algorithms (Kinematic, Takeda and Pivot) were examined to evaluate their suitability in modelling racking connections. For this reason a back bone (or boundary) was needed to be formed to define an envelope curve inside which the cyclic loops will circulate. A method of defining a suitable equivalent cyclic back bone was then proposed to form the cyclic back bone out of monotonic test (or FE) results. By comparing different cyclic algorithms, Pivot hysteresis model was found to be the best option to simply simulate the cyclic tests by specifying appropriate parameters to direct the loading and unloading paths.

3. CHAPTER 3: ANALYSIS OF BASE PLATE CONNECTIONS

3.1 Introduction and literature review

Base plate connections, which are the focus of this chapter, are used to anchor the frame to the floor. They are usually semi-rigid with a non-linear moment-rotation characteristic that depends on many factors such as the floor anchoring arrangement and the axial compression of the uprights. In static analyses, stiffness reduction associated with the semi-rigidity can cause excessive lateral displacements of the structure and thereby lead to further second order effects that must be considered in the analysis and design. In dynamic analyses, the base plate stiffness can influence the fundamental period and consequently the seismic response of the entire frame. “The lack of data on base-plate joint responses is generally reflected in adoption of simplified models of analysis (i.e. frame model with hinged base)” (Baldassino and Zandonini, 2008). Previous studies have pointed out the non-negligible effect of base plate joints on the overall rack response and, as a consequence, an urgent need to investigate the key parameters of the behaviour of the base plate connection was highlighted. (Baldassino and Bernuzzi, 2000)

The Rack Manufacturer Institute, RMI (2012) provides an equation for the initial stiffness of base plate connections based on floor’s modulus of elasticity and base plate thickness. However, the code does not mention the effect of other parameters such as bolt arrangements in the base plates and upright position relative to the base plate. The British Standard EN 15512 (2009) and the Australian Standard AS 4084 (2012) propose an experimental test method for the determination of the moment capacity and stiffness of base plate connections under static loading. The testing arrangement stipulated in EN 15512 (2009) and AS 4084 (2012) leads to inconsistent requirements as described by Gilbert and Rasmussen (2011) who, therefore, proposed an adjustment to the test arrangement. An alternative test arrangement developed by Saleh (2012) was used in obtaining the experimental base plate moment-rotation curves presented in this section. This test arrangement models the same structural conditions stipulated in EN 15512 (2009) but without the test setup drawbacks identified by Saleh (2012) and Gilbert and Rasmussen (2011).

An experimental study was also conducted by European Commission supported by research funds from coal and steel unit (Rosin et al., 2009). They studied the cyclic and monotonic behaviour of typical base plate connections subjected to the lateral forces in both down aisle and cross aisle directions. The base plates they studied were anchored by only two bolts and subjected to different axial compression forces.

Both European and Australian Standards for design of rack structures EN 15512 (2009) and AS 4084 (2012) propose a method to define either the ultimate moment (i.e. capacity) and rotational stiffness of the base plate (or beam to upright) connections using existing experimental test results based on the failure moment 'R_{ni}' (See Figure 3.1). "The stiffness of the assembly shall be obtained as the slope '*Kni*' of a line through the origin which isolates equal areas (A1, A2) between it and the experimental curve, below the design load or moment corrected for yield and thickness, *Rc*," as shown in Figure 3.1.

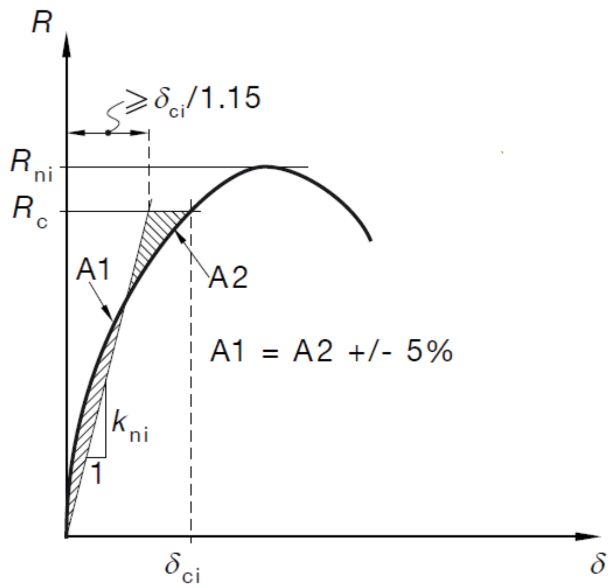

Figure 3.1: The proposed method of deriving a Bi-Linear moment rotation curve from experimental result (AS 4084, 2012, p. 70)

The proposed method requires a failure (ultimate) moment to form the bi-linear curve which does not apply to the base plate connections as in a deformation controlled base plate tests, the ultimate moment cannot be directly determined due to second order effects.

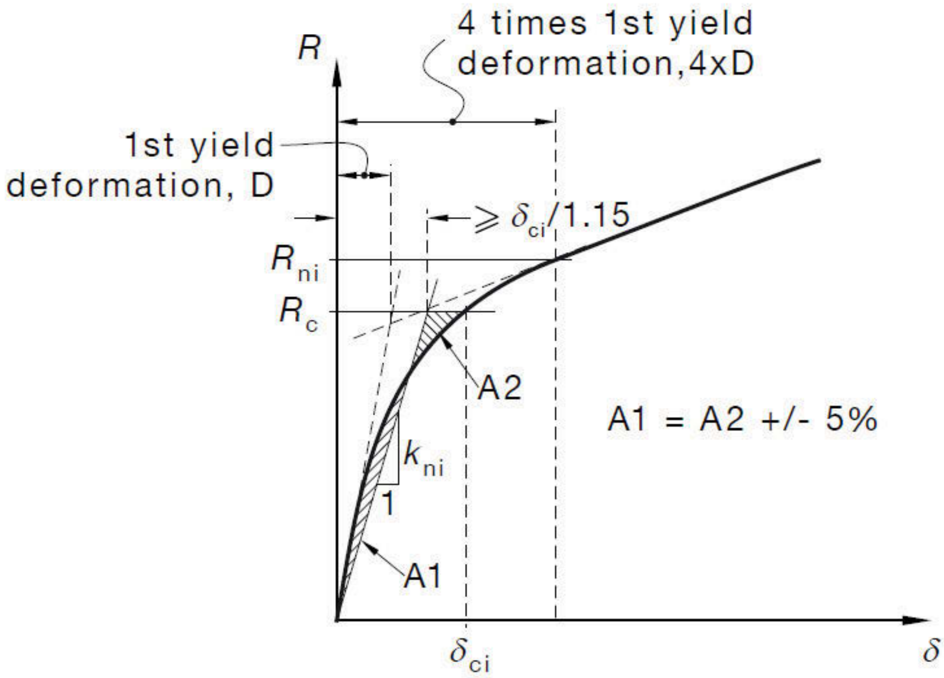

Figure 3.2: The proposed method of deriving a Bi-Linear moment rotation curve from experimental result (AS 4084, 2012. p. 70)

The Australian Standard AS 4084 (2012), therefore, was updated to consider the moment-rotation behaviour of base plate connections based on experimental test results. For this reason the method proposed by Gilbert and Rasmussen (2011) was adopted. The failure (ultimate) moment "R_{ni}" is defined to be the "moment corresponding to four times the first yield deformation if the load or moment-deformation curve does not reach a maximum" as shown in Figure 3.2. "The first yield deformation may be calculated as the deformation at the intersection between a line representing the elastic stiffness deformation and a line representing the inelastic stiffness deformation" (AS 4084, 2012).

However, the codes and specifications have not yet pointed out suitably the behaviour of base plate connection in transverse (i.e. cross aisle) direction. Different base plate geometries can have different behaviour under uplift (i.e. tension) forces and may significantly affect the stability and ductility of the cross aisle system.

In this chapter the moment – rotation behaviour of base plate connections are experimentally and numerically investigated and the ultimate moment and rotation of the base plates were obtained using a theoretical approach. The behaviour of base plate connections under cyclic reversal loads has also been studied by performing Finite Element analysis and a more reasonable seismic design approach is proposed. Finally, a practical approach for modelling the non-linear response of a base plate connection is proposed. This model can be easily implemented in typical frame analysis programs such as SAP2000.

3.2 Geometry, Anchoring configuration and behaviour of base plate connections in down aisle direction

Figure 3.3 shows two typical floor connections where the base plate up-stand bracket is connected to the upright by means of bolts. The base plate has three holes on either side of the upright for anchoring it to the floor.

As indicated in Figure 3.4, in practice two to six anchors are used depending on the design requirements. The moment-rotation behaviour and capacity of base plate connections depends on different factors such as base plate thickness, up-stand bracket geometry, upright section properties and local deformation of concrete floor (Gilbert and Rasmussen, 2010). Different floor anchoring configurations can also lead to different behaviours of the connections as was shown by Saleh (2012) and Rosin et al. (2009). Furthermore, the stiffness and moment capacity of the base plate connection will depend on the magnitude of compressive axial force in the upright which can change due to changing static live loads or seismic actions and can, thereby, significantly change the stiffness and strength of the connections.

In this chapter, the six different anchoring configurations depicted in Figure 3.4 as Type 1 to Type 6 are investigated numerically using Finite Element analyses. The FE models were developed to study the effect of anchoring arrangement on the base plate behaviour by investigating brackets with the same orientation but with different bolting arrangements. The double arrow in the figures indicates that the applied loading causes bending deformation in the down aisle direction (e.g. major axis of the uprights). The FE results of types 1-3 compared favourably with existing experimental results and then the FE results were used to investigate the behaviour of base plate types 4-6 without available experimental test results.

Figure 3.3: Typical base plate connection

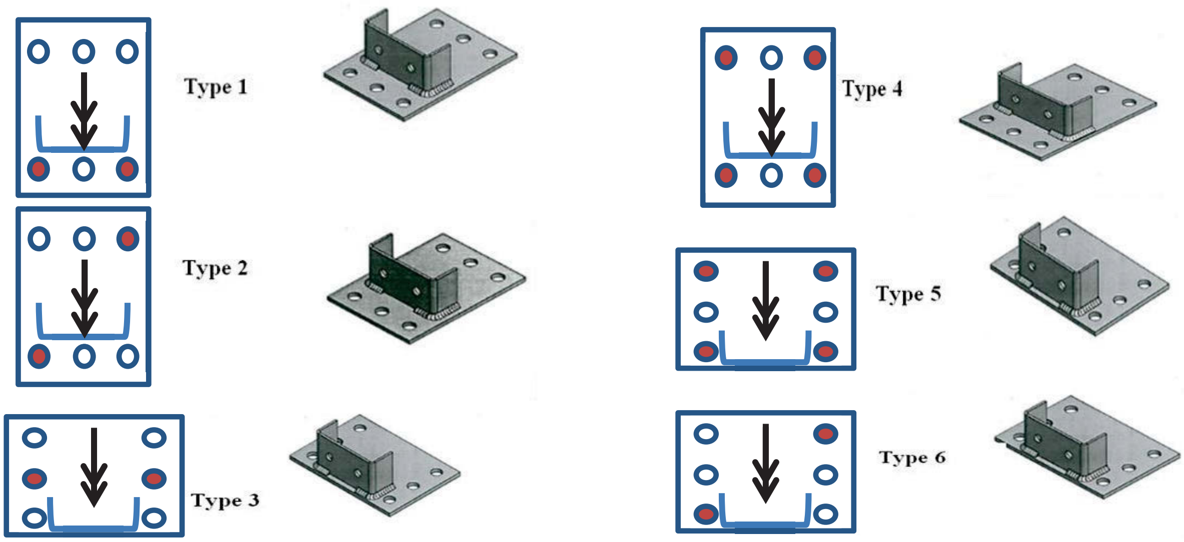

Figure 3.4: Different base plate connections (red dots indicate the position of anchor bolts)

3.3 Experimental Study

The purpose of the tests was to measure the moment rotation characteristics of the connection between upright and floor for a range of axial compression loads up to a nominated design load for the upright. As will be described below, an alternative test arrangement that models the same structural conditions stipulated in BS EN 15512 (2009) was adopted. Figure 3.5 shows the forces and deflections of the test arrangement proposed in the European Norm. As indicated in Figure 3.5, two lengths of upright section fitted with base plates, and bearing onto a concrete cube to represent the floor surface are tested together. Using this test setup, the concrete block must be free to move in the horizontal plane, but restrained from rotating. At the start of the test, the axes of both uprights coincide with the line of action of the compressive load F1, which is increased to its full value and held constant at that value during the test. Then the load F2, which acts transversely on the concrete block, is increased until this load reaches its maximum. Displacements and loads are recorded throughout the test in order to establish the base plate moments and rotations. This test set up has the following practical drawbacks: while the arrangement of Figure 3.5 is symmetric, in practice test specimens are unlikely to perform symmetrically and fail simultaneously in exactly the same way during the test. When testing two specimens together, an averaging of the moments and rotations recorded from both specimens is taken and the test is terminated once one of the two specimens fails. Hence, the failure values observed in the test would be governed by the specimen with the lower strength and / or stiffness and, thereby, the potentially higher values of the second base plate cannot be considered. Furthermore, the EN 15512 (2009) requirement of preventing the rotation of the concrete block, while allowing it to move freely in two orthogonal directions in the plane of bending of the upright, was considered to be difficult to achieve in the laboratory (Saleh, 2012). Therefore, an alternative test arrangement in which only one specimen is tested was developed and adopted. The forces and displacements are as shown in Figure 3.6, the setup is as depicted schematically in Figure 3.7 and the actual test rig is shown in Figure 3.8.

Using this set up, the relative rotation θ_b between base plate connection and concrete block and the corresponding moment M_b are determined from equations (3-1 to 3-3) as follows:

$$\theta_b = \frac{\delta_1 - \delta_2}{d_{12}} \quad (3\text{-}1)$$

$$M_1 = F_2(L - \delta_4) \quad (3\text{-}2)$$

$$M_b = M_1 + F_1\,\delta_3 \quad (3\text{-}3)$$

where:

θ_b: Relative rotation of base plate connection

M_b: Base plate moment

$\delta_1 to\ \delta_4$: Displacements at positions 1 to 4, respectively

d_{12}: Distance between displacement devices for $\delta_1$and δ_2

F_1: Vertical force applied by Jack 1

F_2: Horizontal force at pin above upright

L: Distance between pin above upright and bottom of the base plate

Suitable bearings were used in order to minimise friction under the concrete block and in the pins above the upright that can be subjected to the relatively large force (F_1). As shown in Figure 3.7, the mechanism comprising a four-bar parallelogram linkage allows the horizontal support reaction (F_2) at the top of the upright to be realised and measured directly.

At the start of the test, the vertical compression load (F_1) was gradually increased to the nominated value and held constant throughout the test. The concrete block was then made to slide by activating the horizontal jack while the force (F_2) was observed. The jacking action was continued under displacement control until a large base plate rotation was judged to have been reached or a significant drop in the force (F_2) was observed.

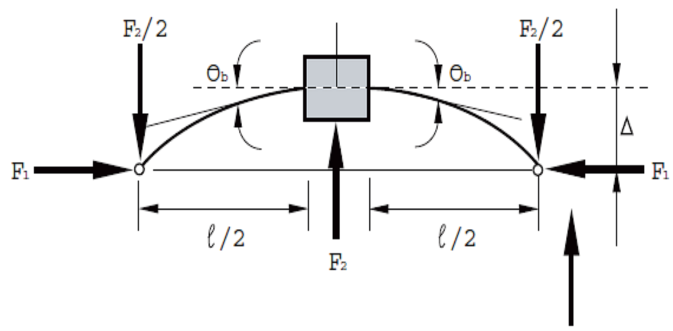

Figure 3.5. Base plate connection test concept with two specimens tested simultaneously as proposed in BS EN 15512:2009

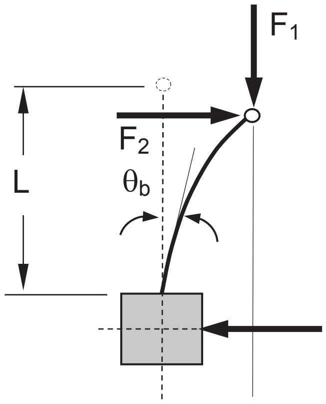

Figure 3.6: Base Plate Test forces and displacements

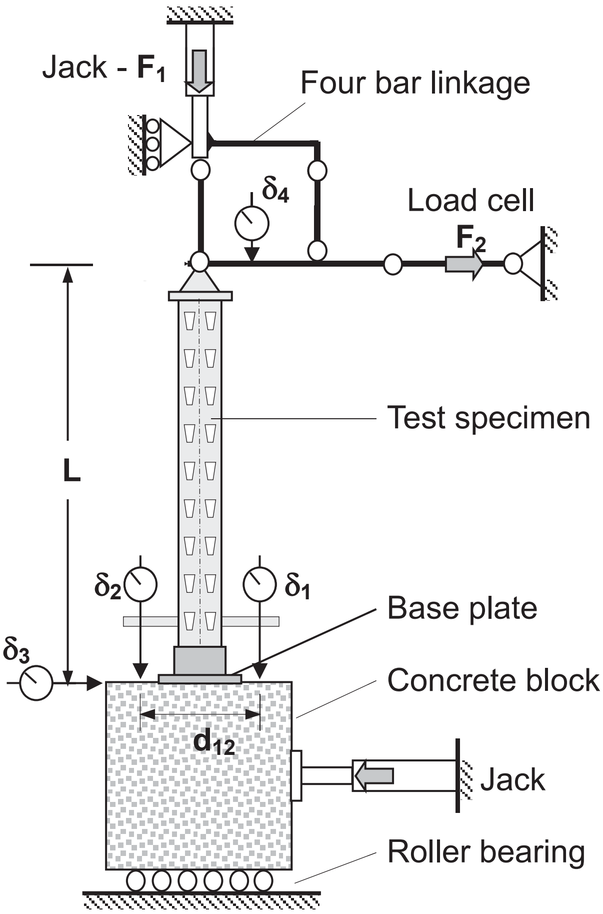

Figure 3.7: Test Setup

Figure 3.8: Base Plate Test arrangement

3.3.1 Test Results and Discussion

Three base plate connection configurations (Type 1, Type 2 and Type 3 of Figure 3.4), which were fitted to the same upright section were tested over a range of six axial loads from 40 kN to 100 kN. All the tests were performed to evaluate the monotonic moment rotation behaviour of base plate connections in the down aisle directions. The corresponding moment-rotation curves are presented in Figure 3.9 to Figure 3.11. It was observed that in almost all cases the moment values continued to increase until the test was terminated when the connection was deemed to have failed and would no longer be able to perform its design function because of large rotations. Plots of the total base plate moment Mb (in equation 3) versus the moment M1, which is caused by the lateral force F2 alone, are presented in Figure 3.12 to Figure 3.14 . It can be noticed that the total moment (Mb) may continue to increase after the moment (M1) has reached its maximum. This effect is attributed to second order effects caused by force (F1).

Similar observations were reported by Gilbert and Rasmussen (2011).

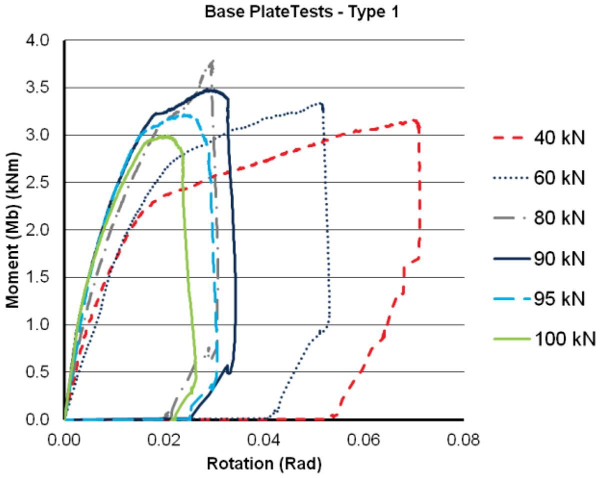

Figure 3.9: Test results for base plate type 1

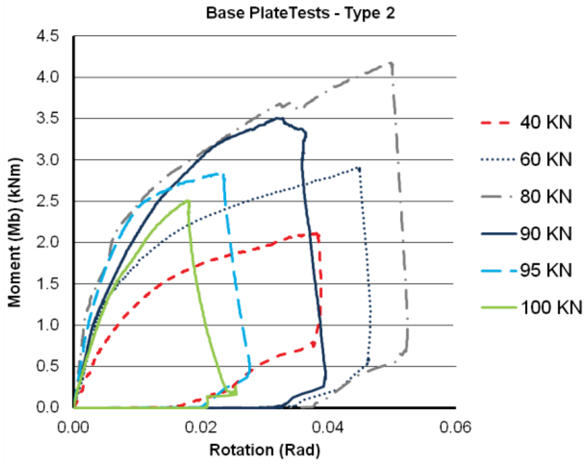

Figure 3.10: Test results for base plate type 2

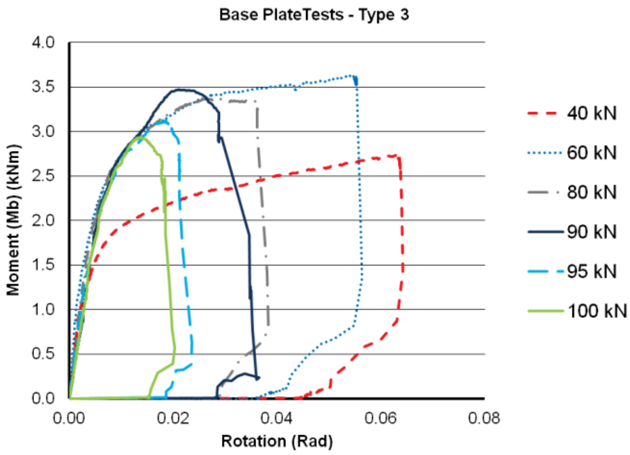

Figure 3.11: Test results for base plate type 3

When no maximum moment can be clearly identified in the experimental moment rotation curve, a criterion for determining the ultimate moment of base plate assemblies proposed by Gilbert and Rasmussen (2011) is to adopt a deformation limit of four times the yield deformation. However, this method seems to be based on a failure criterion for conventional steel connections which may not apply to base plates of storage racks with substantial second order effects (Kosteski and Packer (2003), Yura, Zettlemoyer and Edwards (1980), Beg, Zupančič, and Vayas (2004), Firouzianhaji et al. (2014)).

According to EN 15512 (2009) "the test component shall be deemed to have failed when (a) the applied test loads reach their upper limit, (b) deformations have occurred of such a magnitude that the component can no longer perform its design function". If condition (a) of EN 15512 (2009) is strictly applied, the test would be terminated at the maximum value of M1. In Figure 3.15 to Figure 3.17 the rotations that correspond to the maximum values of M1 for different values of the upright force F1 are plotted.

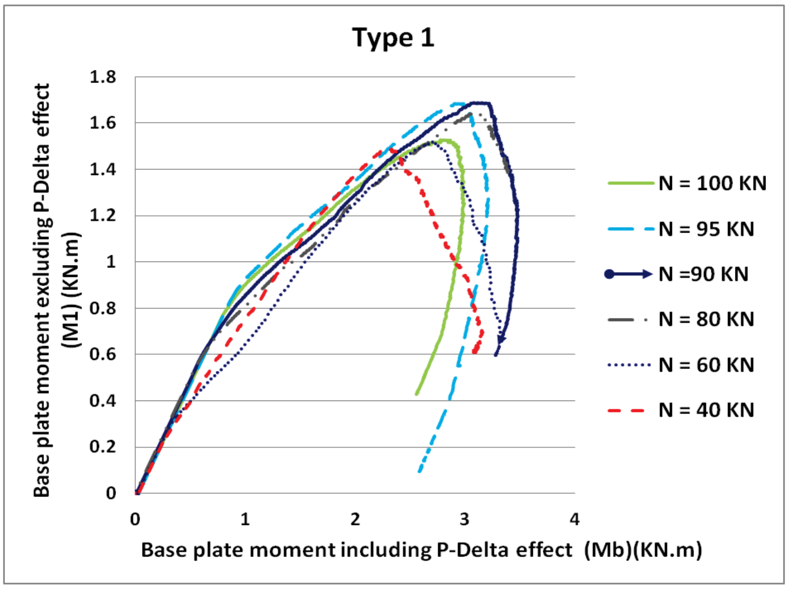

Figure 3.12: Total Moment (Mb) –Moment due to lateral force only (M1).Connection type 2al force only (M1).Connection type 1.

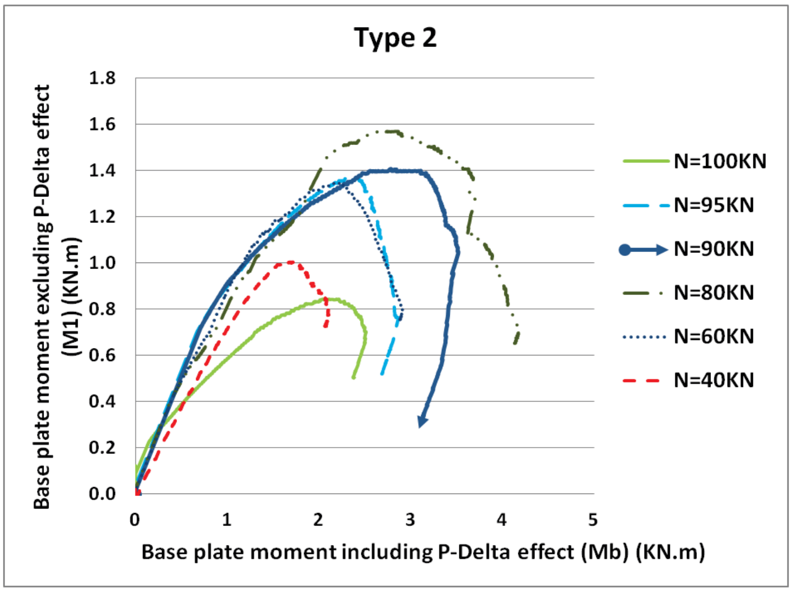

Figure 3.13: Total Moment (Mb) –Moment due to lateral force only (M1).Connection type 2

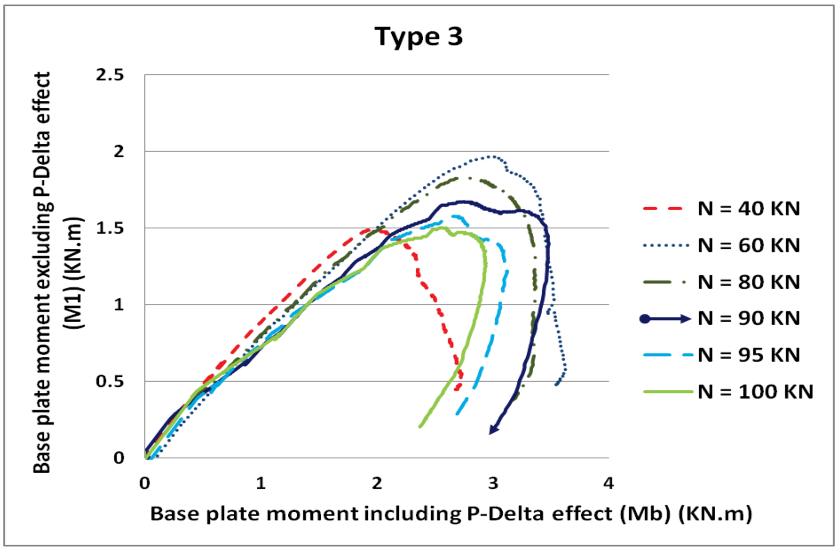

Figure 3.14: Total Moment (Mb) –Moment due to lateral force only (M1).Connection type 3.

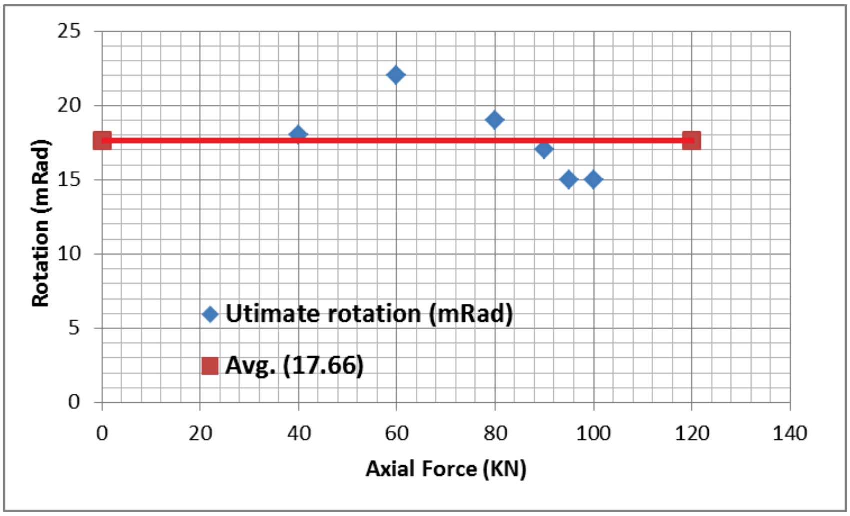

Figure 3.15: Ultimate rotations for base plate type 1

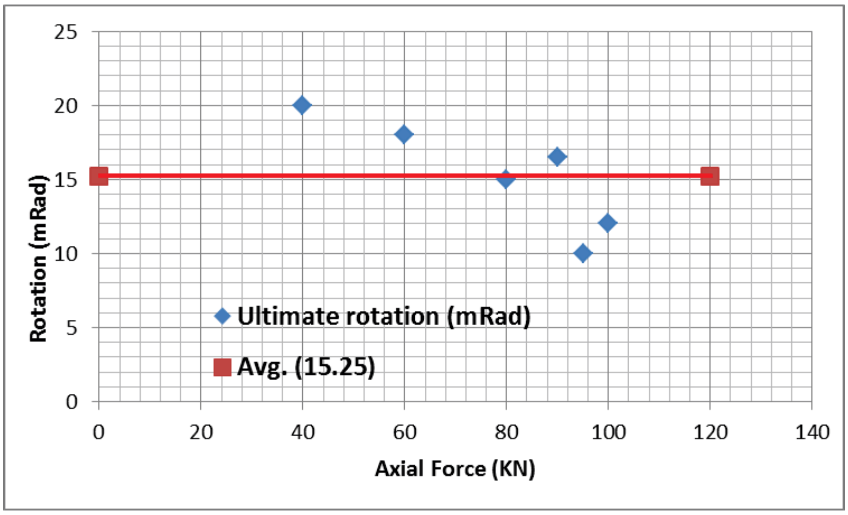

Figure 3.16: Ultimate rotations for base plate type 2

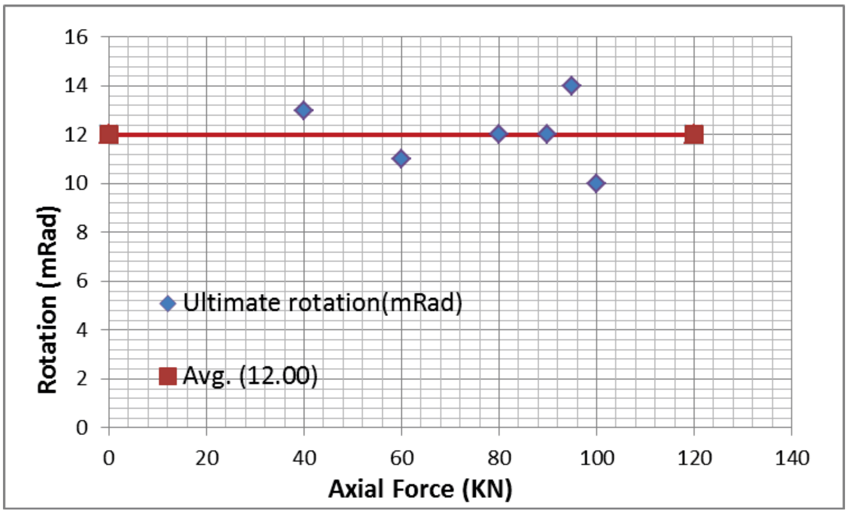

Figure 3.17: Ultimate rotations for base plate type 3

It can be observed that most of those rotation values are of the order of 0.010-0.020 Rad which can be considered as practical deformation limits where the connection would no longer be able to perform its function according to condition (b). It is observed that for the base plate types tested, EN 15512 conditions (a) and (b) would have terminated the test at approximately the maximum load value of F2. Above rotational limit of less than 0.02 Rad may not be worrying for static analysis and design of rack structures when the lateral drift of the structure is usually less than 0.01 rad. However, for seismic design the first level inter-storey drift may pass this limit. Therefore, to satisfy this condition, systems need to be further stiffened by spine bracing members to force the lateral drift to fall within an acceptable range.

3.4 Stability analyses of upright base plates

A stability analysis of upright base plates sheds more light on their ultimate capacity. For such an analysis based on the classic theories of stability of structures, the simplified system is shown in Figure 3.18.

The total potential energy of the system is:

$$U_t = U_I + U_E = \frac{1}{2} M_b(\theta)\theta - F_1 L(1 - \cos\theta) - \frac{1}{2} F_2 \delta_3 \tag{3-4}$$

where:

U_I and U_E indicate the internal and external energy respectively.

In this study any out of straightness in the upright is ignored: ($\delta_3 = \theta L$)[13]

The static equilibrium position is characterised by equation 3-5:

$$\frac{\partial U_t}{\partial \theta} = 0 \tag{3-5}$$

Then:

$$\frac{1}{2}(M_b(\theta) + M_b'(\theta)\theta) - F_1 L sin\theta - \frac{1}{2} F_2 L = 0 \tag{3-6}$$

From Equation 3-2: ($F_2\, L = M_1$)

$$\frac{1}{2}(M_b(\theta) + M_b'(\theta)\theta) - \frac{1}{2} M_1 = F_1 L sin\theta \cong F_1 L\theta \tag{3-7}$$

Therefore, the critical rotation (θ_{ult}) can be calculated by equation 3-8:

$$\theta_{ult} \le \frac{(M_b(\theta) - M_1) + M_b'(\theta)\theta}{2LF_1} \tag{3-8}$$

$$\Longrightarrow \quad (M_b(\theta) - M_1) + M_b'(\theta)\theta \ \ge 2LF_1\theta_{ult}$$

$$\{M_b(\theta) - M_1 = F_1\delta_3 \ \cong \ LF_1\theta\}$$

$$\Longrightarrow \quad M_b'(\theta)\theta \ \ge LF_1\theta_{ult}$$

Then:

$$M_b'(\theta) \ \ge LF_1 \tag{3-9}$$

[13] θ is typically < .05 rad and hence can be assumed to be sufficiently small to accept the approximation of sinθ =θ !

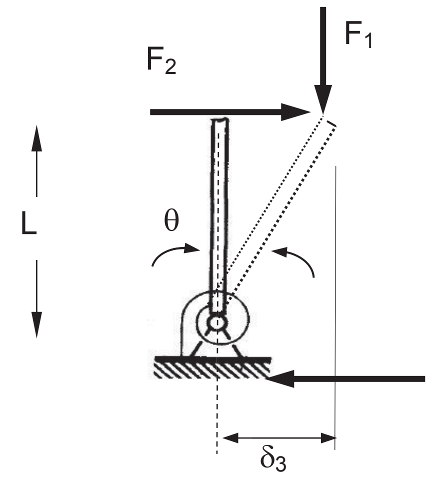

Figure 3.18: Simplified model of the base plate connection

Ultimate rotation can be obtained by trial and error using equation 3-8

The term "$(M_b(\theta) - M_1)$" is the distance between the straight line and the curves in "M_b–M_1" diagram shown in Figure 3.19.

As an example, for base plate Type 1, under 80 kN axial force, the ultimate rotation of "0.019" at which "M_1" starts to reverse, was observed referring to Figure 3.15. Substituting the values in equation 3-8:

$$\theta_{ult} = 0.019 \leq \frac{(M_b(\theta) - M_1) + M_b'(\theta)\theta}{2LF_1} = \frac{1.55(kN.m) + (73\times0.019)}{2\times80\ (kN)\times0.785} = 0.023 \ \ \text{(OK)}$$

where, 'M_1' and 'M_b' can be read from Figure 3.12:

$M_1 = 1.65\ kN.m$

$M_b = 3.2\ kN.m$

Hence, this limit is on the conservative side and a higher rotation limit can be used. This method can be used as a stability check for the ultimate rotation.

Stability check of the base plate systems highlights the importance of post elastic behaviour of the base plate connections. The higher the post elastic (secondary) stiffness, the higher will be the rotation limit.

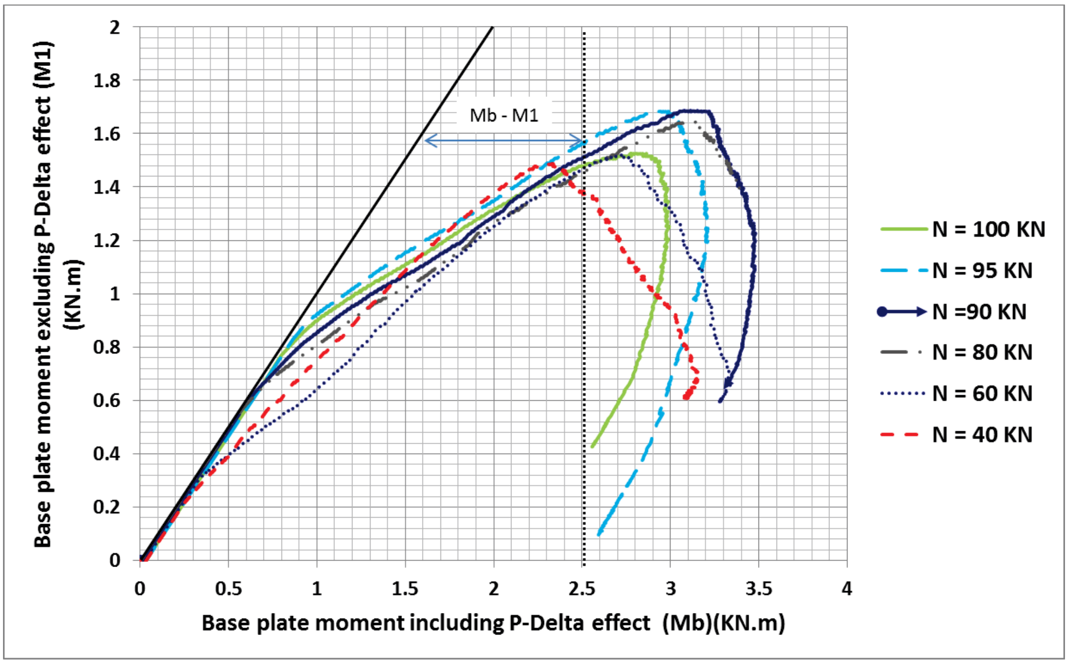

Figure 3.19: M1-Mb diagram (base plate Type 1)

3.5 FE Modelling and discussion of results

While the finite element method is now widely used and is a well accepted tool for accurately simulating complex structural systems, relatively few finite element analyses of storage racks have been reported in the literature [3.13].

In this project, finite element models have been used to determine the stiffness and strength of bolted base plate connections under monotonic as well as cyclic loading.

3.5.1 FE Modelling

Finite Element models were developed using the ABAQUS (2011) software. Two sets of simulations were performed. The first set of simulations served as a verification of the FE models by comparing the results obtained with the experimental results. The second set of simulations was aimed at studying the behaviour of the base plate connection under cyclic loading.

All FE models incorporated material, geometric and contact non-linearity in order to simulate the test conditions as accurately as possible. The material law of base plate assembly and upright were modelled using the tri-linear stress-strain diagram of Figure 3.20 and the values of Table 3-1. For the base plate and column sections, St37 steel grade material was used with a yield stress of 250 MPa and an ultimate stress of 350 MPa. AIII steel material was considered for the anchor bolts with yield and ultimate stress values of 400 MPa and 600 MPa, respectively. Contact interactions between the concrete block, base plate and anchors were ignored while a relatively rigid material was used for the concrete. This assumption was also made for the base plate connection modelling by Díaz, Nieto, Biempica and Rougeot (2006) and Khodaie et al. (2012). Other interactions included: (i) Permitting surface uplift between bottom of upright and base plate as well as bottom of base plate and top of concrete block; (ii) Permitting contact separation but limiting over closure of M12 Bolt-Upright bracket.

The element type used in the models was the 8-node linear brick element (C3D8R) whereby at least two elements were used in modelling the thickness of the upright and base plate sections. The load at the top of the upright was applied by modelling a rigid plate in order to prevent stress concentrations and local buckling in the upright section. In the first set of simulations the loading was applied monotonically in two steps corresponding to the loading sequence of the test. In step 1 the compressive axial load F1 was applied at the top of the upright and in step 2 a lateral displacement Δ was imposed to the bottom of the base plate to induce the required moment (See Figure 3.21). The lateral displacement was gradually increased until failure was judged to have been reached.

In the second set of FE simulations, the models were analysed by applying a cyclic horizontal displacement while a given compression load of 80 kN in the upright was applied and kept constant.

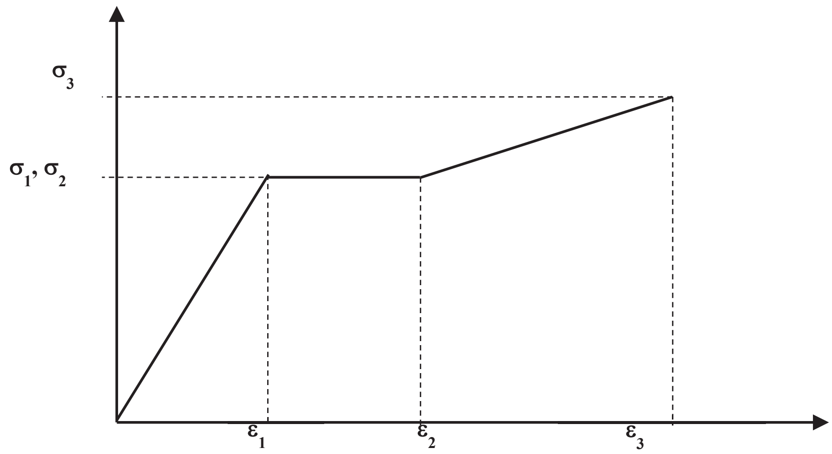

Figure 3.20: Stress-strain law used in FE model

Table 3-1. Material Properties

Components	Base Plate Components	Bolts	Upright
$\varepsilon 1$ (Micro strain)	1250	2000	1500
$\sigma 1$ (MPa)	250	400	350
$\varepsilon 2$ (Micro strain %)	31500	22000	31500
$\sigma 2$ (MPa)	250	400	350
$\varepsilon 3$ (Micro strain)	200000	240000	200000
$\sigma 3$ (Mpa)	350	600	480

3.5.2 FE Results and Discussion

For connection types 1, 2 and 3, a reasonably good agreement in results was observed between the FE simulations and the experiments. As can be seen in Figure 3.22, the FE model was able to predict the entire moment rotation curve.

However FE results provide higher rotational stiffness and ultimate moments which could be attributed to:

1. The concrete block underneath the connections being modelled as a rigid block.

2. Imperfections not being included in this model (i.e. bolts are perfectly engaged to the upright slots and bracket hole)
3. Bearing effect in the bolts may not be simulated accurately due to the relatively coarse mesh used in that region.

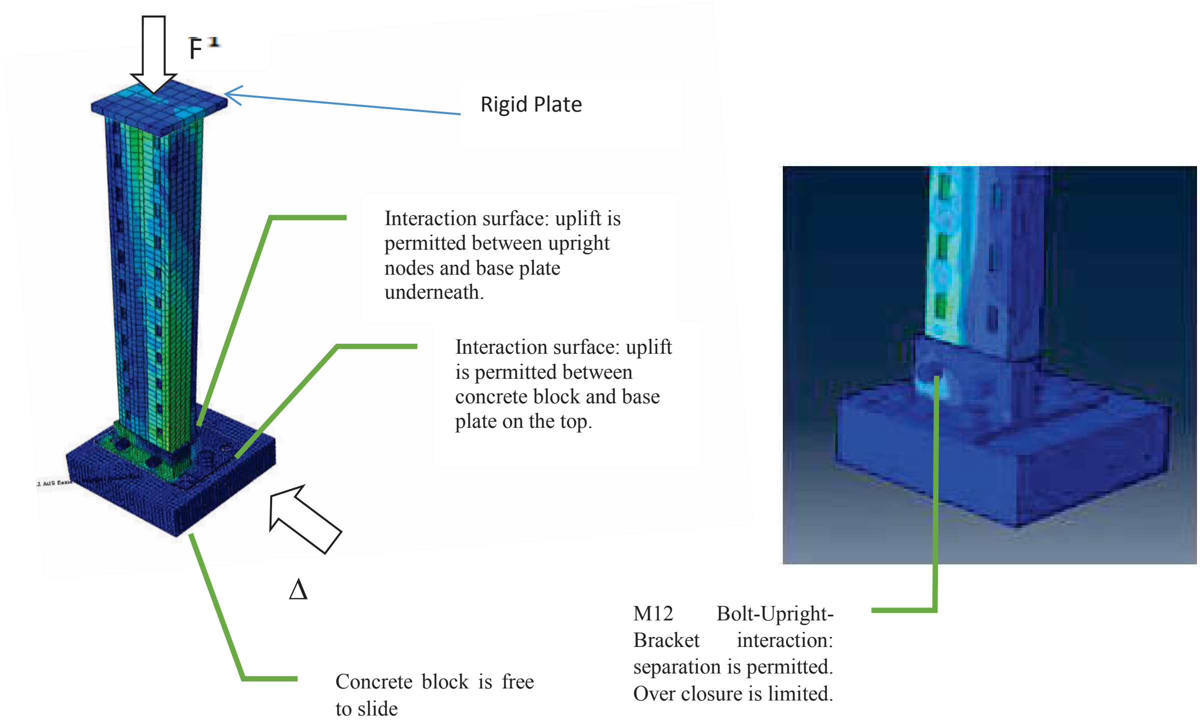

Figure 3.21: Numerical model

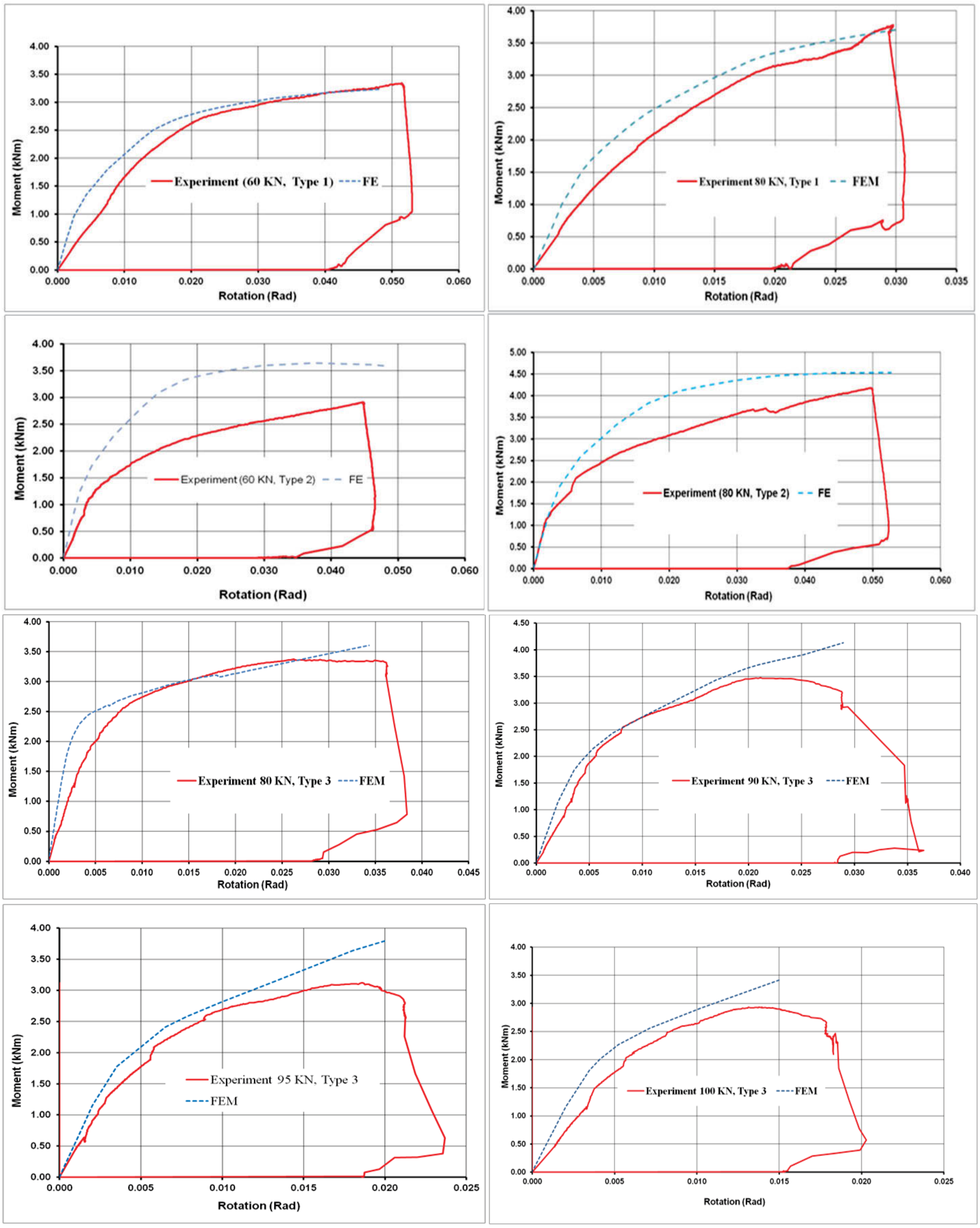

Figure 3.22: Comparison of base plate types 1 and 2, under different axial compression forces

FE models were also used to investigate the behaviour of different base plate configurations of Type 4, Type 5 and Type 6 as shown in Figure 3.4 which were not tested experimentally. Figure 3.23 shows the monotonic moment rotation behaviour of connection types 4, 5 and 6 under 80 kN compression force and an increasing lateral force of “F2”.

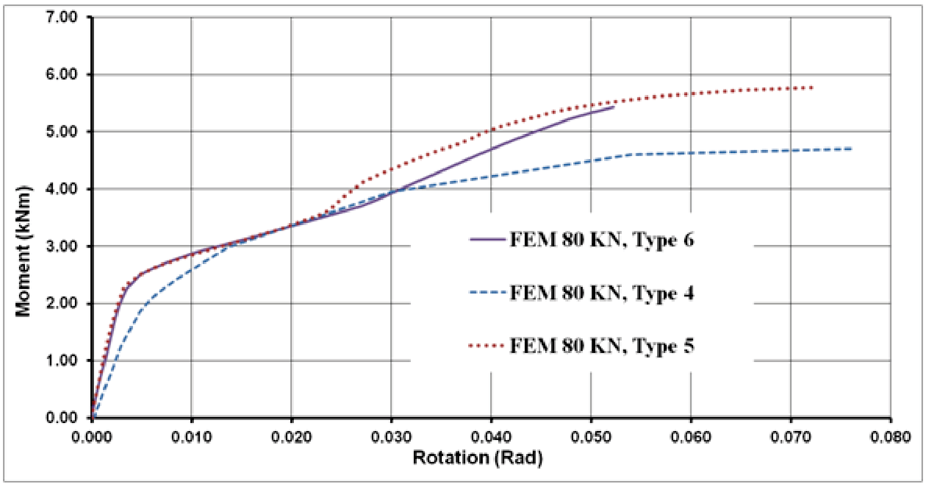

Figure 3.23: FE simulation results

According to Figure 3.24 a comparison of base plate types 1 and 2, under different axial compression forces indicates that the initial *secant* stiffness of base plate type 1 is less than the initial *secant* stiffness of base plate type 2 under the same axial force. However, at higher axial forces the reverse is observed, whereby connection type 1 shows slightly higher initial *secant* stiffness than connection type 2 under the same axial force. This highlights the effect of axial compression force on the initial *secant* base plate stiffness. On the other hand, the initial stiffness of base plate types 1 and 2, according to the method proposed in BS EN 15512 (2009), both have ascending trend relative to the axial compression force and the connection type 1 seems to be stiffer than connection type 2 by 10 to 15 percent (see Figure 3.25). The ascending trend in Figure 3.25was obtained by linear regression. The actual gradient values were not considered to be of interest in the present study.

Finite element result of base plate type 4 with 4 anchor bolts under 80 kN axial force shows that the connection has almost the same initial stiffness as the higher stiffness of connection types 1 and 2, each with 2 anchor bolts (see Figure 3.26). However, slightly higher moment capacity was observed which is due to the higher number of bolts and different boundary connections.

Moment rotation behaviour of base plate types 3, 5 and 6, which have different up-stand to base plate orientation compared to base plates types 1, 2 and 4, are plotted in Figure 3.27.

Base plates type 5 and 6 show almost identical behaviour for rotations less than 0.02 Rad, but base plate type 5 which is anchored at every corner takes more moment at final stage. This may be attributed to different failure modes of the two connections.

Base plate type 3, with two bolts in the middle, shows slightly less initial stiffness compared to the others but its moment rotation behaviour at higher rotations is similar to the connection type 6 and this is due to their similar yield patterns at failure.

Experimental results show that the stiffness of base plate type 3 increases with increasing axial compression force on the upright as shown in Figure 3.28. It is also noticeable that the stiffness of base plate type 3 is 30 to 40 percent higher than that of base plate types 1 and 2 under the same axial compression force. This might be because of limited participation of the baseplate due to particular bracket orientation of the connection type 3. In connection type 3, the two anchor bolts are positioned with more distance compared with base plate types 1 and 2 and this provides a bigger arm to resist the moment.

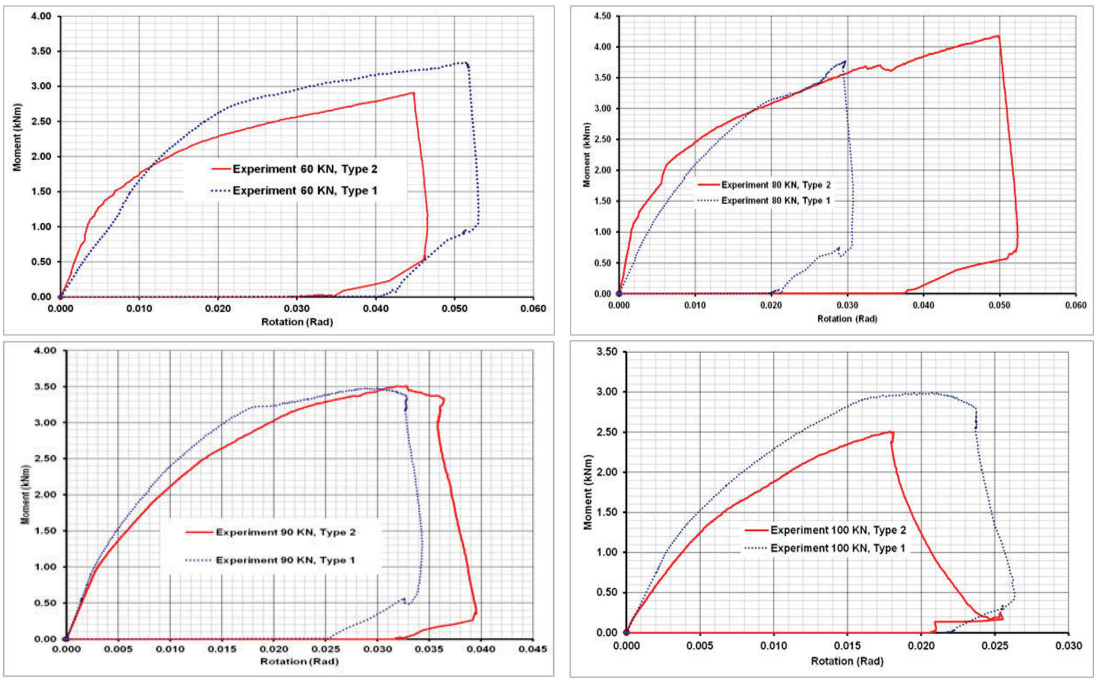

Figure 3.24: Comparison of base plate types 1 and 2 under different axial compression forces

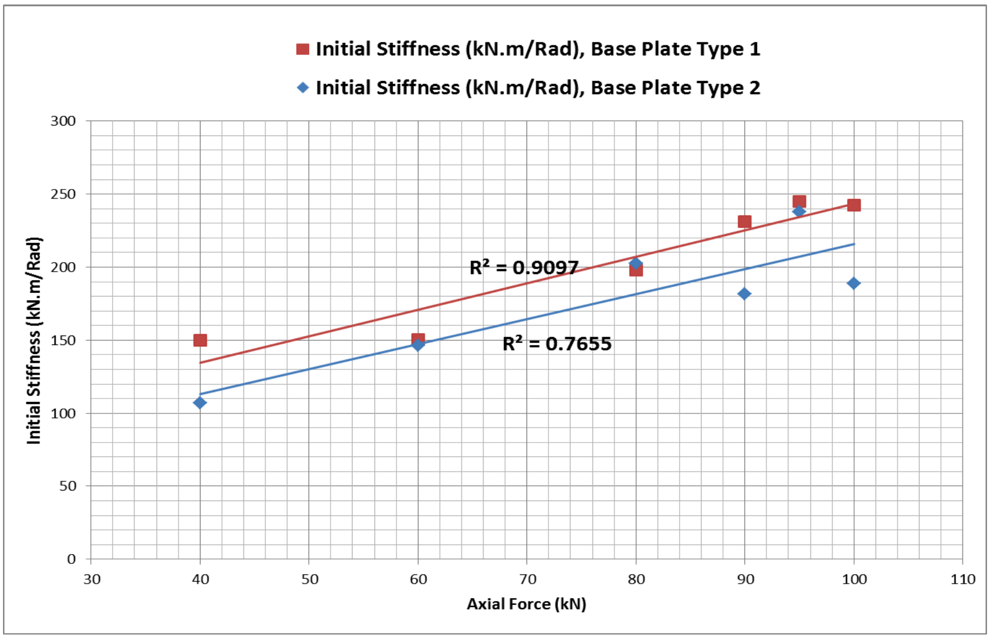

Figure 3.25: Initial Stiffness – Axial Force relations

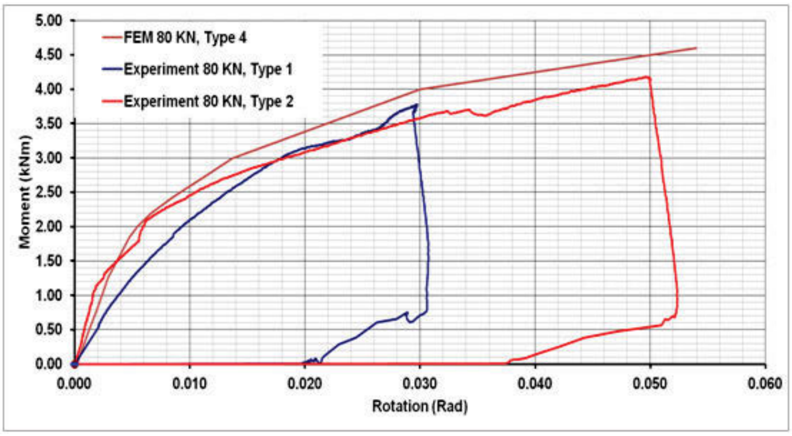

Figure 3.26: FE and Experimental results of connection types 1, 2 and 4

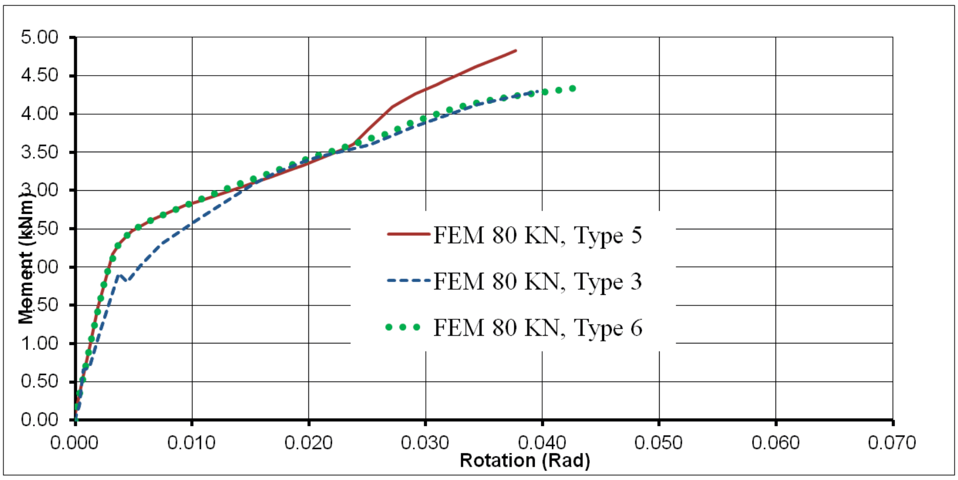

Figure 3.27: FE results of connection types 3, 5 and 6

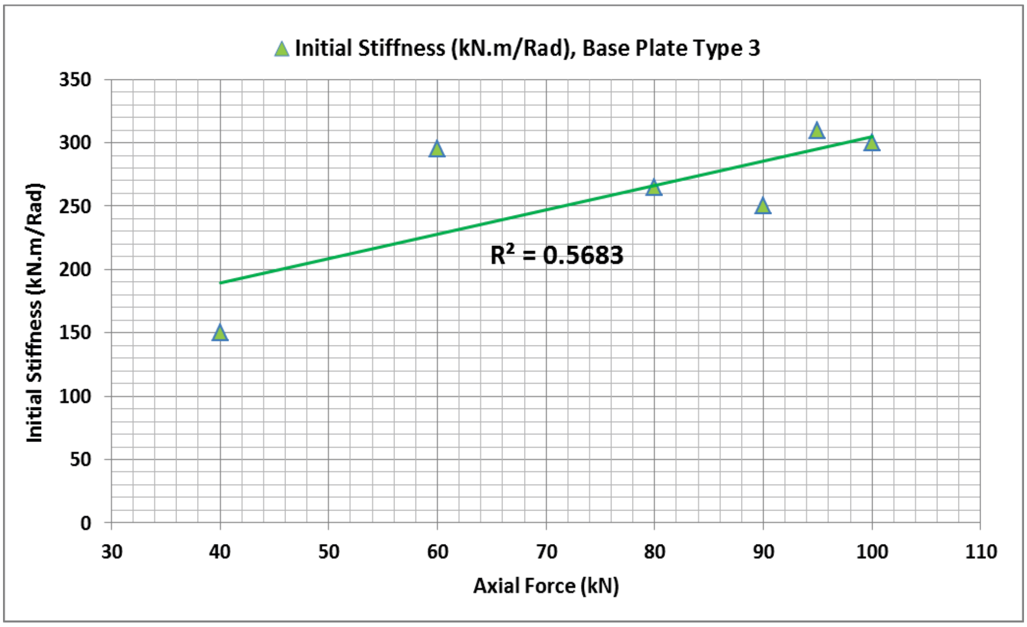

Figure 3.28: Initial Stiffness – Axial Force relation

The above observations lead to two main conclusions:

- The amount of axial force in the uprights affects the stiffness of the base plates with an increasing trend (i.e. base plates under higher compression forces show higher stiffness).
- The effect of bracket orientation in the base plate can be very significant on the stiffness of the connection. This is because the distance they provide between the bolts in each orientation is different. For example, connection type 3 is more than 30 percent stiffer than connections 1 and 2 as the distance between the two bolts of connection type 3 is higher than that of connections 1 and 2.

3.6 Theoretical Analysis

The above observations can be interpreted by considering the failure modes of the connections and corresponding yield lines. Godley (2007) presented a paper on the behaviour of storage racking base plates in which they proposed using a theoretical approach in obtaining the capacity of base plates. A typical failure of an upright base plate is shown in Figure 3.29. It is assumed that the system can take load until plastic hinges form in the base plate. The moment capacity of the base plate system (M_{max}) can be obtained from equation (3-10).

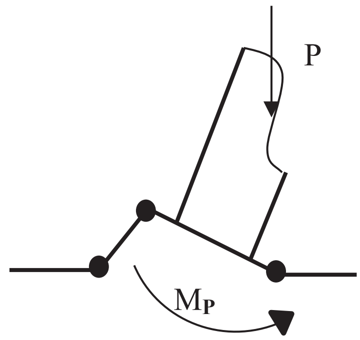

Figure 3.29: Failure mechanism for the upright base plates (Godley, 2007, p. 438)

$$M_{max} = M_p + P\frac{d}{2} \qquad (3\text{-}10)$$

where "*d*" is the upright width and "M_p" is the capacity of the base plate which can be found by using yield line theory based on virtual work procedure (Timoshenko & Woinowsky-Krieger, 1959). "M_p" is equivalent to upper limit of "M_1" in equation 3-2.

Finite element results were used to investigate the possible yield line patterns in the base plates. Figure 3.30 to Figure 3.35 show the vertical deformation contour in the base plate assembly for base plate types 1 to 6, respectively. Yield line patterns were then drawn based on the deformation contour for each type (up-stand bracket to base plate weld failure is ignored).

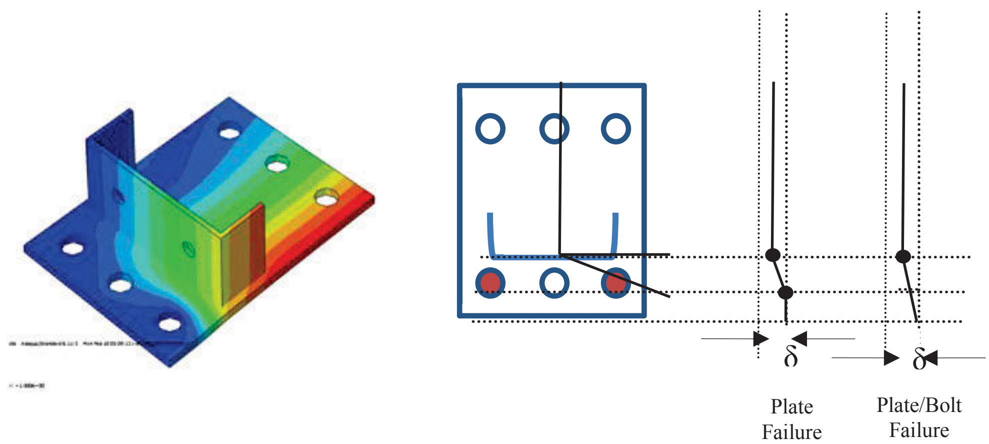

Figure 3.30: Deformed shaped with vertical displacement contour for connection type 1

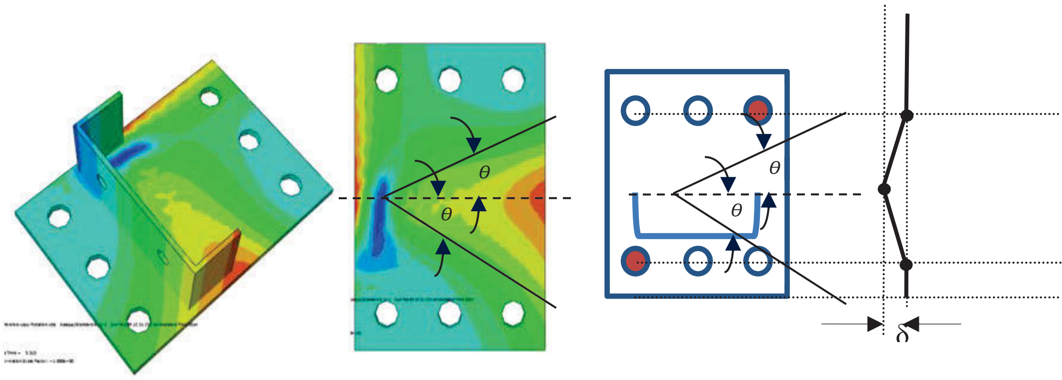

Figure 3.31: Failure mechanism with vertical displacement contour for connection type 2

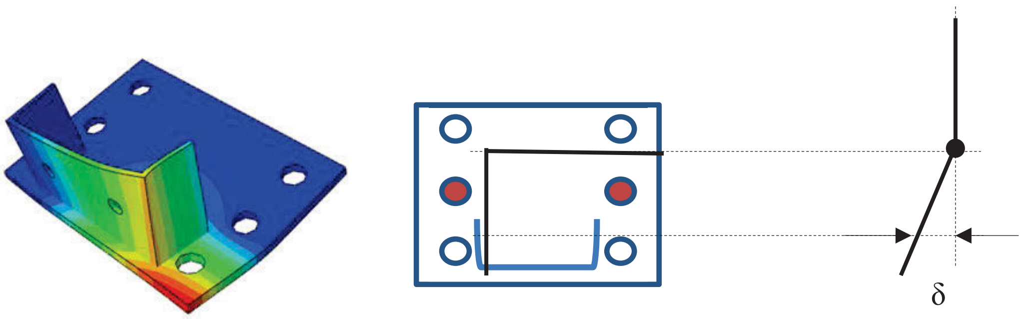

Figure 3.32: Failure mechanism with vertical displacement contour for connection type 3

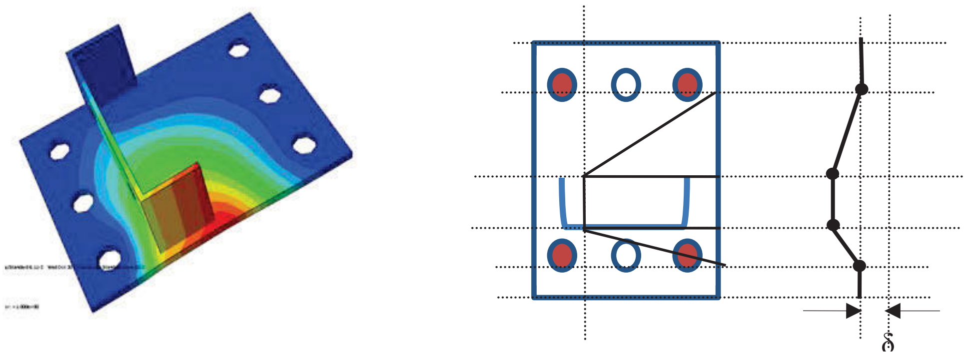

Figure 3.33: Failure mechanism with vertical displacement contour for connection type 4

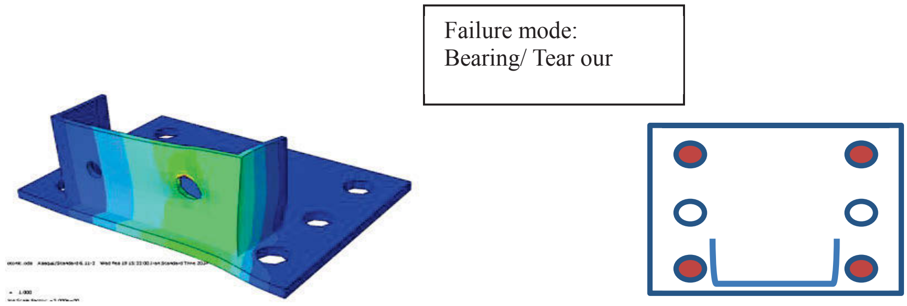

Figure 3.34: Failure mechanism with vertical displacement contour for connection type 5

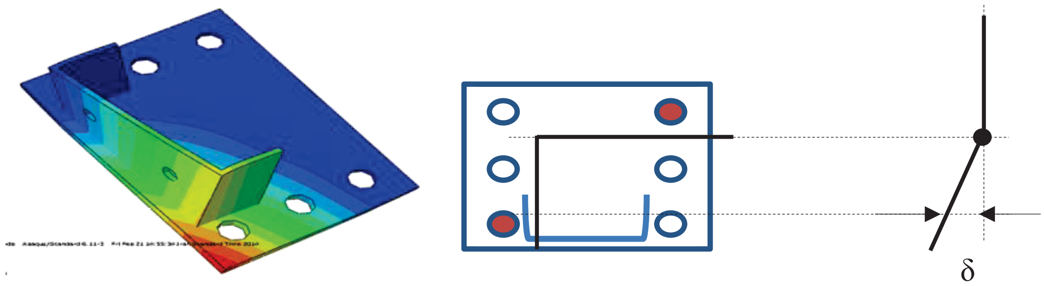

Figure 3.35: Failure mechanism with vertical displacement contour for connection type 6

As an example, details of calculation of obtaining the ultimate capacity of base plate type 4 are presented below. The reason that connection type 4 was selected is that its boundary condition (4 bolts, one, at each corner) is preferable to be used for seismic design as usually 4 bolts or more are required to withstand the upright uplift under heavy seismic forces.

Ultimate moment (moment capacity) of the connection can be calculated by using equation (3-11):

$$M_p\theta = m_p \sum_{i=1}^{5} l_{eff_i}\theta_i \tag{3-11}$$

where

d : Upright width

$m_p = \frac{t^2 f_y}{4}$: Plastic moment capacity per unit length

$\theta = \frac{\delta}{w_1}$

$l_{eff_1} = \sqrt{w_1^2 + e^2}$

$$l_{eff_2} = l_{eff_3} = w_1$$

$$l_{eff_4} = b$$

$$l_{eff_5} = \sqrt{m^2 + {w_1}^2}$$

$$\theta_1 = \theta_2 = \frac{\delta}{e}$$

$$\theta_3 = \theta_5 = \frac{\delta}{m}$$

$$\theta_4 = \frac{\delta}{w_1}$$

M, e, b, w_1, t, f_y and m_p are shown in Figure 3.36.

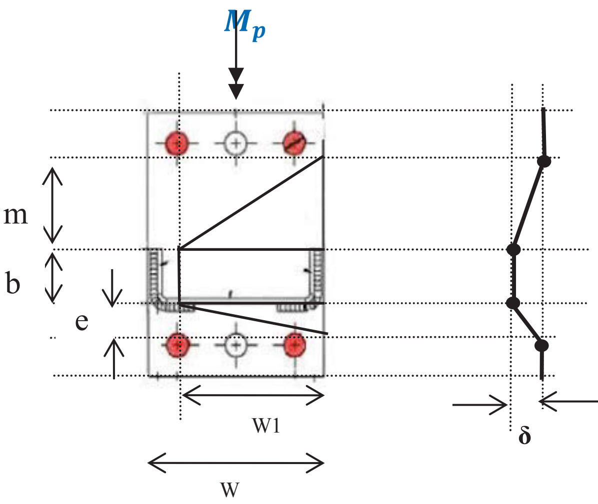

m	*65*
e	*23*
b	*35*
w1	*100*
t	*5*
fy	*250*
mp	*1562.5*

Figure 3.36. Yield line mechanism for the base plate type 4

A plastic moment (M_p = 1.95 KN.m) was obtained from the above calculation for base plate type 4. According to Figure 3.37 the calculated 'M_p' is in reasonable agreement with the moment at which the M_1 curve starts to reverse ($M_1 \approx 2.0$). The ultimate moment ($M_{max} = M_p + P\frac{d}{2} = 5.51\ (kN.m)$) was then calculated based on Godley's model and 'P' and 'd' are '80 kN' and '0.090 m', respectively. This Moment which includes the second order effects (M_b) may be able to be reached at high rotations, however the base plate system would have already failed at lower rotations as discussed in sections 3.4 and 3.5.

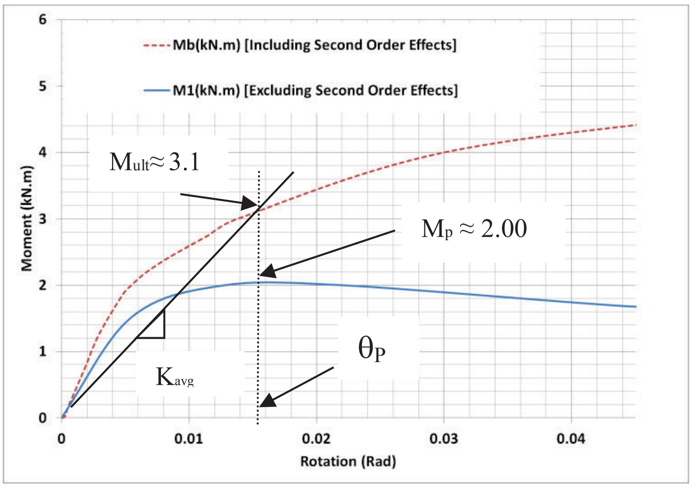

Figure 3.37: Base Plate Type 4, M_b versus M_1

3.6.1 Calculating the Base Plate Connection's stiffness

Using the above relations, the amount of Plastic moment 'M_p' (at which the 'M_1' curve starts to reverse) can be calculated. The average base plate stiffness 'K_{avg}' can be calculated from equations (3-12) and (3-13):

$$K_{avg} = \frac{M_{ult}}{\theta_p} \tag{3-12}$$

$$M_{ult} = M_p + F_1\delta_3 = M_p + F_1\,\theta_{b,p}\,L \tag{3-13}$$

where;

$\theta_{b,p}$ is the value of θ_b at failure.

F_1, $\theta_{b,p}$, δ_3 and L are shown in Figure 3.6.

M_p can be calculated from equation (3-11).

M_{ult} is the base plate moment, including second order effects, corresponding to M_p. (see Figure 3.37)

As was discussed earlier in section 3.4, and referring to Figure 3.15 to Figure 3.17, '$\theta_{b,p}$' varies within a range of 0.01 to 0.02 Rad. Figure 3.37 also shows a θ_b of 0.015 Rad.

Application of the proposed formula leads to 2.9 kN.m which is in good agreement with the value of 'M_{ult} = 3.1' kN.m computed by FE simulation result shown in Figure 3.37.

The example of using this average stiffness for cyclic loading conditions will be explained at the end of this chapter.

3.7 Base Plate Connections under Horizontal Cyclic Forces

Under seismic conditions, connections can be subjected to a wide range of load combinations including load reversal and, therefore, the connection can be expected to perform differently in comparison with its response to monotonic loading. To study the behaviour of base plate connections under repeated load reversal, hysteresis curves were established using FE simulation and different phenomena, related to cyclic loading, such as stiffness degradation are observed.

To obtain the cyclic response of the base plate connections, a lateral static cyclic load was imposed at the concrete block using displacement control. A combined isotropic-kinematic cyclic hardening material was used for all the components of the base plate. Base plate type 3 was analyzed under a range of axial forces from 40 kN to 100 kN and a cyclic lateral displacement. A cyclic displacement was applied slowly whereby the connection was cycled through increasing levels of displacement, three cycles to each increment, until failure occurred. The displacement amplitudes were applied in constant increments of 3 mm with an initial amplitude of 3 mm. Hence, the sequence used in the test was, 3 mm, 6 mm, 9 mm, 12 mm, etc.

Figure 3.38 shows the moment rotation hysteresis curve of Base plate type 3, whereby different amplitudes are shown in different line styles. The solid curve shows the first three cycles with the same amplitude. The energy absorption capability was observed in the first cycle, however, the next cycles with the same amplitude cannot absorb as much energy as the initial cycle.

Clear stiffness degradation and low energy dissipation was also observed for the next sets of three cycles. An alternate cyclic load pattern, shown in Figure 3.39, was used for further investigations of other base plate types. This load pattern was adopted to focus on the stiffness degradation and energy absorption capability of the connections during few cycles with increasing amplitudes. The cyclic responses of the connections are shown in Figure 3.40 (a to e)[14]. Monotonic results were used to identify the range of meaningful displacement amplitudes. At least three cycles were used to investigate the behaviour of the connection. Each cycle represents a different seismic severity from low seismic to high seismic forces. A Similar cyclic load protocol was also used by Wang, Shi, Wang, and Shi (2013). It can be seen from the hysteresis curves that stiffness degradation takes place after each cycle. The slope of the moment rotation curves at the beginning of the second and third cycles are almost identical to the slope of the unloading curves of the corresponding previous cycles.

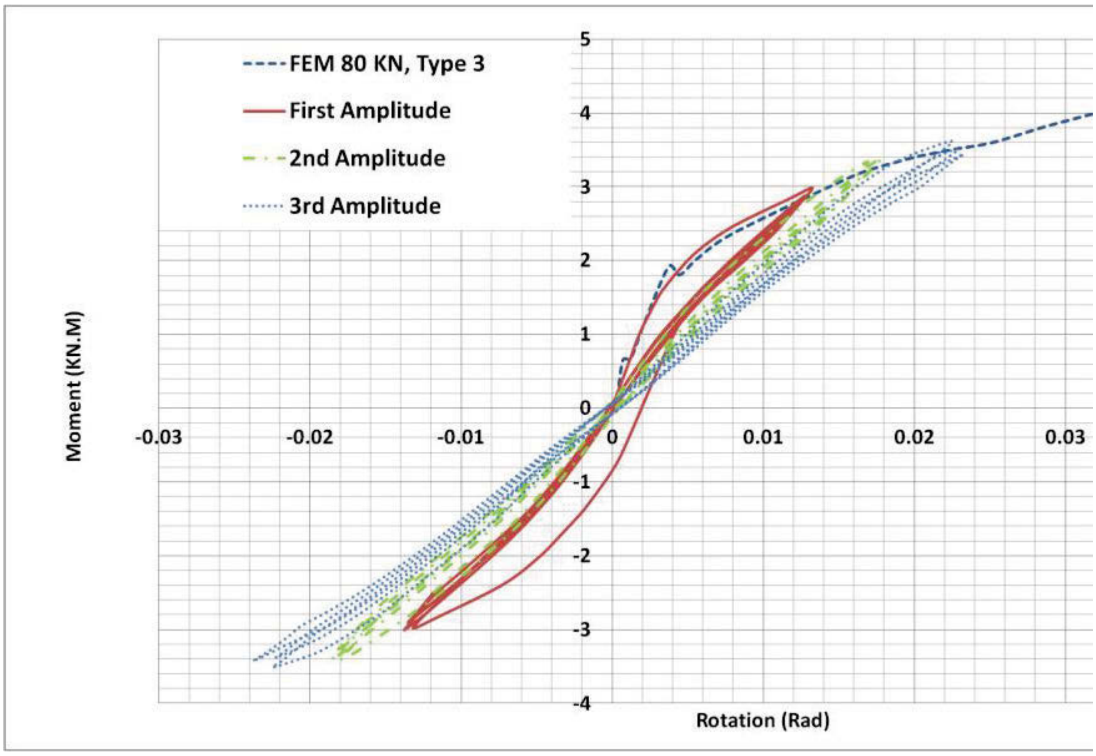

Figure 3.38: Cyclic curves of base plate type 3

[14] In Figure 3.40, the time on the horizontal axis refers to analysis steps used by the Abaqus FE software. Also connection type 3 was not modelled again under this load pattern as it was already investigated (See Figure 3.38)

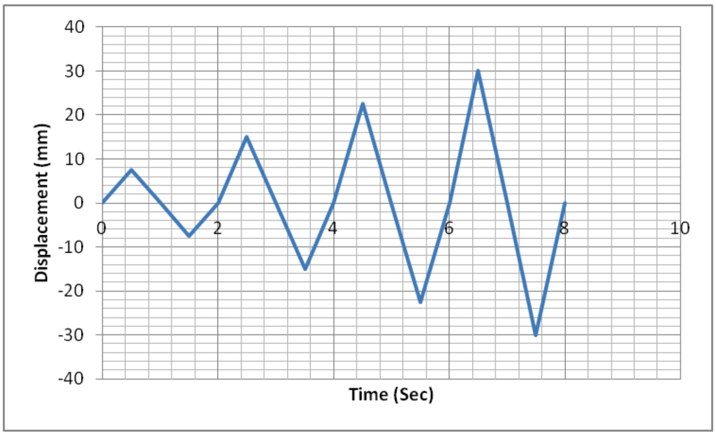

Figure 3.39: Cyclic load protocol

Figure 3.41 illustrates three different stiffness coefficients (K1-K3) that can be established for the base plate connections for the three cycles analysed. This shows that the stiffness of the base plate connection is very much dependant on the ultimate rotation of the base plate connections and, hence, the conservative value for the stiffness is the average stiffness which conservatively represents the base plate behaviour would be the average stiffness defined in section 3.6.1.

For seismic design, based on the equivalent static lateral force method (ESLF), it is recommended to apply the initial stiffness (secant stiffness) of the base plate for the modal analysis to obtain the fundamental period of vibration. This approach is justified since the structure is not subjected to significant horizontal forces and remains elastic unless it experiences a severe earthquake. However, for a nonlinear static analysis and design of the structure, an average stiffness (K_{avg}) based on the maximum rotation of the base plate should be applied. The base plate stiffness for seismic analysis can be obtained from equations 3-12 and 3-13 in section 3.6.1. Also a stability check should be performed by comparing the maximum rotation of the base plate against the ultimate rotation.

The following steps explain a rational method of modelling the base plate connections in seismic design of rack structures according to Equivalent Static Lateral Force method.

- Step 1. Calculate the fundamental period of vibration and the corresponding seismic actions by applying the secant rotational stiffness of the base plate connections from moment-rotation curve. However, if the moment-rotation curve of the base plate connection was not available, the connections can be conservatively[15] modelled as fully rigid.

- Step 2. Assume a reasonable ultimate rotation (between 0.01 to 0.02) and then calculate the corresponding average stiffness of the base plate (K_{avg}).
- Step 3. Perform both non-linear analysis and elastic buckling analysis of the structure under seismic forces obtained from Step 1 and with base plate stiffness of K_{avg}.
- Step 4. Check if the first level inter-storey drift is less than the assumed ultimate rotation of Step 1. If the first level inter-storey drift is less than the assumed ultimate rotation, it is deemed OK, otherwise, the system should be stiffened more and redo all the above steps.

3.7.1 Hysteretic Modelling of Base Plate Connections

To be able to perform the Non-Linear dynamic analysis of the structures, the moment rotation response of the base plate connections under cyclic loads was also modelled by Pivot cyclic model. The Pivot model as was discussed in Chapter 2, was first proposed by Dowell et al. (1998) to model the non-linear hysteretic behaviour of concrete structures. Pivot cyclic model is available in SAP 2000 software to model the hysteresis curves based on the observation that loading and unloading curves are directed towards specific points, known as pivot points. To define a Pivot model, "Two α parameters govern unloading; two β parameters locate the pivot points for reverse loading; and η determines the amount of degradation of the elastic slopes after plastic deformation" (see Figure 3.42) (Reyes, 2013).

[15] This is conservative as the period of vibration of stiffer structures are shorter and hence attracts more seismic forces.

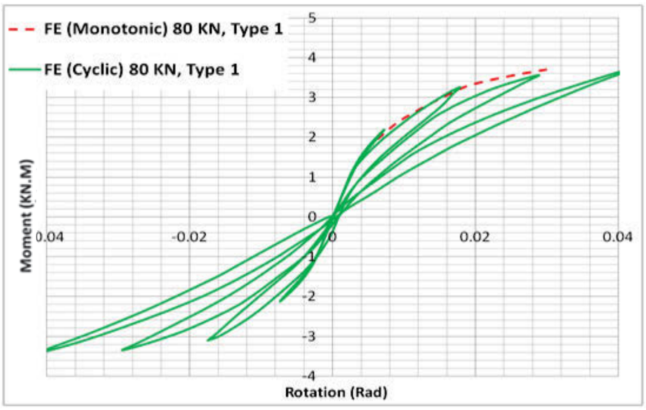

(a): Cyclic and monotonic curves of base plate type 1

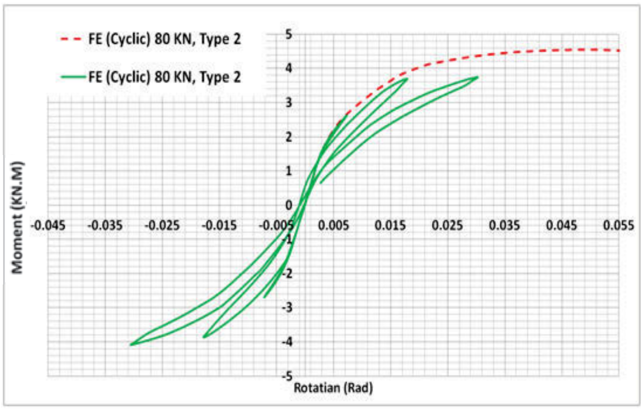

(b): Cyclic and monotonic curves of base plate type 2

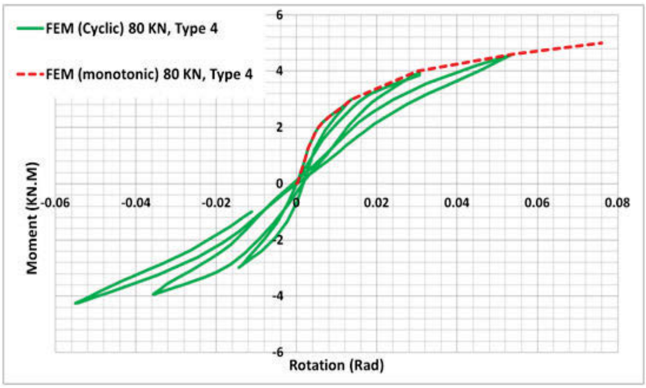

(c): Cyclic and monotonic curves of base plate type 4

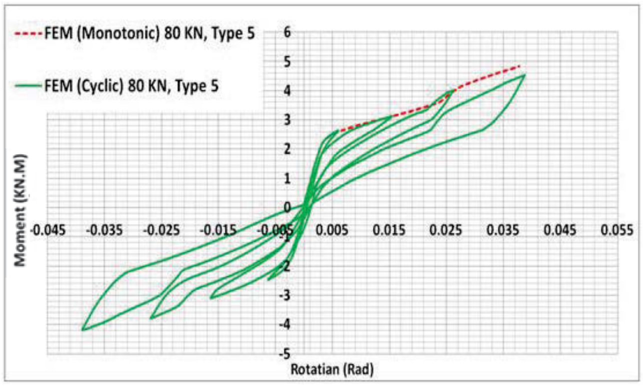

(d): Cyclic and monotonic curves of base plate type 5

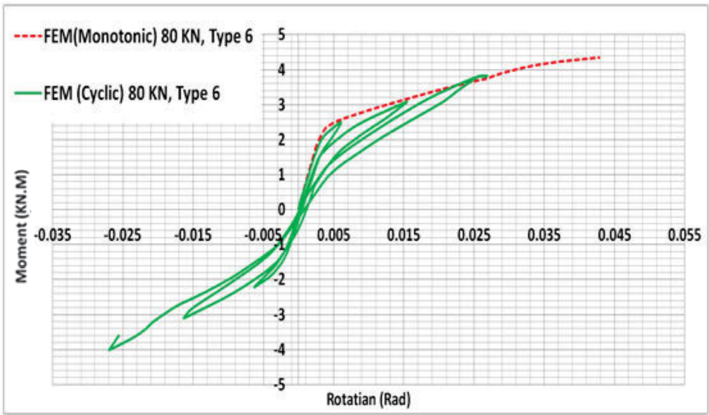

(d): Cyclic and monotonic curves of base plate type 6

Figure 3.40: Cyclic and monotonic curves of base plates

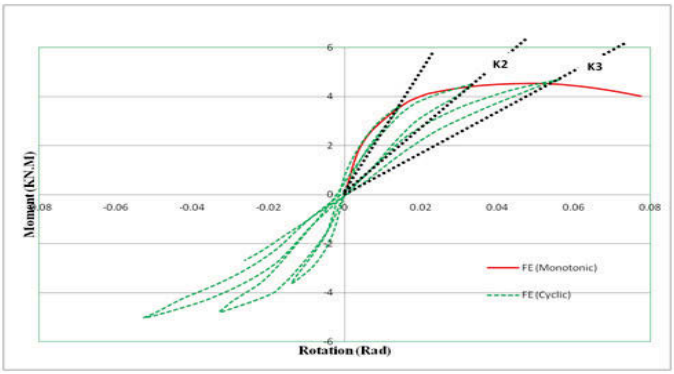

Figure 3.41: Different stiffness related to each cycle

A backbone curve is also needed to define the boundaries of the hysteresis loops. As all hysteresis curves show that the loading and reverse loadings pivot around the origin, then the hysteresis curves can be produced by using Pivot Cyclic Model when all “α” and “β” and the “η” factors are equal to zero. Multi-Linear monotonic moment rotation curve was used to define the backbone of the pivot model in SAP 2000 (see Figure 3.43).

Figure 3.44 (a to c) shows that a reasonable agreement is obtained between Pivot models from SAP 2000 and the results of an accurate Abaqus FE model of base plate type 1 at N = 80 kN.

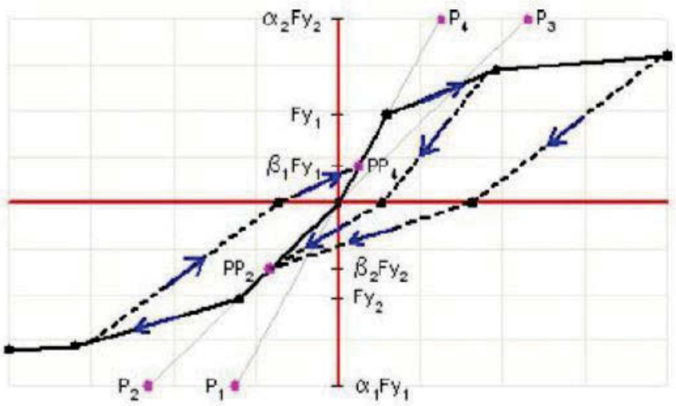

Figure 3.42: Pivot Model from SAP2000 User Manual.

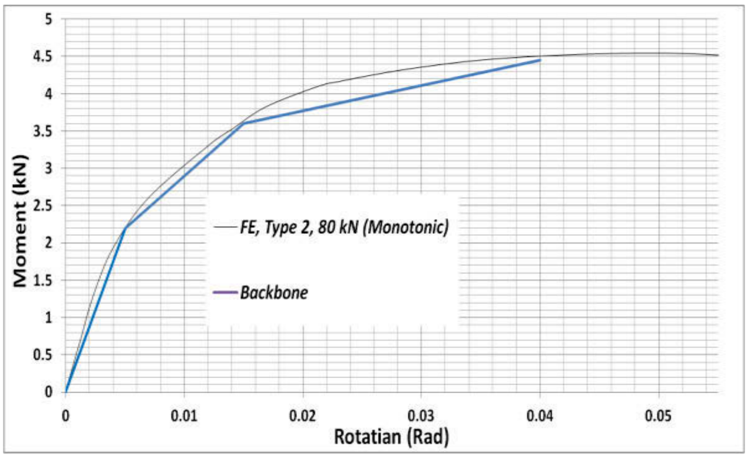

Figure 3.43: Multi Linear backbone definition in SAP 2000.

The proposed Pivot model can be used in more accurate analyses such as dynamic time history analysis to better understand the behaviour of a whole frame under seismic actions.

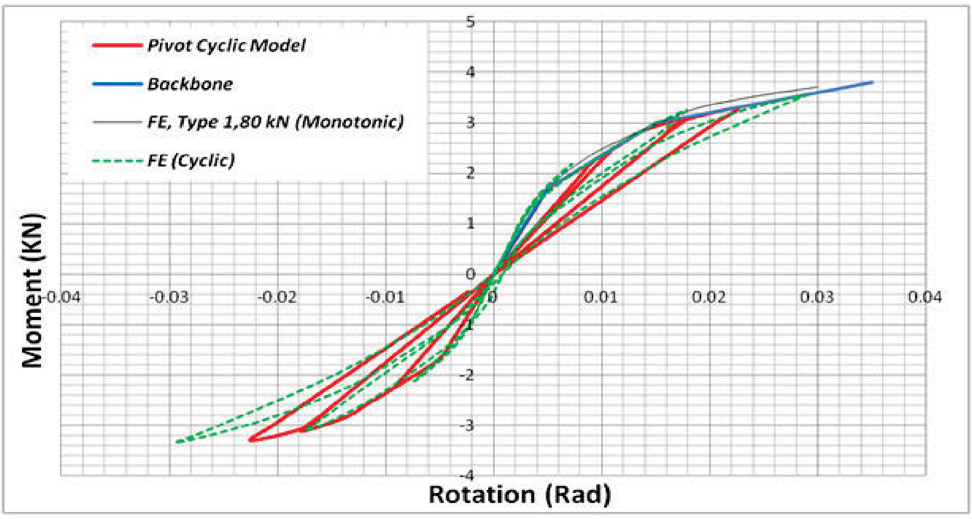

Figure 3.44 (a)

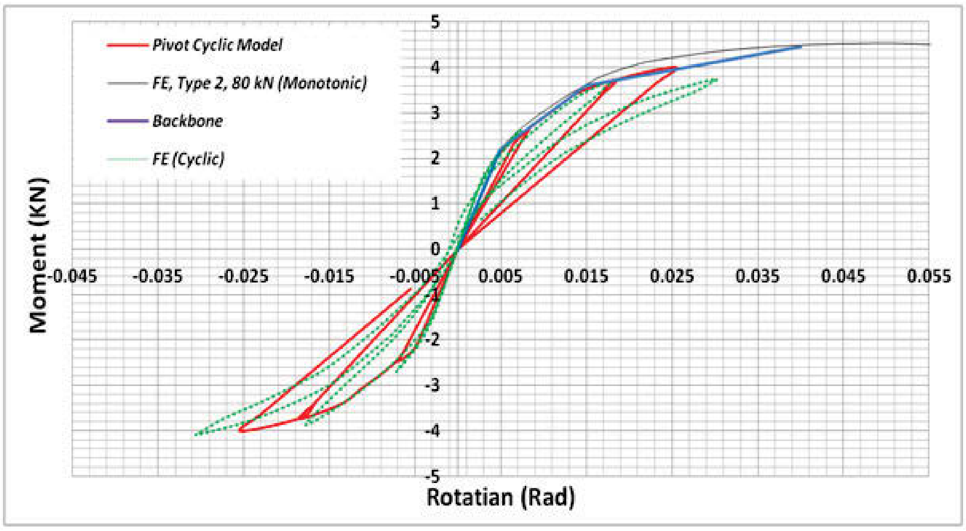

Figure 3.44 (b)

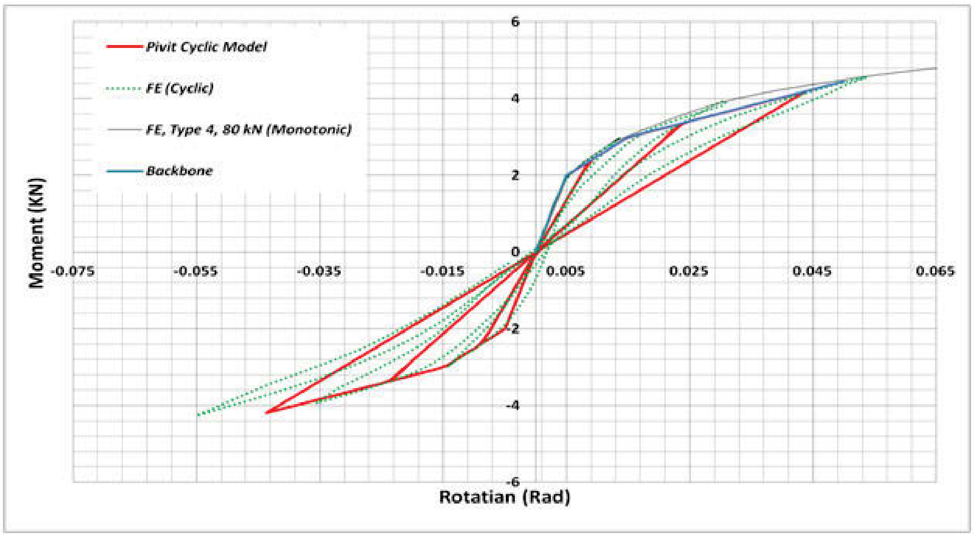

Figure 3.44 (c)

Figure 3.44: Comparison of FE cyclic results (ABAQUS) and pivot cyclic model (SAP 2000)

3.8 Behaviour of Base Plate Connections in Cross Aisle direction

When subjected to transverse loads the rack structure has as a relatively short period of vibration compared to down aisle moment frames. The transverse braced frame can be designed as a free standing cantilever truss. Due to the weight of pallets and the rack frame, both columns are subjected to compression at rest. It is possible that the uprights at one side of the braced frame will unload and reach a zero load level and then go into tension which can cause the base plate to yield in severe seismic situations. On the other hand, the uprights on the other side of the rack take higher compression force during a design level earthquake. The occurrence of yielding in the base plate due to uplift force is accompanied by reduction in the stiffness of the rack and consequently increasing lateral displacement which can lead to instability due to P-Delta effect. It is, therefore, important to investigate the post yield behaviour of the base plate connections under uplift forces.

Base plate connections can then be modelled as translational springs, as shown in Figure 3.45, to account for their uplift-displacement relation.

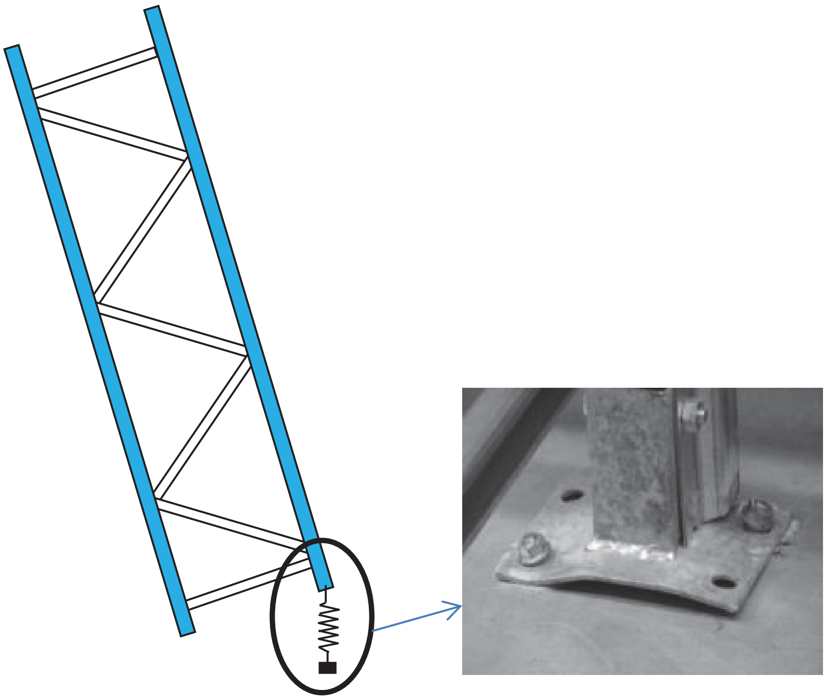

Figure 3.45: Base plate model in cross aisle direction

FE analyses were performed to investigate the uplift - displacement relations of base plate types 1, 5 and 6. The same FE models with different boundary conditions were used (see Figure 3.46). The rigid plate on top of the upright is restrained horizontally and is only allowed to move vertically. This condition is applied to model the effect of bracing and beams in restraining the upright movement in the two horizontal directions. Concrete base was modelled as a fully fixed support. Vertical cyclic load was imposed on the rigid plate on the upright head based on displacement control method.

The cyclic load pattern used for these analyses is shown in Figure 3.47.

Displacement was applied only upward as the base plate assembly cannot penetrate into the concrete base. Figure 3.48 (a to c) shows the cyclic Uplift-Displacement behaviour of the base plate connections. Significant cyclic deterioration is observed from the hysteresis curves.

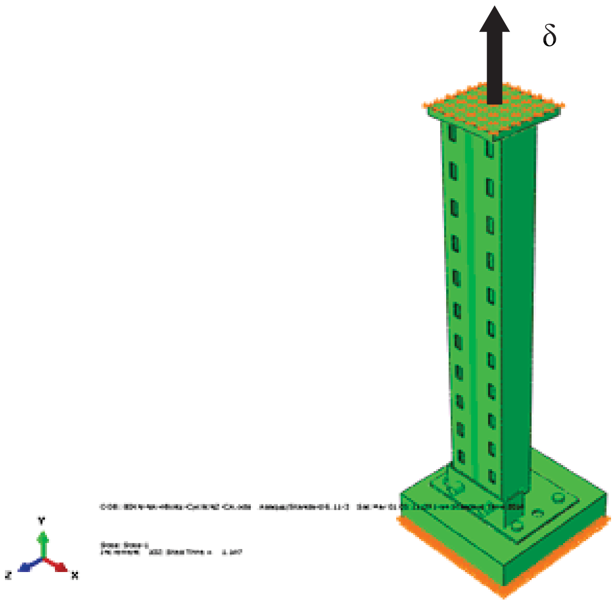

Figure 3.46: FE Base plate model under uplift

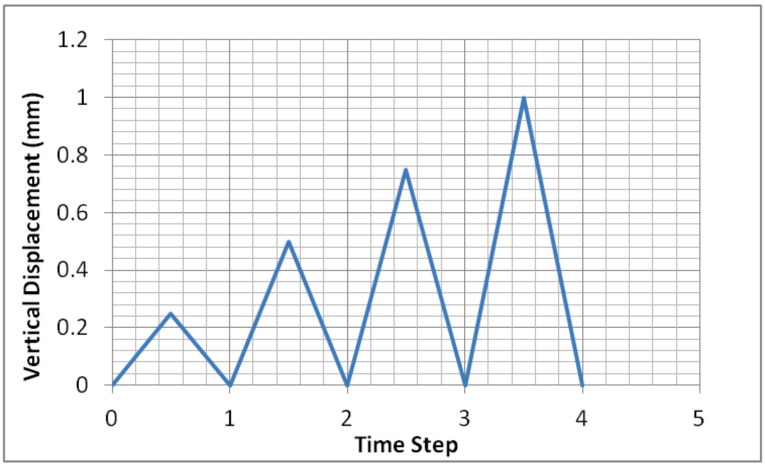

Figure 3.47: Cyclic load protocol

A vertical rigid motion occurs after each cycle leading to a small energy absorption capacity. This effect indicates that after consecutive cycles the base plate connection becomes ineffective under upward forces and can lift up easily, thereby, leading to a significant lateral displacement that can cause total instability. To avoid such instability under lateral seismic forces, it is recommended that no plastic reserve be considered for the base plate design under vertical forces.

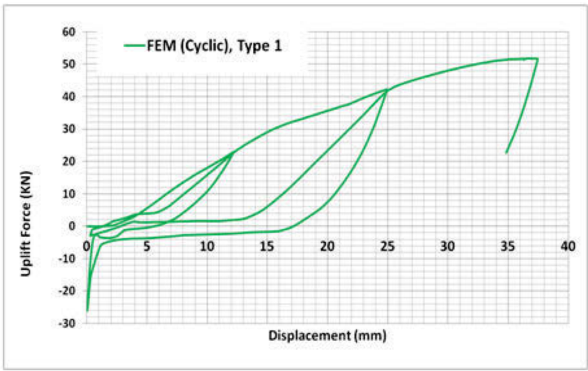

(a)
Cyclic Uplift-Displacement hysteresis curve of base plate Type1

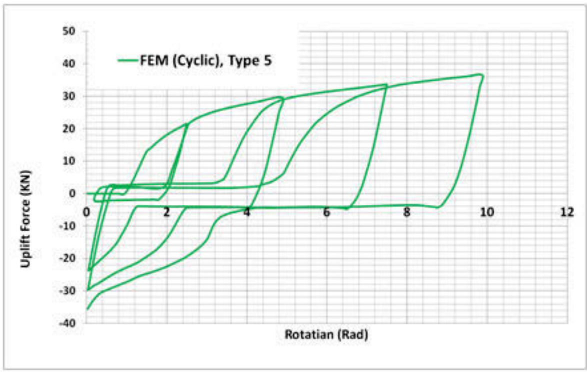

(b)
Cyclic Uplift-Displacement hysteresis curve of base plate type 5

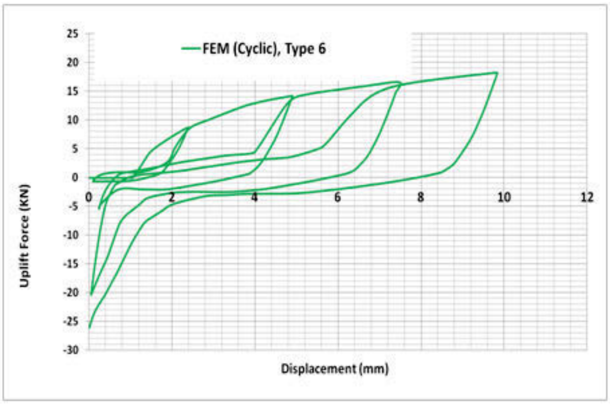

(c)
Cyclic Uplift-Displacement hysteresis curve of base plate type 6

Figure 3.48: Uplift-Displacement hysteresis Curves

3.9 Conclusions

This chapter presents the results of experimental and FE simulations of typical base plate connections used for industrial storage racks with 6 different floor anchoring and bracket to upstand configurations. The experimental results presented, provide moment rotation curves of the base plates for 5 different axial loads imposed on the upright. The experimental setup, models the same structural conditions stipulated in

EN 15512 (2009), but with an alternative test rig setup that overcomes some drawbacks of the test arrangement proposed in EN 15512 (2009). A theoretical stability analysis was performed to define the ultimate moment and rotation of the base plate connections. Using FE models that incorporate material, geometric and contact non-linearity, the base plates were analysed for both monotonic and cyclic loading. The results of the monotonic loading were compared and agreed well with available experimental results. An analytical analysis was also performed using yield line theory to obtain the structural capacity of the base plates.

The hysteresis moment rotation curves of the connections analysed indicated significant stiffness degradation under repeated cyclic loading for all the base plate types. This observation suggests that using monotonic moment rotation curves for seismic design may be unsafe and hence an alternate method of expressing the initial stiffness of base plates for seismic design of rack structures from monotonic experimental or numerical results was proposed.

A practical approach to simulate the cyclic response of base plate connections using a frame-analysis software with beam elements such as SAP 2000 was proposed. The approach involves a pivot model of the base plate connection which is derived from monotonic Moment-Rotation curve of the base plate. The Moment-Rotation curves of the base plates can be found experimentally, by detailed FE analysis or simply from the proposed analytical approach.

4. CHAPTER 4: MODELLING OF BRACING CONNECTIONS IN CROSS AISLE FRAMES

4.1 Introduction and literature review

Braced frame systems are used in cross aisle direction of rack structures to provide stiffness and stability in that direction. This chapter investigates the effect of connection flexibility of bracing members on the shear stiffness of cross aisle frames. Currently, there are two different approaches in obtaining the shear stiffness of a cross aisle frame. One approach refers to Timoshenko and Gere (1961) theoretical equation for deriving shear stiffness of built-up columns. The theoretical equation can easily consider the width-depth aspect ratio, large number of panels and different bracing arrangements. It can also be used in stability evaluation based on shear stiffness. RMI (2012) and AS 4084 (2012) accept Timoshenko and Gere (1961) theoretical formula to calculate the elastic buckling load "P_{cr}" for upright frames braced with diagonals. This approach can be useful for hot rolled structures in which deformation of the connection of the bracing members are negligible. Relatively few investigations have been carried out in the field of cold formed steel frames compared to the hot rolled frames. Another approach in racking specifications is to conduct an experimental test to determine the upright frame longitudinal shear stiffness. In the EN 15512 (2009) the proposed test set up is shown in Figure 4.1. This test set up was recommended by Sajja et al. (2006) to improve the earlier test method of FEM (1998). the Australian Standard AS 4084 (2012) was also updated based on Gilbert and Rasmussen (2012) who proposed an alternate test set up to account for both bending and shear effects. The test set up detail is shown Figure 4.2.

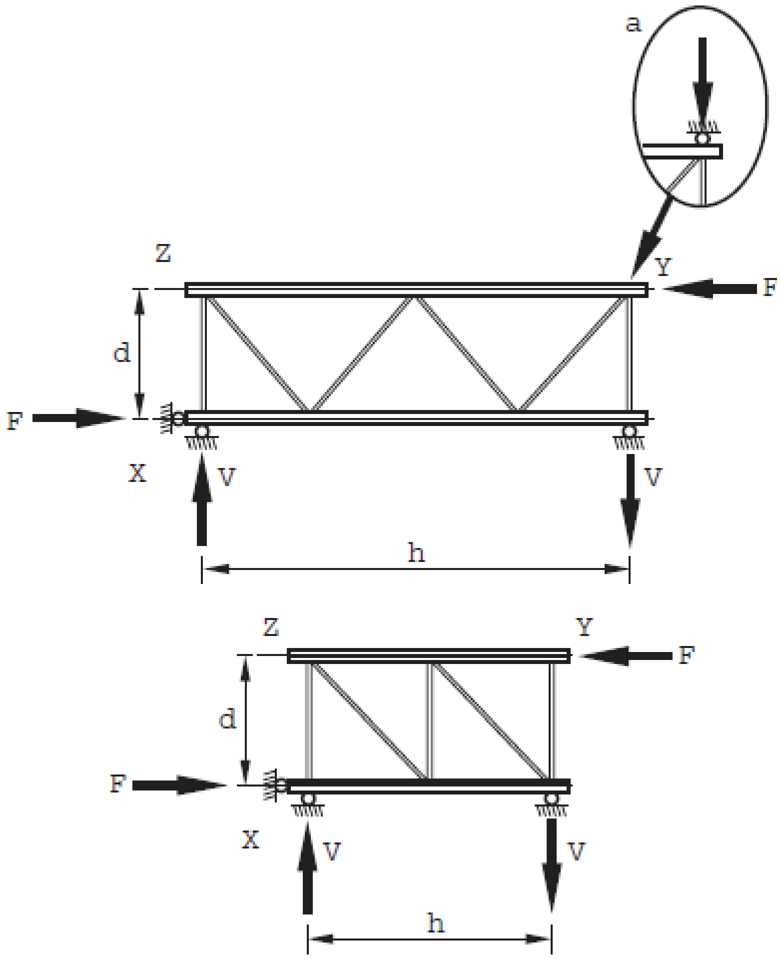

Figure 4.1. Upright frame test set up for measuring the shear stiffness of an upright frame (EN 15512, 2009, p. 112)

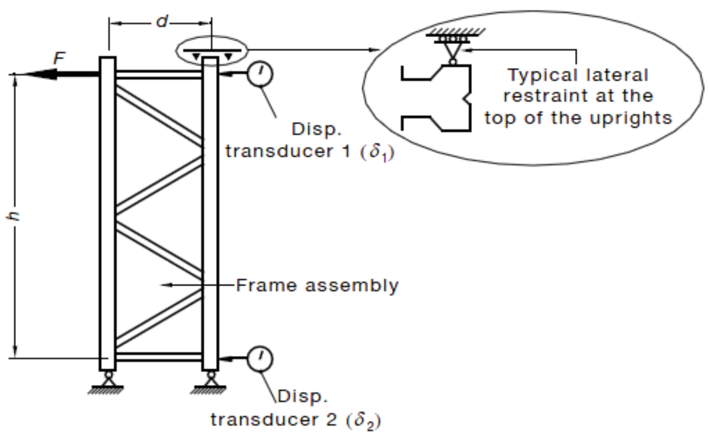

Figure 4.2. Upright frame test set up for measuring the combined shear and bending stiffness of an upright frame (AS 4084, 2012, p. 91)

However, the above experimental approach cannot accurately estimate the behaviour of the braced frames in high-rise rack structures as conducting experimental tests of a tall braced frame is not feasible. This highlights the need of an analytical approach to be used as an alternative method to the experimental approach.

Few investigations have been reported on the shear stiffness of steel storage rack upright frames consisting of cold-formed steel profiles and bolted connections. Rao et al. (2004) and Sajja et al. (2006, 2008) investigated experimentally and numerically the shear stiffness of rack upright frames whereby different numbers of panels, the aspect ratio of panels, upright sizes, restraints and bracing configurations were investigated. Rao et al. (2004) showed the inaccuracy of RMI (1997) specifications in the design of cross aisle braced frames by conducting an extensive experimental program including frames with different aspect ratios and different bracing arrangements. They reported that Timoshenko and Gere (1961) theory overestimates the shear stiffness by a factor of up to 20. Furthermore, their linear numerical models were not able to accurately match the experimental results.

Sajja and his colleagues (Sajja et al., 2008) aimed to focus on more details and components such as bolts which are the main parts connecting braced members to uprights. They developed simple linear FE models which could give them more realistic frame stiffness. Furthermore, by observing separately, each of the effects of the axial and flexural stiffness values of the components, they proved the importance of considering all these effects in the analysis. Gilbert et al. (2012) developed a FE model of the upright frame using ABAQUS and calibrated it against experimental shear stiffness results. The model was built in accordance with EN 15512 (2009) and the upright and bracing members were modelled by beam elements. The proposed FE model was calibrated against experimental results by reducing the cross sectional area of the bracing members by a factor. However, this factor is only an empirical factor and needs to be adopted by changes in sections and assembly method. They have highlighted the need to further investigate the rigidity and ductility of bolted brace to upright connections. As shown in Figure 4.3, the total horizontal displacement at the load point is the sum of shear deformation, rigid body deformation of the frame due to uplift of base plate connection and pure bending of the frame (see cases (a), (b) and (c), Figure 4.3) (Gilbert & Rasmussen, 2009). For high-rise racks the effect of bending deformation may become important.

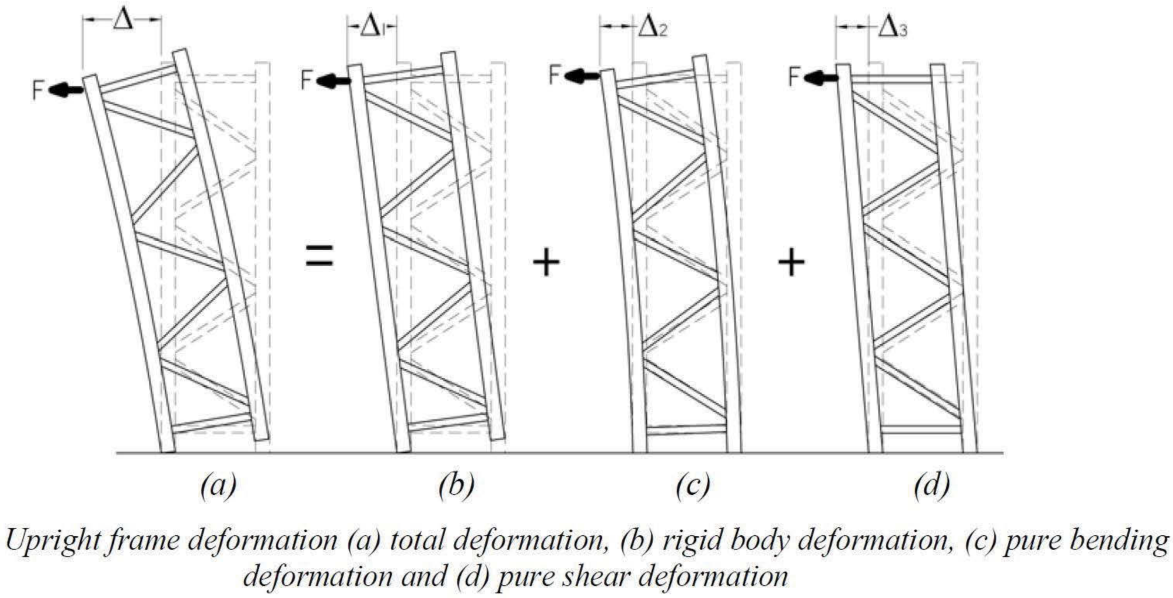

Figure 4.3 Shear frame displacement under transversal loads (Gilbert, 2010, p. 82)

4.2 Experimental Investigations

The test results of four upright frames were provided by Dexion Pty Ltd (Saleh 2012). The test setup of Figure 4.4 was based on the Australian Standard AS 4084 (2012) as depicted in Figure 4.5, whereby the distance (d) between uprights was measured from the front face of each upright. Each upright frame was placed in the test rig with its plane in a horizontal orientation. In the out-of-plane (vertical) direction, the frame was supported on skates that allowed the uprights to slide freely along their axes. To prevent the frame from rotating or moving in the horizontal plane, the end of one upright was pinned (point A) while the diagonally opposite end (point B) of the other upright was roller supported. During the test, a compressive force F was applied at point B by means of a hydraulic jack along the centroidal axis of the upright and the corresponding relative displacement between the uprights (δ) was determined. The required data was recorded using one load cell placed at point B between the jack and the upright, while two Linear Variable Displacement Transformers (LVDTs) were used to measure the displacements at points B and A along the axes of the uprights. The relative displacement (δ) was taken conservatively as the difference between the LVDT readings at A and B. During the test, the load was increased until a linear portion of the load deformation curve could be established (see Figure 4.6). Two further skates were also placed above the upright flanges at the free ends at points C and D. Failure modes observed in frames were consistently the tearing of the bolt hole of one of the bracing members, distortion of upright metal close to the holes and bolt deformation. Typical images of the locations of failure are shown in Figure 4.7.

Figure 4.4. Test rig

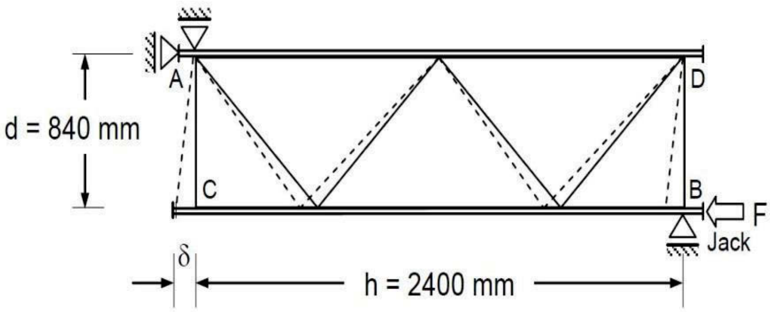

Figure 4.5. Schematic test setup

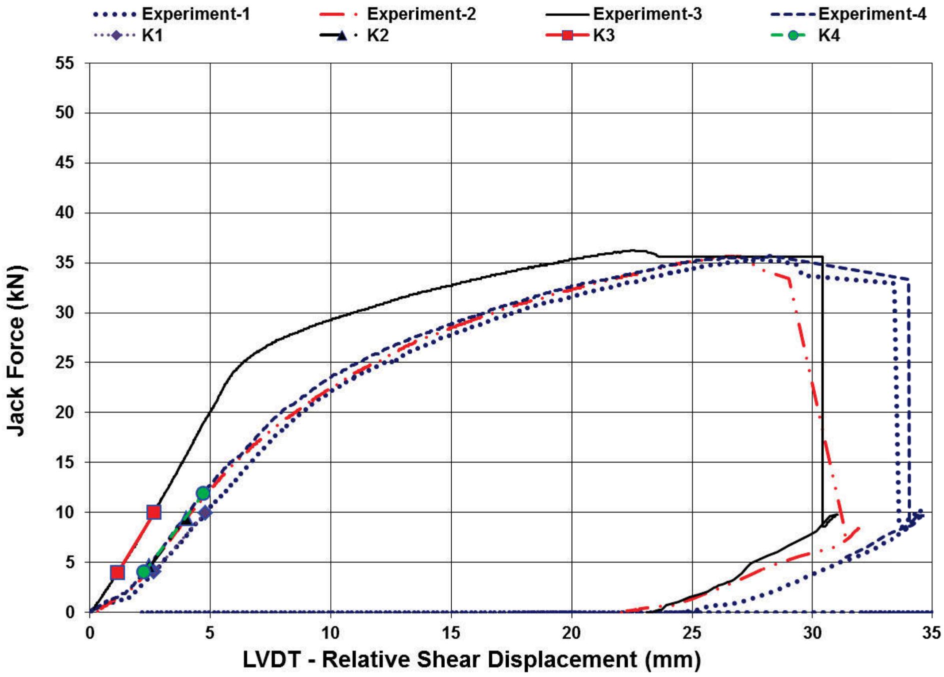

Figure 4.6. Experimental Force – Displacement curves

Figure 4.7. Failure modes (Tearing of the bracing member and bolt bending)

4.3 Numerical Investigation and comparison with experimental results

As part of this research, finite element models are used to simulate and study the behaviour of racking upright frames. In order for the FE models to provide a reliable simulation of the shear frames, the FE modelling approach was first validated by comparing the FE results against experimental data obtained from upright frames which had previously been tested at the University of Technology, Sydney (UTS)

(Saleh 2011). A simple 2D model was first developed using SAP 2000 by adopting beam elements to model upright and bracing members and the joints were modelled as hinged connections. As expected, a significant difference of stiffness was observed (See Table 4-1). It is noted that the model used in SAP 2000 performs according to Timoshenko's equations and, therefore, cannot represent the real cold formed system in which the flexibility and eccentricity of the bolted brace –upright connections are considered.

ABAQUS software was then used to simulate the experiment by applying the same load and boundary conditions. All FE models incorporated material, geometric and contact non-linearity in order to simulate the test conditions as accurately as possible. The material law of base plate assembly and upright were modelled using the Bi-Linear stress-strain relation. For the brace member and column sections 350 steel grade material was used with a yield stress of 350 MPa and an ultimate stress of 450 MPa. AIII steel material was considered for the anchor bolts with yield and ultimate stress values of 400 MPa and 600 MPa, respectively. Soft contact method, which simulates the local plastic deformation between bolt shaft and bolt hole, was used in modelling the behaviour normal to surfaces of bolts, bracing members and uprights, while a frictional interaction with a friction coefficient of 0.3 was used in tangential direction. The "softened" contact pressure-over closure relationships were used to model a soft, thin layer on one or both surfaces. The "softened" contact relationships are specified in terms of over closure (or clearance) versus contact pressure. A linear function with relatively high stiffness was defined for pressure - clearance between the contact surfaces of the model to simulate the hard contact condition. All members were modelled by hexahedral elements (8-node brick element) with an acceptable aspect ratio whereby two elements were generated through the thickness of the upright. The boundary conditions applied in the FE model are shown in Figure 4.8. The load was applied on a rigid plate based on displacement controlled method.

A reasonable agreement was observed between the numerical and experimental (Experiment-1) results as shown in Figure 4.9 and Table 4-1. As the model could not properly model the tearing of the steel at the connection area, the analysis was terminated prior to the experimental ultimate deformation.

A stiffness of 4.4 kN/mm was derived from the FE simulation which is quite close to the shear stiffness obtained from the test results. The deformed shape of the FE model is shown in Figure 4.10.

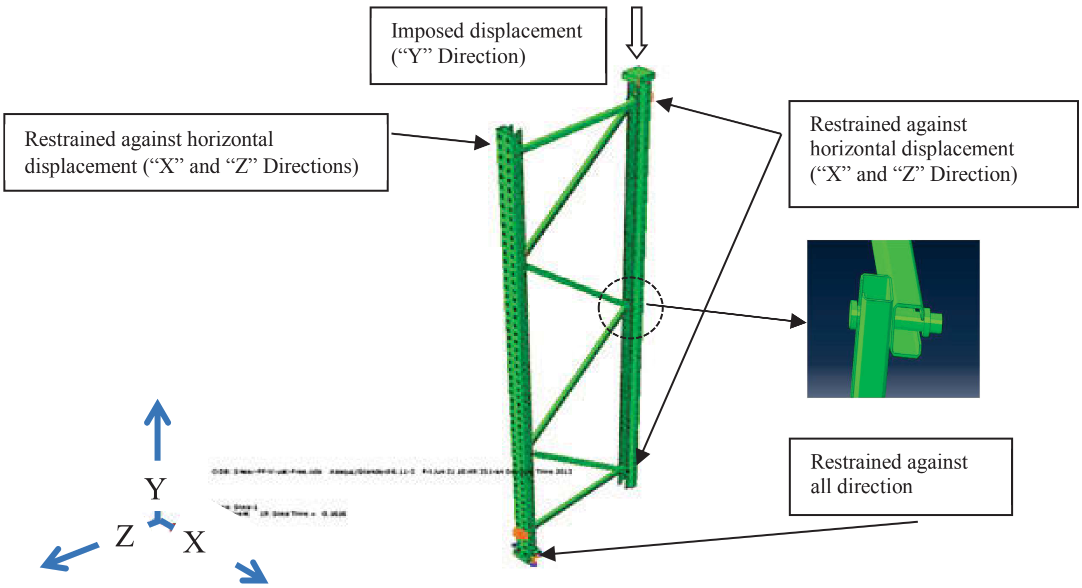

Figure 4.8. FE Model details

Table 4-1. SAP and ABAQUS models vs test results

Test / Simulation	Stiffness (kN/mm)	Error
Experiment	4.0	-
2D SAP 2000	23	475 %
3D ABAQUS	4.4	10 %

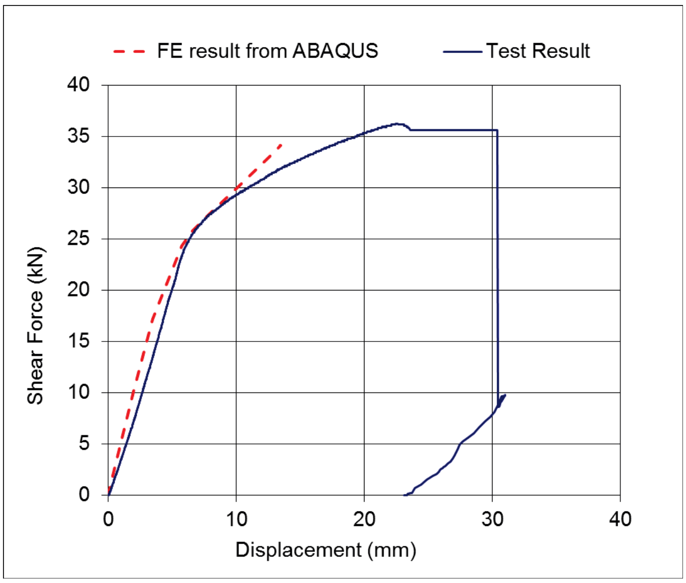

Figure 4.9. FE results vs. Experiment

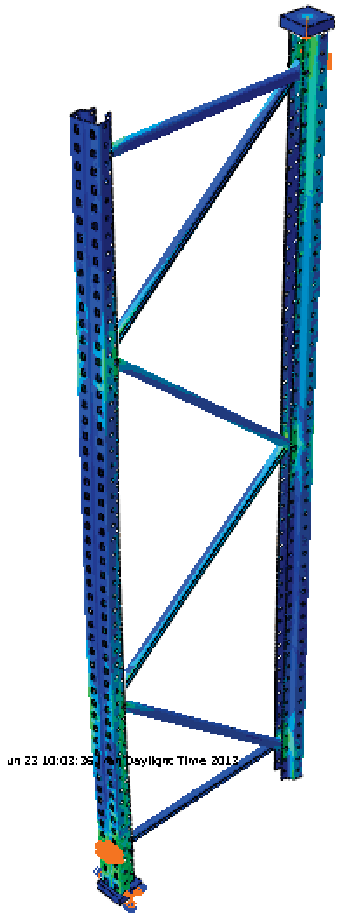

Figure 4.10. FE analysis result with von-mises stress contour

In shear frames used in industrial racking, bracing members may be arranged and bolted either back-to-back or front-to-front (lip to lip) as shown in Figure 4.11. Experimental results reported by Rao et al. (2004) indicate that the braced frames made up of lipped C channels assembled in ‘back to back’ arrangement show higher shear stiffness than those frames with ‘lip to lip’ (i.e. front to front) bracing arrangement.

The effect of each of those configurations on the behaviour, load carrying capacity and stability of the shear frame has been investigated in this chapter.

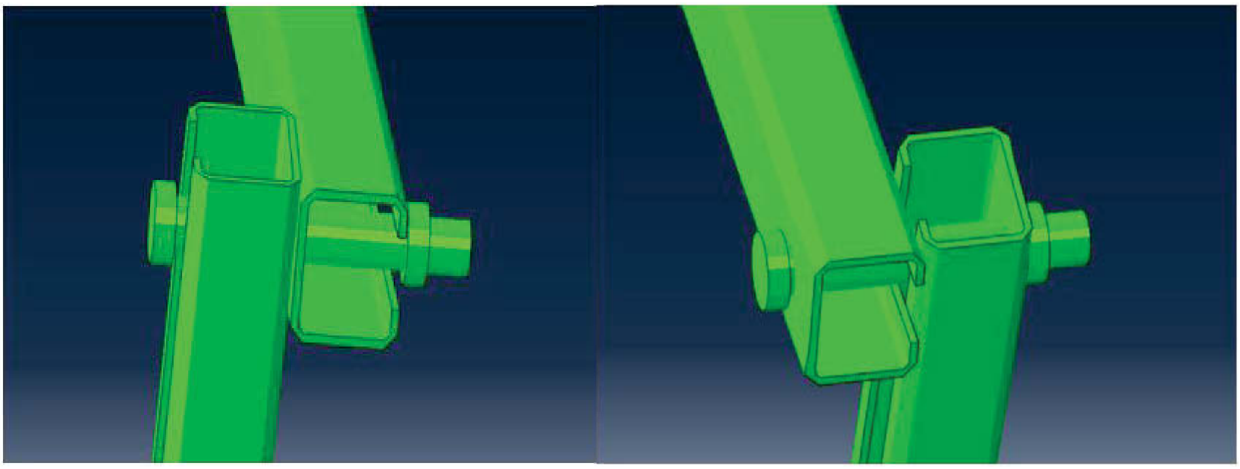

Figure 4.11. Different brace member arrangements in the open upright section

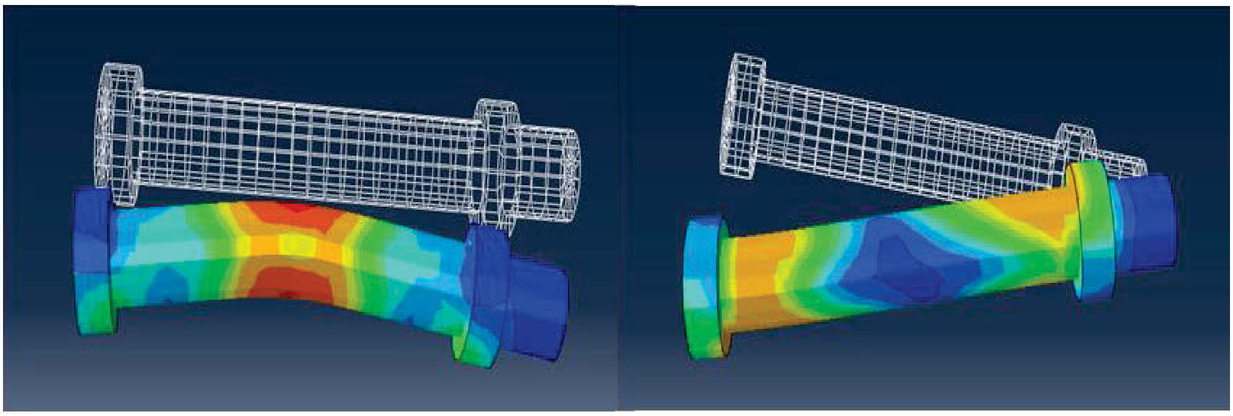

Figure 4.12. Bolts in different bracing arrangements at failure with von-mises stress contour

It was observed that these two arrangements can lead to a significantly different behaviour. As shown in Figure 4.12, for the back to back bracing arrangement the failure mode occurred as a result of a flexural plastic hinge in the middle of the bolt because of the bending due to the bracing member forces which act at the centre of the bolt. In contrast the failure mode in the front to front brace arrangement is by pure shear failure as the bracing member forces are applied near the ends of the bolt shaft, close to the upright flanges and hence bending action is insignificant. Also a larger shear force will be transferred to the upright holes by the bolts and as a consequence a larger bearing force is applied to the perforated sections. As the loads in the case of front to front brace arrangement are applied at bolt ends, they cause torsion in the upright. Furthermore, a significant torsion will be applied to the upright due to the joint eccentricity at joint location. The torsion induced by this bolting arrangement can have a destabilizing effect on the entire rack. The force deformation curves of these two different systems are provided in Figure 4.13. Figure 4.13 shows that the stiffness of the system with back to back bracing system is significantly higher than the stiffness of front to front system.

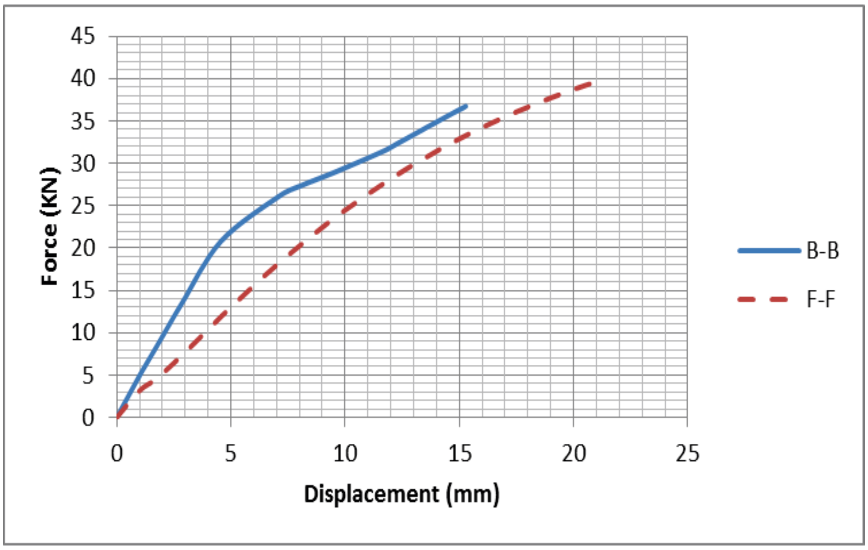

Figure 4.13. Back to back brace stiffness vs. front to front brace stiffness

4.4 Theoretical Analysis

4.4.1 Stiffness calculation

A theoretical analysis was carried out to reproduce the stiffness of the frame based on mathematical equations with simplifying assumptions. Bracing members, as individual components contributing to a composite joint stiffness, are considered in the analysis of the frame and are modelled to consider the effect of joints. The total joint stiffness can be found as a combination of bearing stiffness of the bolt, axial stiffness of brace member and upright and bolt bending stiffness.

By referring to the mathematical equation proposed by Zaharia and Dubina (2006) for bearing stiffness of bolted joints of cold formed steel trusses, the bearing stiffness is determined using equation 4-1.

$$K_{bearing} = 6.8 \frac{\sqrt{D}}{\frac{5}{t_b}+\frac{5}{t_u}-1} \ (kN/mm) \tag{4-1}$$

t_b: Brace member thickness

t_u: Upright member thickness

D: Nominal diameter of bolt

Bolts can be modelled as simply supported beams with the span equal to the distance between upright flanges. Therefore, the bolt stiffness can be approximated by the simply supported beam stiffness from the following equation (equation 4.2).

$$K_{bolt} = \frac{48\,E\,I_b}{l_b^3} \quad (KN/mm) \tag{4-2}$$

E: Elastic modulus

I_b: Moment of inertia of bolt section

L_b: Distance between flanges

Finally, the bolted connection can be simplified as an assembly of springs as shown in Figure 4.14 with a combined stiffness according to equation 4-3:

Figure 4.14. Theoretical model of the joint

$$K_{joint} = \frac{1}{\frac{1}{K_{bolt}} + \frac{1}{K_{bearing}}} \tag{4-3}$$

This stiffness is defined along the line of action of the force acting on the bolt connecting the bracing members and the upright and can be assumed to be directed along the upright axis as this is also the direction of the force resultant of the bracing members.

For practical applications, using frame analysis software, it would be convenient to derive a reduction factor that can be applied to the bracing member stiffness in order to take account of the flexibility of the joint in equation 4.3. The derivation is completed in two steps given below.

Firstly, with reference to Figure 4.15 and considering force and displacement components of the bracing members in direction of the upright, it can be shown that the effective joint stiffness along the bracing member axis, inclined at angle α is given by:

$$K'_{joint} = K_{joint} / \sin^2 \alpha \tag{4-4}$$

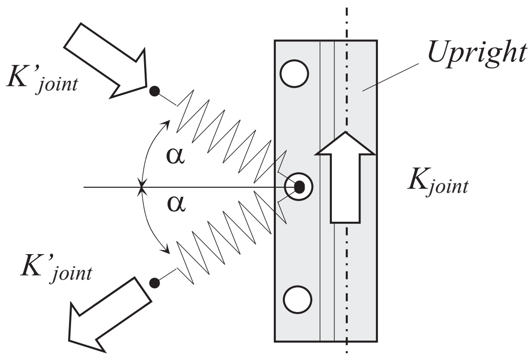

Figure 4.15. Joint stiffness component along brace

where "$K'\,joint$" is defined as the joint stiffness in the direction of the bracing member.

In the next step, the stiffness of the bracing member and the inclined joint stiffness of the bolted connections at both ends are assembled and lead, thereby, to an equivalent stiffness K^*_{member} that incorporates the connection flexibility as shown in Figure 4.16 and equation 4-5.

$$K^*_{member} = \beta K_{member} \tag{4-5}$$

$$\beta = \frac{1}{1 + \frac{2K_{member} \sin^2 \alpha}{K_{joint}}} \tag{4-6}$$

where:

In practical applications, the proposed reduction factor "β" of equation 4-6 can be used to reduce the cross sectional area of the bracing member prior to conducting structural analysis of a braced frame.

$$A^*_{bracing\ member} = \beta A_{bracing\ member} \tag{4-7}$$

A new 2D model was created in SAP 2000 by using beam elements with the new reduced bracing member cross sectional area ($A^*_{bracing\ member}$). As shown in Table 4-2 the error in predicting stiffness value decreased from 475% (refer to Table 4-1) to 28% (see Figure 4.17).

Braced frames such as those considered in this research with 'Force - Deformation' curves shown in Figure 4.6, typical values of 'K_{joint}' and 'K_{member}' are in the range of:

K_{joint} = 2 to 4 (kN/mm);

K_{member} = 25 to 30(kN/mm).

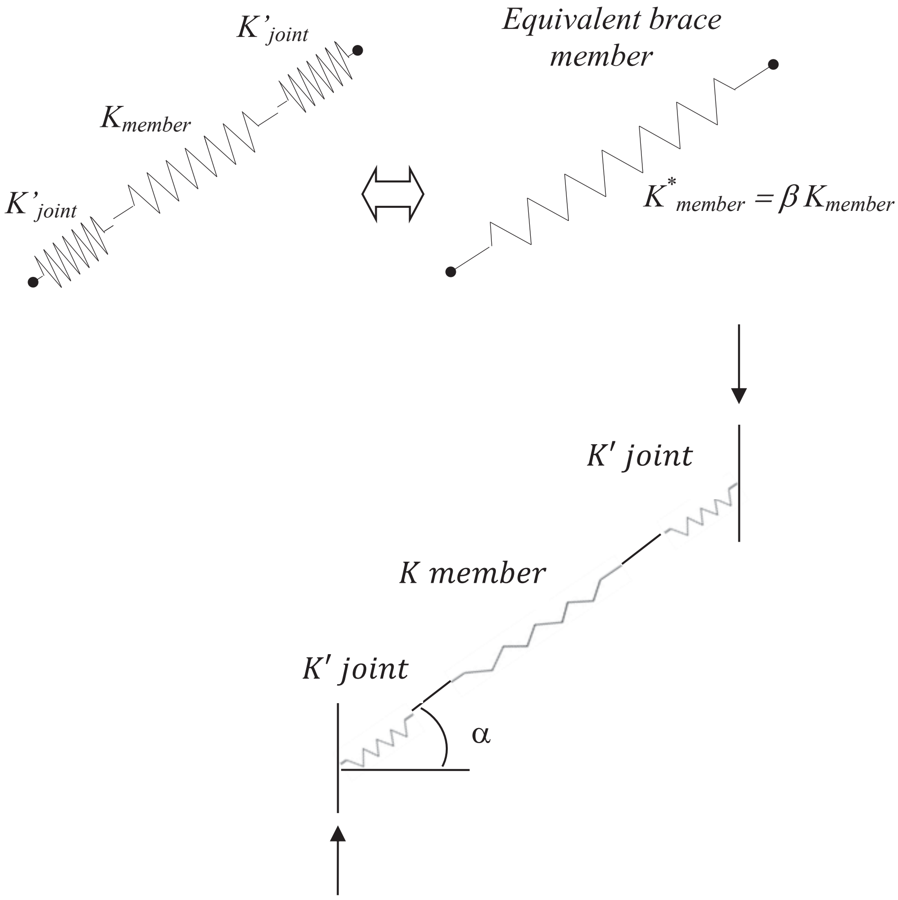

Figure 4.16. Equivalent models of a bolted brace member

It can be seen that "K_{joint}" is very much lower than" $\mathrm{K_{member}}$" and in such cases a rough estimate of the system stiffness can be calculated by using equation (4-8).

$$K_{Frame} = \frac{N_{brc}\,K_{joint}}{2} \tag{4-8}$$

N_{brc} : Number of bracing members in the upright frame

Table 4-2 shows an example comparing different methods in calculating the shear stiffness of an upright frame.

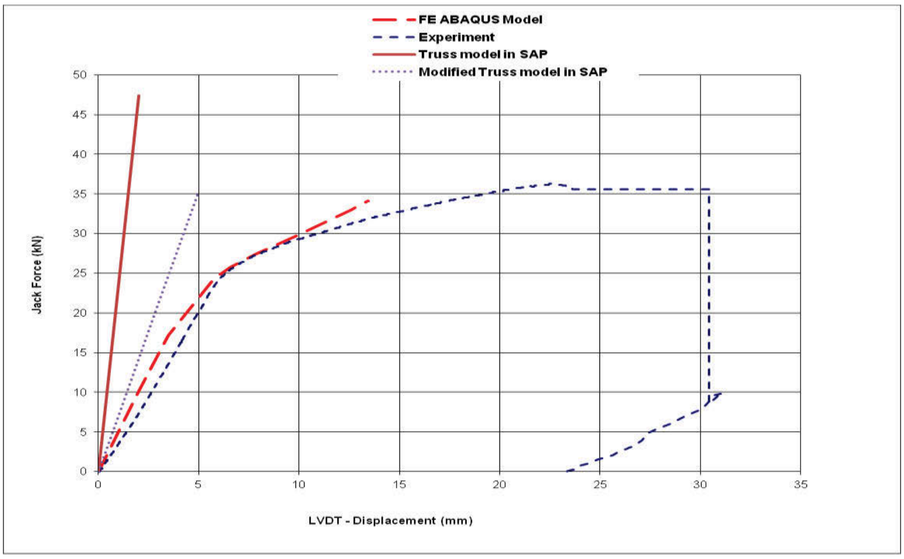

Figure 4.17. Numerical, analytical and experimental results of upright frame analysis

4.4.1.1 Stiffness calculation

Uplift-displacement behaviour of the base plate connections under the frame also plays a significant role in changing the stiffness of a full assembled frame including base plates as shown in Figure 4.18. The uplift-displacement of the base underneath the shear frame should, therefore, be considered using a spring system (with stiffness of K_{uplift}) which is connected to shear frame in series. Therefore, the total stiffness which should be used for stability analysis can be obtained from equation (4-9):

$$K_{Shear_{tot}} = \frac{1}{\frac{1}{K_{shear}} + \frac{1}{K_{uplift}}} \quad (4\text{-}9)$$

According to AS 4084:2012 and BS EN 15512:2009, equation 4-10 is used to find the transverse shear stiffness of an upright frame 'S_{ti}' from the stiffness obtained from the test results.

$$S_{ti} = \frac{K_{shear}\, d^2}{h} \quad (4\text{-}10)$$

h = length of the frame (see Figure 4.5)

d = distance between the centroidal axes of the upright sections (see Figure 4.5)

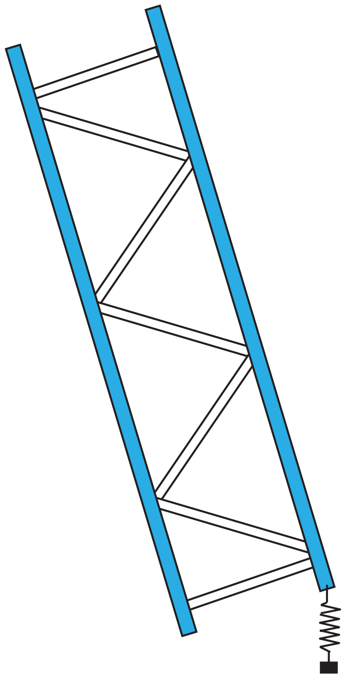

Figure 4.18. Base plate model in cross aisle direction

Table 4-2. Numerical, Analytical and Experimental results

Simulations	Stiffness (kN/mm)
3D ABAQUS	4.4
Rough estimation	4.2
Error (%) for the rough estimation	5

In the above table (Table 4-2), the values are for the tested braced frame configuration where number of brace members 'N_{brc}' is 4 and K_{joint} is equal to 2.1 kN/mm.

To consider the uplift-displacement stiffness of the base plate connections, $K_{Shear_{tot}}$ should replace K_{shear} in equation (4-10).

4.5 Conclusions

This chapter investigates the effect of connection flexibility on the behaviour of braced frame systems in cross aisle direction of rack structures under the influence of lateral forces. Experimental observations first revealed the common failure mode which took place in the connection areas. The experimental test condition was then simulated using ABAQUS software package and the FE model was verified by the test results. The FE analyses were further extended to investigate the effect of bracing arrangement in the frame.

An analytical method was developed to determine the shear stiffness of a bolted braced frame. The analytical model considers the effect of frame depth and height, bracing angle, bolt size and upright thickness.

5. CHAPTER 5 : SHAKE TABLE TESTS (EXPERIMENTAL STUDY)

5.1 Introduction and background

Although the seismic behaviour of normal structural systems has been well investigated and there are well established design philosophies proposed during the last decades, there is an urgent need to better understand the behaviour of cold formed storage rack structures under seismic and static loads (FEMA 460, 2005). Rack structures are mainly designed for seismic actions based on different structural codes, however, the only codes that are specific to rack systems are RMI (2012) and FEM seismic code (FEM 10.2.08, 2010).

A simple performance based design method is proposed in FEMA 460 (2005), however, the most popular strategy for seismic design of rack structures is the equivalent static method. It is obvious that the load pattern, seismic reduction factors and stiffness of the structure are key parameters for seismic design of structures based on the equivalent static method.

5.1.1 Christchurch earthquake collapse observations

To examine whether the rules in the codes are adequate and sufficiently accurate for rack systems, it is worth investigating their performance under severe seismic ground motions. For this reason a preliminary investigation was first carried out on the actual earthquake collapse of rack structures in New Zealand before conducting a series of shake table tests in the structural lab of the University of Technology, Sydney.

Being part of the Pacific Ring of Fire, which is geologically active, New Zealand has experienced many large earthquakes in the past. One of the recent large earthquakes was the 2010 Canterbury earthquake (also known as the Christchurch earthquake or Darfield earthquake) that rocked the south island of New Zealand with a magnitude 7.1 on the Richter scale. The examples of actual rack collapse that took place during the Christchurch earthquake is presented in order to study the mechanisms that lead to rack instability as a result of seismic events.

Different rack failure mechanisms are shown in Figure 5.1 to Figure 5.6. Some of the frames collapsed when a plastic hinge was formed in the uprights, which resulted in further drift and amplification of second order effects and thereby causing failure (see Figure 5.1). Allowing a plastic hinge to occur in the uprights also causes unacceptable failure mechanisms which contradict the recommendation of proposed seismic design methods. One possible reason of forming plastic hinges in uprights could be the tearing of upright metal due to deteriorative cyclic loads during the earthquake, which usually occurs in thinner uprights (less than 2 mm) (Reyes, 2013). This phenomenon was described in Chapter 2 of the current dissertation. Figure 5.2 also shows that despite the basic assumptions for seismic design and stability analysis “linear deformation of the frame” is not an accurate assumption and, therefore, not all the connections experience the same rotation along the frame height. Figure 5.3 shows that welding the beam at the top of the connector angle is not an optimised design for seismic applications as not all the hooks are in effect. As shown in Figure 5.3, the connection only relies on two hooks and the other three are not effective. By welding the beam at the middle of the connector a better rotational stiffness might be gained as more hooks become effective.

Figure 5.5 shows an example of a weld failure which ruptures the beam from beam end connector angle and this highlights the importance of the beam/connector weld design to avoid such brittle failure mode.

Figure 5.6 shows that inaccurate seismic design of the rack structures can also cause damage in the warehouse building by impacting its structural elements.

Another possible failure might take place in upright splices at mid storey height, which causes failure as shown in Figure 5.7. It seems using the splice connections close to the cross aisle frame bracing junction causes torsion and shear to the splice connections leading to upright instability if the splice is not designed properly.

Another key parameter is the base plate connection which can provide stiffness to the structure. Base plate failure can cause a significant displacement that can lead to collapse. Significant cyclic deterioration of the base plate strength and stiffness also contributes to the overall instability. The use of insufficient number of bolts in typical base plate connections can cause excessive rotation and failure of the base plate as shown in Figure 5.8 and Figure 5.9. This observation highlights the fact that, similar to beam to upright connections, base plate connections should be modelled as rotational springs for analysis and design of a rack system. Cyclic deterioration of such connections should also be considered, however, current racking codes and specifications are silent about cyclic features of the connections. The stiffness of the base plate connection will be changed during the earthquake because of its progressive damage under load reversals and this phenomenon was investigated by Firouzianhaji et al. (2014). This phenomenon significantly affects the forces in the uprights at the bottom levels.

A proper base plate design method is also needed in cross aisle direction where it can be damaged under uplift which leads to cross aisle frame failure and causing progressive collapse of all frames in the warehouse (see Figure 5.10).

It was observed that frames with a front to front bracing arrangement collapsed due to upright instability near the bracing connection. An example of such a collapsed frame is shown in Figure 5.11. The reason for such a failure could be that the front to front bracing arrangement induces significant torsion into the upright, however, no accurate method of buckling analysis is yet available to design the uprights under combined axial force, bending and torsion (refer to AS 4600, 2007).

Figure 5.12 shows an example of a rack collapse in an entire aisle because of distortional buckling of an upright at the bottom level. Such failures might be avoided by considering cyclic deterioration of the base plate connections in design as well as the torsion imposed by the frame bracing connections.

Figure 5.1: Down aisle mechanism

Figure 5.2: Down aisle mechanism

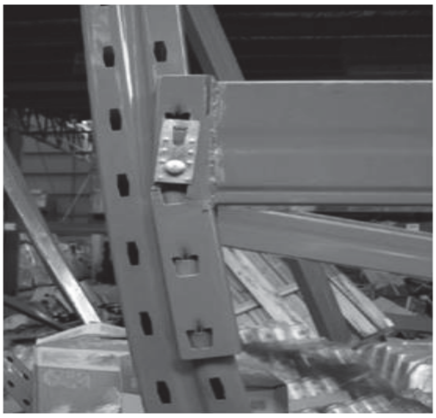

Figure 5.3. Connector bending during the 2011 magnitude-6.3 Christchurch Earthquake (Bruneau, Clifton, MacRae, Leon, & Fussell, 2011, p. 20)

Figure 5.4. Down aisle mechanism-connection failure during the 2010 magnitude-8.8 Chile Earthquake (adopted from: www.FEMA.gov)

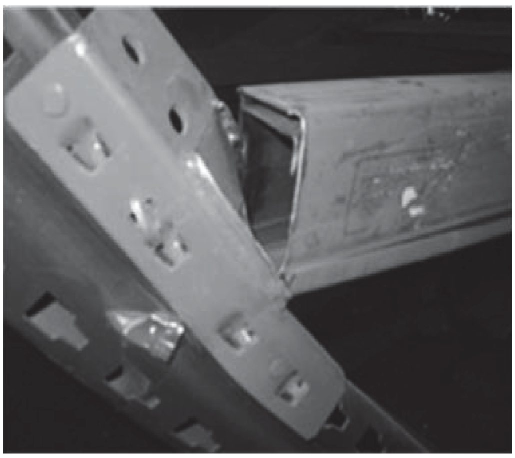

Figure 5.5: Down aisle mechanism- weld failure during the 2010 magnitude-8.8 Chile Earthquake (adopted from: www.FEMA.gov)

Figure 5.6: Down aisle mechanism-impacting the structural components

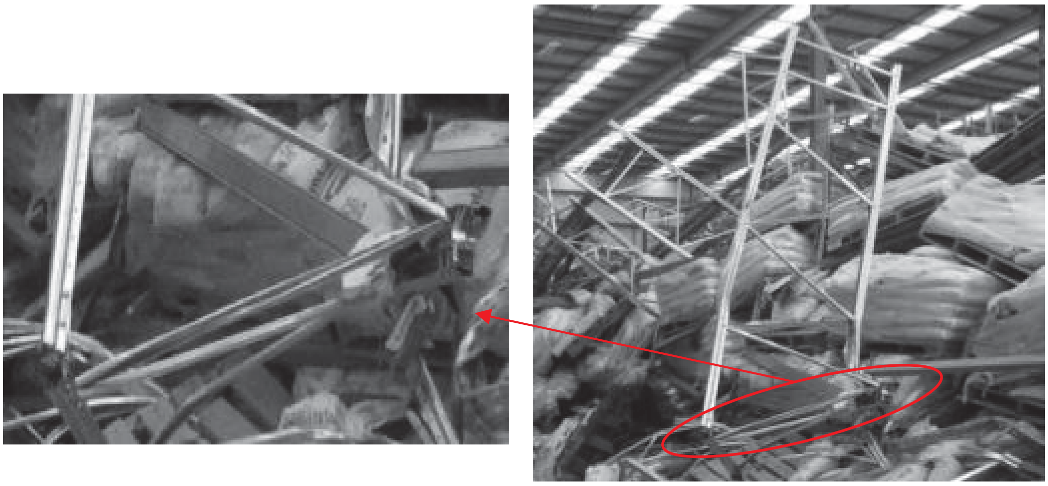

Figure 5.7: Cross aisle frame mechanism - upright splice failure

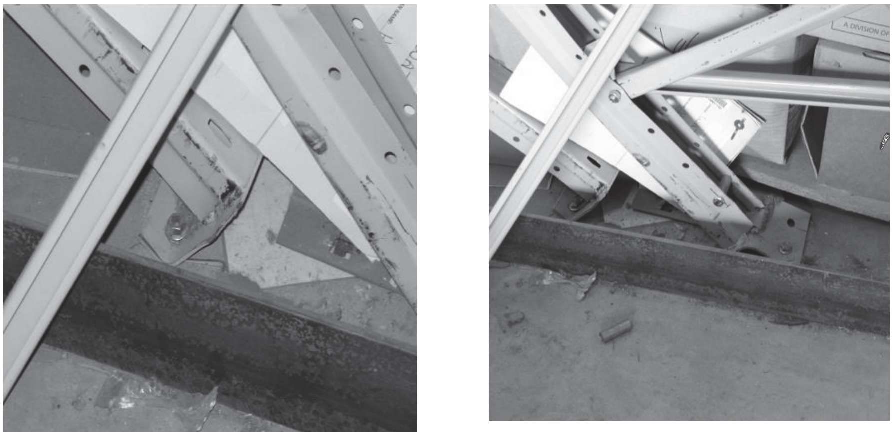

Figure 5.8: Base plate deterioration in cross aisle direction

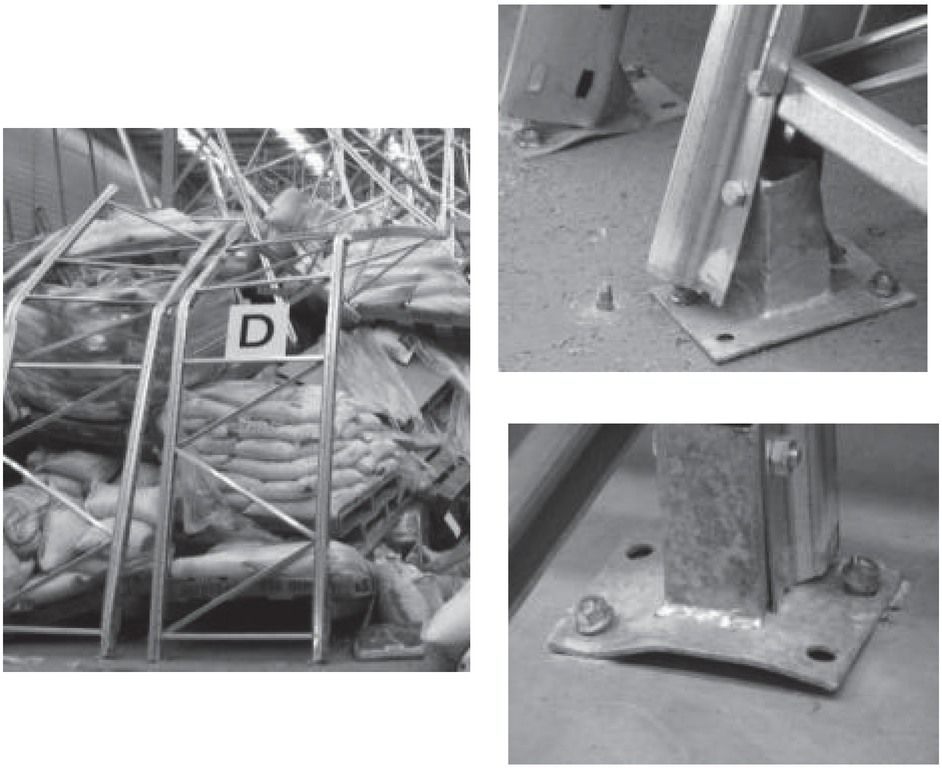

Figure 5.9: Base plate deterioration in down aisle direction

Figure 5.10: Progressive collapse of the entire system

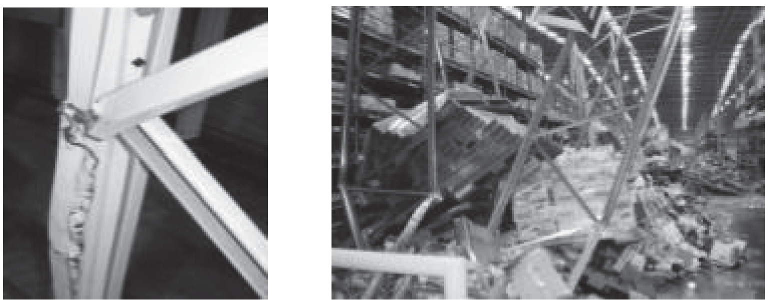

Figure 5.11: Frame instability because of twisting of the upright close to bracing junction

Figure 5.12. Entire rack instability due to distortional buckling of an upright at the bottom level

5.1.2 Theortical Background

"The amount and way that a structure deforms in an earthquake, termed its response, is a function of the strength and dynamic properties of the ground shaking, as well as those of the structures itself. The principal dynamic properties of importance to structural earthquake response are the structure's modal properties and its damping" (Hamburger, 2009, p. 9)

Structures can be modelled either as 'Single Degree of Freedom (SDOF)' or 'Multi Degree of Freedom (MDOF)' systems. A single degree of freedom model basically has all of its mass (m) concentrated at a single location attached to a vertical column with stiffness (k). The natural frequency of such a system can be calculated by Equation (5-1):

$$T = 2\pi\sqrt{\frac{m}{k}} \tag{5-1}$$

A three dimensional frame can be simplified by two SDOF models, each representing the frame's behaviour in the two orthogonal lateral directions. However, the vertical displacement and rotational degrees of freedom are ignored in a SDOF model.

A MDOF model has all of its masses in each storey lumped at a single point along the vertical axis of the column. MDOF models have one natural period, *Ti*, for each mode with a unique deformed shape, Φi, of free vibration, referred to as mode shape.

Figure 5.13 illustrates a MDOF model representing a three-storey building.

Applying the principle of superposition, the total displacement response of a MDOF structure can be expressed by equation (5-2).

$$u = \sum Y_n(t)\ \emptyset_n \qquad (5\text{-}2)$$

where, parameter '$\emptyset_n$' indicates the time-independent vector of the system's nth mode shape and '$Y_n(t)$' is a time varying displacement function.

The overall response of a MDOF system under a given dynamic action is mainly governed by the mode shape related to the mode with the lowest frequency (and longest period) which is called the 'fundamental' mode of vibration.

In any given natural vibration mode of a MDOF system, some of the masses move more than others causing a portion of the structure's total mass to be effectively excited during vibration. The effective or modal mass for mode i (M_i) is expressed by equation (5-3)

$$M_i = \frac{\left(\sum m_j \emptyset_{i,j}\right)^2}{\sum m_j \emptyset_{i,j}^2} \qquad (5\text{-}3)$$

where, mj is the lumped mass at degree of freedom j, and $\emptyset_{i,j}$ is the relative deformed shape displacement for mode i at degree of freedom j.

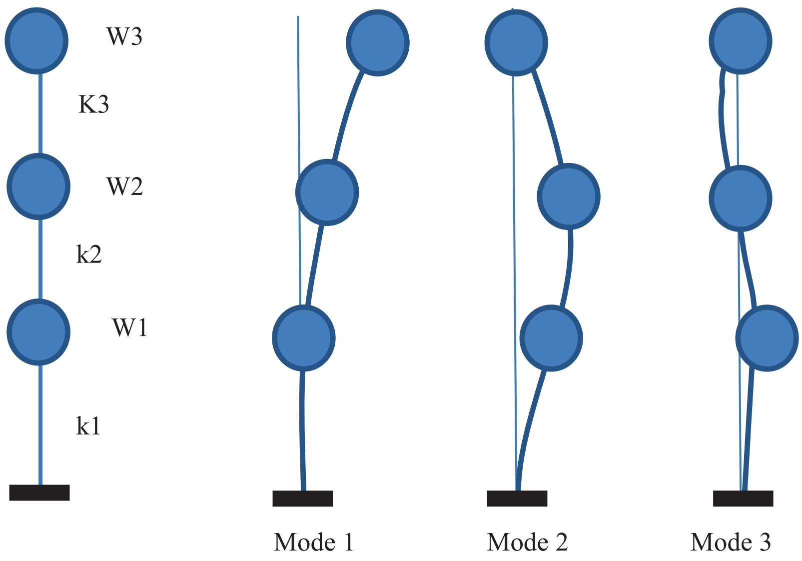

Figure 5.13. A MDOF Model representing a three-storey frame

Another important dynamic characteristic is the structure's damping that could be a significant source of energy dissipation.

"Sources of damping in buildings include energy dissipated by non-structural elements, frictional dissipation of energy at bolted connections and yielding of structural members." (Hamburger, 2009, p. 11) "It seems impossible to identify or describe, mathematically, each of these energy dissipation mechanisms in an actual building" (Carneiro, Jalali, Teixeira, & Tomás, 2006, p. 610).

This dynamic characteristic of structures and buildings is mathematically known as damping ratio (ξ) which is the normalised damping coefficient of the structure with respect to its critical damping.

Damping in a MDOF system is associated with each mode and can be expressed in a matrix form known as damping matrix.

According to the above paragraphs, the fundamental period of vibration, T, and its corresponding damping ratio are the main parameters to predict the behaviour of buildings and structures under given dynamic loads.

One of the few practical ways to determine the fundamental period of a structure and the damping ratio related to that period is by obtaining the frequency-response curve experimentally. This task can be done by performing a sinusoidal sweep testing (a forced vibration test) using sinusoidal (harmonic) loading over a range of frequencies. The concept is to excite the structure with harmonic loading such that at certain periods (periods of vibration, *Ti*) the structure experiences resonance. Damping ratios corresponding to each frequency of vibration can be determined by using half power band method as displayed in Figure 5.14.

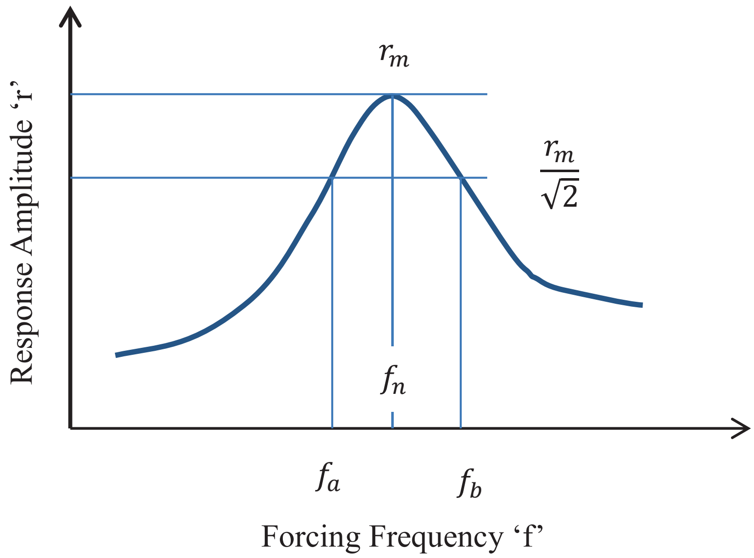

Figure 5.14. Evaluating damping from frequency-response curve (Chopra, 1995, p. 79)

The damping ratio can be calculated by equation 5.4;

$$\zeta\,(\%) = \frac{f_b - f_a}{2f_n} \tag{5-4}$$

where:

f_n is the forcing frequency at resonance and f_a and f_b are the calculated frequencies at a response amplitude of '$1/\sqrt{2}$' of the peak response amplitude (Chopra, 1995).

It is also possible to determine the damping ratio of a structural system from its free vibration peaks following a method known as "Logarithmic Decrement" which is a well established method (Clough and Penzien,1993). The seismic behaviour of typical structural systems can be fairly predicted by knowing the main characteristics of structures as mentioned above, however, full scaled shake table tests are the most direct and accurate way to assess the seismic behaviour. Unfortunately, this kind of testing procedure is very expensive and time consuming compared with other static tests and hence very limited shake table tests have been conducted on rack structures so far.

The first shake-table studies reported on storage racks was conducted at the University of California, Berkeley and was reported by Chen, Scholl and Blume (1980_a and 1980_b and 1981). The test was performed on a 400 square feet (≈ 36 square meters) shake-table. Four types of full-scale industrial steel storage racks were subjected to scaled ground motions of 1940 El Centro and 1966 Parkfield earthquakes. The types of storage racks tested were: single standard pallet racks, back-to-back pallet racks, drive-in (Drive-through) racks, and stacker racks. The fundamental periods of vibration ranged from 2-3 sec for the down aisle direction and 0.5-1.0 sec in the cross-aisle direction. The first mode damping ratios were much larger in the down-aisle direction (in the order of 3 to 9 percent of critical) than in the cross-aisle direction (0.5 to 3 percent of critical). It was also observed that the ductility and energy dissipation capacity of the racks were much larger in the down-aisle, moment resisting frame direction, than in the cross-aisle, braced frame direction. Also the shake table tests proved that the second order (P-delta) effects contributed significantly to the response of the racks in the down-aisle direction.

Five different pallet racks loaded with real merchandise were tested by Filiatrault et al. (2006), on a uni-axial shaking table under a ground motion recorded during 1994 Northridge earthquake in California. Tests were conducted in both cross aisle and down aisle directions. Again the ductility and energy dissipation capacity of the frame was significantly more in the down-aisle direction than in the cross-aisle direction. The fundamental periods of vibration were around 1.4 sec in the down-aisle direction and 0.6 in the cross-aisle direction.

Rosin et al. (2009) conducted shaking table tests on four steel pallet racks loaded by concrete blocks to simulate pallet loads. Their experimental results proved that eccentric bracing configurations can lead to a significant torsional response. The authors stressed the importance of a regular configuration of bracing systems.

A comprehensive shake table program was conducted at the University of Buffalo on four different steel storage pallet rack configurations including racking system with bolted beam-to-upright connections (Filiatrault and Wanitkorkul, 2004). All tests were performed in down aisle directions.

The effect of beam to upright connections on the behaviour of the moment frame in down aisle direction was investigated and very ductile behaviour was observed in the down-aisle direction with inter-storey drifts of greater than 7%.

As mentioned, only a few full scale shake table tests were reported in the literature and hence the lack of sufficient experimental test results on different racking systems provides a need for further experimental and numerical studies. In this study an experimental investigation as well as numerical modelling was carried out. This chapter presents the experimental set up and the test results and the next chapter presents the Finite Element simulation of the experimental studies undertaken.

5.2 Experimental Investigation

This study was conducted in two stages. In the first stage, a two-storey two-bay rack frame was shaken by low intensity records of both "El-Centro" (1940) and "North-Ridge" (1994) earthquakes. Also in order to find the fundamental period and damping ratio of the system, both forced and free vibration tests were carried out. The main objective of the first stage of the test was to verify the key assumptions made in the numerical FE model which was used to design the second stage of the tests. As running the full scaled shake table tests under higher intensity records falls in the category of high risk experimental tests, a comprehensive investigation was required before designing and conducting the tests. For this reason, the test condition was simulated by FE modelling to find the key parameters of 'overall over turning moment' and 'top level displacement' and to check them against the maximum allowable values of the shaking table device.

Figure 5.15, Figure 5.16 and Figure 5.17 show a schematic view of the test set up and the position of LVDT's and accelerometers.

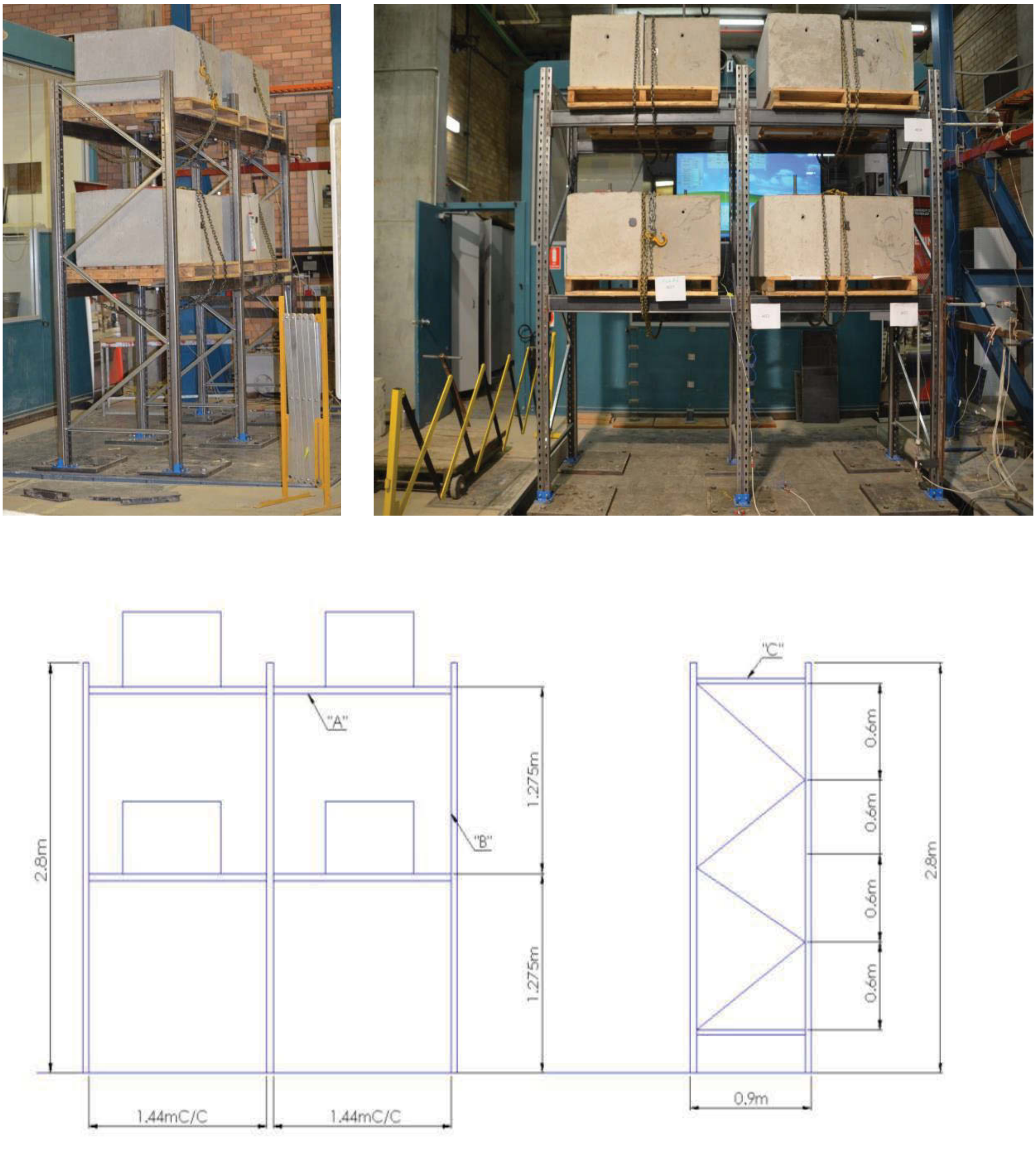

Figure 5.15. Test set up, Schematic views and dimensions of Down Aisle frame (on the left) and Cross Aisle frame (on the right)

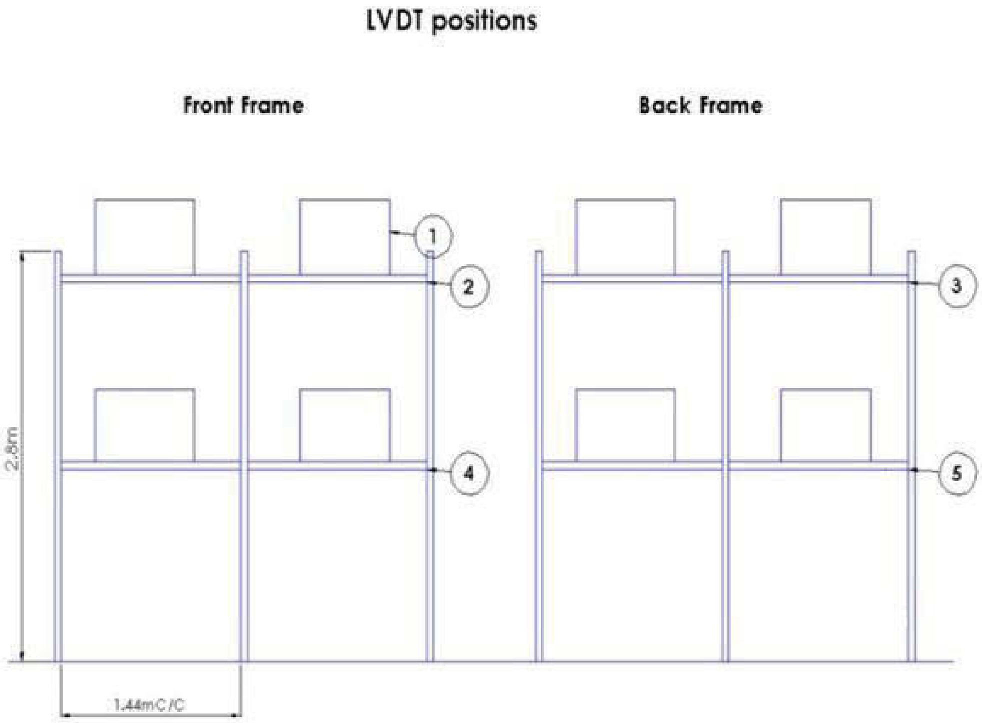

Figure 5.16. Location of position sensors (LVDT's)

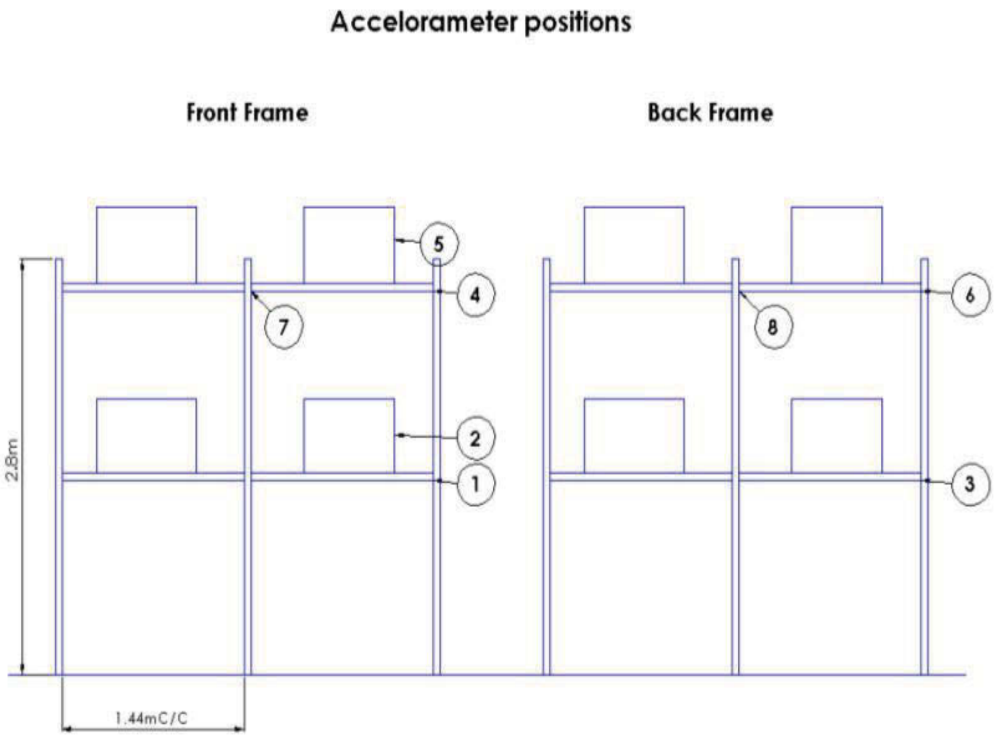

Figure 5.17. Location of accelerometers

Eight accelerometers and five displacement transducers (LVDT) were used to record the response of each rack specimen. Six accelerometers were attached to the frame and the rest to the blocks to measure the accelerations. Four LVDTs were recording the displacements of rack frames and one measuring the displacement of a typical pallet. Figure 5.18 and Figure 5.19 show a typical accelerometer and LVDT, respectively.

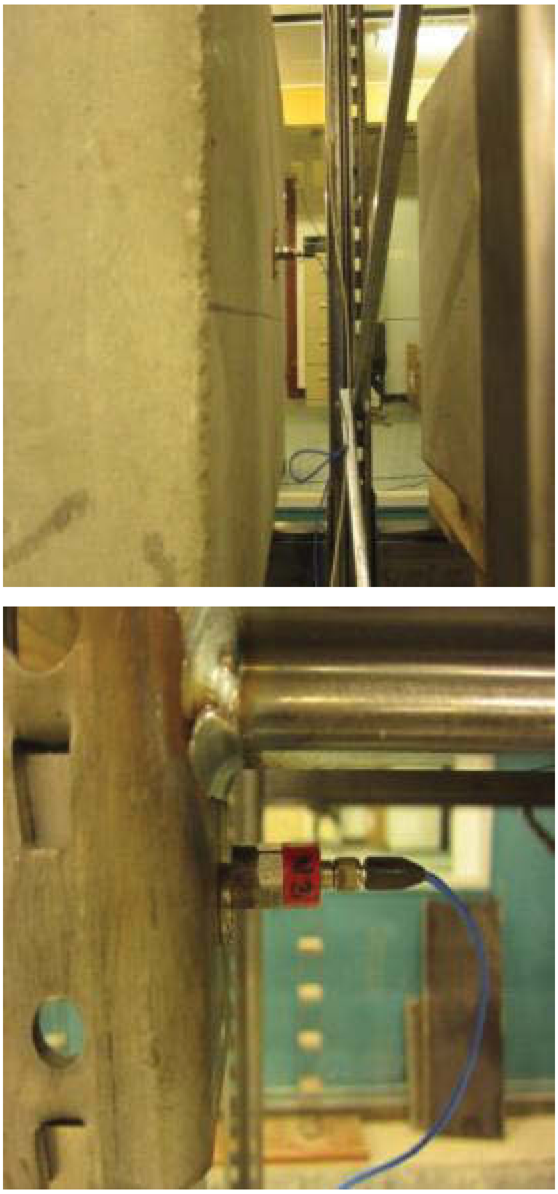

Figure 5.18. a) Accelerometer attached to the block b) Accelerometer attached to the frame

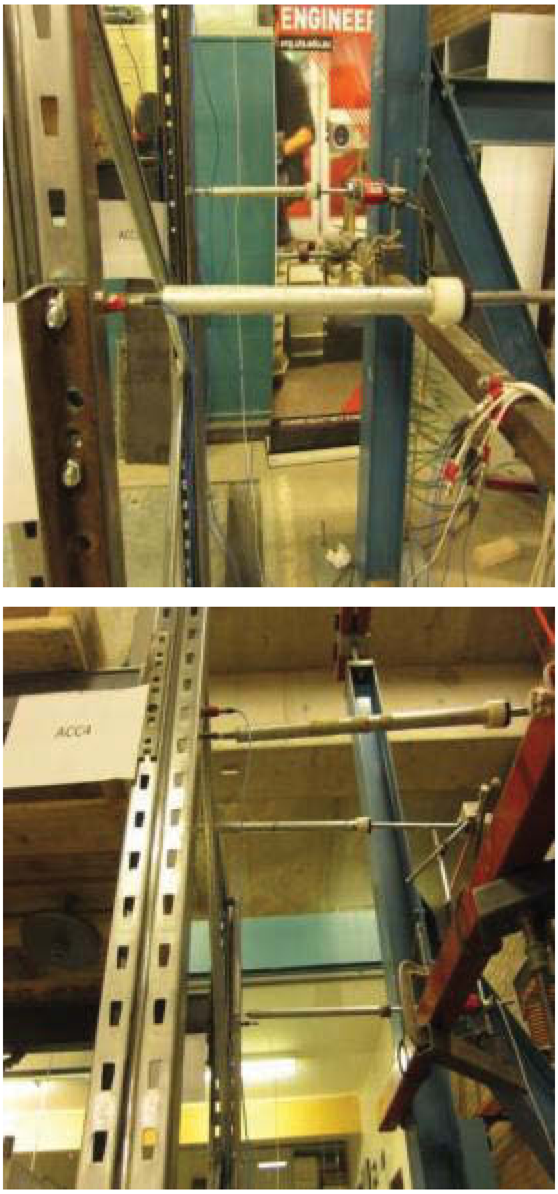

Figure 5.19. a) LVDT attached to the frame b) LVDT attached to the block

Details of different sections A, B and C, as shown in Figure 5.15, are presented in Table 5-1.

Table 5-1. Section profiles

Section		*Length(mm)*	*Area(mm^2)*	*Ix(mm^4)*	*Iy(mm^4)*
A	*Box105×50-1.6 mm*	*1350*	*597*	*1,023,099*	*237,210*
B	*90 Upright 2.35 mm*	*2800*	*578.6*	*700,217*	*325,825*
C	*25 × 30 × 1.8 (⊏ Channel)*	*1062*	*217*	*19,956*	*11,388*

To prevent the concrete blocks from sliding on the pallets, they were fixed to the timber pallets by means of steel rods and bearing plates (see Figure 5.20).

Figure 5.20. Concrete blocks were tightened to the timber pallets

Pallets were also chained to the beam to prevent them from falling off the frame. (see Figure 5.21)

Figure 5.21. Concrete blocks chained to the timber pallet

Table 5-2. Summary of the experimental tests

Time Scaling factor*	Earthquake record	Intensities (%)	Test Phase
1	Northridge (1994)	10	1
1	El Centro (1940)	20	1
1	El Centro (1940)	40,60,70,80	2
2	El Centro (1940)	40,60,70,80,100 120,140,160,180,200,220	2

* The earthquake record's scaling factor in time domain

5.2.1 Stage one of the Experimental Study

Figure 5.22 to Figure 5.24 show the numerical and experimental results of accelerations and displacements of the rack frame with boltless connections under seismic base excitation of 20% 1940 El-Centro and 10% 1994 Northridge earthquakes imposed in down aisle directions. The numerical analyses will be discussed in Chapter 6, however, the numerical results of stage one are shown in Figure 5.22 to Figure 5.24 to show the satisfactory agreement between numerical and experimental for the structure while performing linearly.

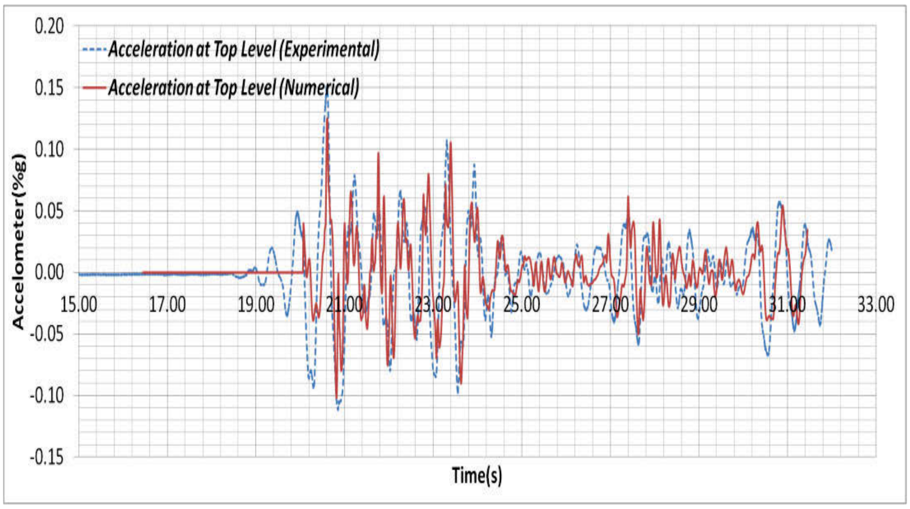

Figure 5.22. Comparison of experimental and numerical results for acceleration at the top storey level (20% 1940 El Centro record).

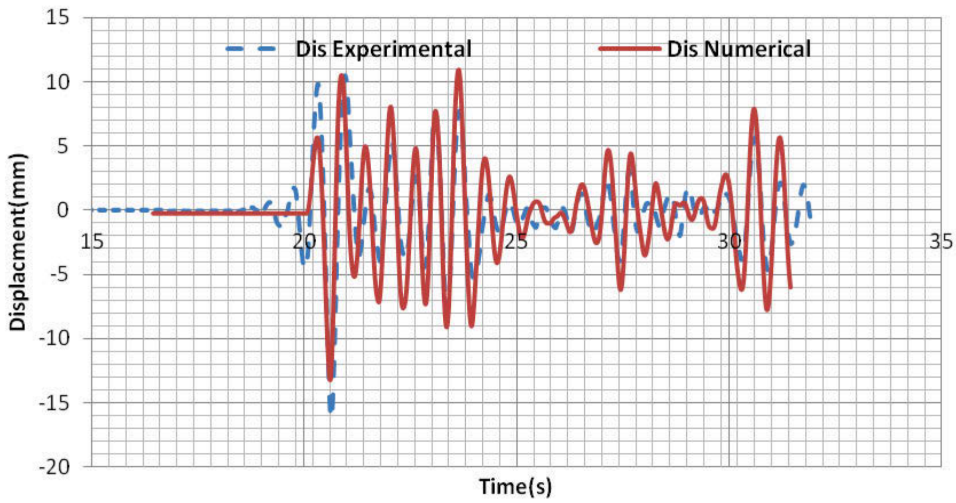

Figure 5.23. Comparison of experimental and numerical results for displacement at the top storey level (20% 1940 El-Centro record).

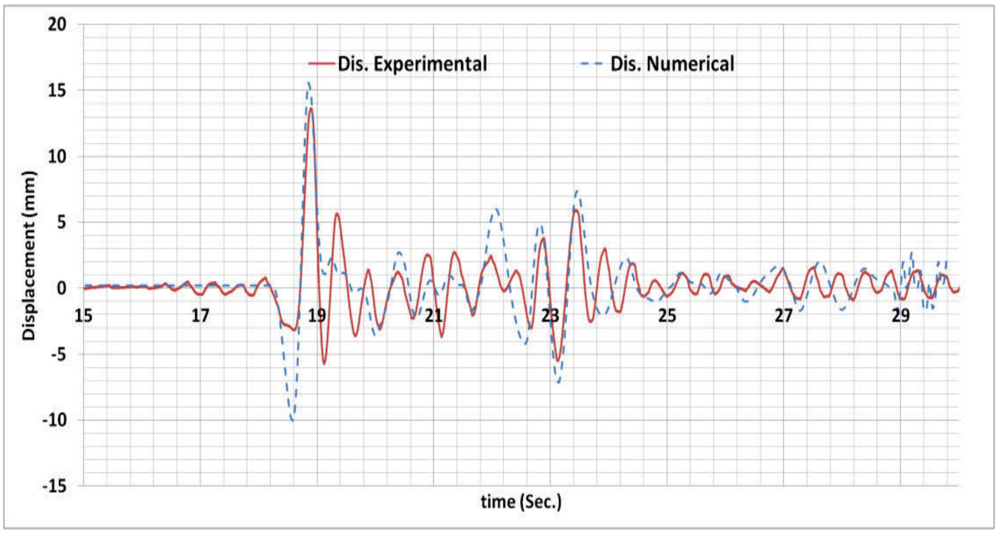

Figure 5.24. Comparison of experimental and numerical results for displacement at the top storey level (10% 1940 El Centro record).

Prior to the first test, a Sine sweep test was used to determine the natural period of the rack system in its original condition. For this purpose, a full-cycle acceleration time-history at a frequency range of 1 to 20 Hz with a rate of one octave per minute and an amplitude of 0.02 g was generated by the shake table in the down aisle direction of the rack.[16]

Sine sweep test results are presented in the form of Fast Fourier transform (FFT) to

[16] The frequency range was later shortened to '1 to 10 Hz' as the first model observed frequency was less than 2 Hz

easily determine the frequencies of vibration and damping ratio (see Figure 5.25). The sine sweep test results were converted to FFT format using a pre-programmed laboratory software.

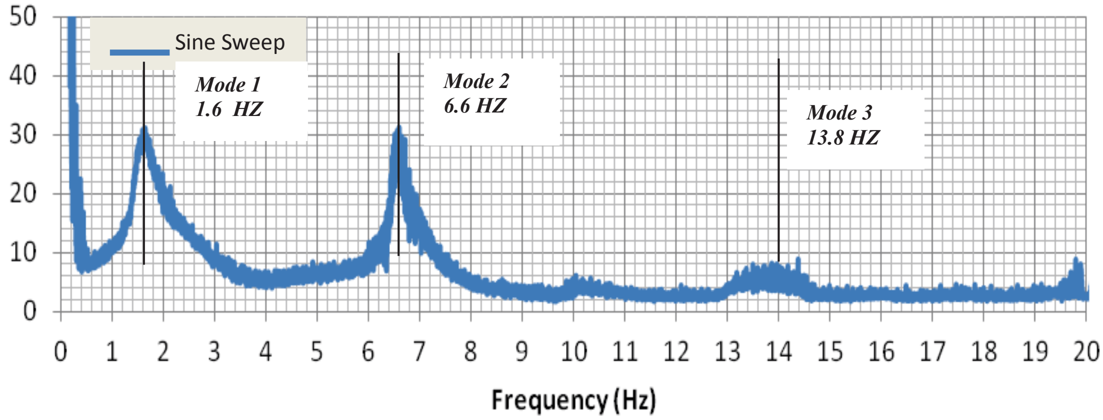

Figure 5.25. FFT of sine sweep test of the specimen before being exposed to any seismic actions

Figure 5.25 shows that the fundamental frequency of vibration is around 1.6 Hz which corresponds to the vibration period of 0.63 second.

Mode shapes where similar to those reported by Krawinkler, Cofie, Astiz, and Kircher (1979). The First and second modes of vibration were quite visible, however the third mode was not visible to the naked eye. Figure 5.26 schematically shows the first and second modes of vibrations.

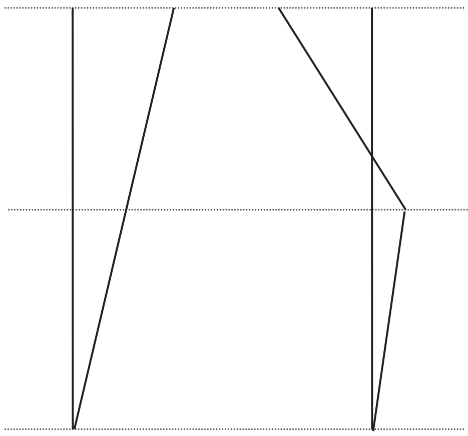

Figure 5.26. First and second modes of vibration observed in sine sweep test

As mentioned earlier, the preliminary test schedule of phase 1 was only conducted to give us an indicative understanding of the rack system's behaviour under dynamic actions in order to modify and improve the numerical models which was used to design the second stage of the test program. FE models were then calibrated against the recorded experimental results and were used to simulate the second phase of this experimental study.

5.2.2 Stage two of the Experimental Study

The second phase of the shake table testing program was conducted to subject the same system to higher seismic forces than in phase 1 to enable formation of local plastic deformation in the structure.

Precaution needed to be taken to ensure safety and avoid global instability of the structure. The excitation intensity was, therefore, applied in an incremental fashion. The loading schedule was:

a. Starting the tests at Peak Ground Acceleration (PGA) of 40% of 1940 El- Centro earthquake record.
b. Increasing the earthquake record by steps of 10% or 20%

Before the next increment, comparative checks between experimental results and their numerical counterparts were made to ensure that the following step to be applied is safe[17].

To minimise the risk of pallet sliding and also to check the strength of the timber pallet under the seismic force, preliminary sliding tests were conducted. For this reason, a pallet was placed on two beams which were fixed to four short uprights very close to the table as shown in Figure 5.27. The table was then shaken using the acceleration recorded at the top level of the low intensity test of Phase 1. The acceleration record was magnified incrementally to simulate the pallet movement on the top storey for higher intensity shakes. Although the acceleration which the pallets on the top level experience would be different than the accelerations recorded from the tests conducted in Phase 1, this method provided a rough estimate of how critical the sliding of the pallets would be. However, the accelerations and displacements of the above safety assurance test were not recorded and assessed as the test was only performed and passed visually.

To prevent catastrophic collapse of the rack subjected to higher seismic records in Phase 2, support structures were designed and constructed to allow the structure to lean against in case of failure. Figure 5.28 shows the test set up in which the test specimen and support structures on both sides of the rack can be seen.

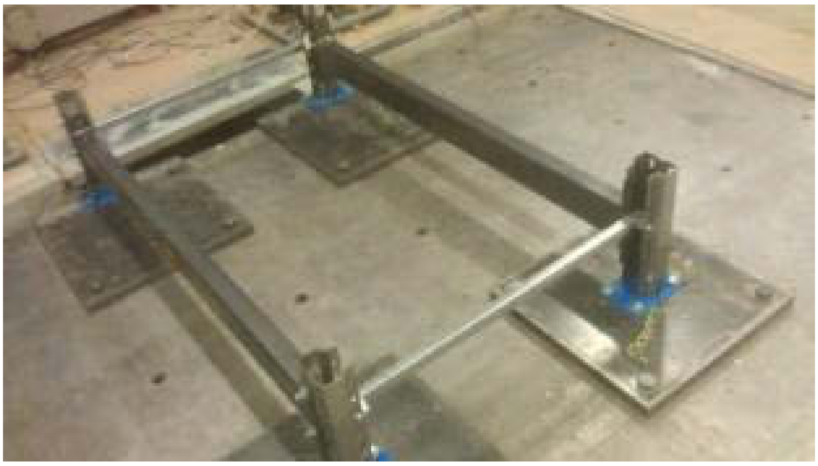

Figure 5.27(a)

[17] Sine Sweep tests with a low intensity (0.02g) was conducted after every step to monitor possible period elongation due to damage in the system and evaluate the damping ratio

Figure 5.27(b)

Figure 5.27. Pallet Sliding test set up

(a)

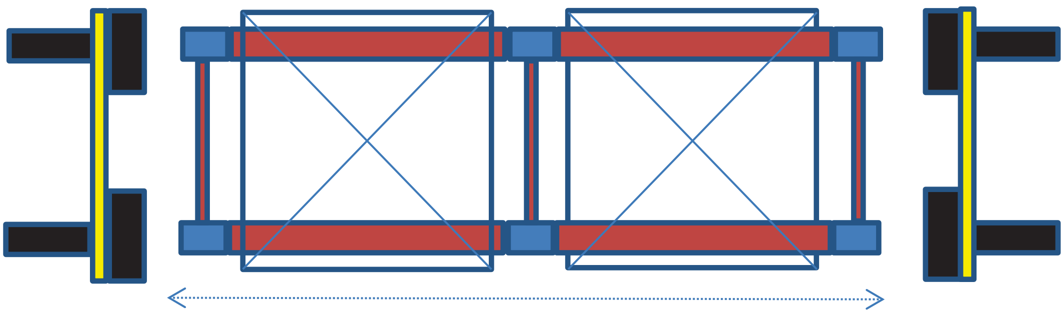

(b)

Figure 5.28. Rack frame and support structures (a. Test rig, b. Schematic plan view)

Details of shake table test results on different rack frames are expressed as follows.

A series of uni-axial earthquake tests in the down aisle direction were performed on two specimens. In the first set of tests the specimen was excited by the original 1940 El-Centro earthquake without any time scaling, while the second specimen was subjected to the same record but scaled down by a factor of two in the time domain[18] (i.e. the time increments in the standard El Centro record were halved)

Tests were started from lower intensities and continued to higher intensities in steps of 10 to 20%.

The details of shake table test results of the frames with boltless connections and non braced in down aisle directions (BL-NB) are described below:

5.2.2.1 Test 1: 1940 El-Centro Earthquake, Non-Scaled in time domain

Figure 5.29 to Figure 5.33 show the structural responses under 20% to 80% 1940 El-Centro earthquake record. Tests were carried out in consequent steps which lead to cumulative plastic deformation in the frame. It was decided not to subject the specimen to a record greater than 80% of 1940 El-Centro as the recorded acceleration of the top level indicated a peak acceleration near '1.0 g' which was close to the capacity of the table under a 4 tonne structure. For this reason, the collapse and failure mode was not observed from the shake table test results and the results were mainly used to verify the computer simulations with the proposed model of beam to upright connections.

No significant pallet movement was observed during tests with intensities of less than 60% and maximum sliding of around 20 mm was observed in the top pallet for the last test with an intensity of 80% of 1940 El-Centro. For this reason the top pallet acceleration[19] started to deviate from the acceleration that was recorded from the accelerometer mounted to the upright.

Another interesting observation was that the deformed shape of the structure under seismic actions indicated that the inter-storey drift of the first level was significantly higher than the second level inter-storey drift (see Figure 5.34). This trend becomes clearer by increasing the seismic intensity which was indicative of a soft storey failure mode of the structure. This observation is in line with the failure mode

[18] The purpose of re-running shake table tests with the same record intensity but different scale factor in time domain was to better simulate the sensitivity of higher racks with longer periods

[19] Effective Design Acceleration (EDA)

reported in the report prepared by Rosin et al. (2009).

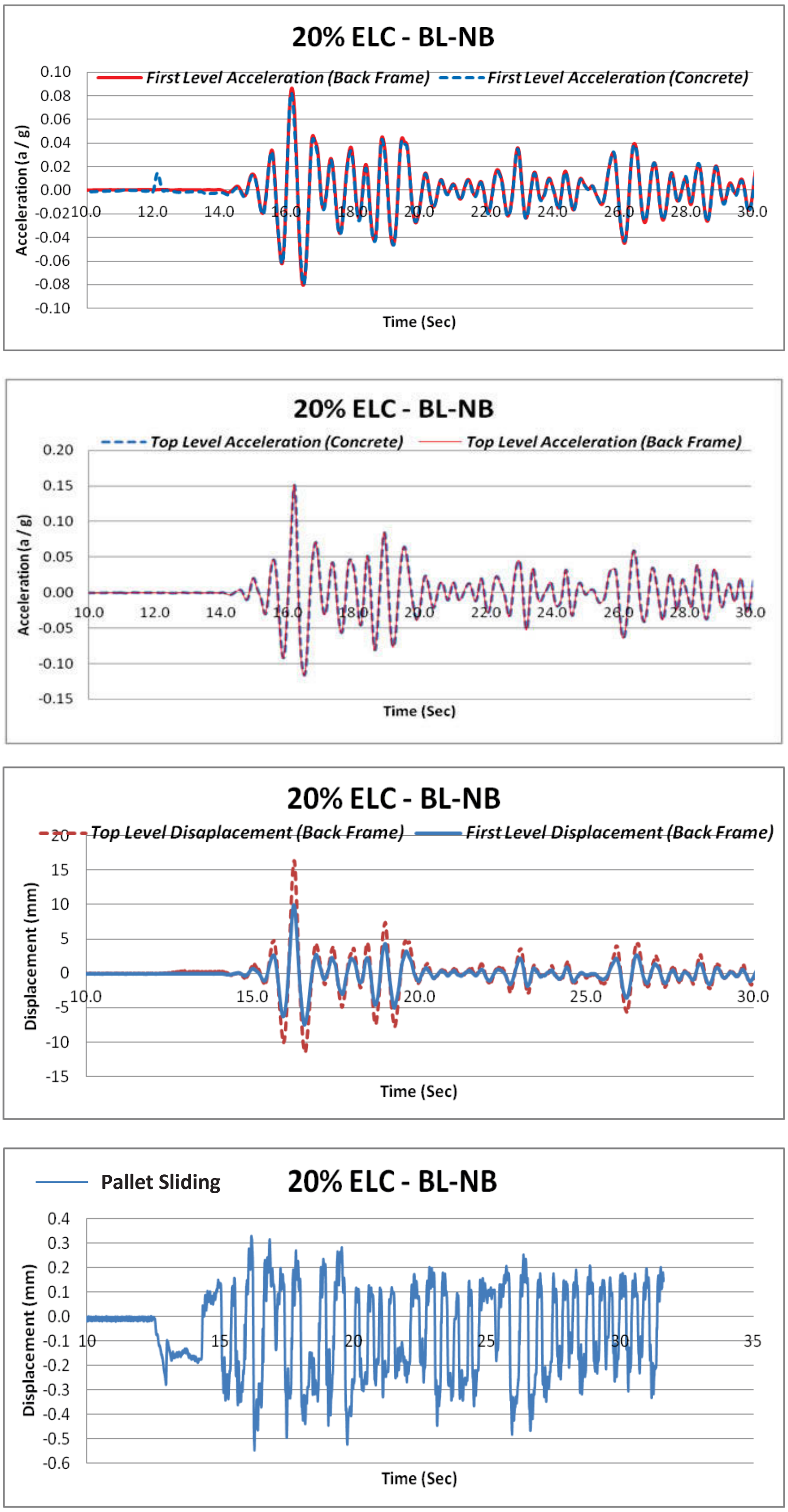

Figure 5.29. Structural response under 20% 1940 El-Centro earthquake record / Non-Scaled in time domain

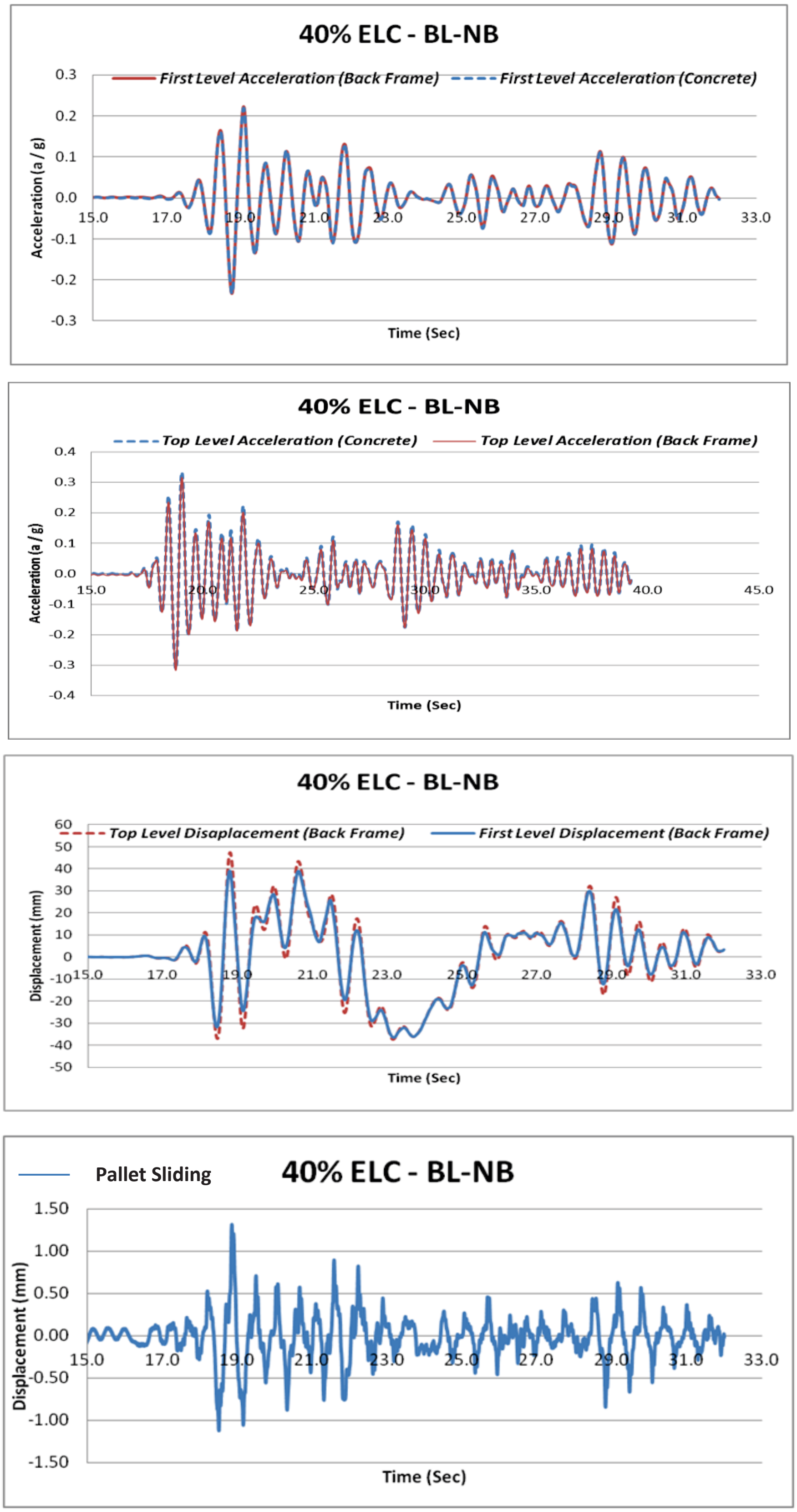

Figure 5.30. Structural response under 40% 1940 El-Centro earthquake record / Non-Scaled in time domain

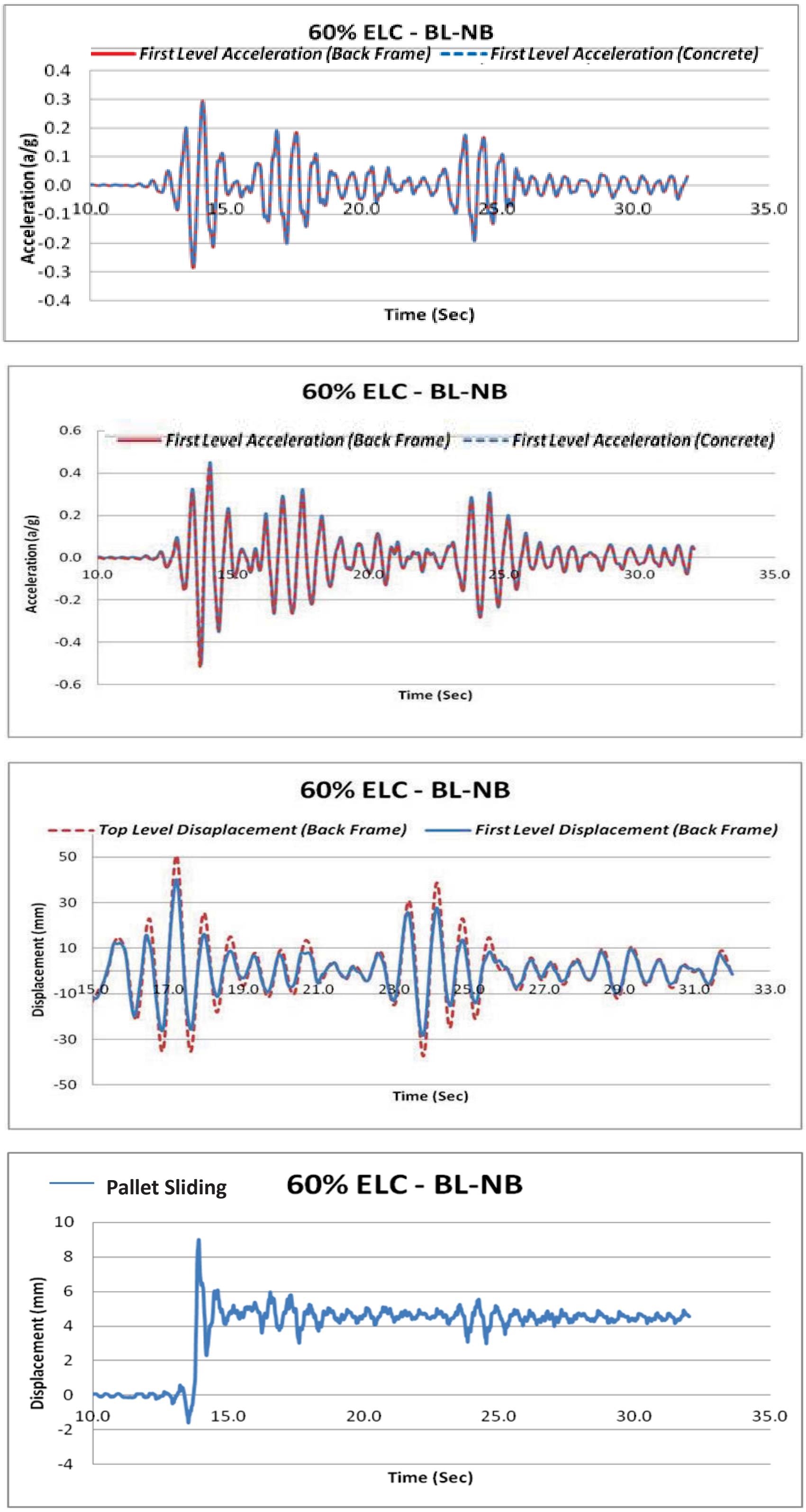

Figure 5.31. Structural response under 60% 1940 El-Centro earthquake record / Non-Scaled in time domain

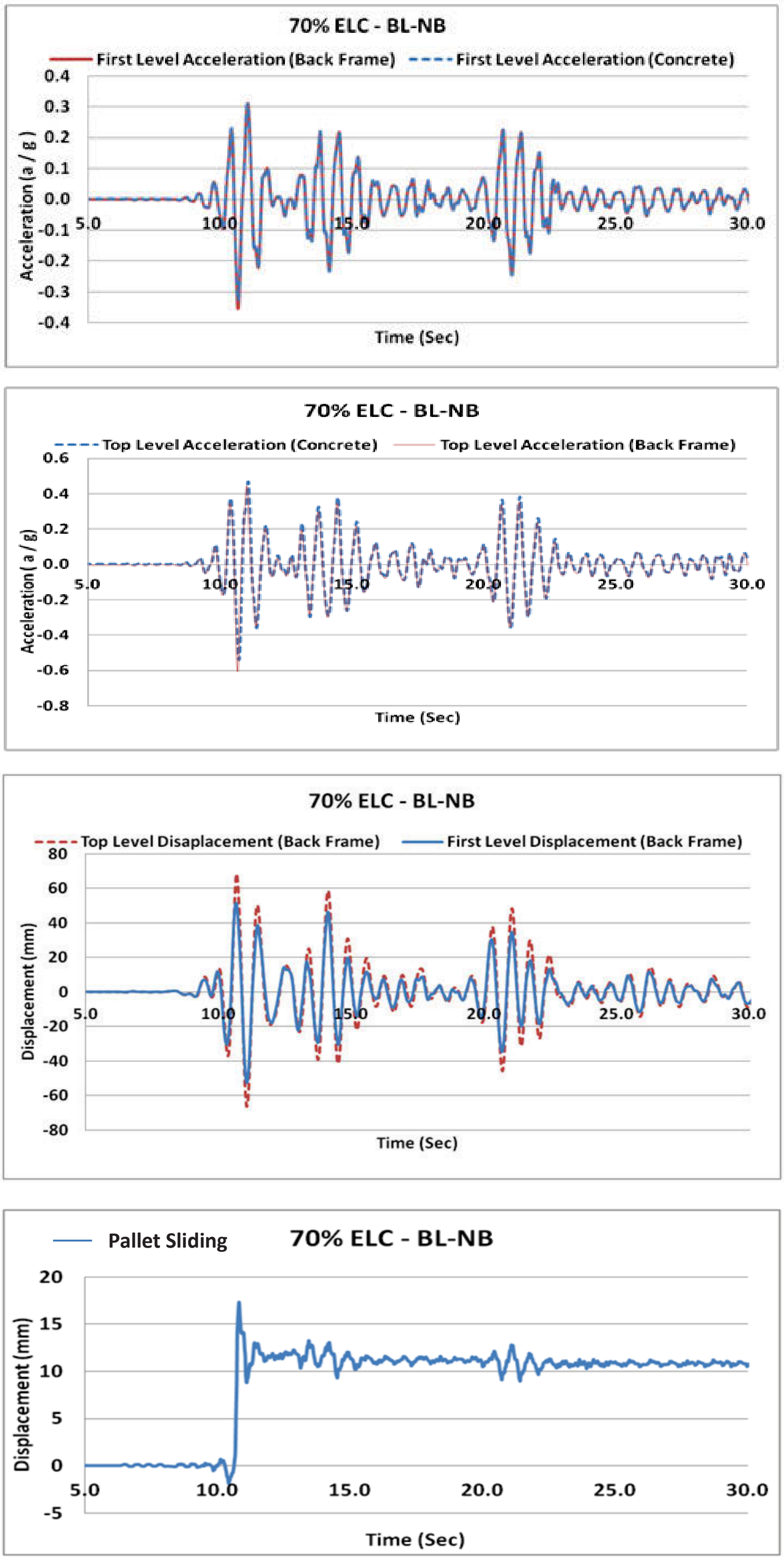

Figure 5.32. Structural response under 70% 1940 El-Centro earthquake record / Non-Scaled in time domain

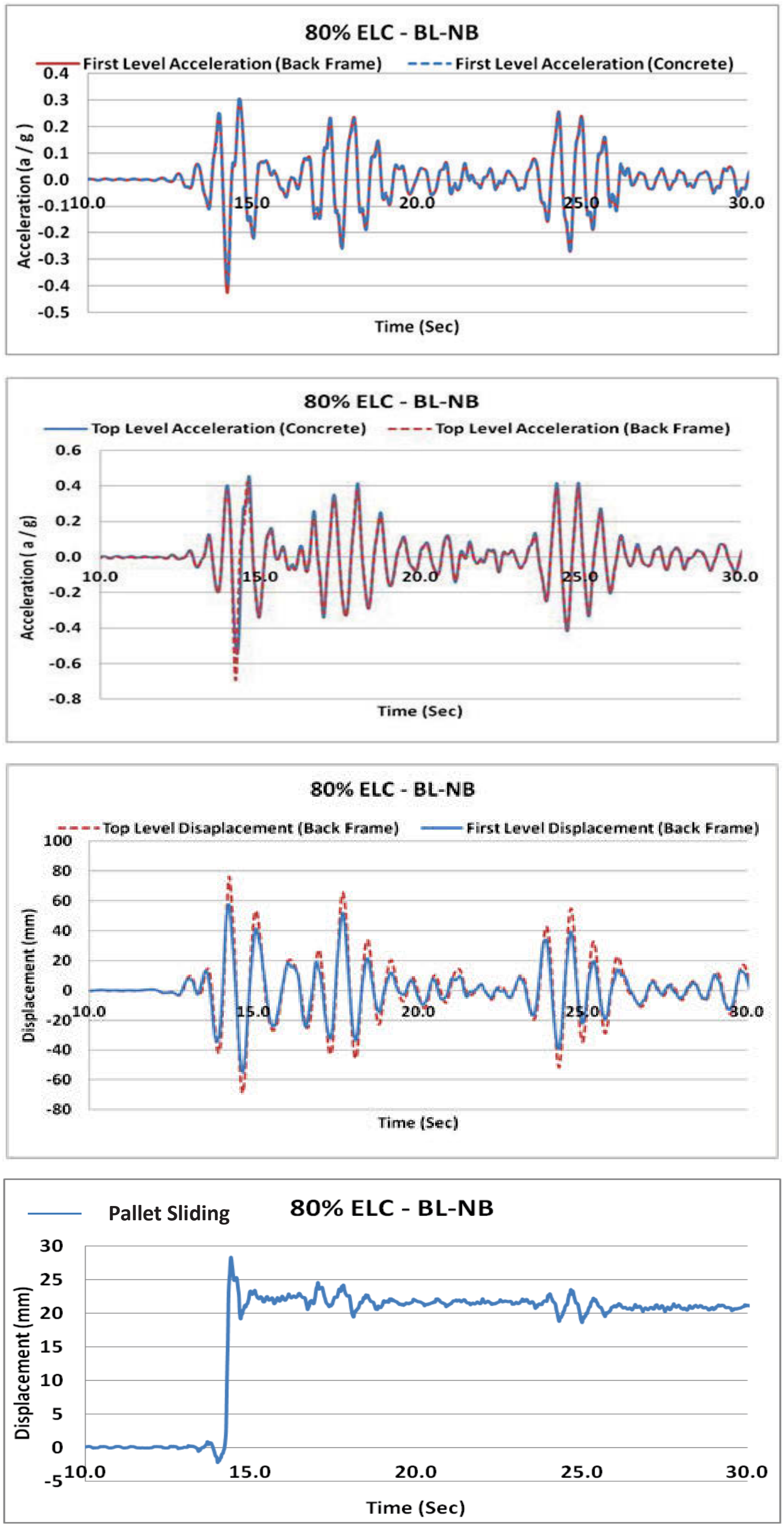

Figure 5.33. Structural response under 80% 1940 El-Centro earthquake record / Non-Scaled in time domain

Table 5-3 shows the details of the test results.

Table 5-3. Peak responses of structure under seismic actions

Intensity (% ELC)	Top Level Disp. (mm)	1st Level Disp. (mm)	Top Level Acc. (a/g)	1st Level Acc. (a/g)	Top Level Pallet Acc. (a/g)	1st Level Pallet Acc. (a/g)
20	16.4	10.0	0.15	0.086	0.15	0.083
40*	47.5	39.1	0.31	0.23	0.33	0.23
60	60.6	47.7	0.52	0.29	0.5	0.285
70	68.4	52.6	0.61	0.35	0.54	0.327
80	76.2	58	0.69	0.425	0.545	0.396

*The shake table test results of 40% 1940 El Centro earthquake record was not reliable as the input acceleration record was not based on 1940 El-Centro record and was performed as random vibration, but with the correct intensity. However, it is included in this table as the seismic record intensity is equivalent to 40% 1940 El-Centro earthquake.

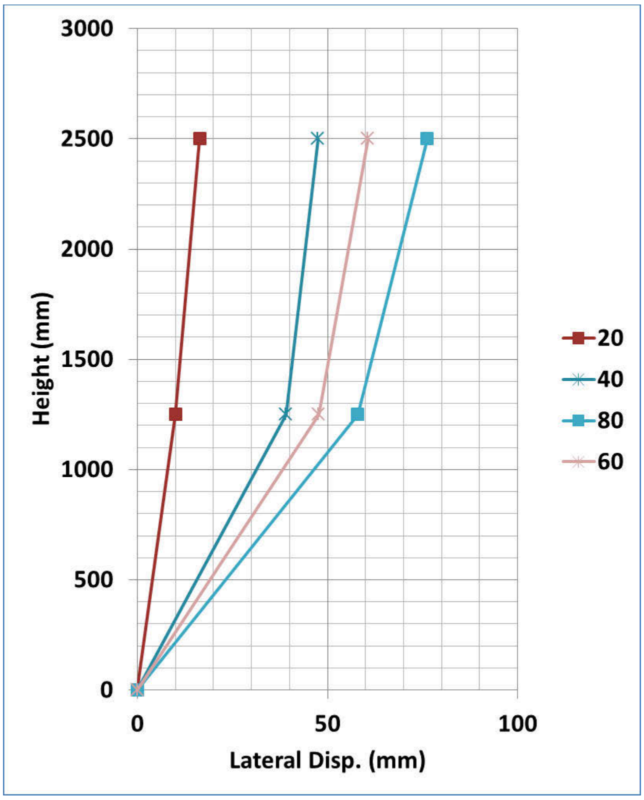

Figure 5.34. Lateral displacement of the rack

5.2.2.2 Test 2:1940 El Centro Earthquake, Scaled down in time domain by factor of two

As the test specimen was limited to 3 meters height, the results may not be extendable for higher racks with a period longer than 0.63 Sec of the tested specimen. For this reason, to estimate the behaviour of higher rack frames under the same seismic actions, a similar rack configuration (2storey- 2 bay frame with boltless connections without spine bracing in down aisle direction) was subjected to the same 1940 El-Centro earthquake record but scaled down in the time domain by a factor of two. By using this technique, instead of changing the structure to obtain a longer period (two times longer), the same structure was subjected to faster earthquake. Therefore, the behaviour of a system with a given natural frequency under a squeezed time history record (e.g. faster earthquake) simulates the behaviour of a virtual structure with longer period under non-scaled earthquake in the time domain.

Figure 5.35 to Figure 5.47 show the structural responses for the 40% to 220% scaled

1940 El- Centro earthquake records. Pallets started to slide on the beam after 160% intensity tests. The tests were continued until the automatic acceleration sensor raised alarm of reaching a high acceleration at the top level close to the table capacity during the 220% intensity test. After running the 220% intensity scaled test, three more tests were conducted with smaller intensities of 160%, 100% and 40% of the same record (named as: 160R, 100R and 40R).

The structure's deformed shape again showed a higher inter-storey drifts at the first level (see Figure 5.48). However, the difference between the accelerations recorded from the beam and pallet at the top level of the last three tests were obviously more than those of the previous tests with similar intensities. This can be explained by the reduction of the friction coefficient between the timber pallet and the beam due to the large number of tests using the same pallets and beams which smoothed the contact surfaces of the timber pallet with the beam flange. By reducing the friction coefficient, the seismic forces induced to the structural mass (pallets) was reduced as explained in FEM 10.2.08 (2010).

Table 5-4 shows more details of this series of tests.

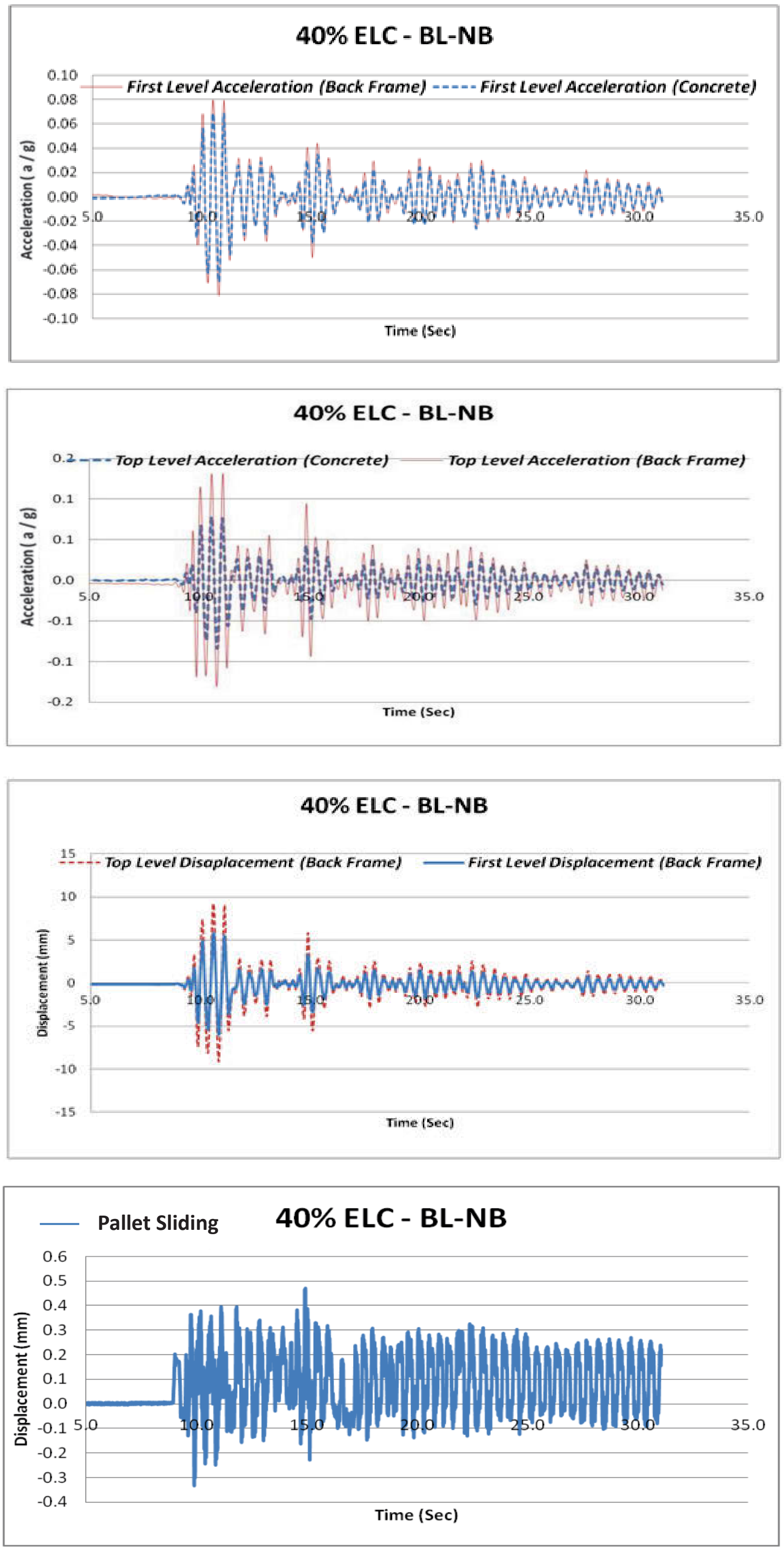

Figure 5.35. Structural response under 40% 1940 El-Centro earthquake record / Scaled down in time domain by a factor of 2

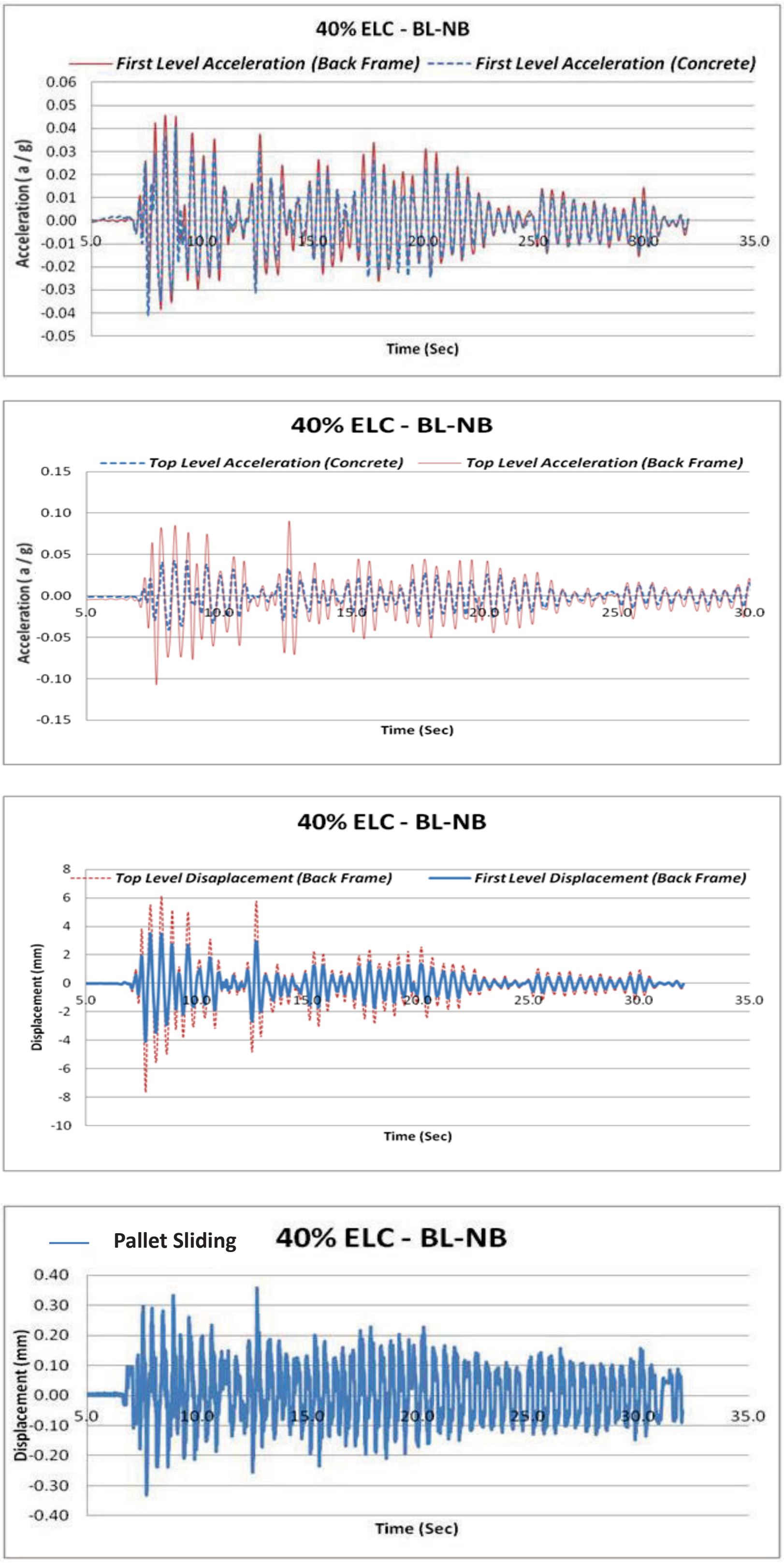

Figure 5.36. Structural response under 40% 1940 El-Centro earthquake record / Scaled down in time domain by a factor of 2 (After running higher intensities)

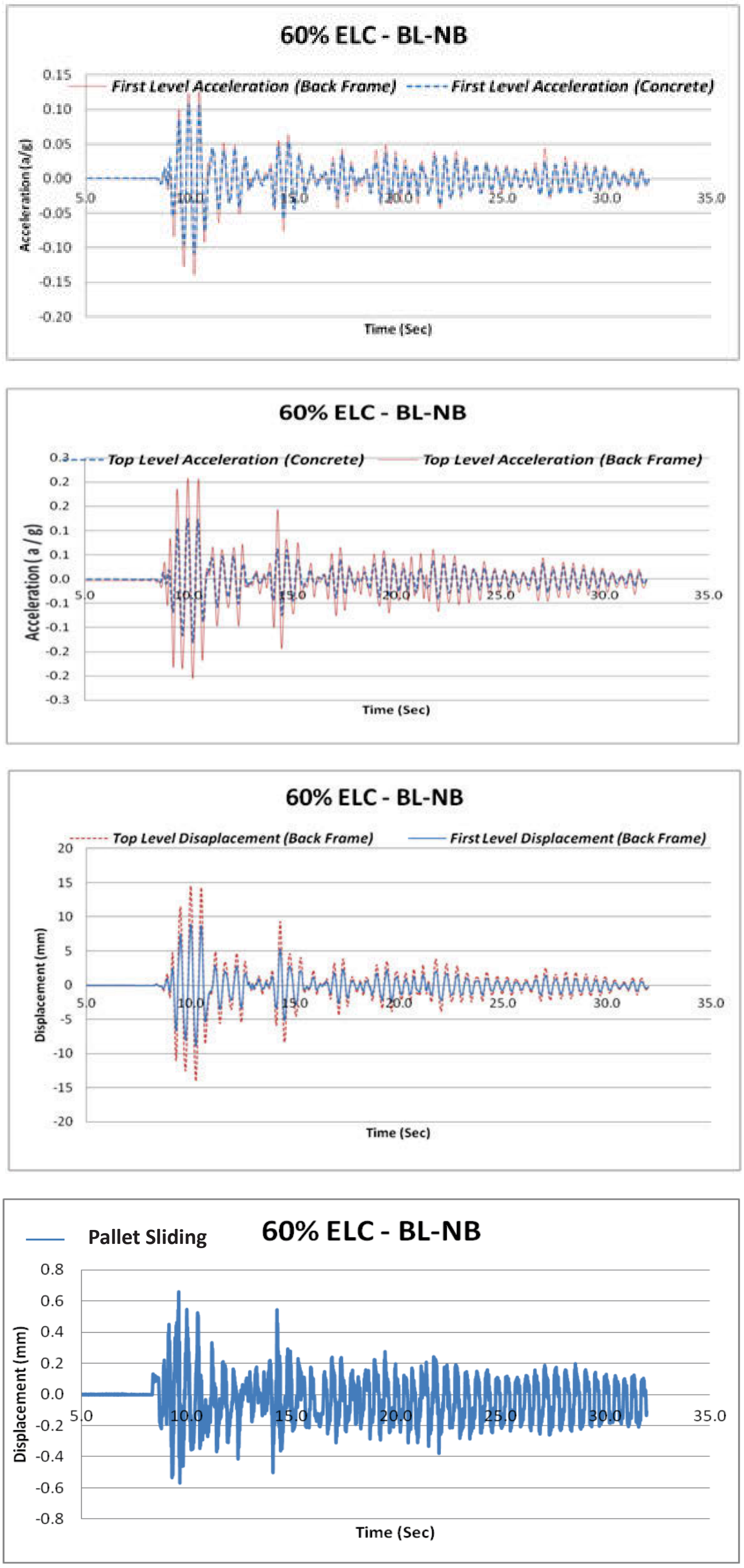

Figure 5.37. Structural response under 60% 1940 El-Centro earthquake record / Scaled down in time domain by a factor of 2

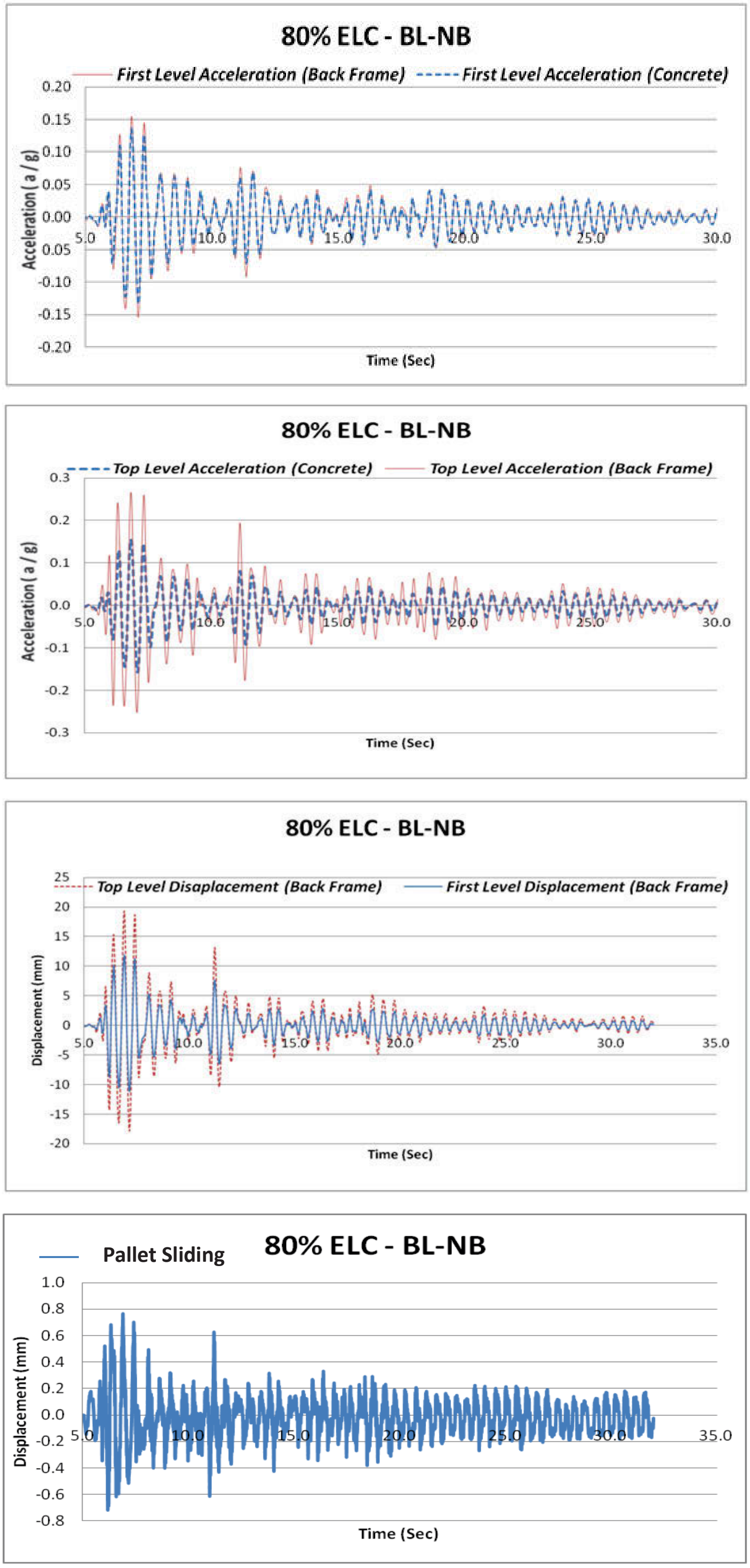

Figure 5.38. Structural response under 80% 1940 El-Centro earthquake record / Scaled down in time domain by a factor of 2

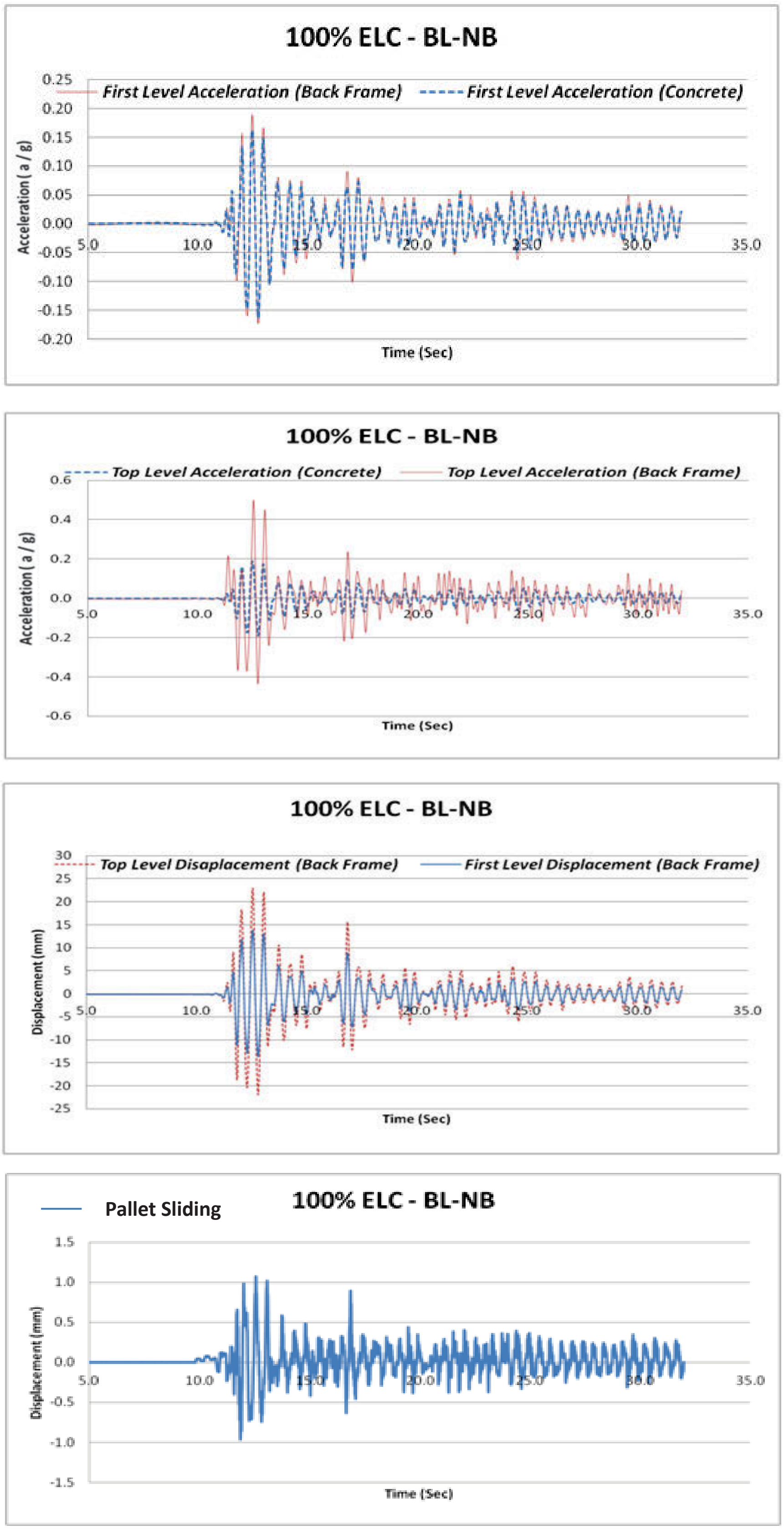

Figure 5.39. Structural response under 100% 1940 El Centro earthquake record / Scaled down in time domain by a factor of 2

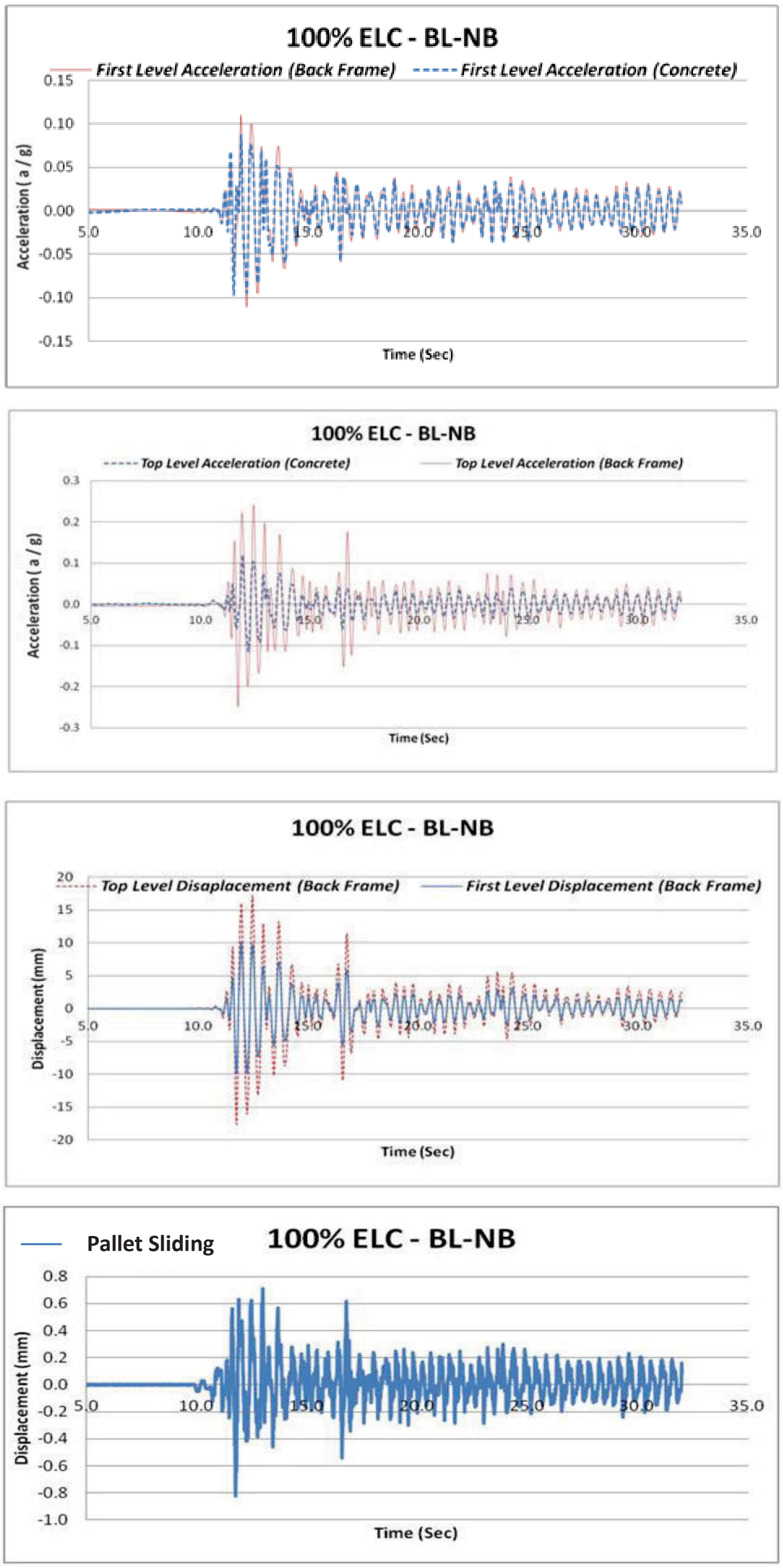

Figure 5.40. Structural response under 100% 1940 El-Centro earthquake record / Scaled down in time domain by factor of 2 (After running higher intensities)

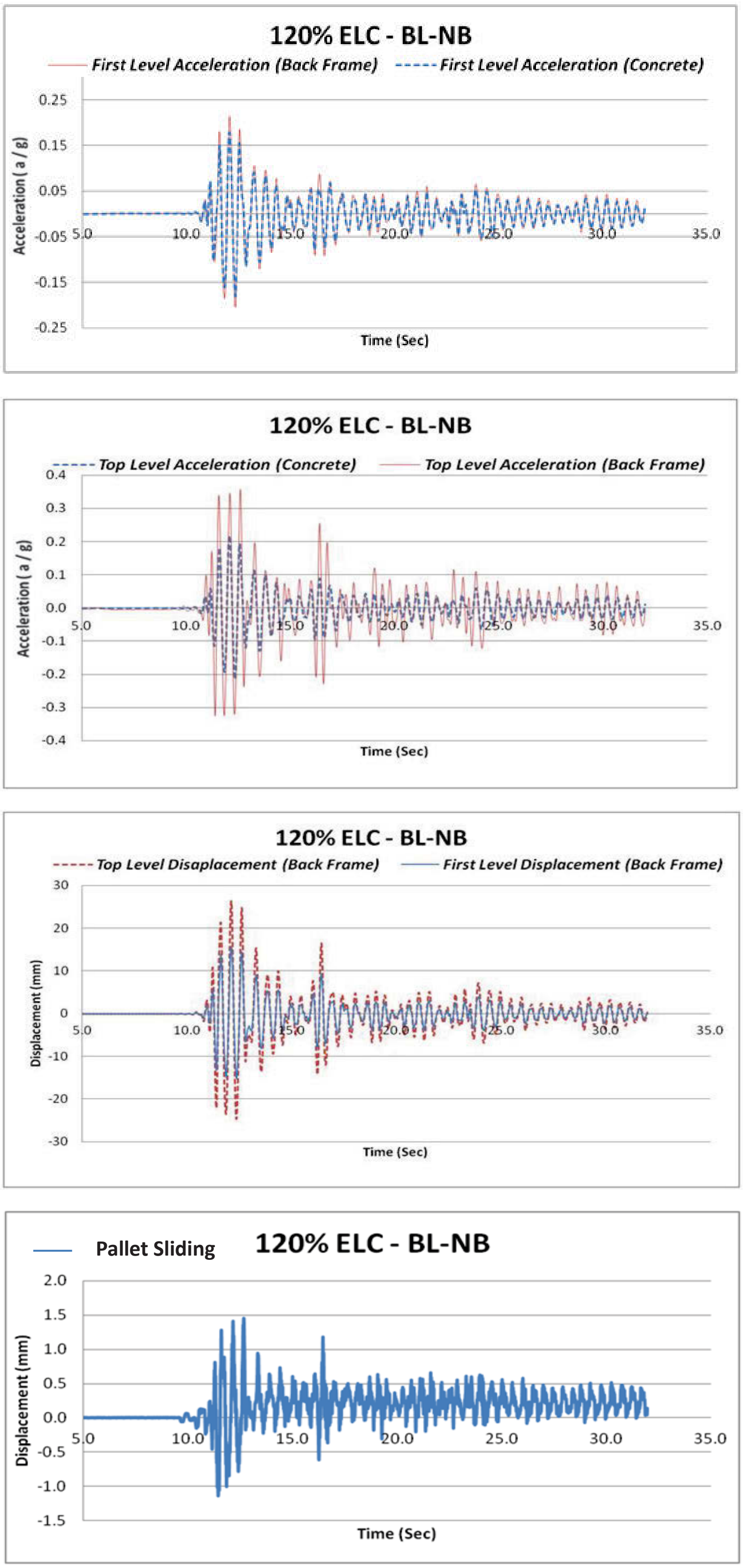

Figure 5.41. Structural response under 120% 1940 El-Centro earthquake record / Scaled down in time domain by a factor of 2

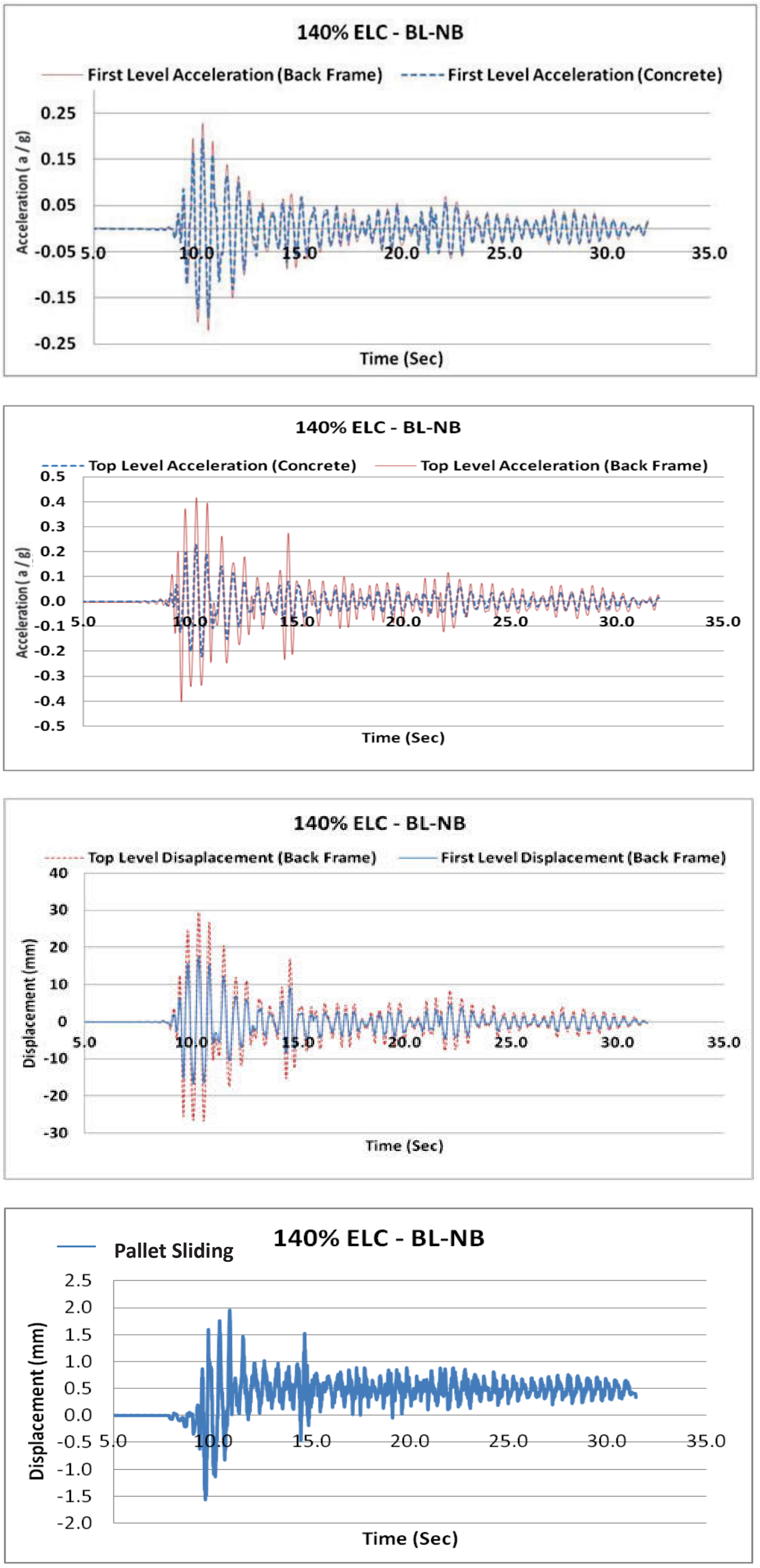

Figure 5.42. Structural response under 140% 1940 El-Centro earthquake record / Scaled down in time domain by a factor of 2

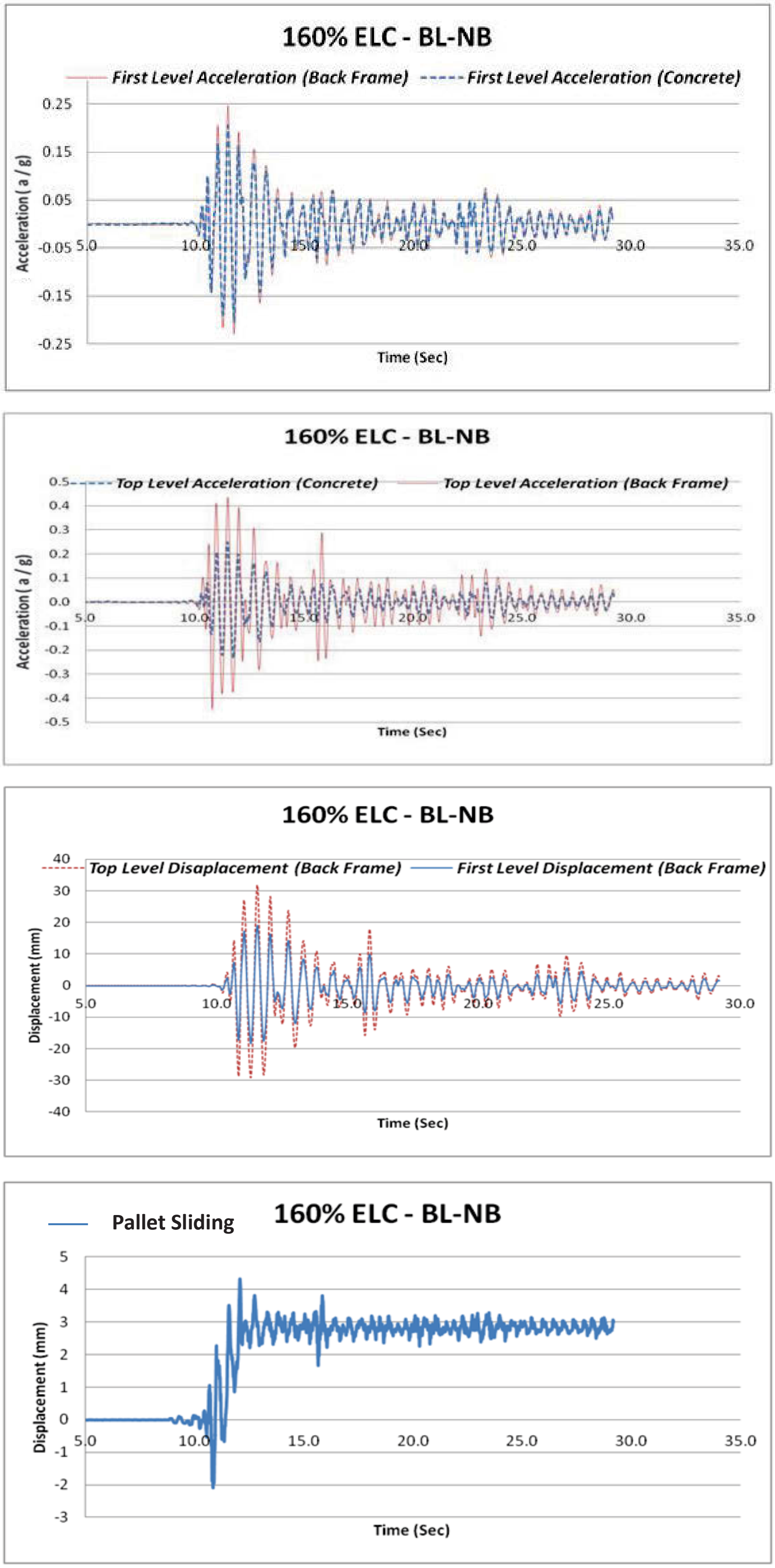

Figure 5.43. Structural response under 160% 1940 El Centro earthquake record / Scaled down in time domain by a factor of 2

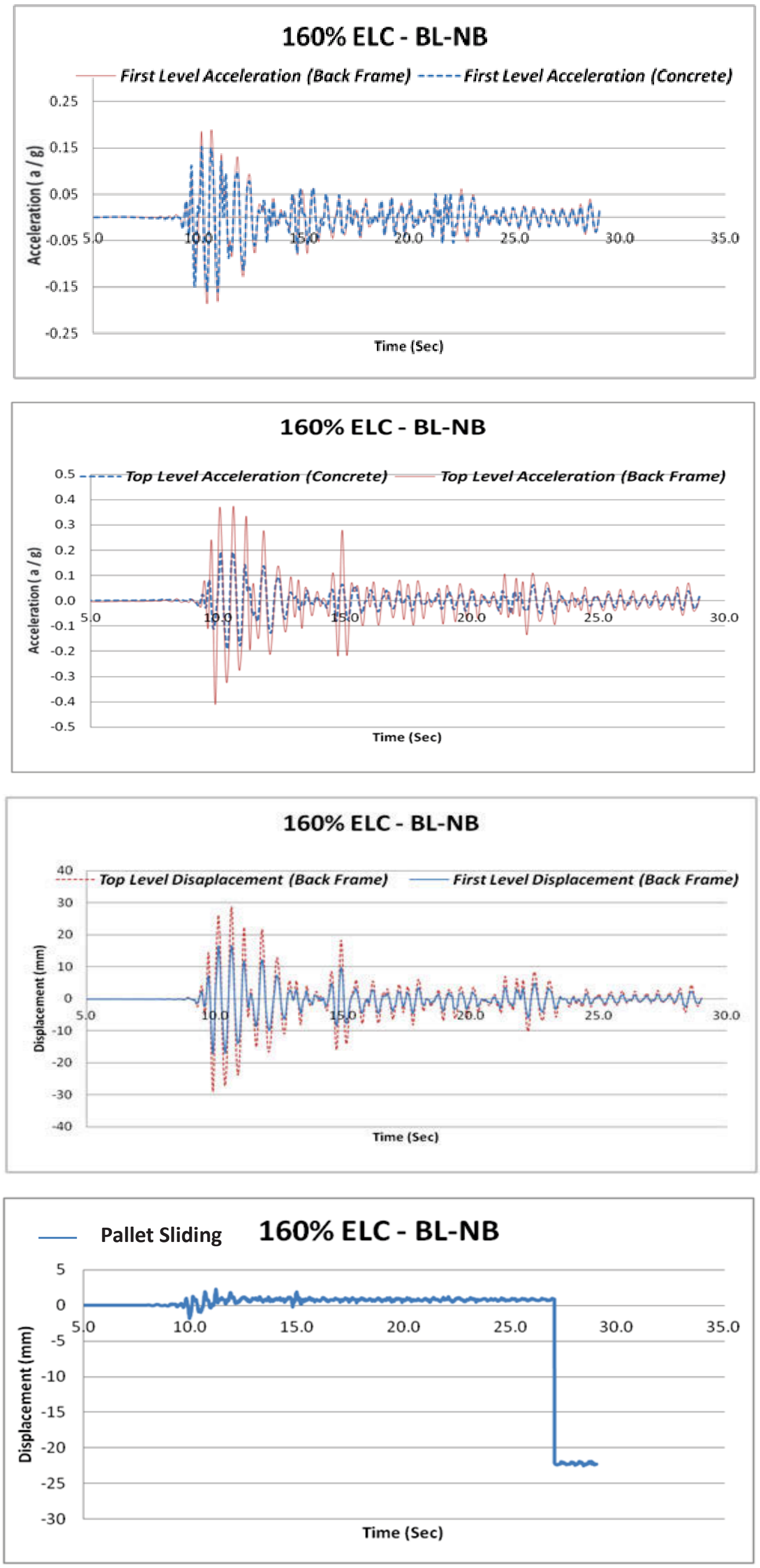

Figure 5.44. Structural response under 160% 1940 El Centro earth quakerecord / Scaled down in time domain by a factor of 2 (After running higher intensities)

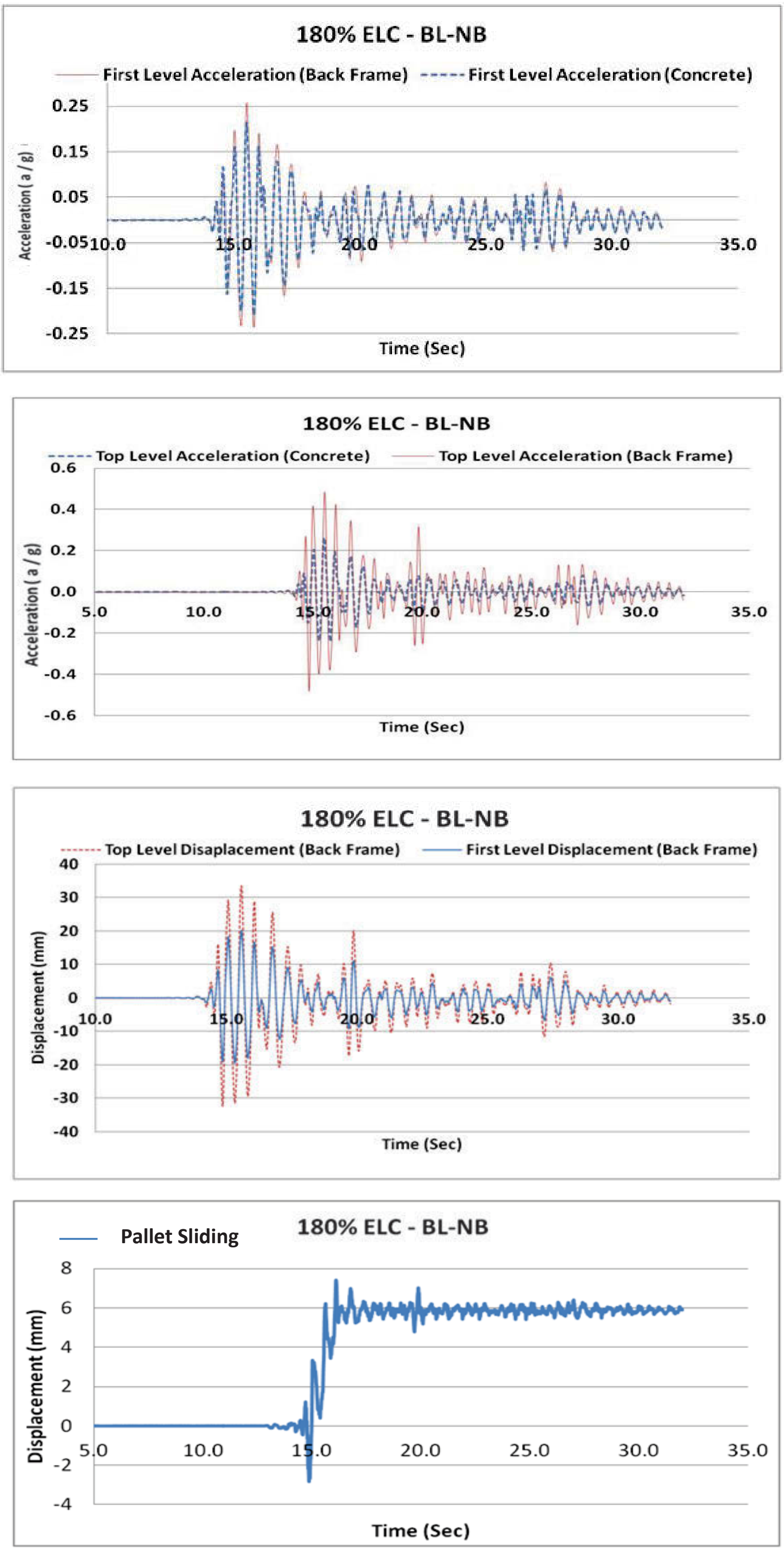

Figure 5.45. Structural response under 180% 1940 El-Centro earthquake record / Scaled down in time domain by a factor of 2

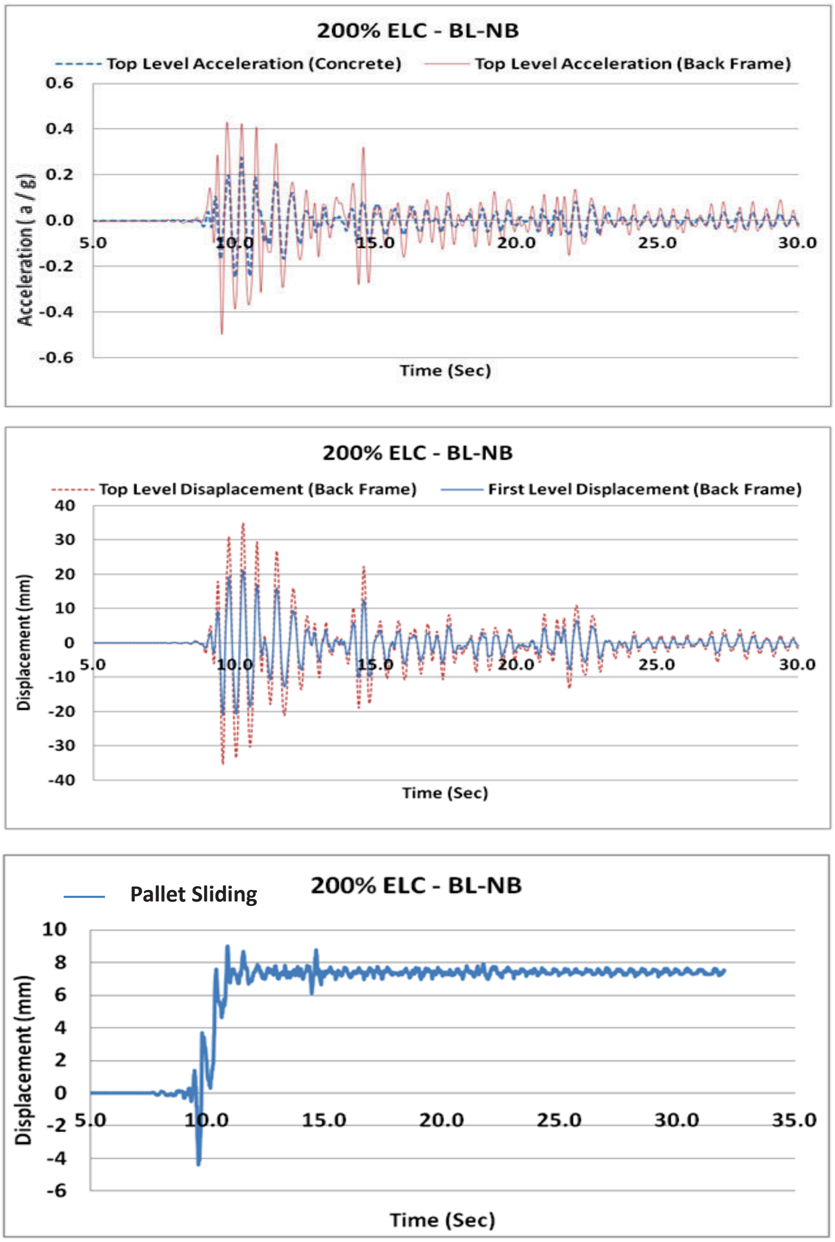

Figure 5.46. Structural response under 200% 1940 El-Centro earthquake record / Scaled down in time domain by a factor of 2*

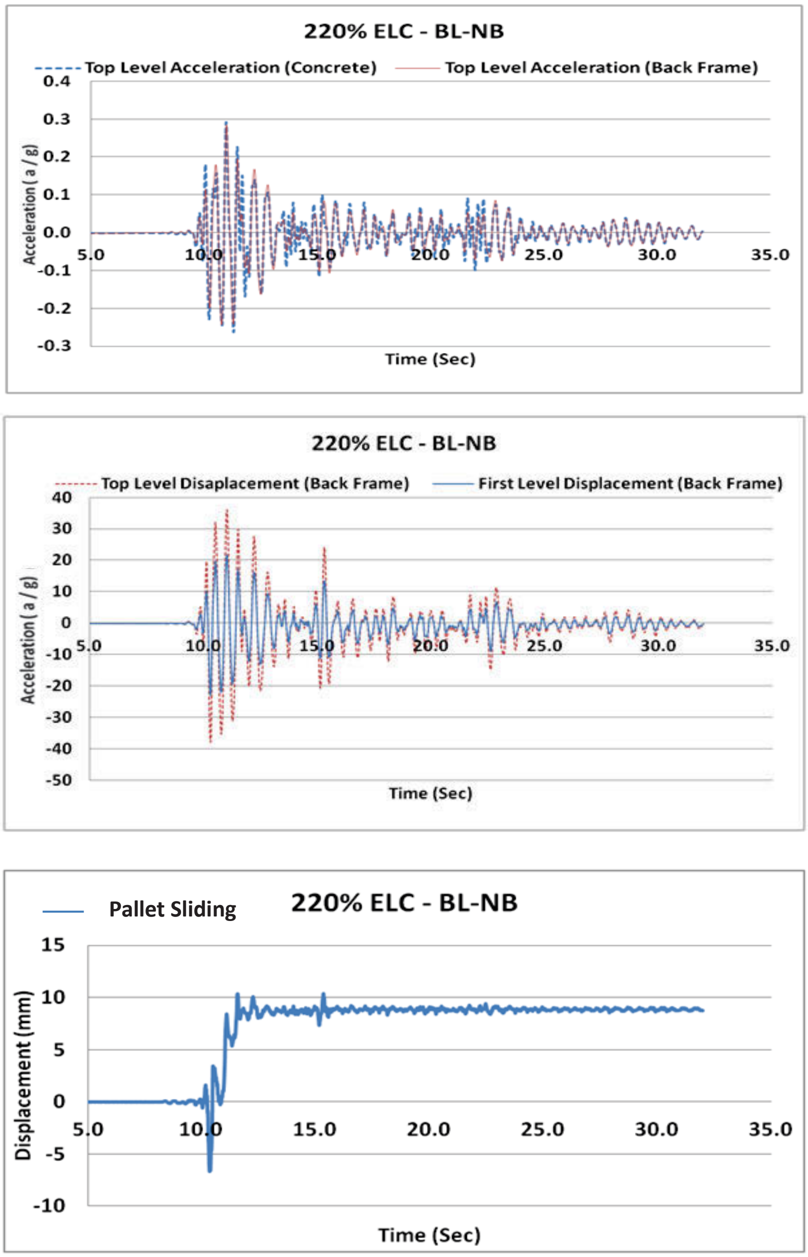

Figure 5.47. Structural response under 200% 1940 El-Centro earthquake record / Scaled down in time domain by a factor of 2

Table 5-4. Peak responses of structure under time scaled seismic actions

Intensity (% ELC)	Top Level Disp. (mm)	1st Level Disp. (mm)	Top Level Acc. (a/g)	1st Level Acc. (a/g)	Top Level Pallet Acc. (a/g)	1st Level Pallet Acc. (a/g)
40	9.21	5.76	0.132	0.08	0.078	0.068
40R	7.76	4.12	0.10	0.045	0.043	0.041
60	14.56	8.95	0.21	0.14	0.13	0.11
80	19.31	11.84	0.27	0.16	0.16	0.14
100	22.94	13.81	0.33	0.19	0.19	0.16
100R	17.68	10.10	0.25	0.11	0.12	0.10
120	26.36	15.70	0.36	0.21	0.22	0.18
140	29.43	17.45	0.42	0.23	0.23	0.19
160	31.85	19.05	0.45	0.25	0.25	0.21
160R	29.04	17.09	0.41	0.19	0.19	0.16
180	33.42	20.20	0.48	0.26	0.26	0.21
200*	35.39	21.19	0.50	0.27	0.28	-
220**	37.82	22.91	0.29	0.23	0.29	-

*and**: the accelerometer showed unreasonable results due to connection problem with the acquisition system.

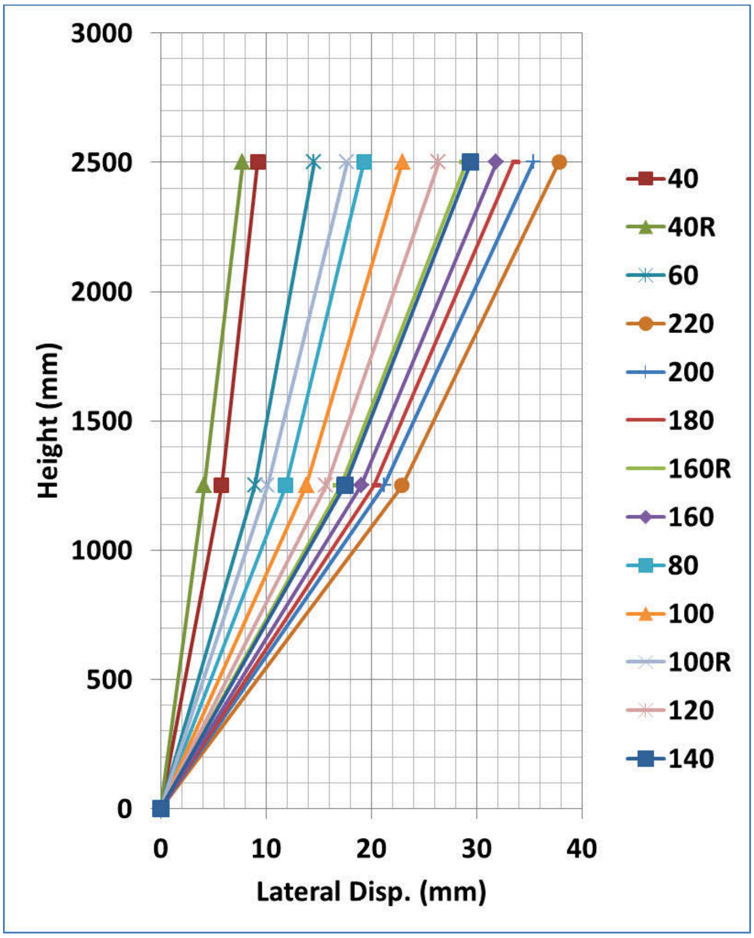

Figure 5.48. Lateral displacements of the rack

5.2.2.3 Damping of the System

Limited investigations on the damping of rack structures are reported so far from previous shake table tests. Krawinkler et al. (1979) emphasised the effect of amplitude of motion on the damping ratio. "The structural damping which will come primarily from the beam-to-post connections will be strongly amplitude dependant (amplitude of motion) and will be affected by the looseness of the connections" (Krawinkler et al., 1979, p. 13). "At large amplitudes, the grip-type connectors were moving with respect to the perforations in the posts providing significant damping. Once the connectors locked at smaller amplitudes, the damping dropped drastically to a very small value" (Krawinkler et al., 1979, p. 13).

However, a damping ratio for seismic design of rack structures has not yet been proposed with high level of confidence. Although proposing an accurate damping

ratio is beyond the scope of this study and indeed needs more in situ testing of loaded and unloaded racks, performing a preliminary investigation on the damping of the system was attempted.
As mentioned previously, in order to evaluate the damping ratio and vibration period elongations due to cumulative damage in the system after every step of shake table tests, the structure was subjected to a sweep sine wave with an acceleration amplitude of ‘0.02g’. Table 5-5 and Table 5-6 show the damping ratios as well as the fundamental vibration period of the system calculated from the sine sweep tests conducted after each of the test steps for both non-scaled and scaled tests, respectively. Damping ratios were calculated by applying the half power band method on the sine sweep test results as expressed earlier in this chapter.
Figure 5.49 and Figure 5.50 show the Frequency – Response curves of the sine sweep test results used to obtain the damping ratio as well as fundamental period of vibration. For the non-scaled tests the period was visibly changed due to apparent damage of the system in dissipative zones (e.g. connections) and system lost stiffness. Damping was also increased and it can be seen in the graphs by focusing on the width of the curves that were broadened after higher seismic intensities. The same observation can also be noticed in Figure 5.50, however, as the displacement amplitude in the scaled tests in time domain were smaller, the amount of damage of the connections was less significant and, therefore, less effective on the vibration period of the system.

Table 5-5 and Table 5-6 show an increase of the damping ratios after each increment of shake table test with increasing seismic intensity. The corresponding increase in the amount of lateral movement of the frame is basically the result of the interactions of the hooks in the beam end connectors and upright slots.

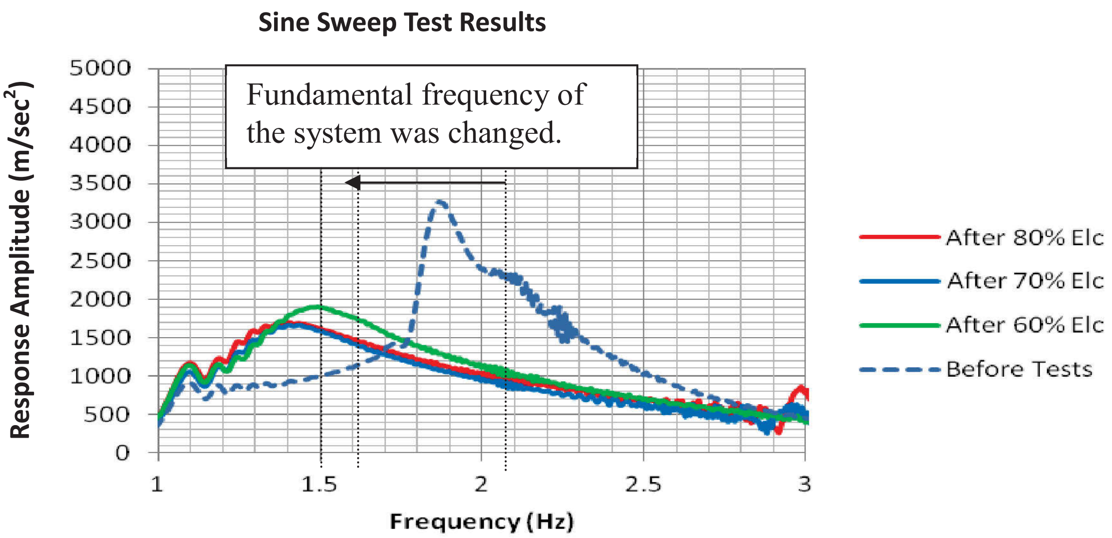

Figure 5.49. Sine Sweep test results of the Non-Scaled test in time domain

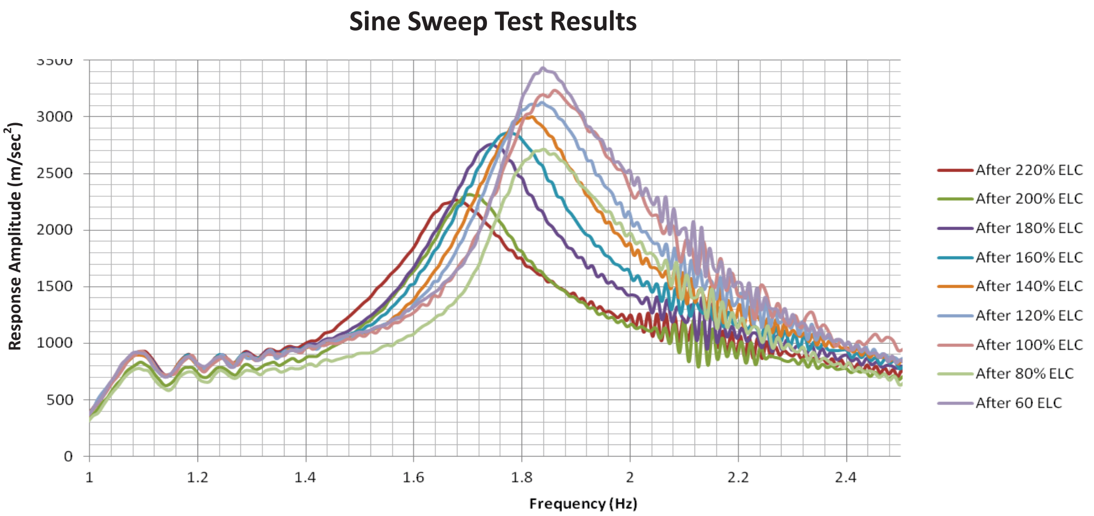

Figure 5.50. Sine Sweep test results of the Scaled test in time domain

Table 5-5. Dynamic features of the system under 1940 El-Centro test record/Non scaled in time domain

Intensity (%ELC)	Frequency (Hz)	Damping Ratio (%)	Top Level Displacement (mm)
60	1.5	16.7	60.4
70	1.4	18.6	68.4
80	1.35	19.2	76.2

Table 5-6. Dynamic features of the system under 1940 El-Centro test record/Scaled in time domain

Intensity (%ELC)	Frequency (Hz)	Damping Ratio (%)	Top Level Displacement (mm)
Before Tests	1.85	5.3	0
40	1.85	6.8	9.21
60	1.85	6.8	14.56
80	1.85	7.4	19.31
100	1.85	7.4	22.94
120	1.85	7.5	26.36
140	1.80	7.7	29.43
160	1.80	7.3	31.85
180	1.75	7.7	33.42
200	1.70	8.1	35.39
220	1.65	8.0	37.82

However, unlike damping ratios, the fundamental period of the structure has not been significantly shifted after higher seismic records.

Nevertheless, both effects of 'sharp damping increase' and 'negligible vibration period change' cannot be extrapolated to the overall nonlinear behaviour of every rack structure. This is because all these results are derived from sine sweep tests with very low acceleration intensity of '0.02 g' during which the system experiences small displacements and hence the system behaves elastically. On the other hand, increasing the acceleration intensity is unsafe and impractical due to uncertainties of the system at resonance.

The damping ratios determined from structural motions that are small are not representative of the larger damping expected at higher amplitudes of structural motion. (Chopra, 1995)

Under such low intensity sine sweep tests, the hooks mainly slide in the slots which cause high damping ratios due to the hook-to-slot friction. After running high intensity seismic records in which the structure experiences greater lateral movement, the hooks in the connection area cut into the upright slots and create a higher travel pass for the next hook-slot interactions. This may explain why the damping ratios calculated from the sine sweep tests performed after high seismic shake table tests are drastically higher. The above explanation can be supported by the phenomenon of making loud noises while running sine sweep tests. The noise was possibly because of sliding and the relative movement between the hook and upright slot.

However, the system still showed more damping after it was subjected to higher seismic intensities, or in general, when the system is no longer linear, it shows more damping. This increase of the damping ratio was proved by the last three tests of the scaled 1940 El-Centro test series. In the last three tests with intensities of 160%, 100% and 40% of scaled 1940 El-Centro after the structure has already experienced up to 220% intensity scaled 1940 El- Centro earthquake record, almost 30% smaller peak displacement and base shear was observed compared to the results of the previously tested structure with the same intensity records (see Table 5-6)

5.3 Conclusions

Details of experimental shake table tests including setup and results are presented in this chapter. A 2 Storey - 2 Bay frame was subjected to 1940 El-Centro earthquake records with different intensities in an increasing fashion from low to high intensities. Lateral displacement of the frame under dynamic actions was recorded as well as acceleration at different locations of the frame. Damping ratio of the system at each step was also calculated and an increasing trend in the damping ratio versus maximum lateral displacement of the systems was discovered. Shake table test results proved that the inter-storey drift at the first level of the structure was greater than that of the second level and this effect became more obvious at higher intensity earthquakes. This effect could have been justified by the low rotational stiffness of upright base plate connections. A difference between the recorded acceleration data from the accelerometers mounted on the beams and the data from accelerometers mounted at the concrete blocks (on the pallets) highlighted the effect of sliding in reducing the seismic base shear for seismic design.

6. CHAPTER 6: FINITE ELEMENT SIMULATIONS

6.1 Introduction and Literature Review

This chapter presents the details of FE Modelling and comparison of FE simulation results against shake table test results. Non-Linear Dynamic Time History analysis was performed to simulate the shake table test condition as accurately as possible. As was mentioned in chapters 1 and 5, compared to structural systems there are only limited data bases available for engineers to better understand and then design racking systems and consequently not many comprehensive numerical investigations were carried out so far to accurately evaluate the seismic and non-seismic behaviour of different rack systems.

An equivalent lumped mass numerical model was developed by Blume and associates (1973) in order to predict the fundamental period of vibration of the racking systems in both directions. Rigid beam to upright connections were modelled in down aisle directions and pinned base connections were assumed for both longitudinal (down aisle) and transverse directions (Cross aisle). Although the model was a very simple linear model, it was able to fairly predict the fundamental modes of vibrations.

Another linear model was developed by Chen et al. (1980) to perform frequency analysis and to compare the analytical result with the mode shapes and periods of vibration derived from previously conducted low amplitude forced vibration (shaking table) test as well as free vibration (pull-release) tests. The outcomes of the above investigation were used to support the American standard of 'Uniform Building Code (UBC, 1997)'. He also concluded that a 2-Dimentional model with net cross sectional area of beams and uprights with correct centreline dimensions is enough to perform a modal analysis.

Chen et al. (1980) then developed the first nonlinear numerical model of a racking system by considering semi-rigidity of both beam to upright and upright base connections. Bi-Linear moment rotation curves were then defined based on previous experimental tests on the local components. A time history dynamic analysis was carried out to simulate the behaviour of racking systems under dynamic loads. Their preliminary model was able to fairly predict the dynamic behaviour of investigated racking systems.

Another interesting investigation was carried out both numerically and experimentally by Blume and associates (1987) in order to evaluate the seismic applicability of eccentric braced frame in cross aisle direction of rack structures. Promising results were achieved as was expected for hot rolled steel storage racks. Significant amount of inelastic deformation was observed by the eccentric bracing system without overall instability.

The most recent numerical investigation report on the European cold formed steel storage racking systems was provided by Rosin et al. (2009). They developed a three-dimensional (3-D) numerical model using the 'Perform' software package and as a result the amount of pallet sliding on the beam was approximately calculated. However the peak displacements and accelerations at the top beam levels could not be perfectly matched with the corresponding experimental shake table test results.

Limited experimental and numerical studies on the seismic behaviour of steel storage rack structures established a platform to develop the current seismic codes and specifications for rack structures. The most popular seismic design codes specific to rack structures are RMI (2012) and FEM 10.2.08 (2010). Rack Manufacturer Institute standard RMI (2012) is an American code which is basically written based on International Building Code (IBC, 2005) and Federation Europeenne de la Manutention (FEM 10.2.08, 2010) is essentially based on the European Seismic Code EN 1998-1 (2004). Both specifications present an *Equivalent Static Method* for the analysis and design of steel storage rack structures. However, FEM 10.2.08 (2010) provides more stringent conditions for design of rack structures based on more recent investigations particularly on rack structures. It suggests using more advanced analysis methods (such as Response Spectrum Analysis, Modal Analysis and/or Time History Non-Linear Analysis) based on the regularity of the rack structures (in plan and height).

In this chapter, first a brief overview of different analysis methods will be presented as a background and then the most advanced method (e.g. Non-Linear Dynamic Time History Analysis) will be used to both simulate the shake table tests presented in chapter 5 and to evaluate the overall rack frame behaviour under seismic loads.

6.1.1.1 Equivalent Static Lateral Force Method

The Equivalent Static Lateral Force method (ESLF) is based on elastic static analysis and is summarised as follows:

1. Treat the structure as a linear elastic SDOF model.
2. The total elastic base shear of the structure (Ve) is calculated based to the structure's fundamental period of vibration corresponding to the design response spectrum curve.
3. Reduce the elastic base shear (Ve) by dividing it by the force reduction factor (R or q)[20] to obtain the equivalent inelastic base shear force.
4. Distribute the equivalent lateral inelastic base shear force over the height of the structure by assuming a given shape[21].
5. Analyse the structure under the seismic forces mentioned above.
6. Design the main components of the structure such as beams and columns (other than those that undergo inelastic deformations) for the internal actions obtained from the analysis results.
7. Check the capacity of dissipative zones (the components that provide ductility to the structure such as beam to upright connections or bracing members and connections) for the magnified internal actions obtained from seismic analysis results[22].

---

[20] Seismic reduction factors are the most important factors in ESLF method that are dependant to the ductility and the degree of indeterminacy of structures. American codes (i.e. RMI, UBC & IBC) call the reduction factor as 'R' factor while the European Standards (FEM & EC8) call their reduction factor as 'q' factor. Australian/ New Zealand seismic codes 1170.4 & 1170.5, separately consider the effects of ductility of structures ($\boldsymbol{\mu}$) and degree of indeterminacy (Sp) and as a consequence a total reduction factor of ($\boldsymbol{\mu} / \mathbf{S_p}$) will be calculated.

[21] 'Inversed triangular' shape or 'first mode' shape is commonly used.

[22] Dissipative zones should be designed for corresponding internal actions amplified by an over-strength factor of 'Ω' which is defined in the seismic codes.

8. Assess the inter-storey drifts and/or overall lateral displacement[23] of the rack against serviceability as well as stability criterion.

6.1.2 Modal Analysis

Structures undergoing free vibrations, oscillate according to certain ‘natural modes’ at particular ‘natural frequencies’. These shapes and frequencies are described as natural since they are a property of the structure, independent of external loading (Chopra, 1995).

As described in Chapter 5, MDOF systems have ‘n’ natural modes of vibration corresponding to their ‘n’ degrees of freedom, while the SDOF structures are only allowed to vibrate in their unique mode shape and frequency.

The total displacement ($\boldsymbol{v}$) of a MDOF structure can be displayed as an assemblage of the structure’s mode shapes. An example of a cantilever column with three vertical translational degrees of freedom is shown in Figure 6.1. As shown in Figure 6.1, the displaced shape of any system can be expressed by superimposing the suitable amplitudes of the natural mode shapes (Clough and Penzien, 1993).

$$V = \varphi_1 Y_1 + \varphi_2 Y_2 + \cdots + \varphi_n Y_n = \sum \varphi_i Y_i \quad (6\text{-}1)$$

Or in matrix format:

$$V = \phi\, Y \quad (6\text{-}2)$$

When $\boldsymbol{\phi}$ matrix is a time-independent matrix and **Y** matrix is a time dependent matrix.

[23] Lateral displacements obtained from analysis results should be amplified by a magnification factor (‘Cd’ for RMI and ‘q’ for European Standard) to account for equivalent nonlinear (inelastic) drift of the structure.

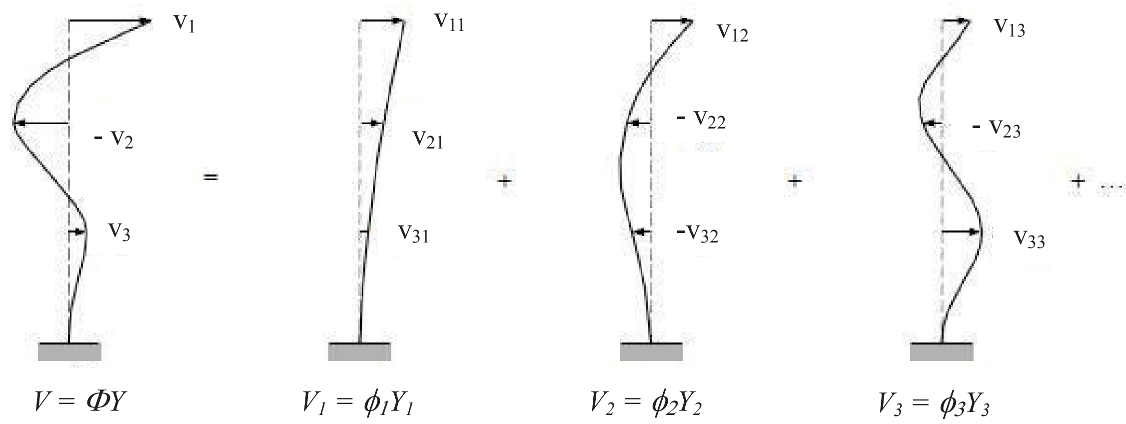

Figure 6.1. Representing deflections as sum of modal components. (Clough and Penzien, 1993, p. 220)

By substituting equation 6-2 into the equation of motion (equation 6-3) the overall response of a MDOF structure can be calculated by solving the differential equation.

$$m\ddot{V}(t) + c\dot{V}(t) + kV(t) = p(t) \qquad (6\text{-}3)$$

For seismic analysis, the external earthquake actions (dynamic load vector) can be expressed by equation 6-4:

$$p(t) = -m\ddot{u}_g \qquad (6\text{-}4)$$

6.1.3 Non-Linear Time History Dynamic Analysis (NLTH)

The most accurate method for the dynamic analysis of non-linear structural systems is the direct numerical integration of the dynamic equilibrium equations using Newmark method presented by Newmark, (1959).

In the Newmark formulation, the basic integration equations for obtaining velocity and consequently displacement of the structural system are expressed as follows:

$$\dot{v}_1 = \dot{v}_0 + (1-\gamma)h\ddot{v}_0 + \gamma h\ddot{v}_0 \qquad (6\text{-}5)$$

$$v_1 = v_0 + h\dot{v}_0 + \left(\frac{1}{2} - \beta\right)h^2\ddot{v}_0 + \beta h^2\ddot{v}_1^2 \qquad (6\text{-}6)$$

By using β=1/6 and γ=1/2 the most general Newmark integration equations will be derived:

$$\dot{v}_1 = \dot{v}_0 + \frac{h}{2}(\ddot{v}_0 + \ddot{v}_1) \tag{6-7}$$

$$v_1 = v_0 + h\dot{v}_0 + \frac{h^2}{3}\ddot{v}_0 + \frac{h^2}{6}\ddot{v}_1^2 \tag{6-8}$$

The details of integration method based on linearly varying acceleration is shown in Figure 6.2.

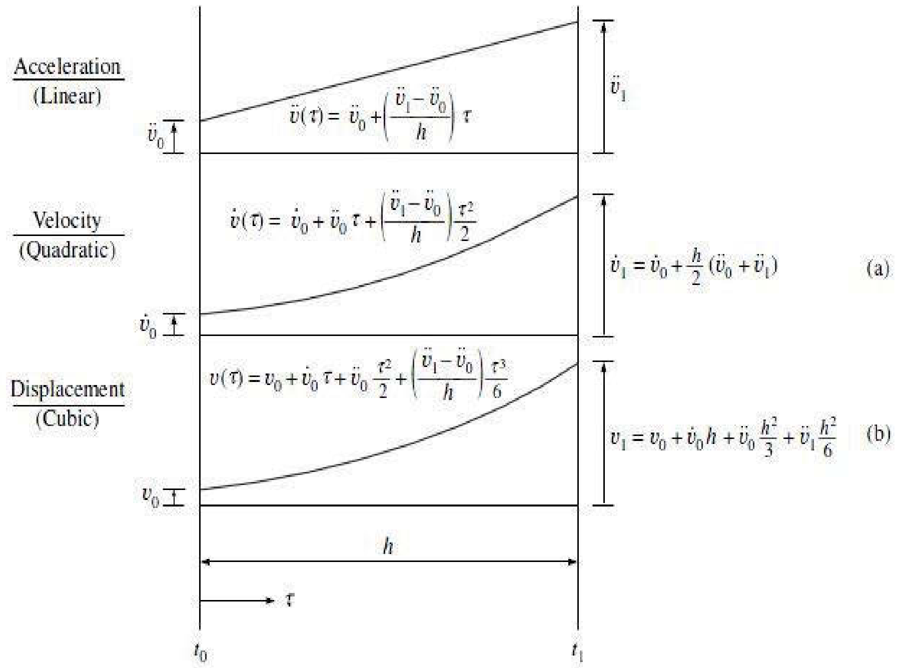

Figure 6.2. Motion based on linearly varying acceleration (Clough and Penzien, 1993, p. 121)

By substituting equations 6-7 and 6-8 into the equations of dynamic equilibrium at time 't_1' (equation 6-9), structural response at time 't_1' can be calculated using a piecewise step by step integration method.

$$m\ddot{v} + c\dot{v} + kv = P \tag{6-9}$$

Stiffness '*k*' in equation 6-9 is not constant when performing non-linear time history analysis (e.g. *k=f(v)*)

Calculation of the structural response at any time can then be calculated from the structural responses at the previous time step.

6.1.4 Non-Linear Static Pushover (NLPO)

Non-Linear Push Over Analysis (NLPO) is a non-linear static analysis of a structure under predefined lateral load pattern that monotonically pushes the structure until a failure occurs (see Figure 6.3). NLPO analysis results are generally presented in terms of plots of lateral deformation of a certain point versus structure's base shear.

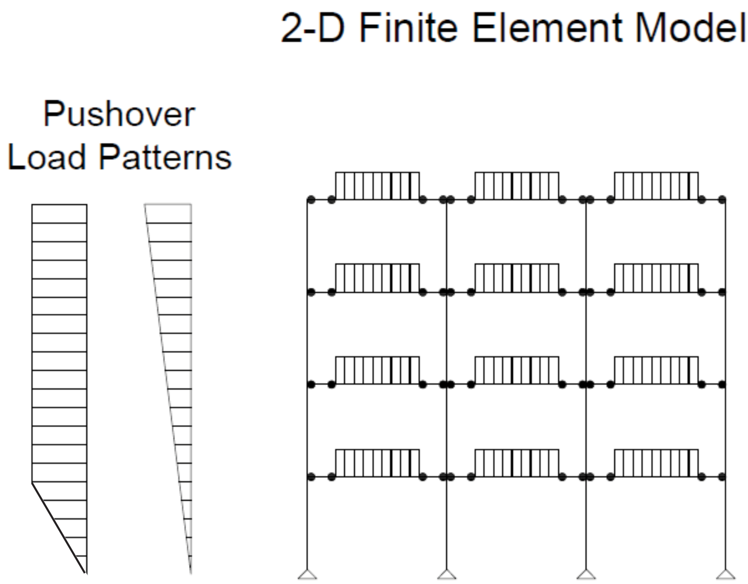

Figure 6.3. Numerical NLPO analysis using linear and uniform 'fixed' load patterns.

Such analysis can be conducted either experimentally or via computer software packages. Experimental push over tests can also be conducted cyclically with increasing amplitude of each cycle until instability occurs. Details of such an experimental analysis will be discussed more in Chapter 7.

Compared to non-linear time history dynamic analysis (NLTH), static push over analysis method has its own advantages and disadvantages as outlined below:

- Advantages:
    - It is simpler (Numerically) and cheaper (Experimentally)
    - Easy to interpret by giving the equivalent lateral force imposed on the system corresponding to a desired inter-storey/overall drift.

- Considers all possible failure mechanisms by making plastic hinges at potential energy dissipative zones.
- When subjected to static lateral loads, this approach is more under control and can be loaded either by displacement control method or load control method.

- Disadvantages
    - It is a static test and dynamic features of the structure such as equivalent viscous damping ratio and natural periods of vibration cannot be determined.
    - Higher mode effects cannot be observed in static push over test.

    > "[Higher modes] can significantly affect inter-storey drifts, plastic hinge rotations, storey shears and overturning forces. The contribution to inter-storey drifts stems directly from the higher mode shapes being more torturous and, therefore, having a greater contribution to inter-storey drift. Consequently, estimates of inter-storey drift based on a first mode pushover analysis is prone to be inaccurate as the number of stories and period increases." (FEMA, 2005, p. A-11)

    - Static push over analysis needs an accurate lateral load pattern to push the structure so that it can behave similar to its performance under dynamic actions. This lateral load pattern needs dynamic analysis to be determined.

    > "The response of the buildings is sensitive to the shape of the lateral load distribution." (Mwafy and Elnashai, 2001, p. 419)

Figure 6.4 shows a typical static push over curve (base shear versus top level displacement) and f_y indicates the point at which the structure starts to yield (yield strength) at yielding deformation of u_y and after that the yielding continues at almost constant force of f_y until failure at the ultimate deformation of u_m. Ductility with respect to displacement of structure can be simply defined as the ratio of maximum (ultimate) deformation, u_m, to the yielding deformation of u_y. (Chopra, 1995)

Ductility: $\mu \left(or\ R_{\mu}\right)(Ductility) = \frac{u_m}{u_y}$ (6-11)

Over Strength Factor: $\Omega = \frac{u_y}{u_o} = \frac{f_y}{f_o}$ (6-12)

Seismic Reduction Factor: $R = \frac{u_m}{u_o} = \frac{u_m}{u_y} \times \frac{u_y}{u_o} = R_{\mu} \times \Omega$ (6-13)

where, u_o is the first yield displacement and f_o is the corresponding force.

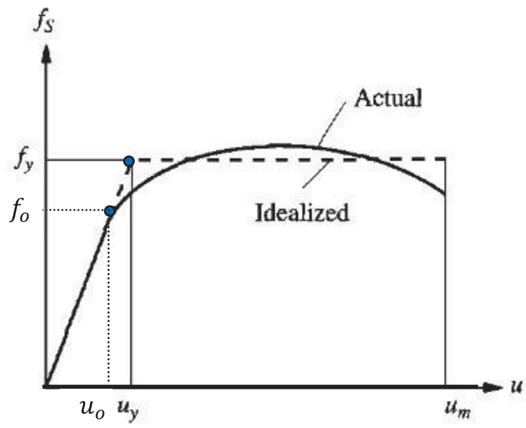

Figure 6.4. Static Push Over curve; actual and elastoplastic idealization (Chopra, 1995, p. 246)

The above ductility factor is also known as 'μ' in Australian and New Zealand Seismic codes and is applied as a reduction factor to the calculated elastic seismic base shears.

6.1.5 Incremental Dynamic Analysis (IDA)

"Incremental Dynamic Analysis (IDA) determines peak response quantities (e.g. roof drift) by a series of independent nonlinear dynamic analyses of a structure subjected to one or more scaled ground motions. The scale factor ['λ'] is increased successively from a small initial value, and peak response quantities are plotted against a measure of the ground motion intensity." (FEMA, 2005, p.A-12)

Incremental Dynamic Analysis (IDA) results are basically presented in the format of plotting an intensity indicator (or Intensity Measure, IM) of the imposed acceleration record (PGA or λ) versus the maximum displacement or inter-storey drift (Damage Measure, DM) of the system under corresponding accelerogram intensity (Vamvatsikos and Cornell, 2002).

Although IDA method is computationally (and experimentally) very time consuming as it requires many steps of NLTH analysis, it is very useful and efficient because of giving an overview of various steps of NLTH analysis results and providing much better understanding of the structural response under different intensities of a given earthquake record. More details and characteristics of incremental dynamic analysis method and IDA curves are well explained in different papers. (Borzi & Elnashai, 2000 and Mwafy & Elnashai, 2001, Vamvatsikos & Cornell, 2002, Kim and Choi, 2005, Fathi, Daneshjoo, & Melchers, 2006, Dubina, 2008, Asgarian & Shokrgozar, 2009 and Reyes, 2013)

Due to similarity of NLPO analysis concept and IDA concept, IDA curves are also known as Dynamic Non-Linear Push Over curves (DNLPO) and in fact can give us a ductility indication of structures under a particular earthquake record by using the same approach as explained above (Mwafi & Elnashai, 2001).

An evaluation of ductility factor for a typical racking system under different earthquake records using both IDA and NLPO curves is presented below.

6.1.6 Preliminary Investigations

Prior to conducting the shake table program and starting to simulate the shake table test conditions as presented in Chapter 5, a 2-D finite element analysis was performed on a 4-storey 3-bay frame model shown in Figure 6.5. The objective of this preliminary investigation which was conducted jointly with a final year undergraduate student was to better understand the behaviour of the moment frame of the rack structures under widely used seismic actions including El-Centro (1940), Northridge (1994) and Kobe (1995) earthquake records. Different seismic records with different intensities beside different beam to upright connection models were well investigated and reported (Reyes, 2013). This investigation not only shows the approach to the most suitable beam end connector technique, but also checks the ability of connectors in resisting seismic actions by providing ductility to the rack structures.

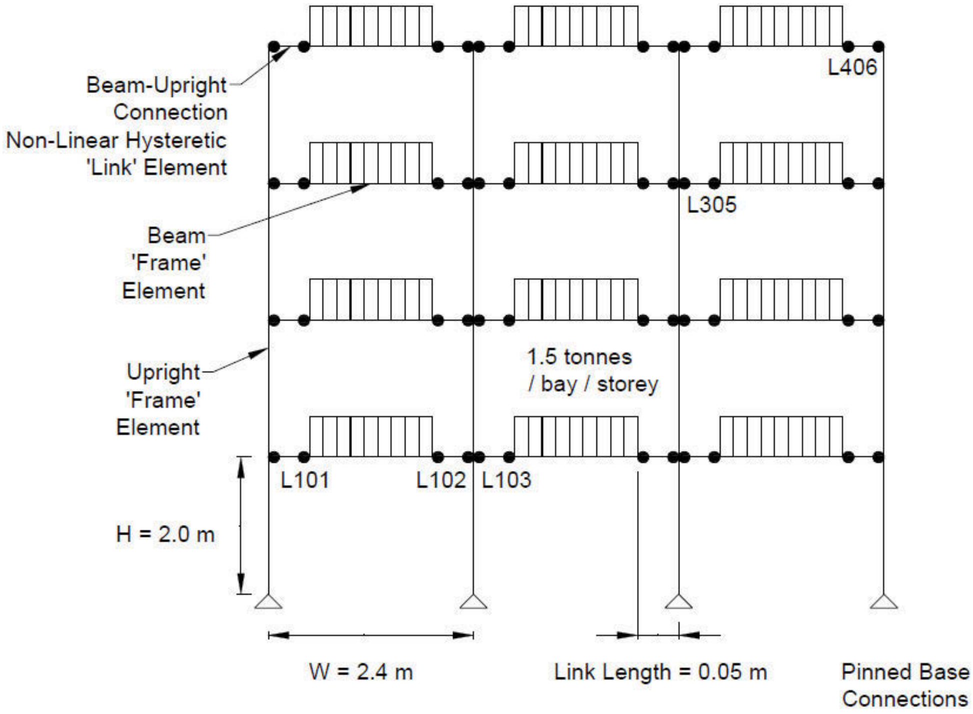

Figure 6.5. Finite Element model of entire rack frame. (Reyes 2013, p. 66)

In this section a summary of that investigation and conclusions will be presented. SAP 2000 (2009) software was used to prepare the FE model and the following assumptions were made to generate the model.

1. The beam to upright connections modelled using the link elements, were the only locations (zones) to allow plastic hinge formation. Beam and upright were assumed not to undergo inelastic deformations. This assumption was supported by Filiatrault et al. (2006) and Bernuzzi and Castiglioni (2001).

> "Although the system exhibits highly nonlinear behaviour up to very large relative rotations between the beams and uprights, it remains essentially elastic in the sense that the behaviour does not cause permanent inelastic deformation in the beams and uprights." (Filiatrault et al. (2006), p. 162)

"It has been shown that frame collapse is generally due to the interaction between instability and plasticity in beam-to-column joints. Columns never achieved their ultimate strength, while in a limited number of cases a plastic hinge occurred approximately at the beam mid-span." (Bernuzzi & Castiglioni (2001), p. 844)

2. Geometric Non-Linearity was considered in the analysis.

3. Referring to FEM 10.2.08 (2011) [6.26], a damping ratio of 3% was specified at a period of 6.18 seconds and 0.06 second using Rayleigh damping model.

4. Upright base plate connections were modelled as hinged connection.

5. Three Different hysteresis models (i.e. Kinematic Model, Takeda Model and Pivot Model)[24] were used to simulate the beam to upright connections.

The model was first excited by El-Centro (1940) earthquake record to investigate the dynamic features of a rack frame such as capacity, energy dissipation capability and permanent drift. The following observations were made;

6.1.6.1 Frame Capacity[25]

The effect of different beam-upright connection hysteresis models on the frame capacity under El-Centro (1940) earthquake record was first investigated. The models that were investigated are mentioned below:

1. Kinematic model:

    a. with experimental monotonic back bone (KIN-MON)
    b. with proposed equivalent cyclic back bone (KIN-EQV)

---

[24] Details of these three individual hysteresis models of the beam to upright connections were presented in Chapter 2.

[25] Frame Capacity was indicated as the maximum PGA (or maximum earthquake intensity) in which the software could not converge or very large and unrealistic drifts were observed in FE results.

2. Takeda Model[26] (TAK-EQV)
3. Pivot models[27]:
    a. with experimental cyclic back bone (PIV-CYC)
    b. with proposed equivalent cyclic back bone (PIV-EQV)

It was noticed that the system with more realistic beam to upright connection model (e.g. Pivot hysteresis model with actual experimental cyclic back bone, PIV-CYC) survived the highest earthquake intensity meaning that all other beam to upright models provide a conservative estimation of the structures capacity under El-Centro (1940) earthquake. However, the structure with "Equivalent Cyclic Pivot connection model" (e.g. Pivot hysteresis model with proposed equivalent cyclic backbone, PIV-EQV) failed at an intensity scale much closer to that of PIV-CYC. Also equivalent cyclic Pivot model, PIV-EQV, does not provide conservative estimation of important response quantities such as base shear and inter-storey drifts. Therefore whilst using PIV-EQV model in the finite element analysis provides an accurate estimation of rack collapse under seismic actions compared to the PIV-CYC model, this method can be used when no cyclic results are available.

Table 6-1 shows the capacity of different models in terms of Peak Ground Acceleration (PGA) (or El-Centro (1940) earthquake scale) and Table 6-2 shows the details of structural responses of systems with different beam to upright connection models under 60% El-Centro (1940) earthquake.

Table 6-1. Summary of El Centro scaling at collapse when using different connection models.

Connection Model	Scale Factor (λ) at Collapse	PGA at Collapse (g)
KIN-MON	0.95	0.333
KIN-EQV	0.65	0.227
TAK-EQV	0.90	0.315
PIV-EQV	1.15	0.403
PIV-CYC	1.30	0.454

[26] Takeda model with proposed equivalent cyclic back bone (refer to Chapter 2)

[27] Refer to Chapter 2

Table 6-2. Response of Rack Modelled with Different Connection models to 60% El-Centro (1940) ground motion

Connection Model	Max Top Storey Deflection ('DY $_{MAX}$', m)	Max Inter-storey Drift Ratio[28] (δ_{MAX} / h)	Max Base Shear ('V $_{MAX}$', kN)	Permanent Top Storey Inelastic Deflection (m)	Total Energy Dissipated by Links (kJ)
KIN-MON	0.225	6.5%	2.02	0.00	0.136
KIN-EQV	0.282	8.1%	1.88	-0.11 [29]	0.206
TAK-EQV	0.214	6.4%	1.88	-0.02	0.212
PIV-EQV	0.189	6.4%	1.88	0.01	0.190
PIV-CYC	0.224	6.3%	2.09	0.02	0.218

Analysis results are shown in Appendix D.

6.1.6.2 Hysteresis Behaviour and Energy absorption

Although the Kinematic model seems to dissipate more energy when subjected to the connection cyclic test, Finite Element results show that the structures modelled with the Kinematic model dissipate less energy compared to the structures modelled with Takeda or Pivot models and indeed fail at lower intensities of a given earthquake record than those with Takeda and Pivot models. This phenomenon can be explained by the inherent hysteretic algorithms directing the moment rotation "paths" or "loops" by each hysteresis model. The rules of Kinematic model allow or push the curves to oscillate about a non-zero point, while subjected to an inelastic cyclic excursion. These later cycles oscillate elastically (e.g. linearly) about the shifted non-zero origin (Figure 6.6). Figure 6.7 shows stages of inelastic deformation progressing up until failure. The outlined part of the figure shows the hysteresis curves of the Kinematic connection from time 39 sec until failure when the system is subjected to 95% scaled El-Centro (1940) earthquake. It can be seen that the moment rotation path will be oscillating linear elastically around a shifted origin.

[28] The max inter-storey drift ratio was always noted to occur in the first storey. Same was observed in the shake table test results presented in Chapter 5.

[29] High permanent deflections are characteristically demonstrated by the KIN hysteresis model close to failure. This is due to the KIN model's elastic oscillations after inelastic excursions, discussed further in section 6.1.5.2.

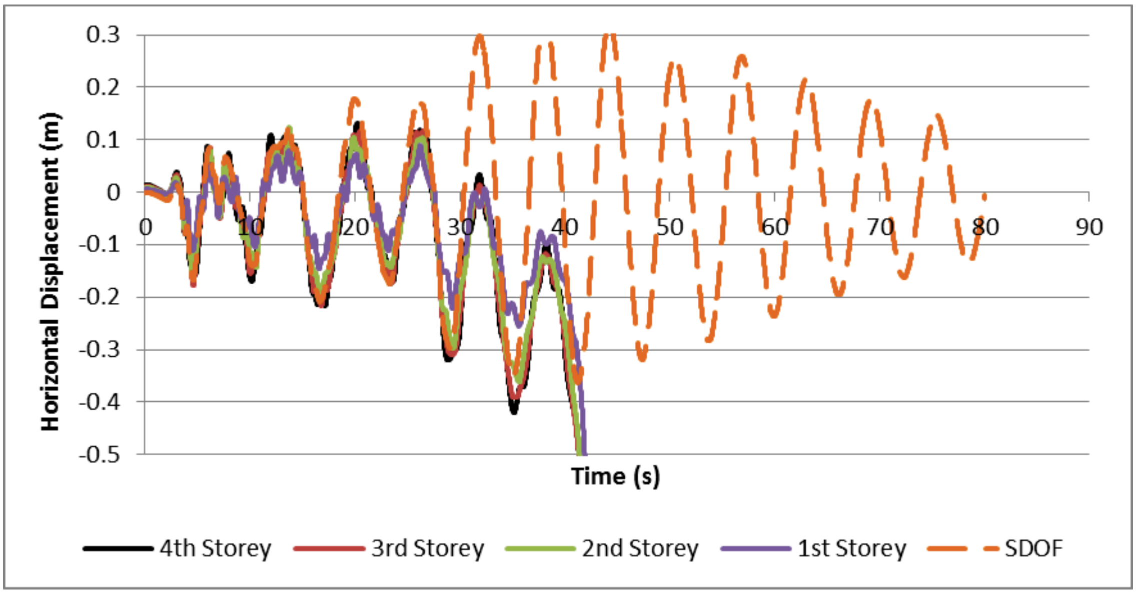

Figure 6.6. Deflection Response of KIN & SDOF Equivalent to 95% El Centro. Instability and collapses occurs at ~40s. (Reyes 2013)

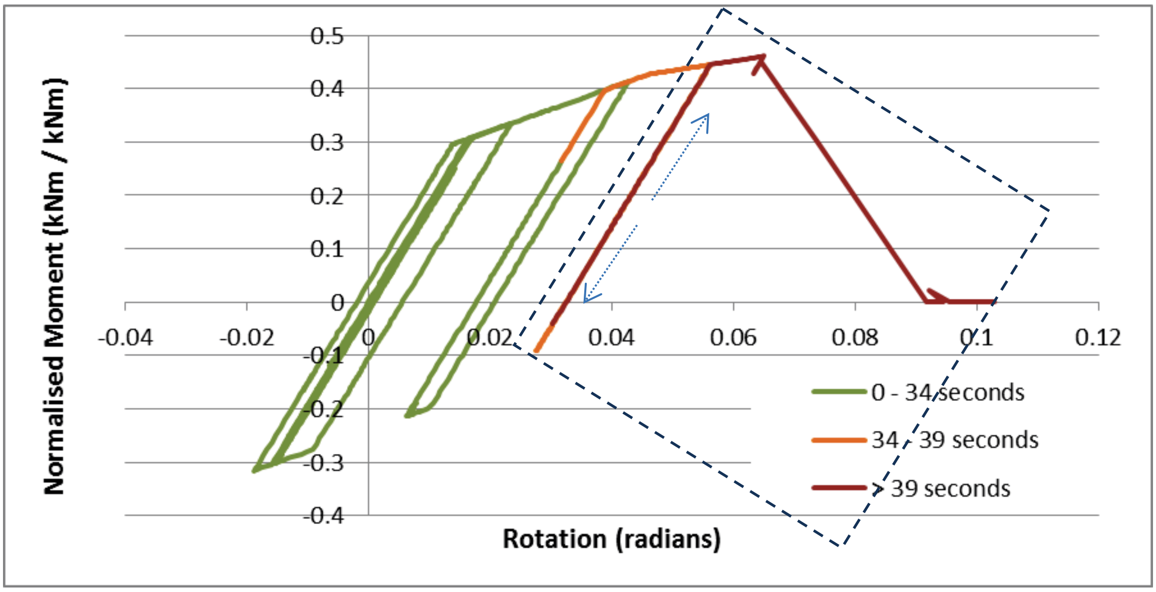

Figure 6.7. Kinematic link response to 95% El Centro (Reyes 2013)

This behaviour has three consequences.

1. As mentioned above, after the structure modelled by Kinematic model is subjected to higher intensity seismic records, the moment-rotation path will be pushed further, following the backbone curve and, therefore, later cycles oscillate about a displaced point which is closer to the defined back bone limit. On the other hand later cycle oscillations in Takeda and Pivot models occur closer to the origin of the back bone curve. This phenomenon can justify the lower capacities of the structures modelled by Kinematic model

when the further inelastic cycles initiate from a higher moment – rotation origin in dynamic time history analysis.

2. Due to the same reason, the amount of energy dissipated by the Kinematic model is significantly less than the amount of energy that Takeda and Pivot models dissipate through their inelastic hysteresis in later cycles.
3. High permanent drift was observed in the system modelled with Kinematic model when almost negligible permanent inelastic drift was observed in the systems modelled with Pivot and Takeda models[30] and subjected to El-Centro (1940) earthquake record. However, it should be noted that this feature of zero permanent lateral deflection for the systems with Pivot connections may not be necessarily valid for other earthquake records.

6.1.6.3 Second order (P-Delta) effects

Another finding of the numerical investigation was the effect of geometrical non-linearity on the dynamic period of vibration. To evaluate the sensitivity of the value of fundamental period of vibration to the second order effects, two dynamic modal analyses were performed with the following conditions:

I. Modal analysis was conducted from zero initial conditions without P-Δ effect.

II. Modal analysis was continued from the end of a previous static non-linear analysis of structure under pallet loads and P-Δ effect is included in the program.

Comparing the results of the two analysis cases, it was observed that the fundamental period of structure in case (I) was 3.49 seconds when the fundamental period of structure in case (II) was 6.18 seconds. Such a significant difference in the fundamental vibration period of structure leads to a reduction of almost 65% in the equivalent seismic base shear of the system for seismic design according to Australian seismic code 1170.4 (AS 1170.4 (2007)).

Theoretical details of P-Delta effect on the fundamental period of vibration is thoroughly explained by Clough and Penzien, (1995). This period elongation due to

[30] This phenomenon was later proved by the experimental shake table test results.

second order effects is more significant in those structures that are heavily loaded close to their overall stability limit and negligible in those structures with lighter Dead/Live loads compared to the frame stiffness. Therefore, unlike most structural systems, this effect becomes a significant parameter in design of high rise steel storage rack structures due to their lightness and high Live Load to Dead Load ratios compare to buildings.

6.1.6.4 Incremental Dynamic Analyses

Effect of different connection modelling approaches on the overall behaviour of a typical unbraced rack system in down aisle direction was investigated in the first round of FE analyses. The significant difference between different connection models highlighted the importance of using correct modelling procedures for further investigations. Therefore, the rack model with connections modelled with Pivot hysteresis model, formed by cyclic back bone from experimental test, was used to continue the investigations by performing an "Incremental Dynamic Analysis (IDA)". For this reason two earthquake records of El-Centro (1940) and Northridge (1994) shown, respectively, in Figure 6.8 and Figure 6.9 were used to derive two sets of Incremental Dynamic Analysis (IDA) curves in order to investigate the ductility of the rack frame with boltless beam to upright connections in down aisle direction.

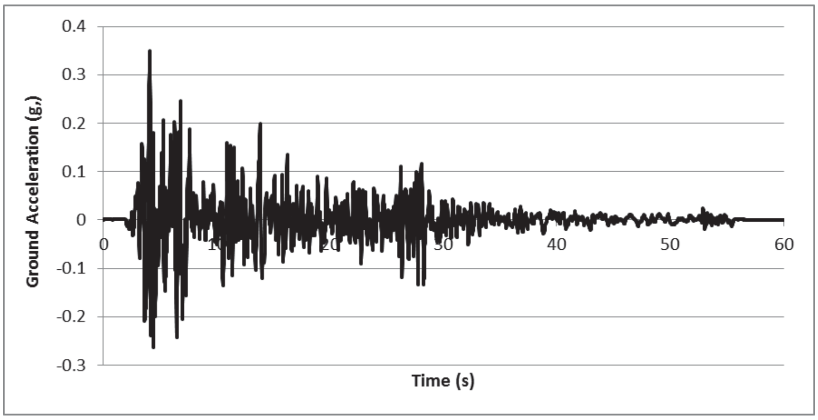

Figure 6.8. El-Centro 1940 Accelerogram. Unfactored Max PGA = 0.35g

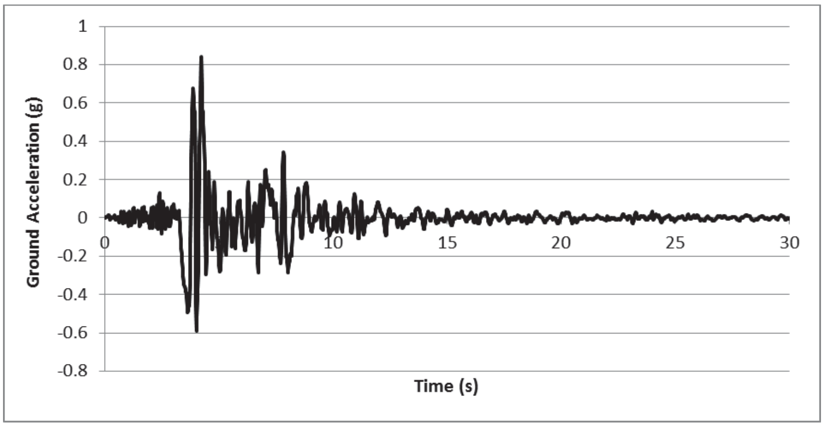

Figure 6.9. Northridge 1994 Accelerogram. Unfactored Max PGA = 0.84g

Incremental non-linear time history analyses were performed by increments of "Δλ = 0.1" for the El-Centro (1940) earthquake (a far field earthquake) and Δλ of "0.05" for the Northridge (1994) and Kobe (1995) earthquakes (near field earthquakes) until the solution reached convergence problems that was deemed as frame failure. The time history analyses were continued for 20 seconds after the earthquake record to consider the free vibration of the frame after the earthquake. Non-linear time history analyses were repeated in each step with linear connections. For this reason, a linear rotational spring simulating the connection behaviour was used to define the initial stiffness of the Pivot model. The purpose of these analyses was to discover the first yield point of the structure, where the nonlinear model starts to deviate from the linear analyses results. Additionally, equivalent Single Degree of Freedom (SDOF) linear-elastic dynamic analyses were performed using the Duhamel Integration method[31] (See Figure 6.10). The reason of conducting SDOF dynamic analyses was to calculate the first mode spectral response of the structure.

[31] This analyses were performed using the excel program developed by Reyes 2013.

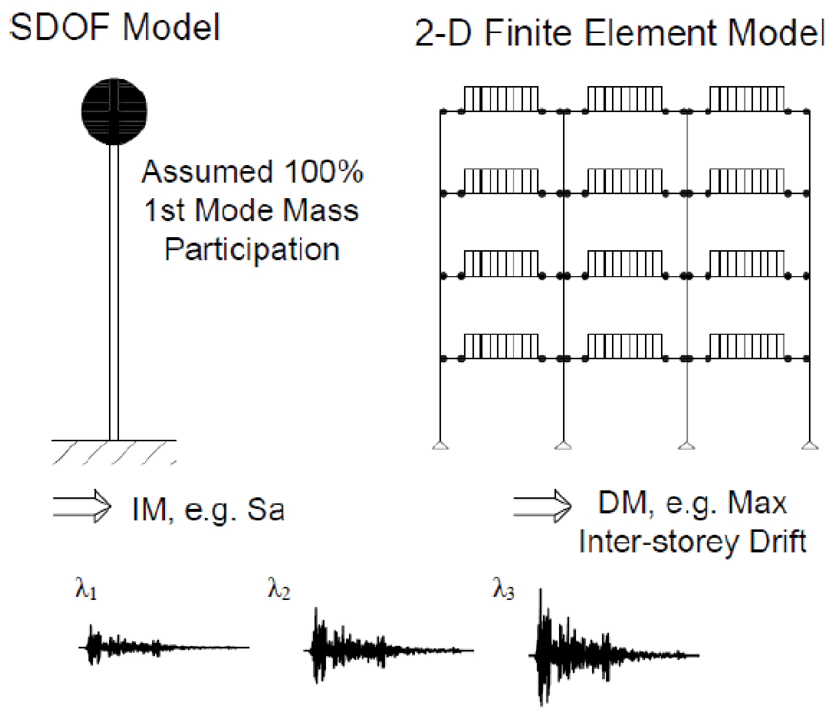

Figure 6.10. Schematic of IDA Analysis Process and Outputs. Note the figure shows three scaled El-Centro 1940 records, leading to three points on the IDA curve. (Reyes, 2013, p. 93)

Details of analysis results such as "energy dissipation", "connection rotation", "top story deflection" and "base shear response" of both nonlinear MDOF and linear SDOF models is well reported in [6.22]. A short summary of analyses results for 1940 El-Centro and 1994 Northridge earthquake records will be described below.

6.1.6.4.1 1940 El Centro Earthquake (Far Field Earthquake)

The frame responded linearly at the first three increments up to "$\lambda = 0.3$" (PGA = 0.3 x 0.35 = 0.105 g) and zero energy dissipation due to plastic rotation of beam-upright connections were observed. However, the structure was pushed to behave inelastically at "$\lambda = 0.4$" (PGA = 0.4 x 0.35 = 0.14 g), when the energy function will not return to zero, indicating plastic deformations. (See Figure 6.11)

Also, Duhamel SDOF solution started to deviate from non-linear time history analysis results (NLTH) at "$\lambda = 0.4$" which is another proof of inelastic deformations.

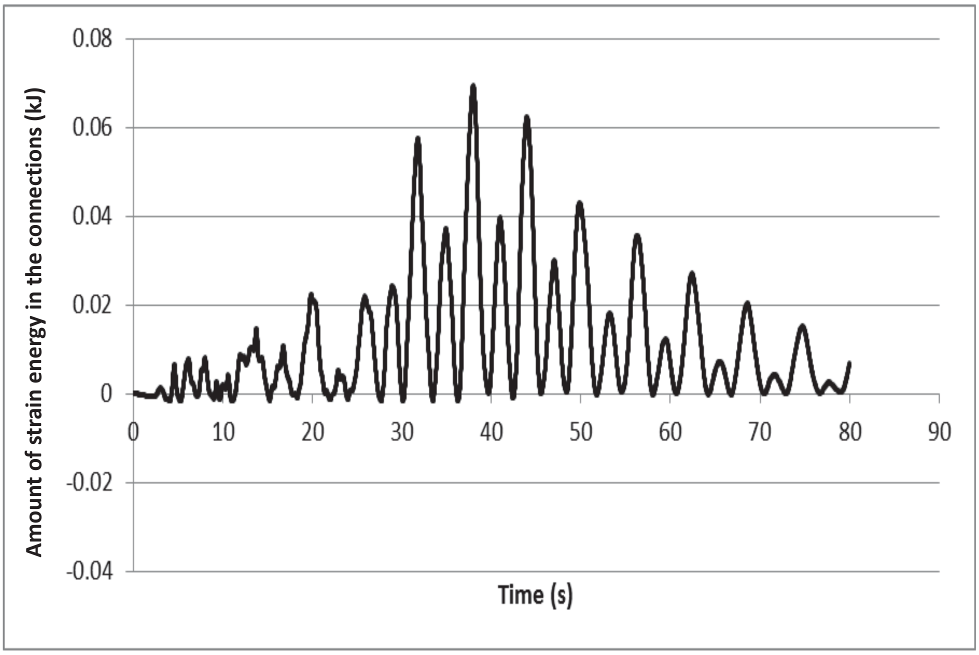

Figure 6.11. (a)

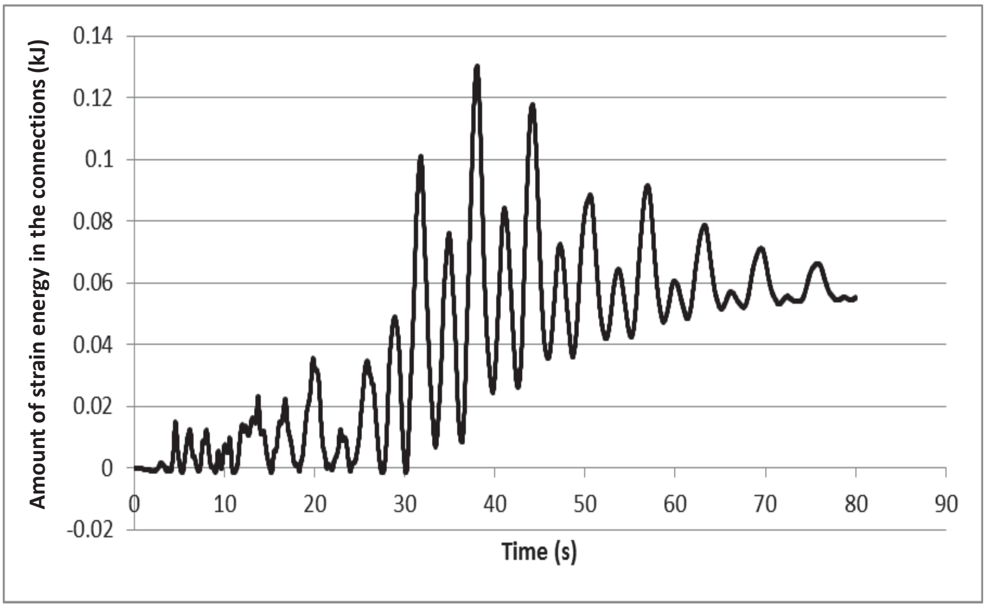

Figure 6.11. (b)

Figure 6.11. Total amount of strain energy in the connections when subjected to 30% and 40% El-Centro (1940) earthquake.

The solution could not converge while running "λ = 1.25". Therefore, the upper limit of "λ = 1.2" (PGA of 0.42 g) was considered as the final step indicating the frame capacity, in which a remarkable amount of energy was *gradually* dissipated by the connections for the full duration of the 1940 El-Centro earthquake (See Figure 6.12).

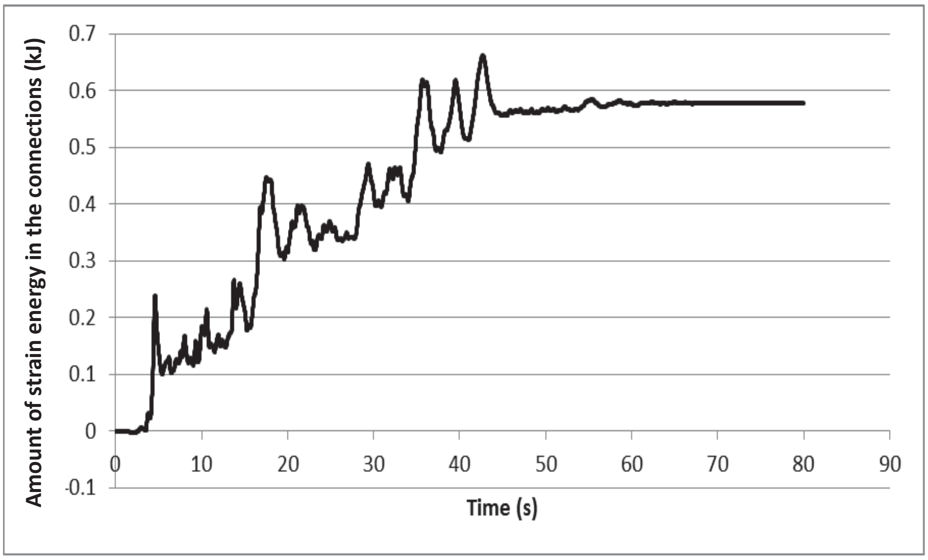

Figure 6.12. Total amount of strain energy in the connections when subjected to 120% El-Centro earthquake.

Significant energy dissipation was observed in the first storey connections while the amount of energy dissipated by higher level connections was almost negligible (See Figure 6.13).

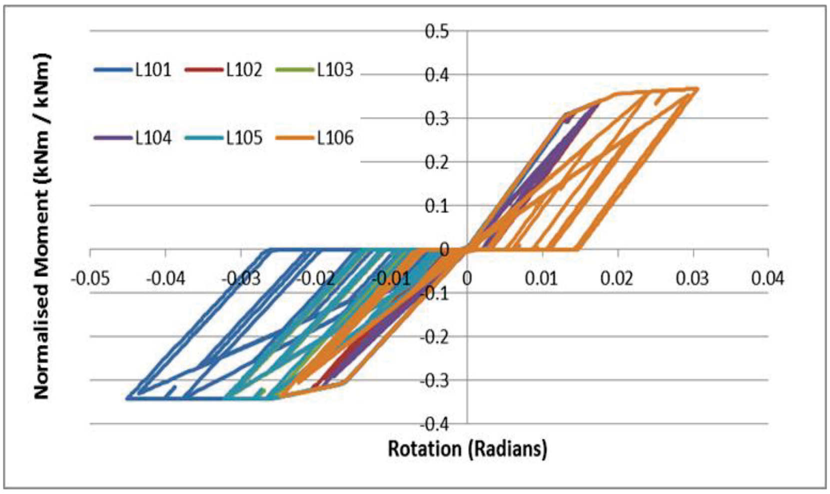

Figure 6.13(a). Connections at 1st Level

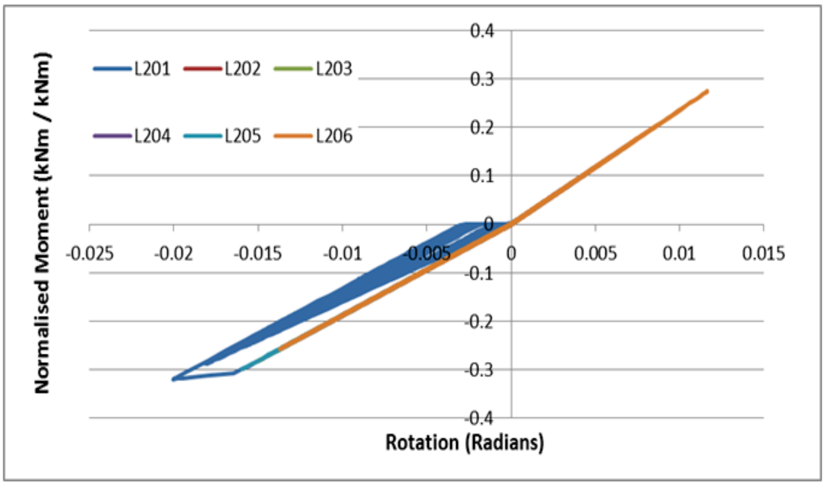

Figure 6.13(b). Connections at 2nd Level

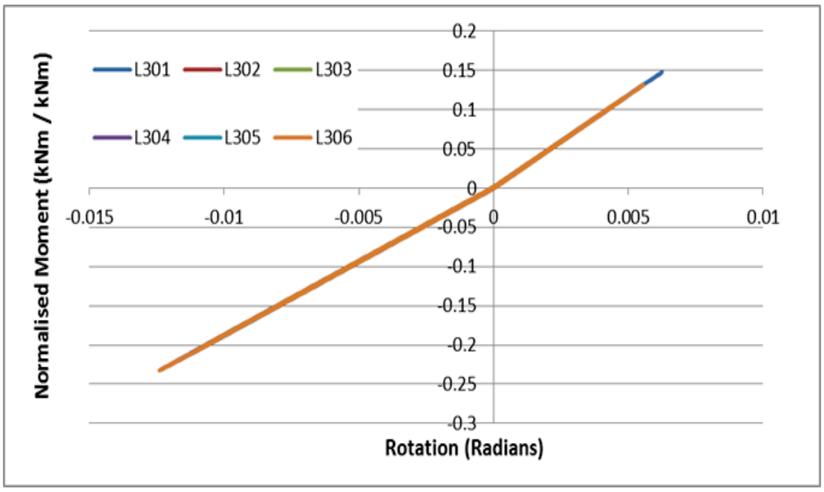

Figure 6.13(c). Connections at 3rd Level

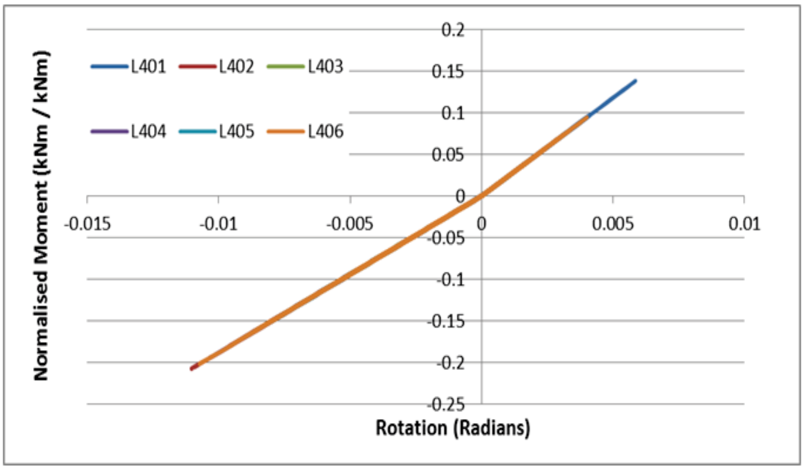

Figure 6.13(d). Connections at 4th Level

Figure 6.13. Moment rotation behaviour of the connections at different levels

This indicates the potential for soft storey failure mode of the frame in which greater inter-storey drift is observed in the first level than the higher levels as shown in Figure 6.14.

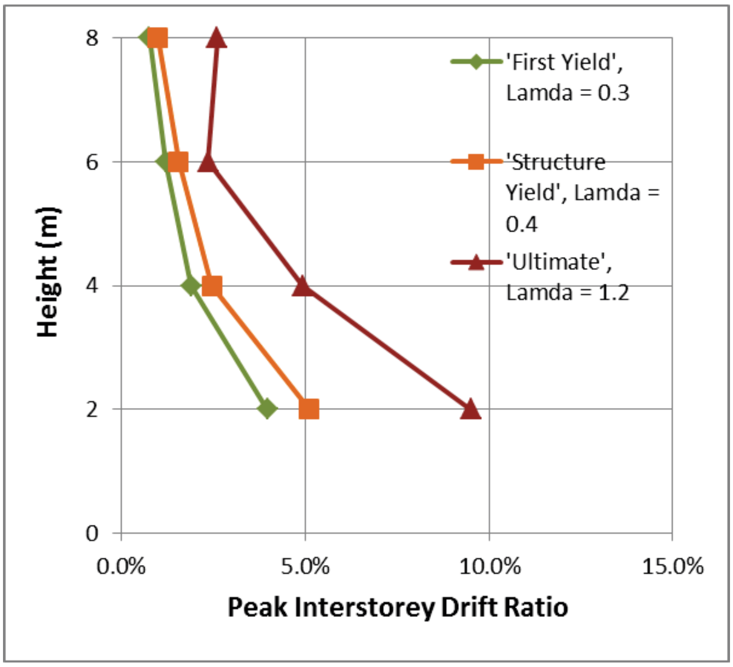

Figure 6.14. Inter-storey drift of the system at different load intensities (soft storey mechanism is obvious).

6.1.6.4.2 1994 Northridge Earthquake (Near Field Earthquake)

Analyses started from "$\lambda = 0.05$" and continued in steps of "0.05" until a numerical convergence problem occurred at "$\lambda = 0.55$". Therefore, "$\lambda = 0.5$" (PGA of 0.415 g) was considered as the final step (e.g. the frame capacity).

Significant permanent top storey deformation was observed at "$\lambda = 0.5$" from non-linear time history analysis results. Surprisingly, the *ratio* of the non-linear dynamic analysis and SDOF Duhamel integration solution maximum base shear was *unity* indicating no ductility in the system[32] (e.g. ductility factor of "R ≅ 1"). Unlike the 120% 1940 El-Centro energy dissipation, the majority of the energy dissipated by the connections took place in the first big "jerk" at the beginning of Northridge earthquake record as shown in Figure 6.15. The amount of dissipated energy then remained almost constant during the earthquake period.

[32] There is no ductility in the system, as Linear analysis result shows almost identical as the Non-Linear analysis results indicating that the system can be modeled by linear analyses method without considering ductility and reduction factors.

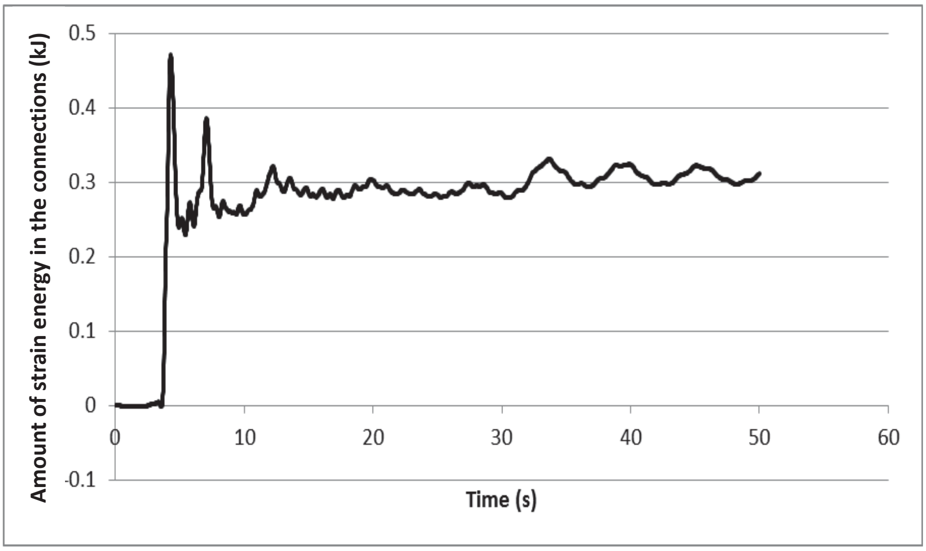

Figure 6.15. Total amount of strain energy in the connections when subjected to 50% 1994 Northridge earthquake.

The significant energy dissipation occurring at the start of the earthquake can be seen clearly by the inelastic deformation undergone by the first level connections which are remarkably greater than the subsequent cycles.

Figure 6.16 shows the moment rotation behaviour of the beam to upright connections at different levels. Greater rotation was observed in the first storey connections compared to higher level connections similar to the 120% 1940 El-Centro results. Also it can be seen from the moment rotation hysteresis curves of first level connections that the curves come into rest at a non-zero point which explains the permanent drift of the top story level.

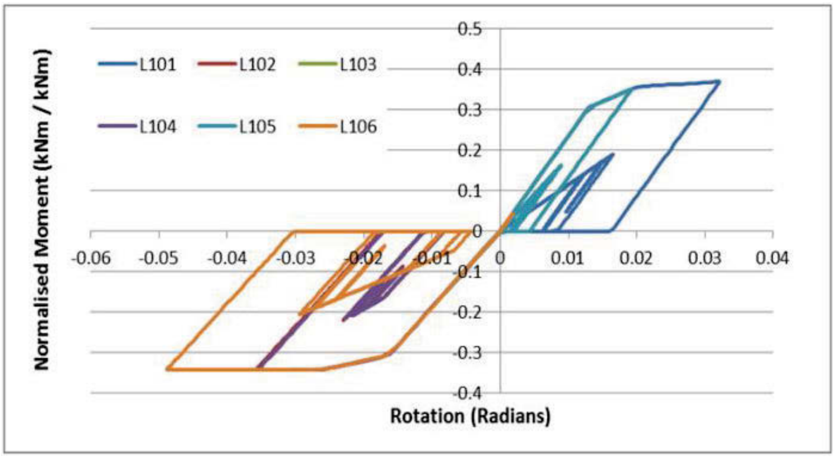

Figure 6.16(a). Connections at 1st Level

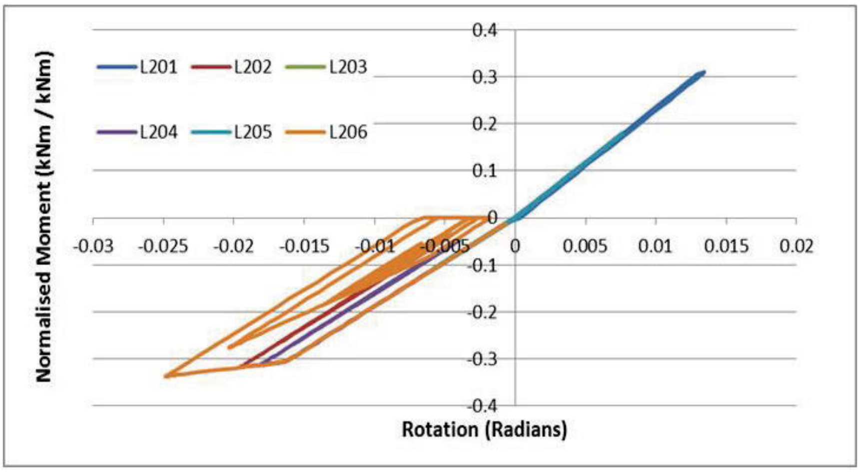

Figure 6.16(b). Connections at 2nd Level

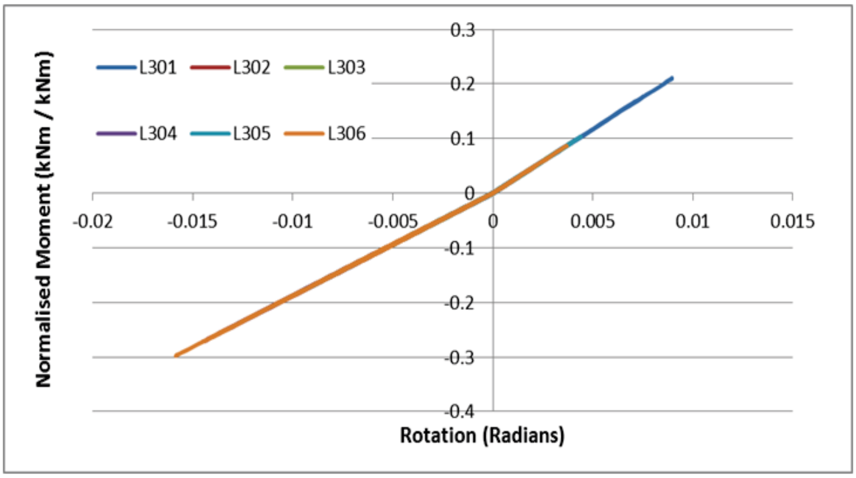

Figure 6.16(c). Connections at 3rd Level

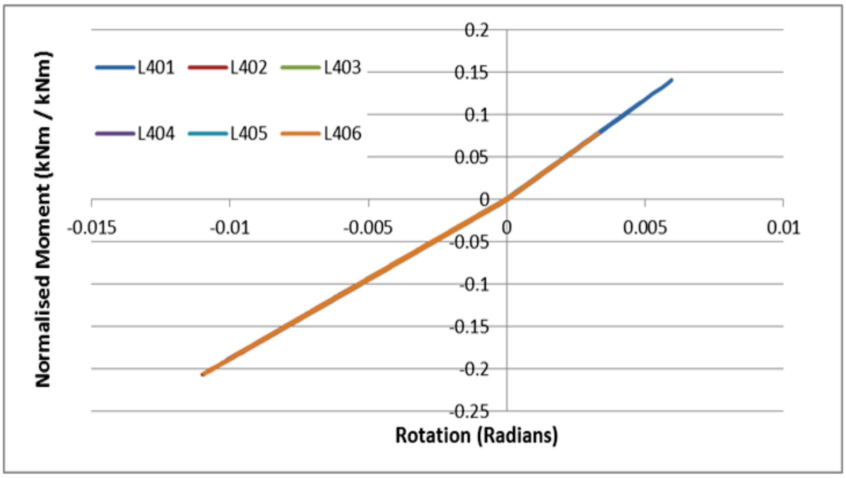

Figure 6.16(d). Connections at 4th Level

Figure 6.16. Moment rotation behaviour of the connections at different levels

6.1.6.4.3 Discussion of analyses results

IDA curves for the three[33] earthquakes are shown in Figure 6.17 and Figure 6.18.

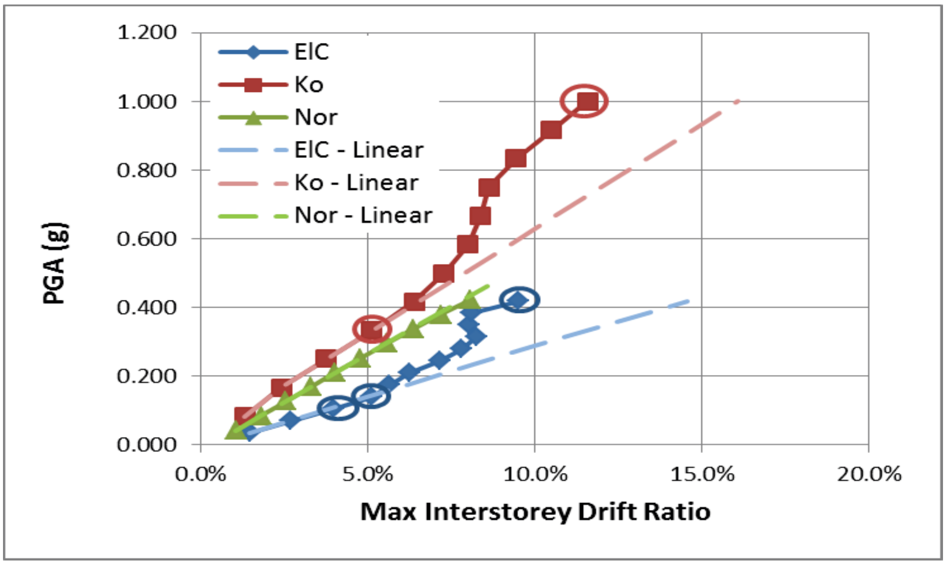

Figure 6.17. PGA vs. Max inter-storey drift ratio IDA curves for 3 different earthquakes.

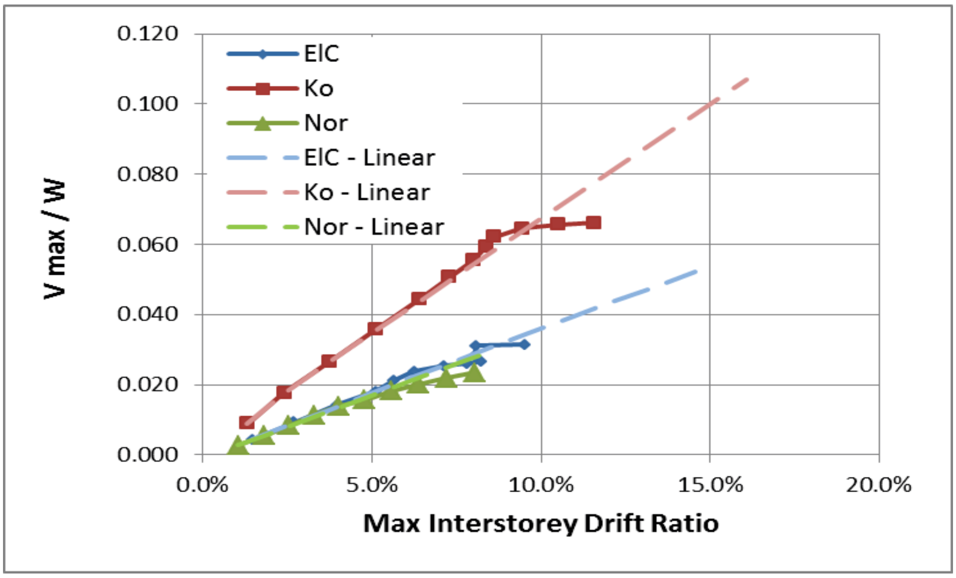

*: W is the weigth og the system

Figure 6.18. 'Dynamic Pushover' style IDA results in the format of base shear coefficient vs. drift for 3 different earthquakes.

As was mentioned earlier, a ductility reduction factor of around "1" for 1994 Northridge earthquake was evident from the analysis results which can be justified by the features of Near Field earthquakes.

[33] The details of analysis results of Kobe Earthquake (Near Field Earthquake) is presented in reference [6.22]

“Near field motions are those that contain one or more large velocity pulses, usually originating from the superposition of waves emanating from the fault as the rupture progresses towards a site.” (FEMA, 2005, p. A-8)

“The R factors associated with such pulses are smaller, in general, than those associated with motions in which resonance contributes to the elastic spectral amplitudes” (FEMA 2005, p. A-8)
On the other hand, 1940 El-Centro earthquake seems to be a more typical ground motion for far field earthquakes “located more than 15km from the fault rupture” (Medina & Krawinkler, 2003, p. 38). Therefore, the R factors calculated from 1940 El-Centro earthquake are more acceptable and applicable in general. Therefore, the seismic design factors were derived based on the results of 1940 El-Centro Incremental Dynamic Analyses.

The circled points in the 1940 El-Centro results (Figure 6.17) represent the “first significant yield”, “structural yield” and “collapse” points. Seismic reduction factors are then presented in the below tables.

Table 6-3. R Factor Calculation via PGA Ratio with respect to ‘first significant yield point’ selection.

From Figure 6.17	**It follows:**
$PGA_{ult} = 0.42$	$R\mu = 3.0$ (0.42/0.14)
$PGA_{structure\ yield} = 0.14$	$\Omega = 1.33$ (0.14/0.105)
$PGA_{first\ yield} = 0.105$	$\therefore R = 4.0$ (0.42/0.105) ($R = R\mu.\ \Omega = 3 \times 1.33 = 4$)

The calculated reduction factor of (R = 4) is 30% less than the proposed reduction factor of (R = 6) in RMI and is 100% greater than that of FEM (q = 2)

6.1.6.5 Non-Linear Static Push-Over Analysis

To evaluate the proposed “R” factor, non-linear push over analyses with two different loading patterns (triangular and rectangular) were also performed (See Figure 6.19).

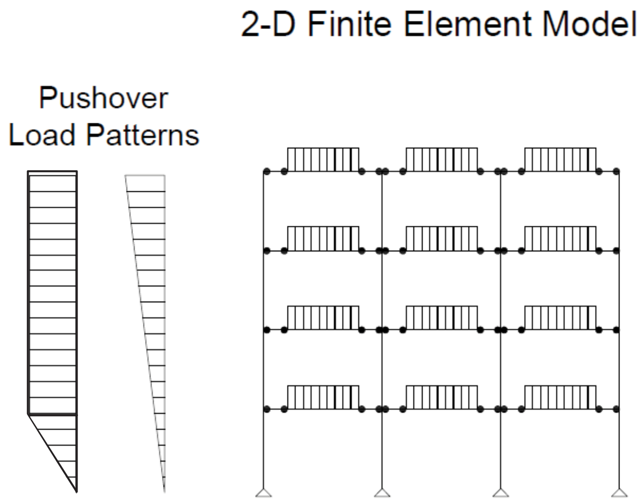

Figure 6.19. Numerical NLPO analysis using linear and uniform load patterns.

Due to the observed failure mode from the dynamic analyses mentioned above, the rectangular load pattern gives a better agreement with the IDA results as seen in Figure 6.20.

"A rectangular pushover load pattern is noted by literature to be appropriate for 'soft storey' structures which is indeed the case for down-aisle unbraced storage racks with pinned bases." (Reyes, 2013, p. 145)

"The use of the uniform load shape may be justified in the light of a possible soft storey mechanism… If this mechanism occurs the response will be controlled by a large drift in the first storey… The inverted triangular (code) and the rectangular (uniform) load shapes also represent the extreme cases from the linear distribution point of view." (Mwafy & Elnashai, 2001, p. 411)

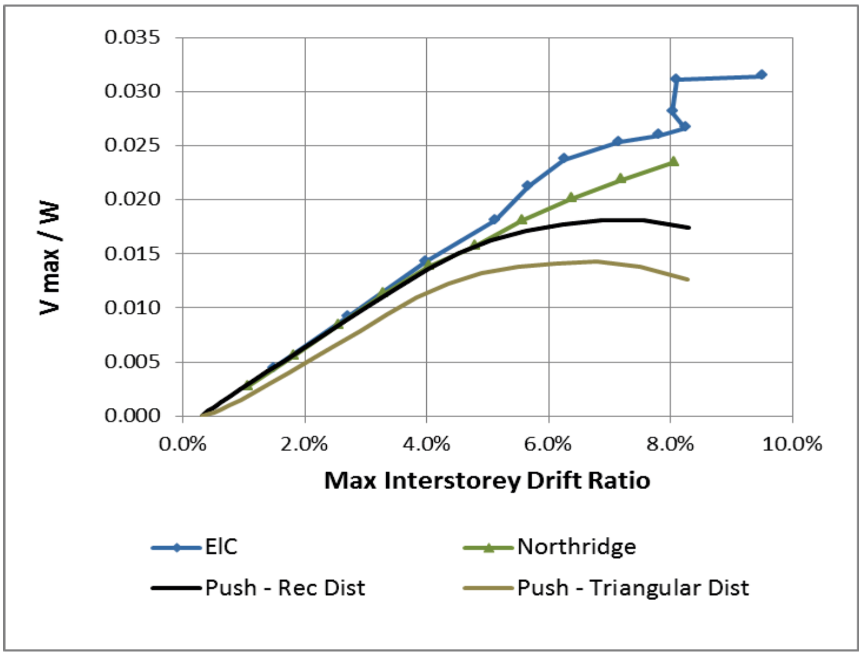

(a)

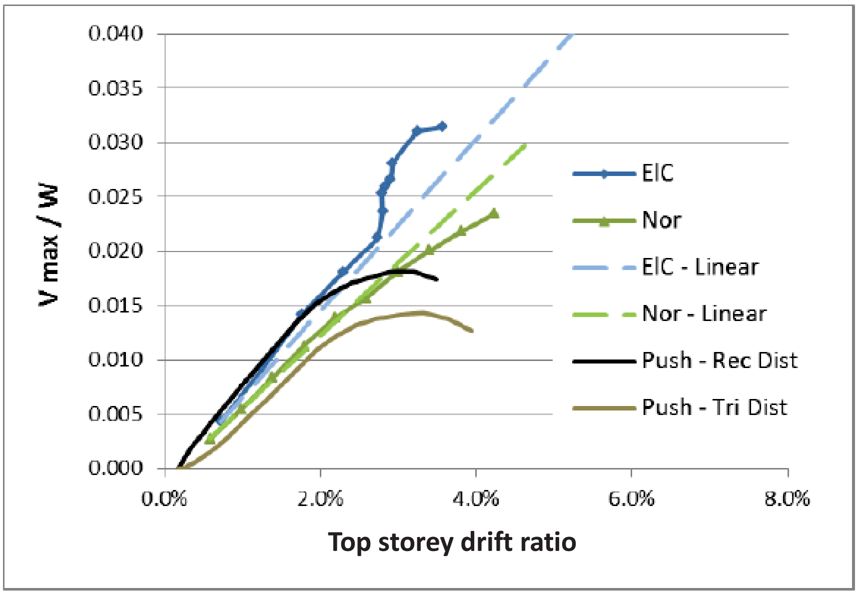

(b)

Figure 6.20. Comparison of static and 'dynamic pushover' curves with respect to (a) max inter-storey drift.(b) top storey drift

Details of ductility factor calculations, using roof drift according to equation 6-11 and 6-12 and Figure 6.21 and Figure 6.22 is presented in the following.

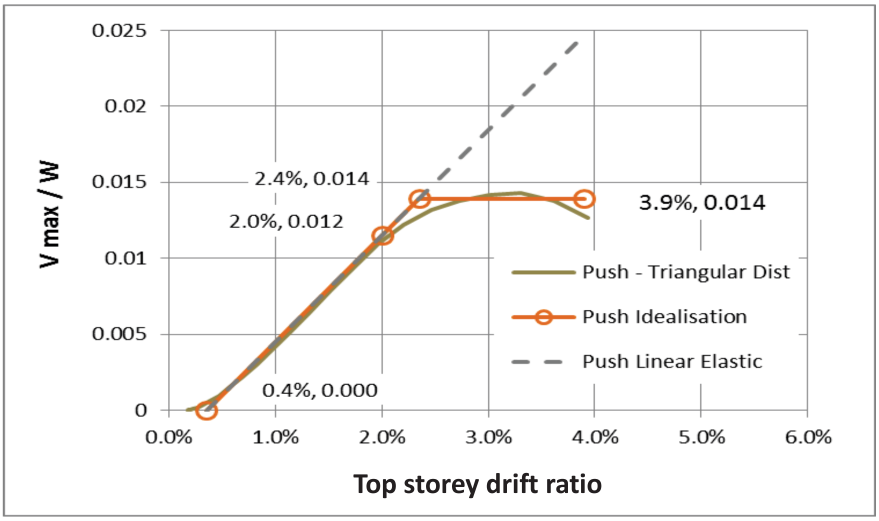

Figure 6.21. Triangular Load Pattern Pushover Curve with respect to top storey drift.

Table 6-4. R factor calculation from triangular load pushover with respect to top storey drift.

Factor	Calculated Value
Rμ	1.62 (=3.9/2.4)
Ω	1.2 (=2.4/2)
R	1.95 (=1.62 x 1.2)

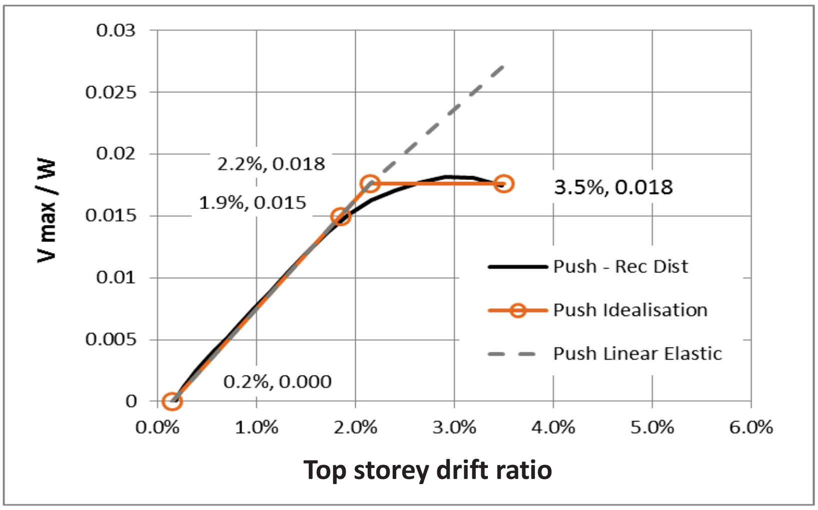

Figure 6.22. Rectangular Load Pattern Pushover Curve with respect to top storey drift.

Table 6-5. R factor calculation from rectangular load pushover with respect to top storey drift.

Factor	Calculated Value
Rμ	1.54
Ω	1.18
R	1.81

Details of ductility factor calculations, using maximum drift according to equation 6-11 and 6-12 and Figure 6.23 and Figure 6.24 is presented in the following.

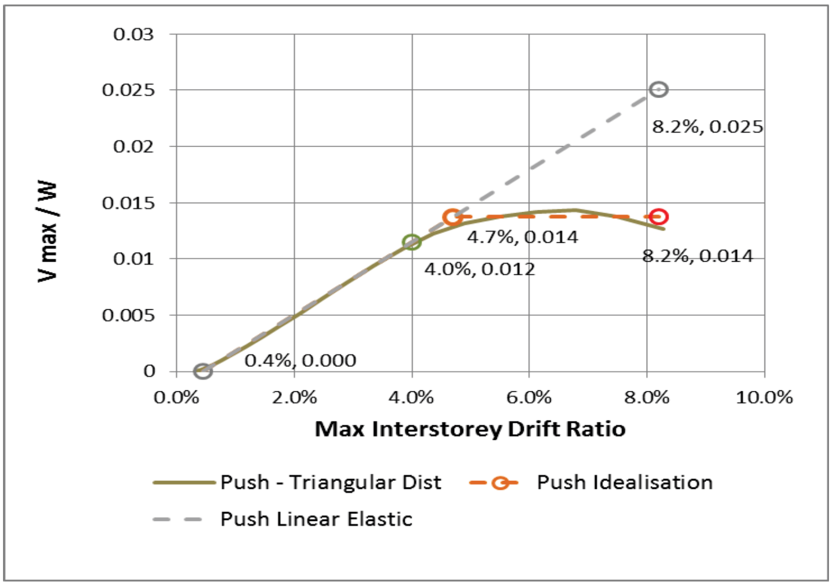

Figure 6.23. Triangular Load Pattern Pushover Curve with respect to max inter-storey drift.

Table 6-6. R factor calculation from triangular load pushover with respect to max inter-storey drift.

Factor	Calculated Value
Rμ	1.82
Ω	1.20
R	2.18

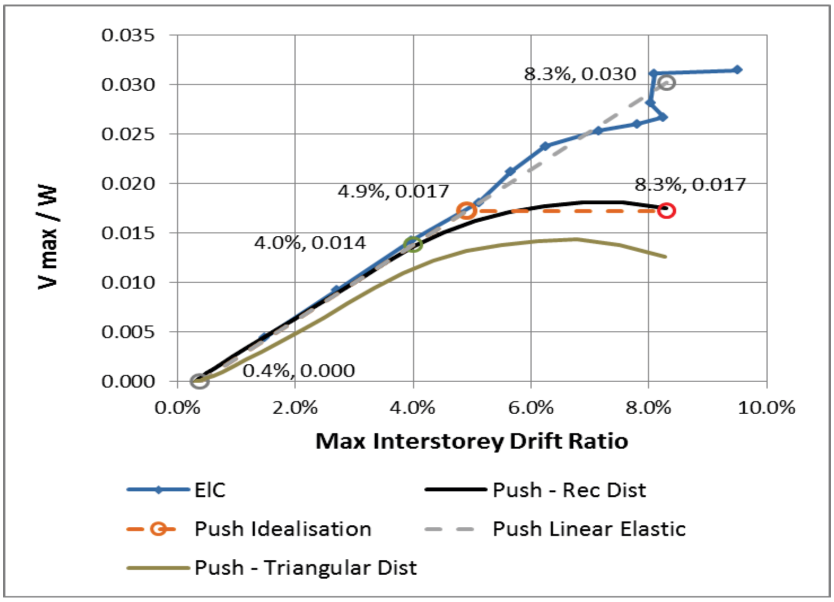

Figure 6.24. Rectangular Load Pattern Pushover Curve with respect to max inter-storey drift.

Table 6-7 R factor calculation from rectangular load pushover with respect to max inter-storey drift.

Factor	Calculated Value
$R\mu$	1.75
Ω	1.520
R	2.19

To come up with the final seismic design reduction factor, NLTH and ESLF analyses results were compared and adjusted. For this reason the structural response parameters such as "Maximum moment in first storey upright", "Maximum first storey drift" and "Maximum top storey drift" were compared between the two analysis results (refer to Appendix D). Finally, the most appropriate seismic design factors for steel storage rack structures with boltless connections in down aisle direction was reported as follows.

Table 6-8. Recommended Seismic Design Factors for ESLF design of unbraced down-aisle steel pallet racks.

ESLF Seismic Design Factor	Recommended Value
Force Reduction Factor, R	1.8
Ductility Reduction Factor, R_{μ}	1.5
Over strength Factor, Ω	1.2

6.2 Shake Table Test Simulation

Numerical investigations were continued by simulating the shake table test. The previously performed analyses assumptions and results needed verification by the real dynamic tests performed at the University of Technology, Sydney (UTS) in order to be generalised. For this reason a '3-D' Finite Element Model as shown in Figure 6.25 was developed with a similar connection model as the above mentioned Pivot hysteresis model. The pivot model back bone was determined based on the experimental cyclic moment-rotation curves and by parameters shown in Table 6-8 (See Figure 6.26).

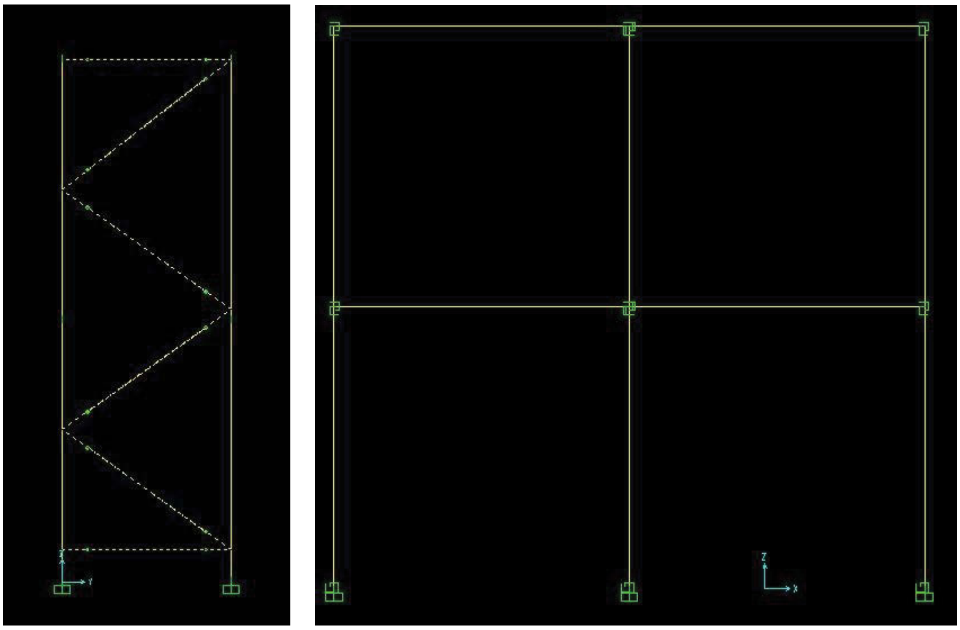

Figure 6.25. FE model, Elevation and Side views

Base plate connections were also modelled as pinned bases due to low compression force in the base plate. Beams and uprights were modelled as beam elements with 6 degrees of freedom at each end. Bracing members were modelled as a 2 D beam elements with the cross sectional area of 10% of the real cross sectional area (refer to Chapter 3) of the bracing member and were connected to the uprights with hinged connections[34].

[34] However in this section the effect of bracing member was not effective on the behaviour of the rack in down aisle direction

The damping ratio was defined as 6% of critical for the lower intensity according to the phase one shake table test results. Damping of 8% of critical was used for higher intensity test simulations (60%, 70% and 80% of 1940 El-Centro, non-scaled in time domain).

Non-Linear Time History (NLTH) dynamic analysis was performed using Newmark Integration method by defining appropriate parameters. The dynamic parameters of Newmark integration method for the non-linear dynamic time history analysis of the structure in SAP 2000 were '$\gamma = 0.5$' and '$\beta = 0.25$'.
1940 El-Centro earthquake acceleration record was imparted to the structure with a gradually increasing intensity scale from 20% to 80% (e.g. 20%, 40%, 60%, 70%, 80%) to simulate the test conditions. The mass was defined at an elevated level from the beams to consider the mass centres of the concrete blocks. FE models were unable to consider the sliding effect which was in fact beyond the scope of this research program[35].

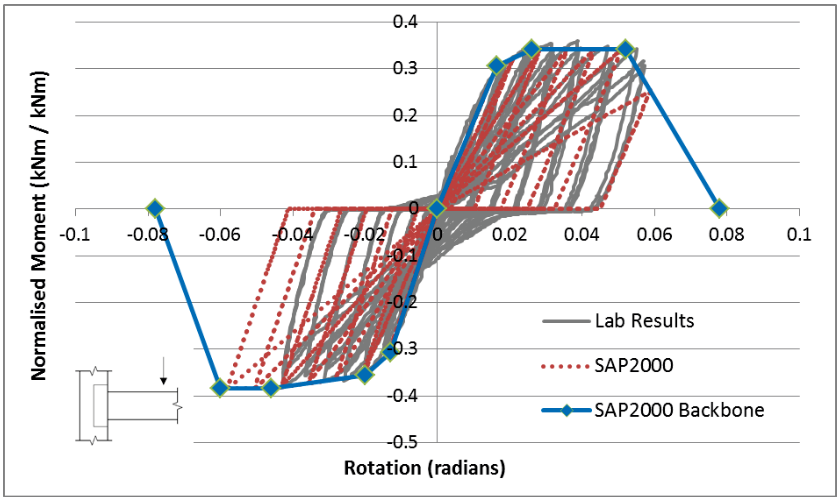

Figure 6.26. Experimental and Numerical Cyclic Test Comparison using LabCyc-PIV Link.

[35] Translational springs were used to model the pallet sliding on top of the beams like a frictional link, however due to complexities, the model could not predict the amount of 'sliding' and the correct 'recorded acceleration' from the pallet and were performing like a rigid links with no sliding. Investigations regarding to sliding of the pallets on the beams are reported in ref [6.5].

Table 6-9. Calibrated Pivot Model Parameters for 'Type A' Beam-Upright Connections

Pivot Parameter	Adopted Value
α_1	100
α_2	100
β_1	0
β_2	0
η	0

As shown in Figure 6.27, to Figure 6.29 FE results show a reasonable agreement with the experimental results.

The trend of the FE results complies with the trends of the test results for both responses of top level displacement and acceleration.

The FE model could predict the maximum top storey displacement, however, the second displacement jerk could not be perfectly predicted. This minor disagreement could be explained by the effect of connection looseness leading to further drift in the structure which cannot be captured in the pivot hysteresis model.

The accelerations monitored on the concrete blocks also could not be predicted by the FE model.

The agreement between finite element analyses results and the experimental shake table test results verifies the results of numerical investigations carried out previously.

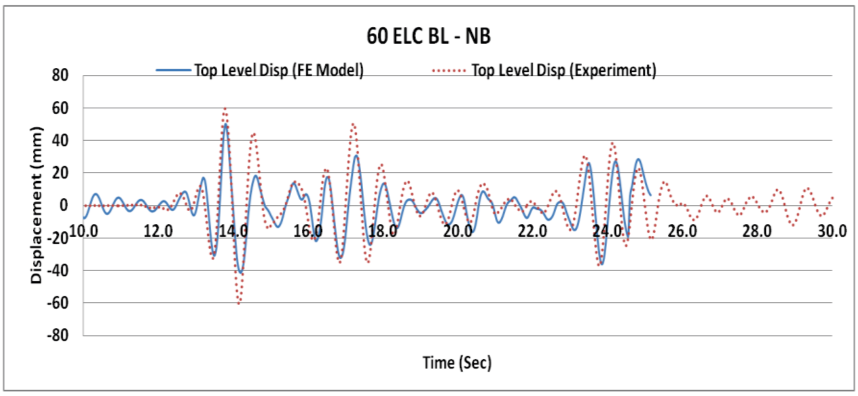

(a). Top Level Displacement response

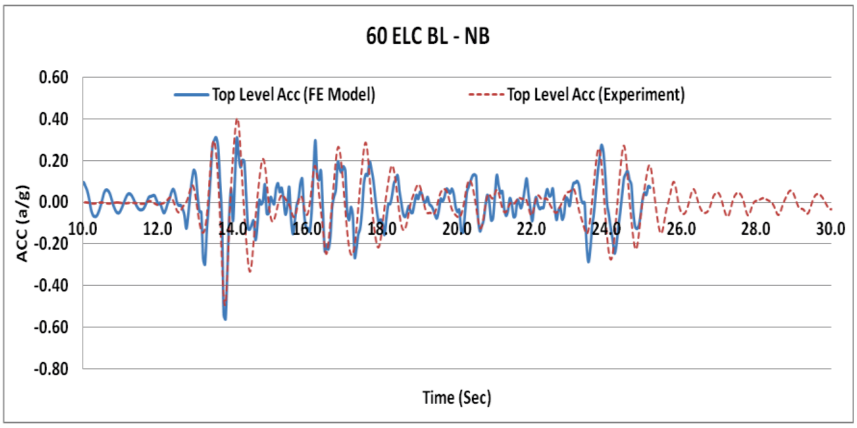

(b). Top Level Acceleration Response

Figure 6.27. (a) and (b): Numerical analysis results vs Experimental test results (60% 1940 El Centro Earthquake – Not Scaled in time domain)

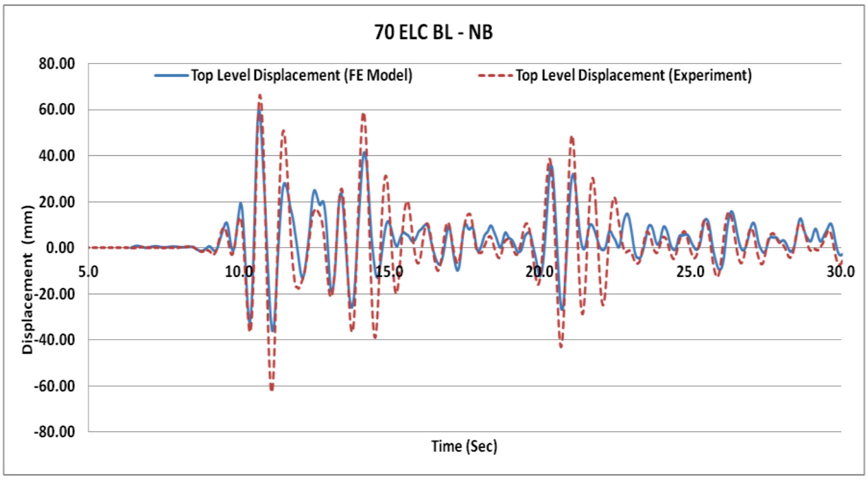

(a). Top Level Displacement Response

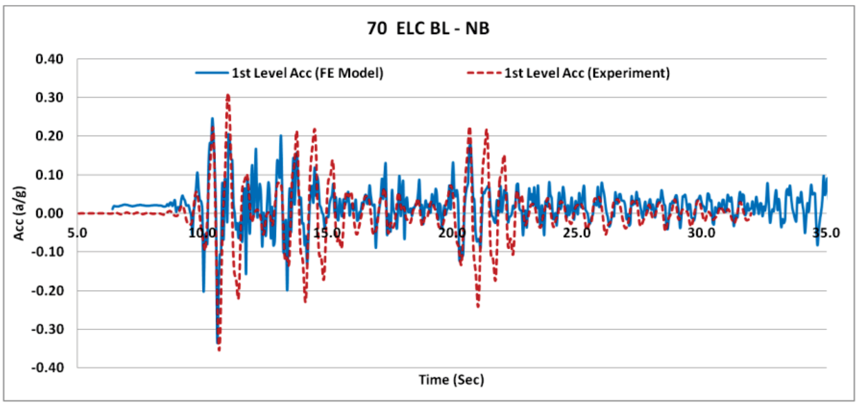

(b). First Level Acceleration response

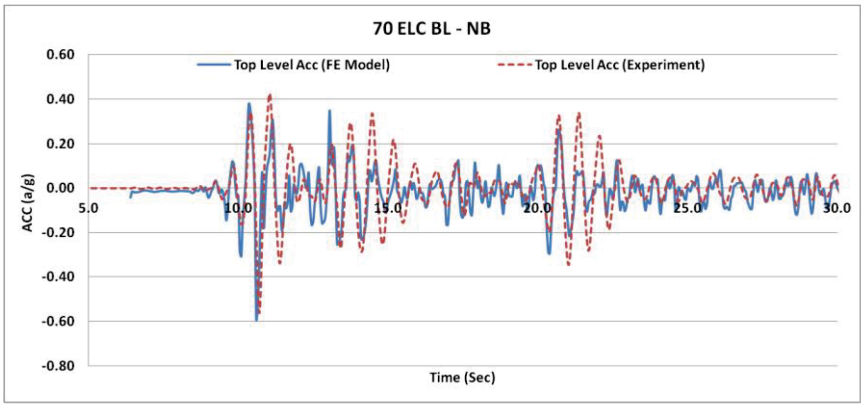

(c). Top Level Acceleration Response

Figure 6.28. (a), (b) and (c): Numerical analysis results against Experimental test results (70% 1940 El Centro Earthquake – Not Scaled in time domain)

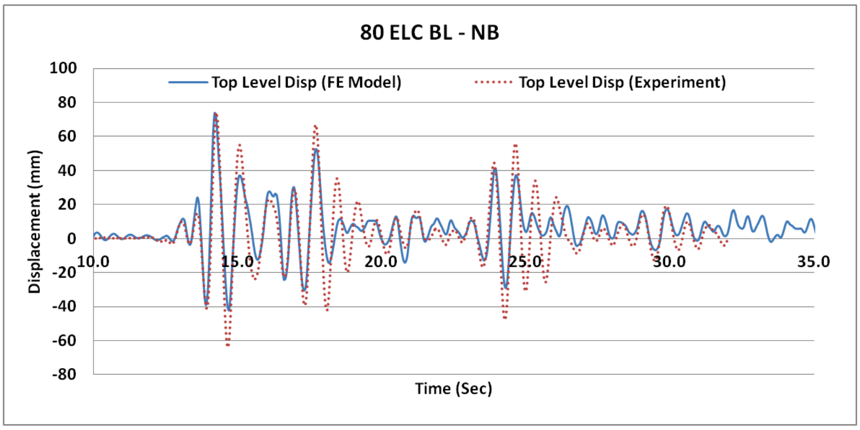

(a). Top Level Displacement response

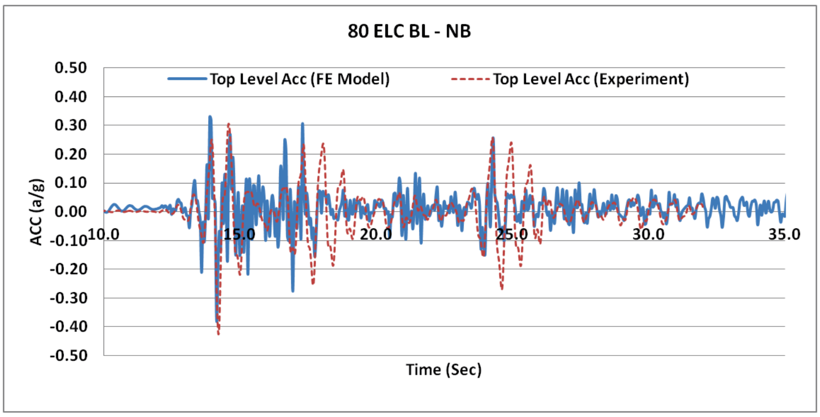

(b). Top Level Acceleration Response

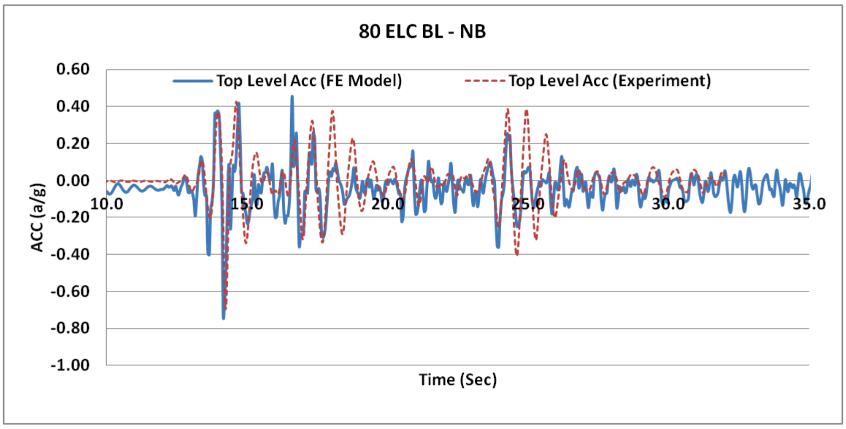

(c). Top Level Acceleration Response

Figure 6.29. (a), (b) and (c): Numerical analysis results vs Experimental test results (80% 1940 El Centro Earthquake – Not Scaled in time domain)

6.2.1 Discussion of results

Figure 6.30 to Figure 6.33 show moment – rotation hysteresis curves of the beam to upright connections in both levels of the model for the higher intensity 1940 El-Centro earthquake record. The most obvious feature of the below figures is that the connections at the second beam level (top level) show a linear behaviour even when the structure is subjected to a high intensity earthquake record, while the connections at the first beam level behave in-elastically and tend to absorb energy. Comparison of responses of the connections at the first beam level with the responses of the connections located at the second beam level clearly indicates the soft storey mechanism of the system which disagrees with the current seismic design assumptions. According to the current displacement based seismic design method, all the connections of the structure experience the same rotation under seismic actions (FEMA 460, 2005). However, the phenomenon of having soft storey failure mode may not initially occur in the higher rack structures as their base plates are heavily loaded and referring to Chapter 3, they show stiffer moment rotation behaviour. However, according to Chapter 3, they may lose their stiffness in higher intensities of seismic actions. This suggests that if the rotational capacity of the base plates in a racking system is less than the rotational capacity of the beam to upright connections, the formation of soft storey failure mode may be most likely to occur.

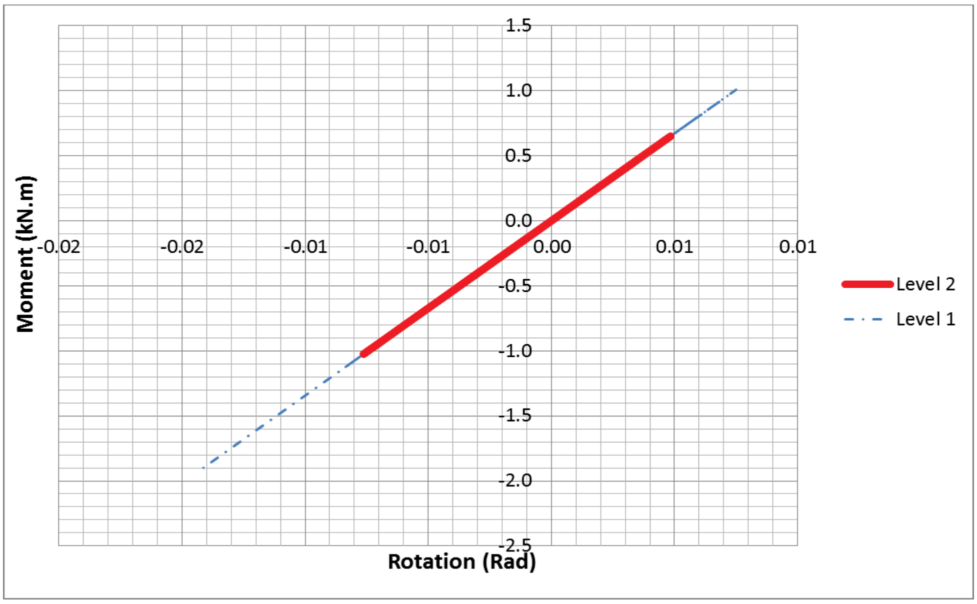

Figure 6.30. Moment – Rotation hysteresis curves of the beam to upright connections at first and second beam levels (60% 1940 El Centro Earthquake record)

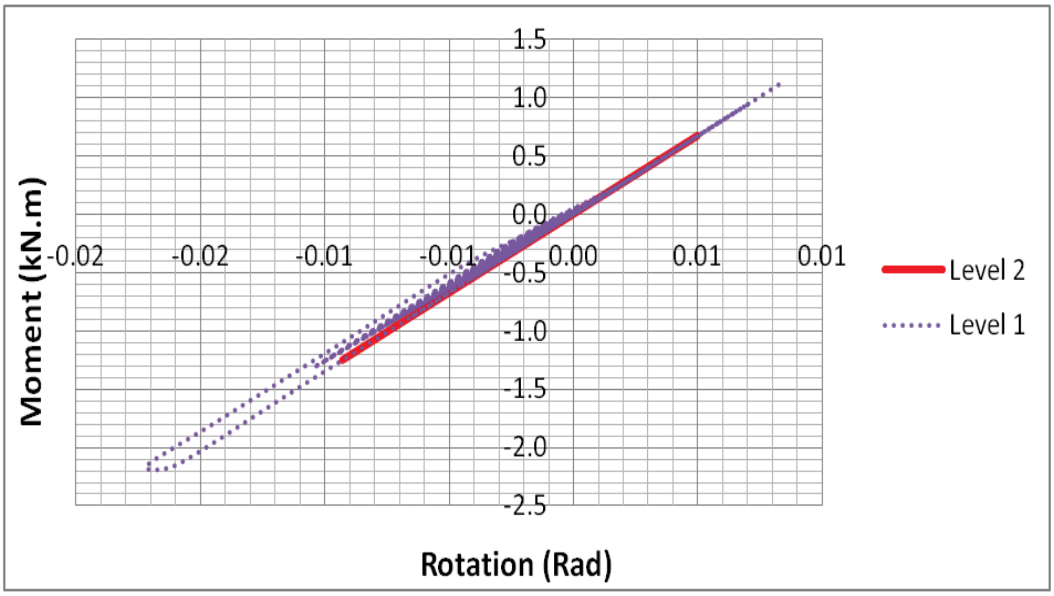

Figure 6.31. Moment – Rotation hysteresis curves of the beam to upright connections at first and second beam levels (70% 1940 El Centro Earthquake record)

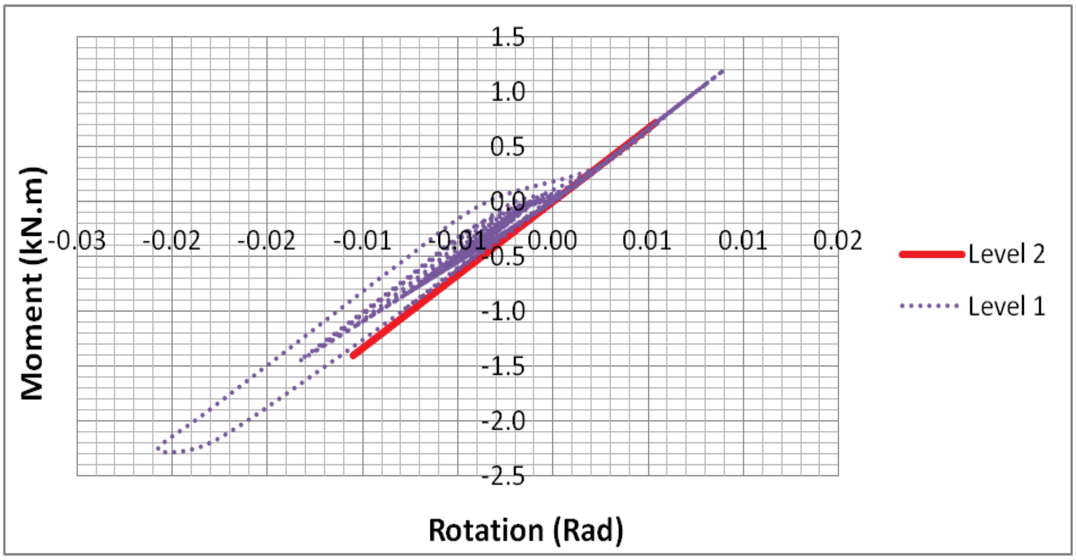

Figure 6.32. Moment – Rotation hysteresis curves of the beam to upright connections at first and second beam levels (80% 1940 El Centro Earthquake record)

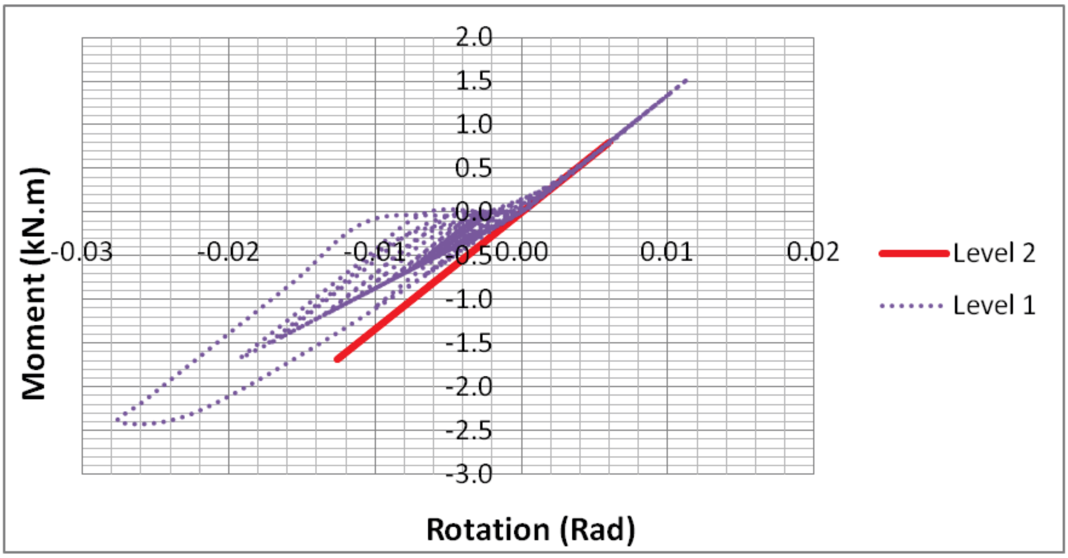

Figure 6.33. Moment – Rotation hysteresis curves of the beam to upright connections at first and second beam levels (100% 1940 El Centro Earthquake record)

Figure 6.30 to Figure 6.33 show a progressive damage of the connections for consecutive steps. One can clearly notice the lag between the solid moment rotation curve (indicating the responses of connections at the second beam level) and the dotted moment rotation curves (which demonstrate the responses of connections at first beam levels) which initiates from 70% 1940 El-Centro test. This lag proves the progressive stiffness deterioration of the beam to upright connections.

IDA curve of the test has also been derived and is presented in Chapter 7 to be compared with the cyclic test results.

6.3 Conclusions

Numerical simulation of the shake table tests was presented in this chapter. First a preliminary investigation was planned and carried out jointly with an undergraduate final year student who was supervised to develop an initial numerical model to be able to accurately model the behaviour of rack structures under seismic actions. The behaviour of racking systems basically relies on their connections and hence the main components such as beams and uprights stay elastic (if not buckled) under heavy dynamic actions so long as the structure maintains its overall stability. Therefore, the main focus of the preliminary numerical analyses was to investigate the behaviour of beam to upright connections and to identify the most suitable connection model for dynamic (time-history) simulation of hysteretic structure behaviour. For this reason, beam to upright connections were modelled by three different popular hysteresis models (Kinematic Model (KIN), Takeda Model (TAK), Pivot Model (PIV)) available in Finite Element software packages like SAP 2000. Behaviour of four '2 dimensional, 4-storeies and 3-bays' FE models, each modelled by a different beam to upright connection, was investigated and the results were compared and summarised below:

- The system modelled by PIV-EXP connection model survived the highest earthquake scaling.
- The system modelled by PIV-EQV connection models failed at an intensity scale much closer to that of PIV-EXP. This proves the reliability of the proposed equivalent cyclic back bone.
- The structure modelled with the Kinematic model dissipated less energy at higher intensities, and, therefore, failed at much lower intensities of earthquake scaling than their Takeda and Pivot counterparts.
- High permanent deflections were demonstrated by the system modelled by KIN hysteresis model close to failure. This observation was due to the KIN model's elastic oscillations after inelastic excursions.
- Pivot connections demonstrate zero permanent inelastic deflection even at higher intensities close to failure.

After a comparison was made among different connection modelling techniques, as mentioned above, further investigations were carried out to evaluate the ductility of a rack structure in its down aisle direction. For this reason, the same structure configuration (2D, 4-Storeies, 3-Bays) was subjected to three earthquake records of 1940 El-Centro (far field earthquake), 1994 Northridge and 1995 Kobe (near field earthquakes) ground motions. Non-linear static push over analysis (NLPO) was also performed to depict static push over curves and then the IDA and NLPO curves were used to calculate the structural ductility factors. The following results were obtained:

- Significant amount of energy was dissipated by the first storey connections while the amount of energy dissipated by higher level connections was almost negligible or in other words, greater inter-storey drift was observed at the first level than the higher levels (Soft storey failure mode).
- P-Delta effect was proved to remarkably change the fundamental vibration period of structures and consequently the equivalent seismic base shear in the structure.
- Remarkable amount of energy was *gradually* dissipated by the beam to upright connections during the 1940 El-Centro earthquake. However, significant energy dissipation occurred at the *beginning* of 1994 Northridge earthquake because of the inelastic deformation of connections at the first storey level under the first big pulse in the 1994 Northridge accelerogram.
- Negligible permanent inelastic drift was observed in the structure subjected to 1940 El- Centro earthquake.
- Rectangular and triangular load patterns were used to push the structure side ways until failure and then force – deformation curves (PO curves) were derived.
- Rectangular load pattern proved to give a better agreement with the IDA results.
- A force reduction factor, R, of 1.8 with a corresponding over strength factor, Ω, of 1.2 was proposed based on the aforementioned numerical investigation.

The most accurate numerical technique was then applied to simulate the shake table test results and check the validity of the above findings. Acceptable agreement was observed between the numerical results and the actual shake table test results. Strength deterioration of the beam to upright connections and soft storey deformation mode was observed in the shake table tests which verified the numerical results.

7. CHAPTER 7: FULL FRAME CYCLIC TESTS (PUSH - PULL)

7.1 Introduction and Literature Review

Full frame cyclic tests could be one of the best and most efficient ways to investigate the full frame behaviour in either directions considering the interactions between different frame components such as beam to upright connections, frame bracing and upright base connections.

Very few experimental quasi-static tests have been reported in the literature. Krawinkler et al. (1979) performed four tests of full 'three stories – two bays' rack for two different rack configurations, two in down aisle and two in cross aisle direction. The frames were subjected to a lateral load imposed to the top level only, however, the results were very valuable and revealed different features of a typical rack frame in both longitudinal and transverse directions. Pinching hysteresis loops with significantly less energy dissipation in the consequent cycles of the same displacement amplitude was observed. Soft storey failure mode was observed in down aisle direction initiated by cracks in the welds between beam and beam end connector angle. Also the second order effects (e.g. P - Δ effect) on the frame stiffness on both sides were highlighted.

Rosin et al. (2009) accommodated two full scaled push over tests in their experimental study. They subjected their '3 storey – 2 bay' frames to cyclic lateral loads and reported the results for both directions (See Figure 7.1). As shown in Figure 7.2 an inverted triangular load pattern was applied to the frame based on displacement control technique to simulate the seismic actions. Rack frames were loaded by 12 pallets (4 at each level) providing a total of 102 kN vertical pallet load. The frame was loaded up to a given displacement and returned to zero followed by pushing to a larger displacement and again back to zero. This trend was continued till failure was observed. Soft storey failure mode was observed as the base plates performed like hinged connections. They first lost their stiffness and became hinged connections as shown in Figure 7.3. Plastic hinges were formed underneath the beam to upright connections and frame then became unstable due to large lateral displacements.

Figure 7.1: Push-Over test set up in both directions (Rosin et al., 2009, p. 59)

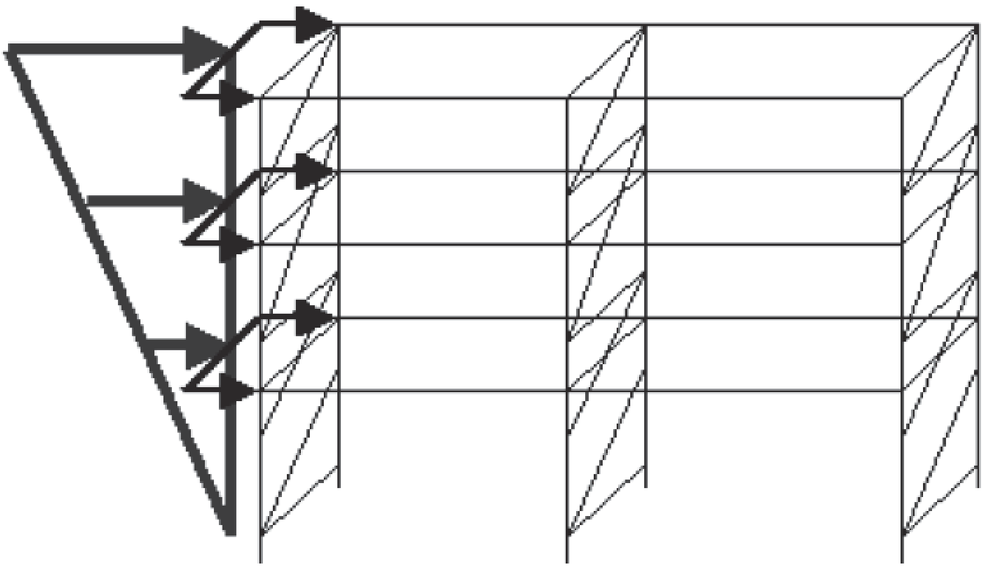

Figure 7.2: Schematic view of the shake table test set up (Rosin et al., 2009, p. 60)

Figure 7.3: Failure of the frame as result of push over test (Rosin et al. 2009, p. 63)

In cross aisle direction, the frame was loaded until a bracing member buckled and consequently frame became unstable. Local deformation of base plates and failures in the bolts were also reported. Figure 7.4 a and b show the structural responses in terms of total base shear plotted vs. the horizontal top level displacement for down aisle and cross aisle frames, respectively. The nonlinearity of the base shear- top displacement hysteresis curves is due to the nonlinear response of the frame bracing members, however, it seems that the nonlinearity of the bracing members under compression force compared to the nonlinearity due to bearing of the upright - bracing connections is negligible.

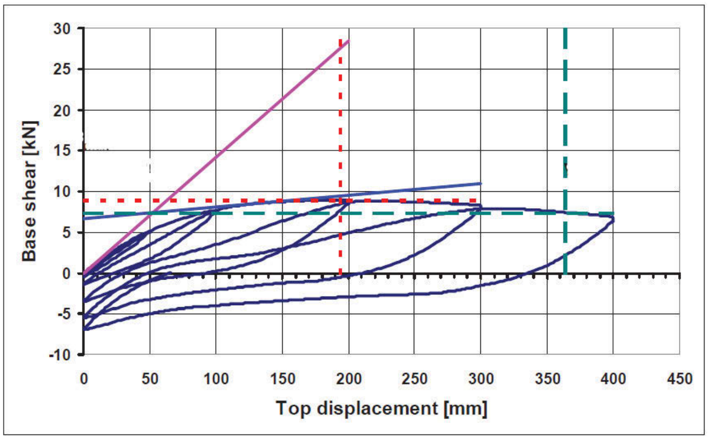

(a)

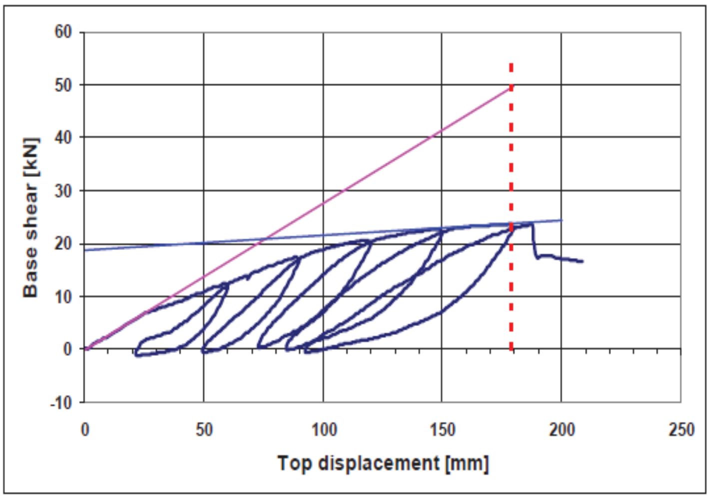

(b)

Figure 7.4: Hysteresis response of the frame in both directions of (a) down aisle, and (b) cross aisle (Rosin et al., 2009, p. 63 & 67)

Ductility factors (q-factor) of 3.7 for down aisle frame and 2.1 for cross aisle frames were reported based on the test results by considering the first yield point and ultimate capacity of the frame. The hysteressis curve of the cross aisle frame response shows a significant permanent drift in the system which was not adressed well in that report (See Figure 7.4 a and b).

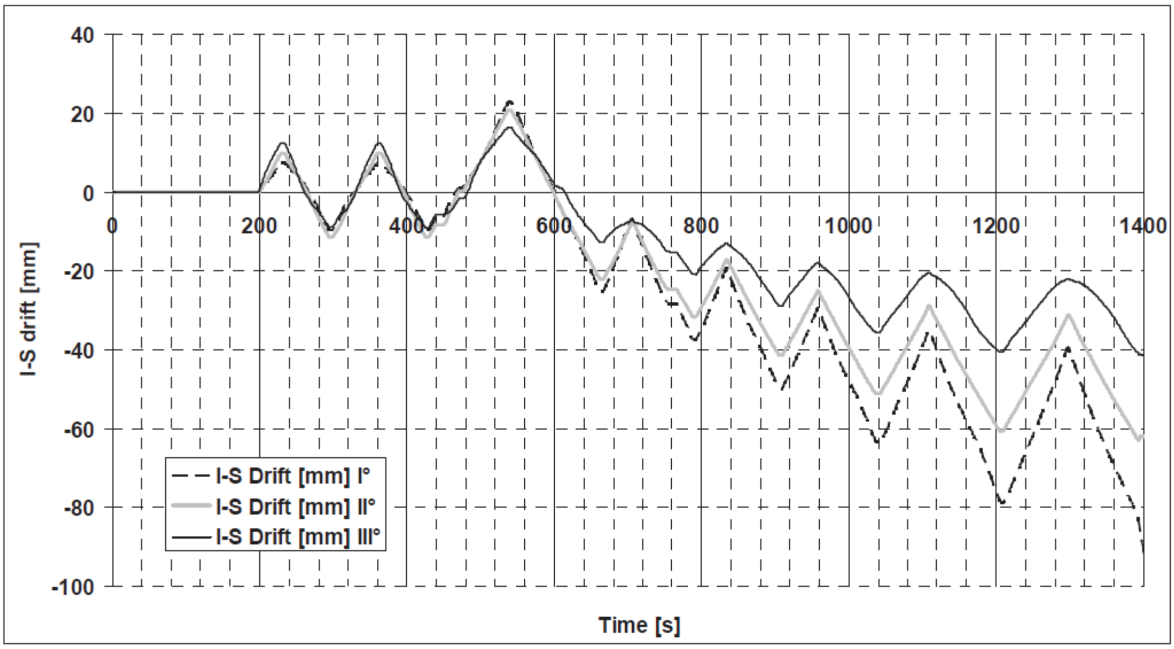

Figure 7.5: Overall drift of the system in cross aisle direction (Rosin et al., 2009, p. 65)

This permanent accumulative displacement could be because of the base plate deteriorations under uplift forces. This phenomenon was presented earlier in this report in Chapter 3.

7.2 Experimental Study / Test Setup

A Static push over test is an efficient procedure to see the behaviour of the frames in a more controlled procedure and with less risk level.

One full scaled test on a 'two storey – two bay' rack frame with boltless connections and non-braced in down aisle direction (similar to the "BL-NB" frame on the shake table) was carried out. Dimensions and vertical loads of the test rack were identical to the rack tested on the shake table as shown in Figure 5.15. The reason to conduct such a complicated test was to make a bridge between the shake table and push over test results. Frames could then be pushed (pulled) further so that they can undergo large displacement which is impossible for the frames on the shake table under dynamic actions due to safety issues. On the other hand, setting up a push over cyclic test is much more time consuming and complicated compared to a shake table test set up.

The cyclic test that is reported in this part has been conducted in the structures laboratory of the University of Technology, Sydney. Base plates were anchored to '30 mm thick' steel plates which were connected to the concrete floor of the structures laboratory as shown in Figure 7.6.

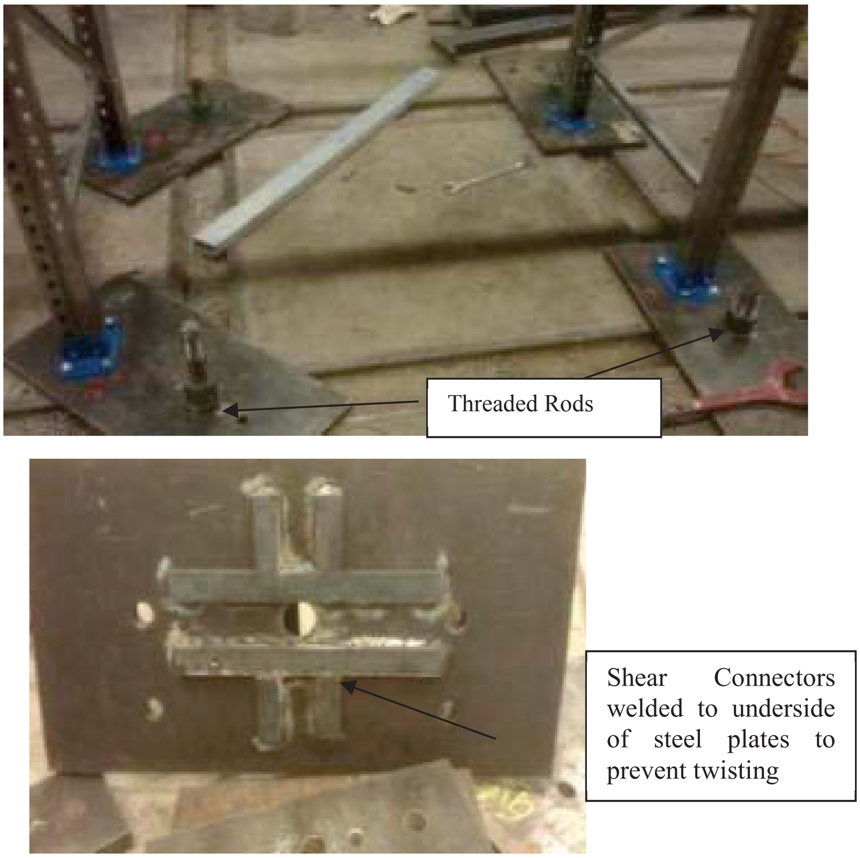

Figure 7.6: Heavy steel plates were locked to the structures laboratory floor by using welded shear connectors

Shear plates were welded on the other sides of the plates to get engaged to the channels on the concrete floor to restrain the plates against twisting and moving due to shear forces in the uprights. The plates were also tied to the concrete floor by heavy duty threaded rods to avoid lifting up in case a significant uplift force is induced in the base plates.

In order to push and pull the frame by the hydraulic jacks, two '25 mm' steel plates were used to sandwich the uprights on top of the connections of the two levels. Sandwich plates were tied to the uprights by two threaded rods per upright. Hard compacted plastic rubbers were glued to the sandwich plates facing the uprights to avoid squashing the upright metal. (See Figure 7.7)

The system was then loaded by two hydraulic jacks at each level and the loads were transferred to each of the two frames by means of heavy spreader beams. Spreader beams were connected to the load cells by a vertical hinge (i.e. the rotation around the vertical axis of ‘X’ in Figure 7.8 is allowed). Also spreader beams were connected to the sandwich plates by two hinges vertically and horizontally oriented to allow the frame to rotate around both ‘Z’ and ‘X’ axes in Figure 7.8 (Also see Figure 7.9)

Figure 7.10 shows the cyclic displacement histories applied to the first and top level of the structure with loading rate of 1.0 mm / sec. The amount of displacement imposed on the first beam level was two thirds of the displacement of top level. This ratio was obtained from the first level and the top level displacement ratio observed from the shake table test results. As shown in Figure 7.10 it was intended to perform the test with steps of loading of three cycles with the same amplitude to see the amount of deterioration after consecutive cycles with the same amplitude. Also after different amplitudes, a smaller amplitude was used to investigate the deteriorations in the structure after consecutive large amplitudes. Figure 7.11shows the full test set up.

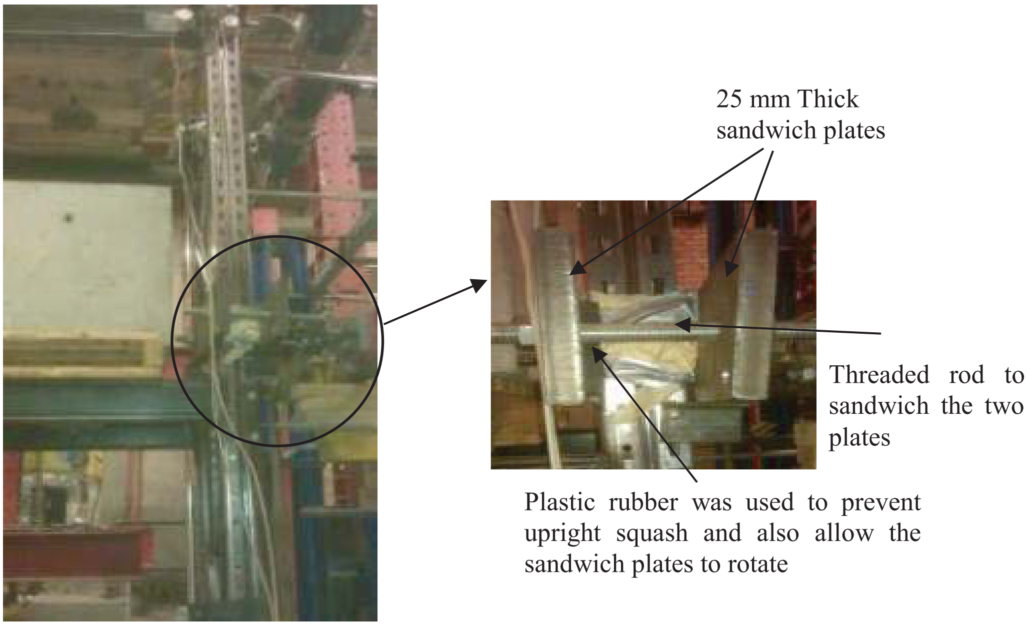

Figure 7.7: Steel plates were used to sandwich the upright

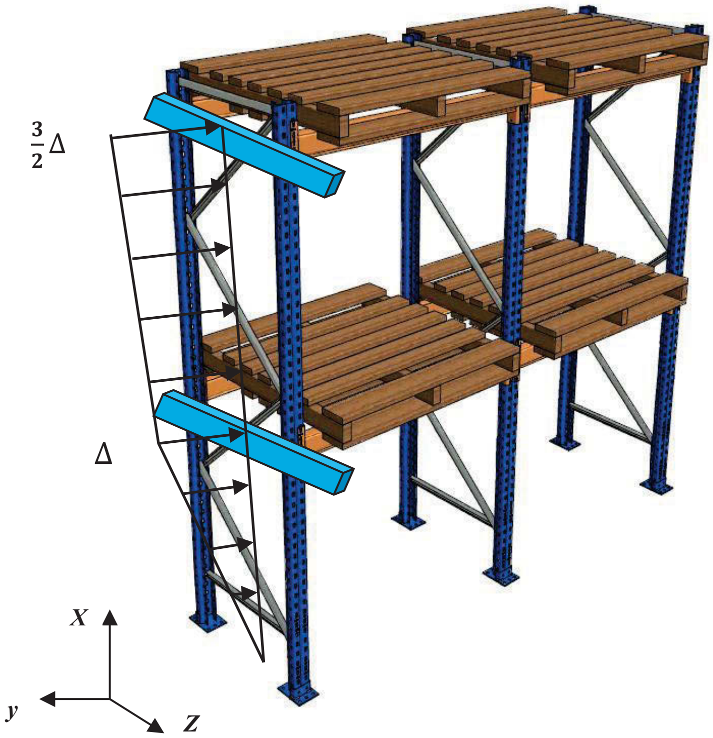

Figure 7.8: Schematic set up 3-D view (Although the rack was loaded by concrete blocks on the timber pallets, they are not shown in this figure)

Figure 7.9: Double hinged connection between spreader beam to the sandwich plates

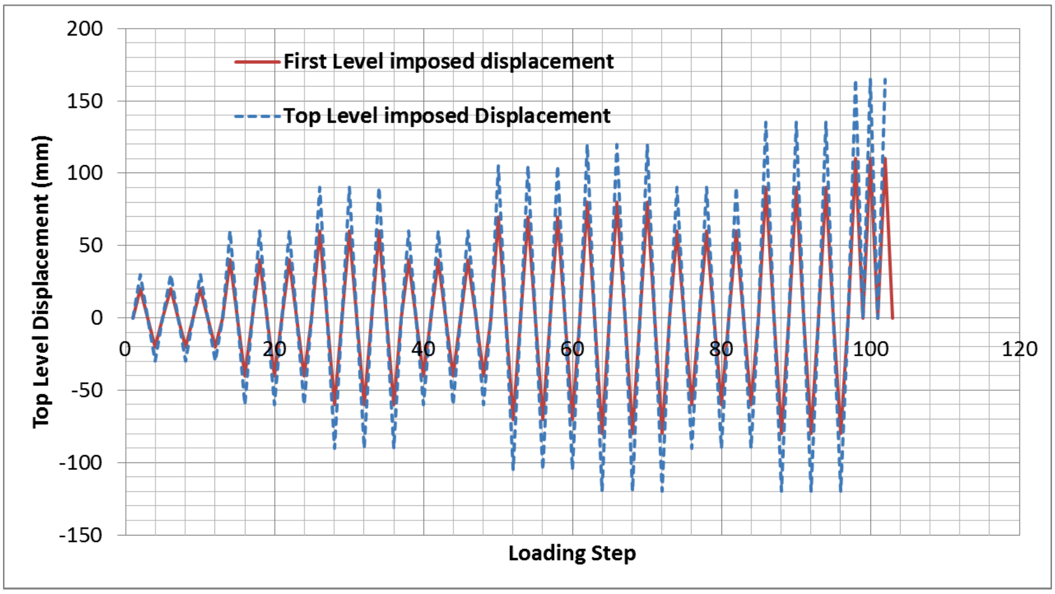

Figure 7.10: Imposed displacement history

Figure 7.11: Frame at ultimate drift

The test was concluded with three cycles of pushing the system up to 165mm top displacement, followed by unloading to zero displacement. These last three cycles were imposed in one direction only as it was beyond the loading stroke to pull the system with such a big displacement. The test was then completed as it reached the maximum allowable displacement of the load stroke. Also the maximum drift of the structure falls beyond the reasonable range of the structural drift in the rack structures. The specimen instrumentation detail is shown in Figure 7.12.

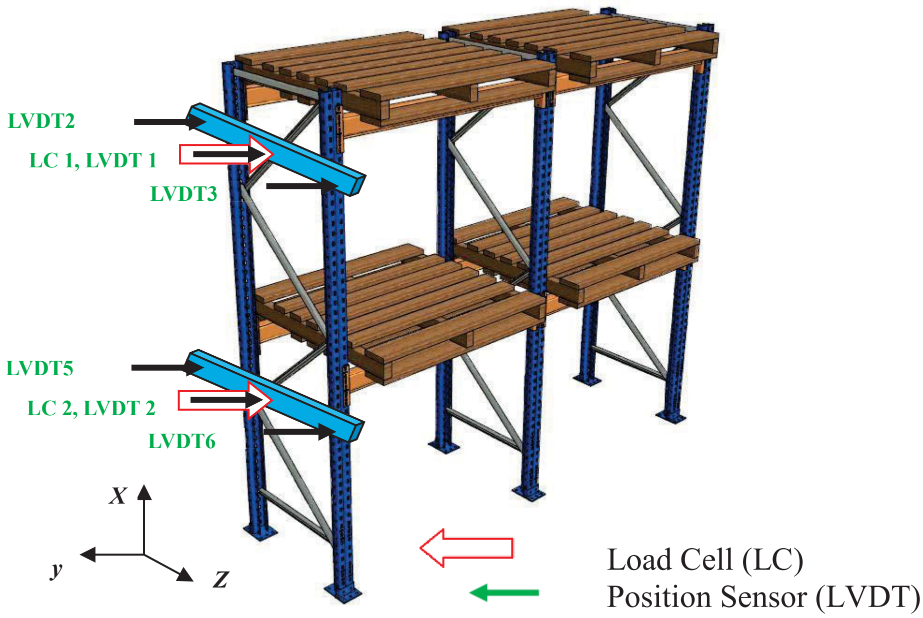

Figure 7.12: Summary of the instrumentation applied to the specimen (Although the rack was loaded by concrete blocks on the timber pallets, they are not shown in this figure)

7.2.1 Structural response and behaviour

Although a visible drift was observed during the tests, the specimen did not collapse. The two LVDT's at each level (LVDT2 and LVDT3, LVDT5 and LVDT6) showed similar displacements which indicates the loads were transferred to the structure symmetrically without twisting the frame. The displacement recorded from LVDT1 was slightly higher than the displacement recorded from LVDTs 2 and 3 and similarly, the displacement recorded from LVDT 4 was slightly higher than the displacements recorded from LVDTs 5 and 6. This is because of the rubber being pressed inside the sandwich plates. However, the difference of the displacement measured from load stroke and the displacement imposed on the frame was negligible and hence not affecting the test results.

No visible damage was observed in the upright base plates. However, indentation was observed close to upright perforation at the beam-upright connection locations due to hook-upright interactions as shown in Figure 7.13.

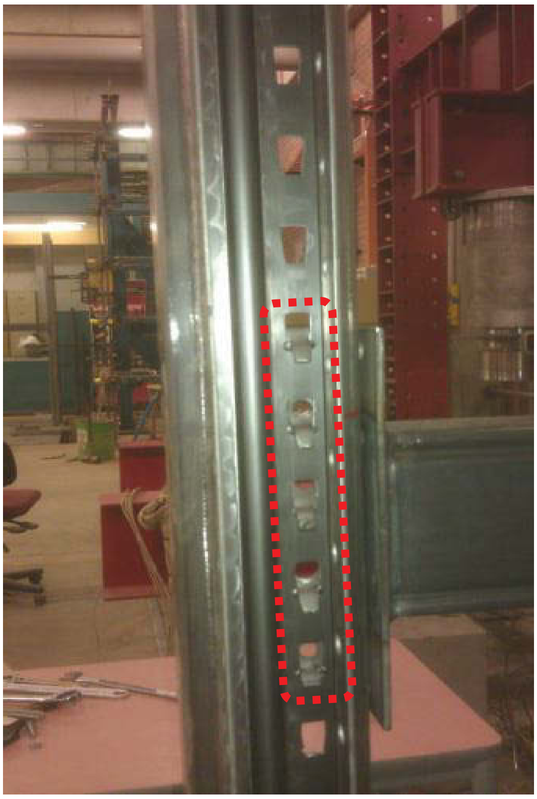

Figure 7.13: Connection zone after the test

The hysteresis curves of the base shear versus top level displacement at displacement amplitudes of ‘A1’ to ‘A9’ are shown in Figure 7.14. A progressive deterioration in the frame stiffness is clearly visible.

Figure 7.15 shows the difference of the hysteresis curves when the system was subjected to the second and forth amplitudes of 60mm top displacement. It can be seen in Figure 7.15 that the frame stiffness has significantly changed after the loading step of “A4” with the displacement amplitude of 60mm compared to the loading step of “A2” with the same displacement amplitude. The reason for such a change in frame stiffness is that the frame underwent the loading step of “A3” with higher displacement amplitude of 90mm, so that the frame was significantly deteriorated. Different behaviour of the system under the same displacement amplitude but different sequence shows that the hysteresis curves pick up forces with the same stiffness as their previous cycle and it means the energy absorption capability of the frames are mainly relied on the history of the load pattern that the structure was subjected to.

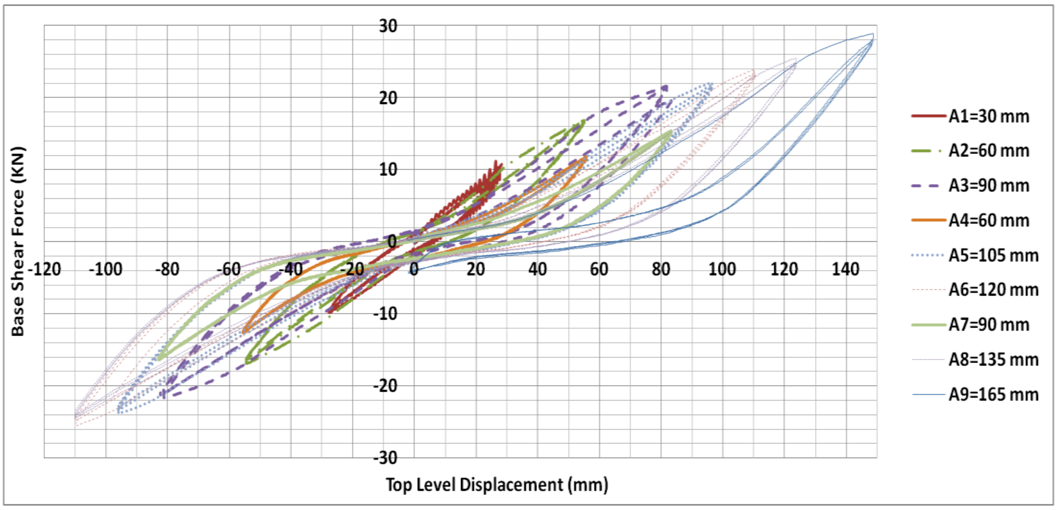

Figure 7.14: Hysteresis response of the frame

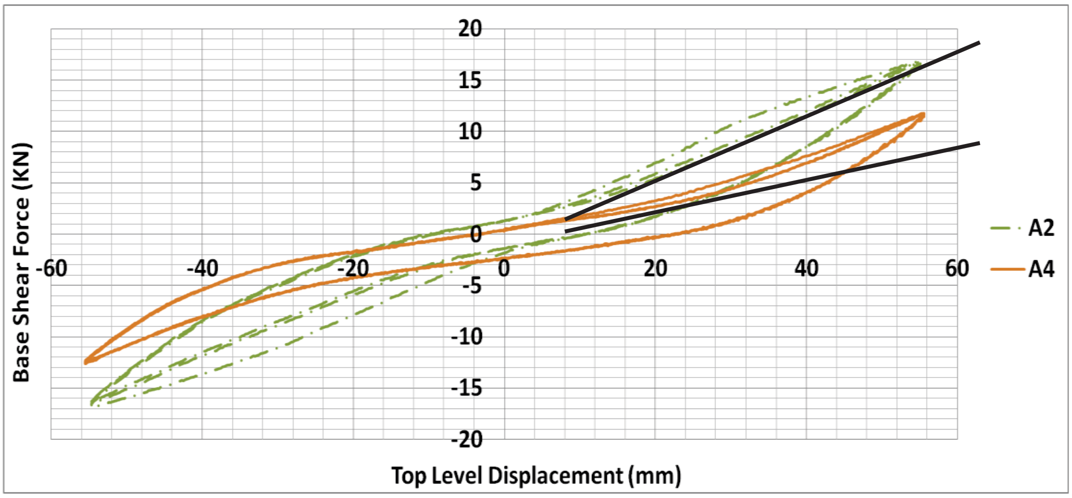

Figure 7.15: Strength deterioration and stiffness degradation after a few cycles of loading

Although progressive deterioration was observed from the cyclic test results, the system shows a good ductile behaviour and the load was never dropped before terminating the test.

It was also noted that the structure was making loud noises when it was unloaded back to zero displacement (e.g. origin). This was indicating the rigid motion of the hooks through the indentations made close to the upright slots. The same noise was heard during the shake table tests at the end of the tests when the structure came back to rest.

The bolts of the upright base plate connections were checked and they were still tied with no local damage in the uprights and base plates.

7.2.2 Ductility Evaluation

Figure 7.16 shows the cyclic envelop curve which passes through the peak points of every displacement amplitude. The Bi-Linear simplified curve was also drawn based on equal energy (area) method. The initial part of the Bi-Linear curve was also continued to estimate the elastic behaviour of the system. Ductility Factor of the structure can then be calculated using equation 7-1

$$\mu = \frac{V_e}{V_{max}} = \frac{60.8}{148} = 2.43 \qquad (7\text{-}1)$$

where;

V_e : Elastic base shear at the maximum monitored displacement of the top beam level

V_{max} : Inelastic base shear at the maximum monitored displacement of the top beam level

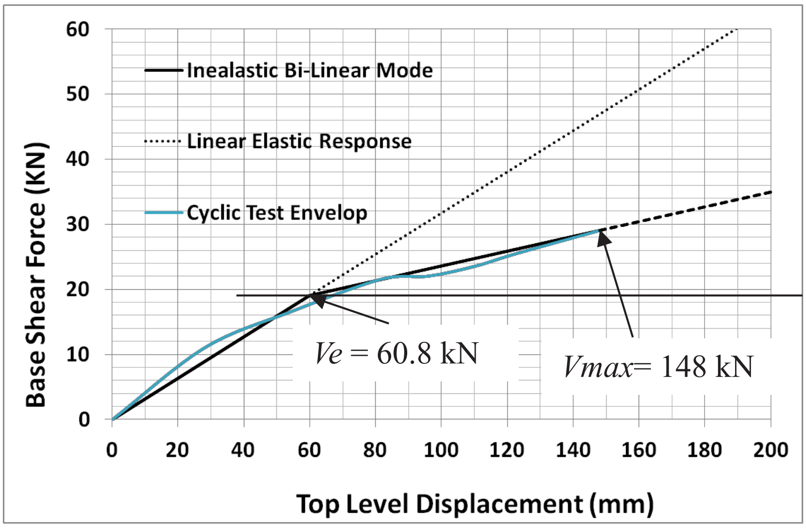

Figure 7.16: Experimental envelop curve vs the Bi-Linear and Linear push curves

The calculated ductility factor ‘μ’ of the structure is smaller than the ductility factor proposed by Rosin et al. (2009). This is because the test was terminated before reaching the ultimate load where the load starts to drop. Obviously, by continuing the secondary stiffness line of the Bi-Linear curve, the ductility factor will be increased.

This simply shows that the ductility factor is essentially related to the maximum drift which the structure experiences. On the other hand, unlike a typical structural system, rack structures are usually loaded up close to their stability limits and this is because of their lightness. The maximum load bearing capacity of the entire rack system is highly sensitive to the stored pallet load (P) and the lateral drift as proved in Appendix E. Hence, stability is another influential parameter which limits the ultimate point and by reducing the ultimate displacement (e.g. drift) the obtained ductility factor will be less.

Also a simple 2-Dimensional FE model was created in ABAQUS to model the envelop push over cyclic curve. For this reason, instead of running the cyclic model, the proposed Equivalent Cyclic Back bone was used to model the beam to upright connections. Base plate connections were assumed to be hinged and all the beams and uprights were modelled using beam elements with 6 degrees of freedom at each node. Figure 7.17 shows the deformed shape of the FE model.

Figure 7.18 also shows the FE results versus experimental envelop curve. The good agreement of the experimental and numerical results, again proved the suitability of the proposed equivalent cyclic moment rotation back bone described in Chapter 2.

A rational displacement based design method will then be proposed at the end of this chapter.

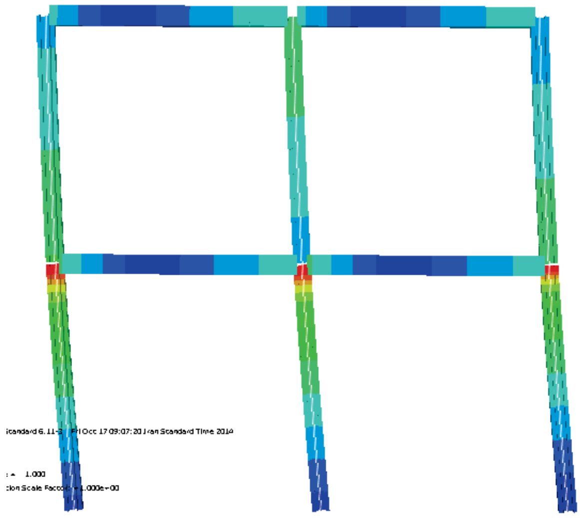

Figure 7.17: Deformed shape of the FE Model (Rendered view)

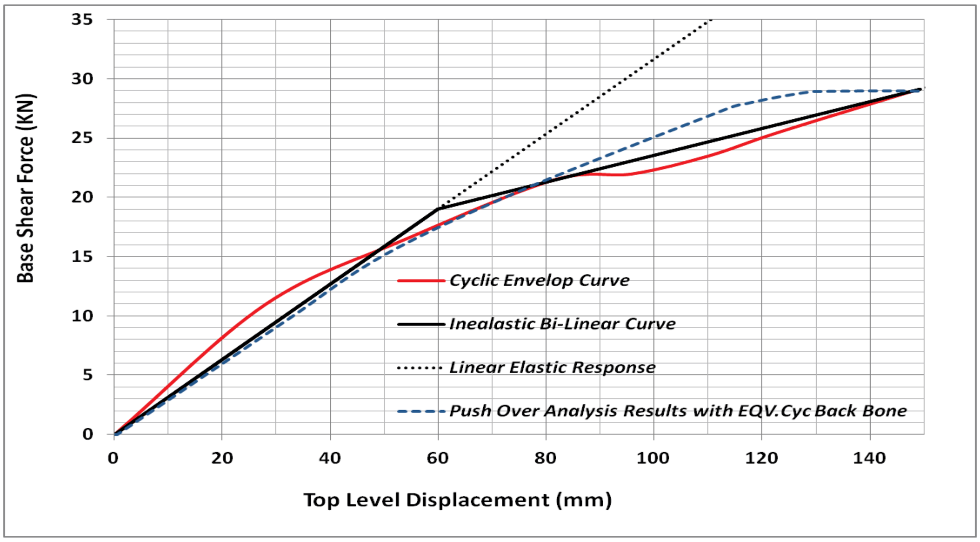

Figure 7.18: Finite Element analysis result vs. Experimental cyclic envelop curve

7.2.3 Cyclic test vs Shake table test results

Incremental dynamic analysis (IDA) curve was derived from the results of 'BL-NB' shake table tests, non-scaled in time domain, and was compared with the cyclic test results as shown in Figure 7.19.

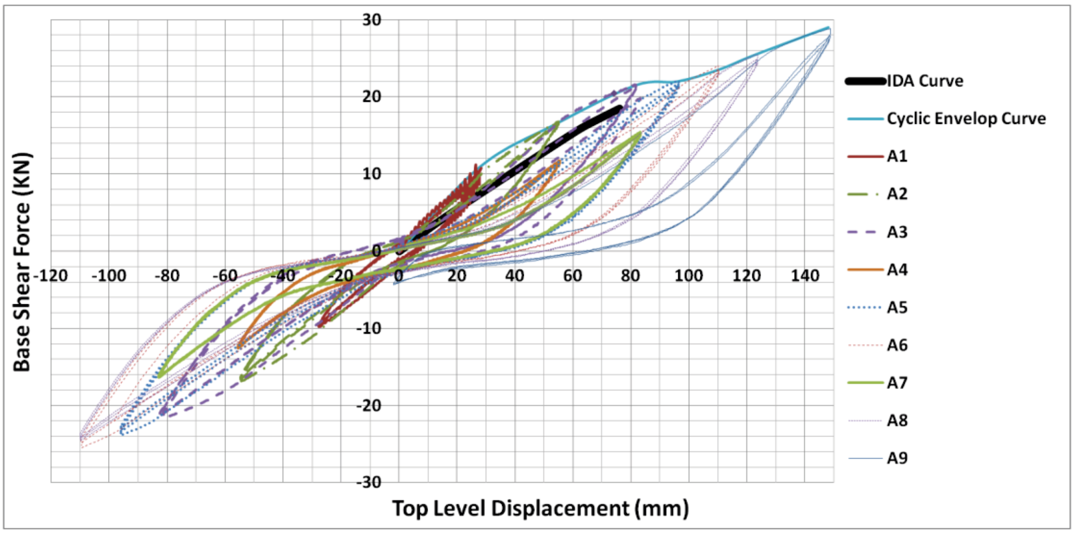

Figure 7.19: Static cyclic test vs Dynamic shake table test results

IDA curve shows the equivalent base shear of the structure under real seismic action vs top level displacement when seismic base shear of the frame was approximately calculated by Equation 7.2.

$$V_{base\ shear} = M_2\, a_2 + M_1\, a_1 \qquad (7\text{-}2)$$

Where M_1 and M_2 represent the masses on levels 1 and 2 while a_1 and a_2 represent the maximum acceleration of the pallets at levels 1 and 2 respectively.

The agreement of the IDA curve and the cyclic envelope curve in Figure 7.19 shows that cyclic test could accurately model the seismic conditions with the given loading pattern in which the imposed displacement at the top level was 50 percent greater than that of the first level. The ratio 1.5 of top level displacement compared with first level displacement was stablished from the response of the frame during the shake table test. Figure 7.20 shows the IDA curve and the cyclic loops with the displacement amplitude equal to the maximum displacement of the IDA curve.

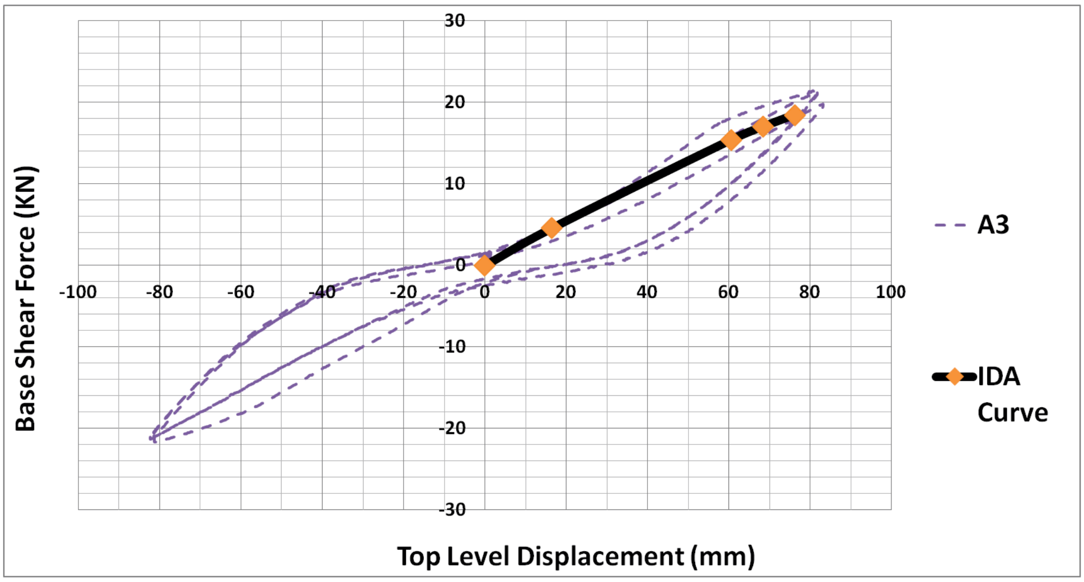

Figure 7.20: IDA curve and the Cyclic curve with the amplitude close to the maximum seismic displacement

7.3 Displacement based method seismic analysis and design by using Capacity Curve

This method is established based on the capacity curve which is the envelope of cyclic push over curve. To derive the capacity curve, a Non-Linear push over analysis based on displacement control technique is required.

Also, a stability analysis is required to obtain the maximum allowable drift of the system under seismic action. Therefore a stability analysis is first presented before proposing the step by step displacement based method of seismic design.

7.3.1 Stability Analysis

In this part the stability analysis method of Lewis (1991) which accounts for the nonlinearity of the beam to upright connections will be improved using the same assumptions by incorporating the stiffness effects of spine bracing and base plate connections. Also in order to use the stability equations for the systems under seismic actions, an approximate model of moment rotation curve of the beam to upright connections will be defined to best model the behaviour of the connections under cyclic loads patterns. In this approach it is assumed that the same loads are applied at each level and their lines of action remain vertical during the displacement of the frame. Simplified models of braced and un-braced frames are shown in Figure 7.24. The bending distortion of the upright is small when compared with the lateral displacement of the upright. The upright rotation as well as beam to upright connections is denoted by "θ". Nonlinear behavior of base plate and beam to upright connections are considered. An initial looseness (out of plumbness) is denoted by "α" which is not shown in Figure 7.24.

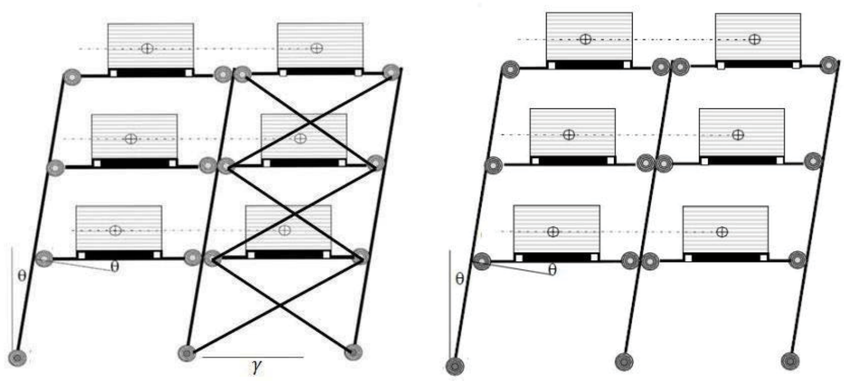

Figure 7.21. Braced and un-braced frames

The total potential energy of the system can be written as:

$$W = U + P_E \tag{7-3}$$

where: U = Internal work

P_E = External work

A significant component of internal work includes the work of semi-rigid connections including base plates and beam to upright connections. In comparison, work due to bending and axial deformation of beams and uprights is assumed to be relatively small and therefore will not be considered in the expression derived below. The work done by semi rigid connections can be expressed as:

$$U = \int N_c f_c(\theta) d\theta + \int N_b f_b(\theta) d\theta \tag{7-4}$$

N_b : Number of base plate connections

N_c : Number of beam to connections

$f_c(\theta)$: Moment rotation function of beam to upright connections

$f_b(\theta)$: Moment rotation function of base plate connections

The potential energy lost by the vertical external loads can be written as:

$$P_E = -N\sum_{i=1}^{c} p\, i\, h(1-\cos\varphi) \tag{7-5}$$

C : Number of storey levels

N : Number of beams at every levels ($N_c = 2\,C\,N$)

φ : $\theta + \alpha$

p : Pallet load distributed at every beam

α : Imperfection (out of plumb)

The total potential energy of the system can be written as:

$$W = N_c \int f_c(\theta)d\theta + N_b \int f_b(\theta)d\theta - \frac{N_c ph(C+1)}{4}(1-\cos\varphi) \tag{7-6}$$

$$\frac{\partial W}{\partial\theta} = N_c \frac{\partial}{\partial\theta}\int f_c(\theta)d\theta + N_b \frac{\partial}{\partial\theta}\int f_b(\theta)d\theta - \frac{N_c ph(C+1)}{4}(\sin\varphi) = 0 \tag{7-7}$$

Therefore:

$$p_{cr} = \frac{4\,[N_c f_c(\theta)+N_b f_b(\theta)]}{N_c h\,(C+1)\,\sin\varphi} \tag{7-8}$$

By applying bracing members, the internal work done by the system will change as follows:

$$U = \int N_c f_c(\theta)d\theta + \int N_b f_b(\theta)d\theta + \frac{N_{brace}h^2\,sin^2\,\varphi\cos^2\gamma\,E_{brace}A_{brace}}{2l_{brace}} \tag{7-9}$$

Where,

N_{brace} : Number of bracing members in tension

γ : The angle between bracing member and horizontal direction (Figure 7.24)

A_{brace}: Cross section area of the bracing member

It is assumed that only those bracing members that are in tension are participating and pallet loads at every beam are of equal values. Using the same methodology and taking the first derivative of the energy function, the load bearing capacity of every beam level will be increased as expressed by Equation 7-10.

$$p_{cr} = \frac{4([N_c f_c(\theta)+N_b f_b(\theta)] + \frac{N_{brace} h^2 \sin\varphi \cos\varphi \cos^2\gamma \, E_{brace} A_{brace}}{l_{brace}})}{N_c h\,(C+1)\,\sin\varphi} \tag{7-10}$$

In order to determine the type of stability of the system, identifying the sign of the second derivatives of the total potential energy function "W" is necessary, which is evaluated as shown below:

$$\frac{d^2W}{d^2\theta} = N_c \frac{\partial^2}{\partial^2\theta}\int f_c(\theta)d\theta + N_b \frac{\partial^2}{\partial^2\theta}\int f_b(\theta)d\theta +$$

$$\frac{\partial^2\left(\frac{N_{brace} h^2 \sin^2\varphi \cos^2\gamma \, E_{brace} A_{brace}}{2 l_{brace}}\right)}{\partial^2\theta} - \frac{N_c p h\,(C+1)(\cos\varphi)}{4} \tag{7-11}$$

Substituting (7-10) into (7-11) leads to:

$$\frac{d^2W}{d^2\theta} = N_c f'_c(\theta) + N_b f'_b(\theta) - \frac{N_c f_c(\theta)+N_b f_b(\theta)}{\sin\varphi}(\cos\varphi) -$$

$$\frac{N_{brace} h^2 \sin^2\varphi \cos^2\gamma \, E_{brace} A_{brace}}{l_{brace}} \tag{7-12}$$

As shown by Lewis (1991) for positive values of α, the sign of equation 7-12 is negative and hence the whole frame will be unstable under any pallet loads greater than p_{cr}. Figure 7.22 shows a typical representation of the equilibrium states of a system with bi-linear connection characteristic. The red line indicates decreasing ultimate loads of imperfect systems by increasing α values.

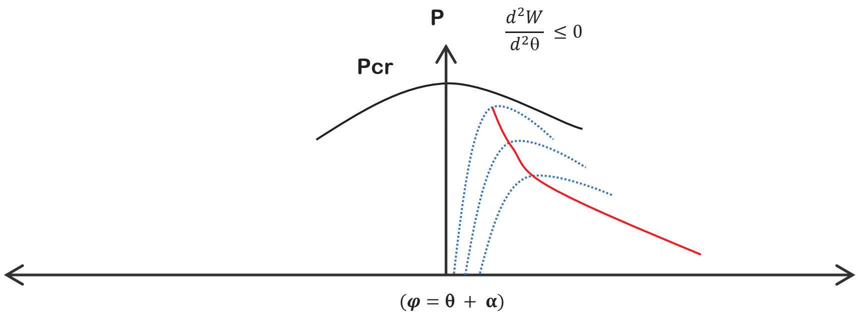

Figure 7.22. Equilibrium states of a system with Bi-Linear connection characteristic

7.3.1.1 Stability of the frames under seismic actions

The approach presented below introduces a stability limit for the seismic design of rack structures where the critical pallet load at the maximum drift of the structure "θ", which is calculated from conventional seismic analyses methods, will be checked against the stored pallet loads on the rack.

In equations 7-8 and 7-10, the stability of the entire down aisle frame in down aisle direction for both braced and un-braced frames essentially relies on the moment-rotation behaviour of beam to upright connections as well as base plate connections. However, to define a stability limit for the maximum drift of the racking system in seismic areas, the monotonic moment-rotation function of the connections may not be reliable because the connections will progressively deteriorate while subjected to cyclic reversal load patterns. However, the stability analysis proposed by Lewis (1991) is only sensitive to strength deterioration while stiffness deterioration has no effect on the final result. By investigating a typical storage rack, it was observed that the dynamic behavior of the system and thereby the maximum seismic drift is significantly dependent on both strength and stiffness deteriorations. A method was proposed in chapter 2 to define an equivalent cyclic moment-rotation back bone that considers the strength deterioration of the connections which can be also used as a moment-rotation function "$f_c(\theta)$" in stability analysis of this down aisle frame. As shown in Figure 7.23, the moment function "$f_c(\theta)$" derived from monotonic tests has higher values compared with moment values obtained from cyclic hysteresis tests for the same rotation "θ". Hence in this case using the monotonic moment rotation curve gives an un-conservative stability limit.

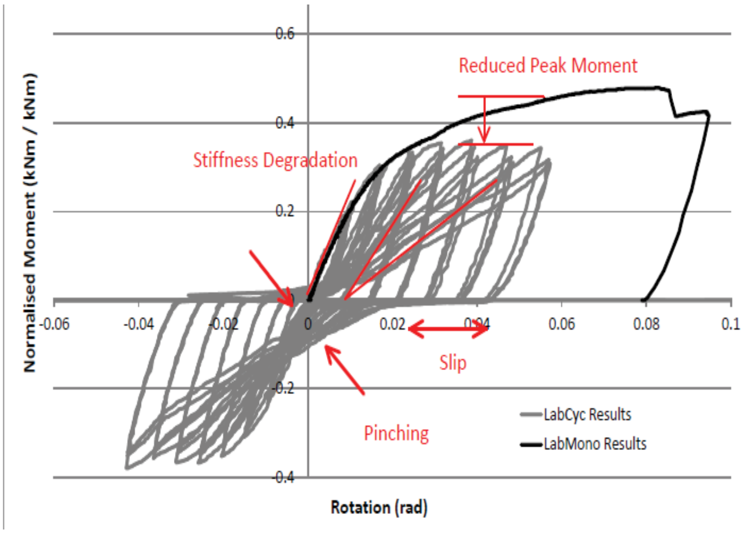

Figure 7.23. Typical Beam-Upright Connection Non-Linear Features (Reyes, 2013, p. 53)

It is therefore proposed that a more realistic stability limit can be obtained from equations 7-8 & 7-10 by adopting a reduced moment according to an equivalent cyclic moment-rotation back bone. Further investigation is required to confirm the validity of this approach to storage racks with other connection types.

7.3.2 Step by step displacement based method

The lateral displacement can be selected as an average of the two extreme patterns of rectangular and triangular[36]. This assumption is made based on the failure modes reported both in Rosin et al. (2009) as well as Chapters 5 and 6 of this thesis. This pattern considers the soft storey failure mode. Similar pattern was also observed in the 2011 Christchurch earthquake as presented at the beginning of Chapter 5. (See Figure 7.24)

A step by step displacement based method will be presented in this chapter to better evaluate the performance of the racking systems.

[36] This is an approximation. A thorough numerical as well as experimental investigations should be conducted to come up with a more accurate displacement pattern.

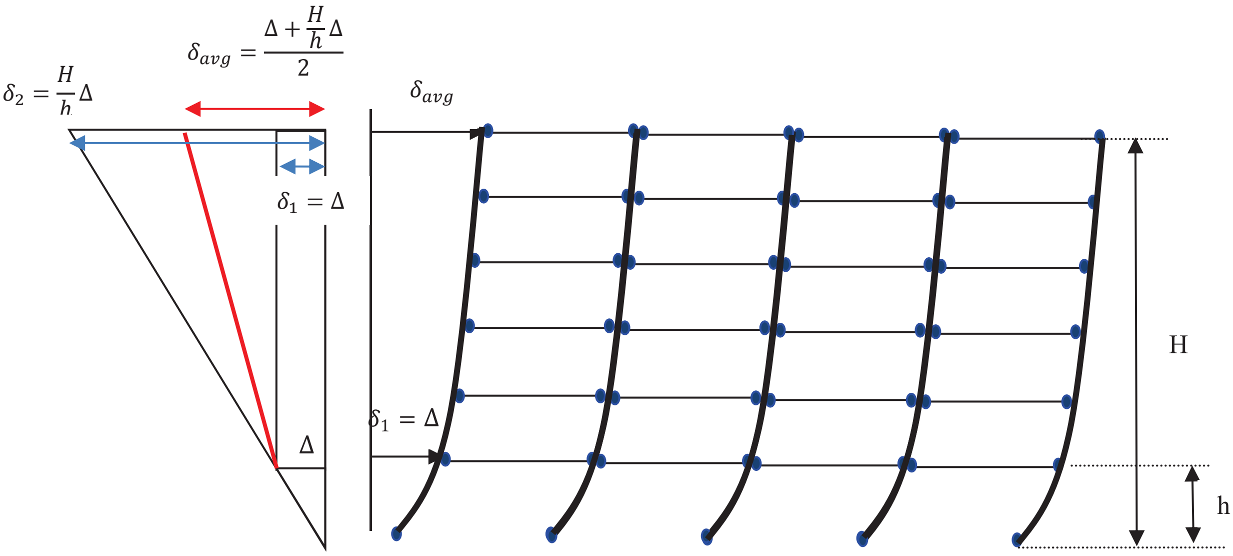

Figure 7.24: Assumed failure mode under seismic actions

I. **Step 1**. Perform Non-Linear static push over analysis based on the equivalent cyclic moment rotation backbone of the beam to upright connections as described above.

II. **Step 2**. A dynamic analysis shall be performed to obtain the fundamental period of vibration[37].

III. **Step 3**. Find the equivalent elastic response displacement, Δ_e, from the 'Design Displacement Response Spectrum' (See Figure 7.25) and then calculate top storey elastic displacement, Δ_{eTop} as expressed in below:

$$\Delta_{eTop} = \frac{\alpha \Delta_e}{\lambda}$$

α: Seismic intensity factor (7-13)

The λ factor is to convert the multi degree of freedom model to the equivalent single degree of freedom model for the seismic design and can be calculated from Equation 7.4. FEMA 460 proposes 0.72 for this conversion, however, the actual shake table test results show a λ factor of 0.9 in this particular case. (See Figure 7.26)

[37] Rational theoretical analysis can be also performed to calculate the fundamental period of vibration as proposed in FEM 460 (2005)

$$\lambda = \frac{(\sum m_i \Delta_i^2 / \sum m_i \Delta_i)}{\Delta_{Top}} \quad (7\text{-}14)$$

where,

m_i is the mass at level i and Δ_i is the lateral movement of level i under seismic loads. Δ_{Top} is the maximum lateral displacement recorded from top beam level.

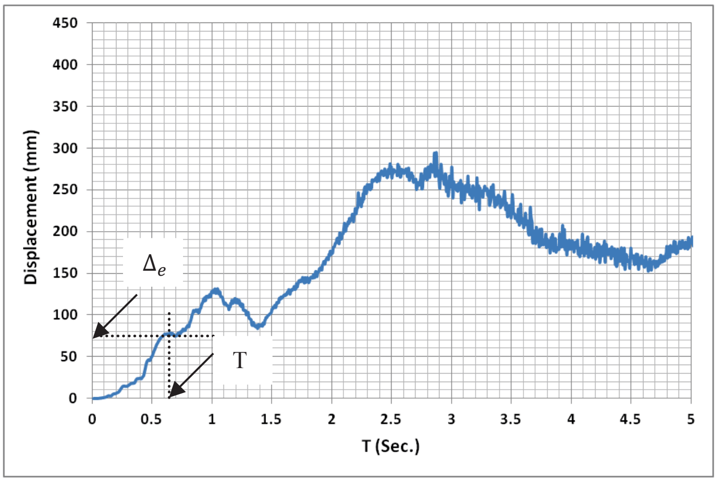

Figure 7.25: Displacement response spectrum

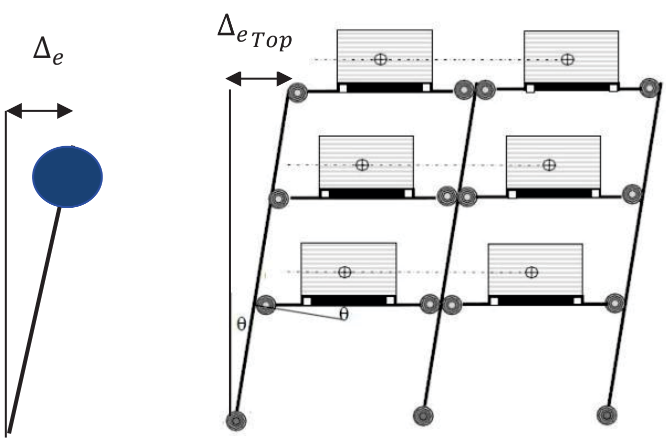

Figure 7.26: Multi degree of freedom model vs Single degree of freedom model

IV. **Step 4**. Find the inelastic top level displacement, Δ_{pTop}, which is the horizontal projection of the elastic top storey displacement, Δ_{eTop}, on the capacity curve (See Figure 7.27)

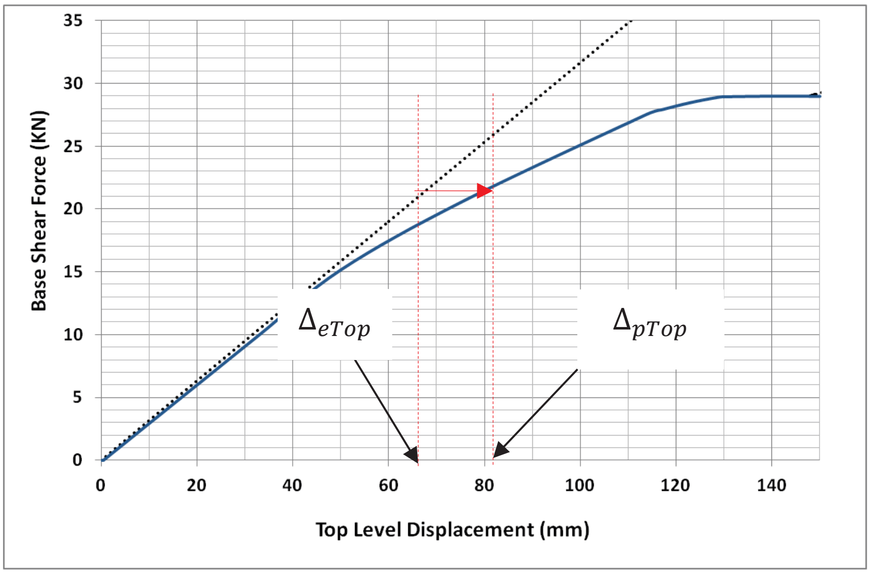

Figure 7.27: The inelastic top level displacement, Δ_{pTop}, the horizontal projection of the linear push curve from the corresponding elastic top level displacement, Δ_{eTop}.

V. **Step 5**. Check if the inelastic top level displacement, Δ_{pTop}, is smaller than the stability displacement limit[38], Δ_S.

- If ($\Delta_{pTop} \geq \Delta_S$) the pallet load should be reduced or the frame needs to be stiffened up by using stiffer beams and beam end connectors or spine bracing members and return to Step 1.
- If ($\Delta_{pTop} \leq \Delta_S$) go to next step.

VI. **Step 6**. Distribute the displacement load according to the pattern shown in Figure 7.24 and based on the top level inelastic displacement.

VII. **Step 7**. Analyse the model to obtain the internal actions.

[38] Stability displacement limit is the maximum displacement at which the structure maintain its global stability. Appendix E explains how to calculate the stability displacement limit of every rack structure. Advanced software packages can be also used instead to calculate the ultimate stability drift.

7.3.3 Example of displacement based design method (Using Non-Linear Static Analysis)

In this section, the 2 Storey- 2 bay frame tested on shake table for 80% 1940 El Centro earthquake ($\alpha = 0.8$) will be checked according to the aforementioned procedure and capacity curve shown in Figure 7.25.

Step 1.

Derive the capacity curve by performing Non-Linear push over analysis. And also find the linear push curve by drawing the secant line passing through the origin of the capacity curve. (See Figure 7.28)

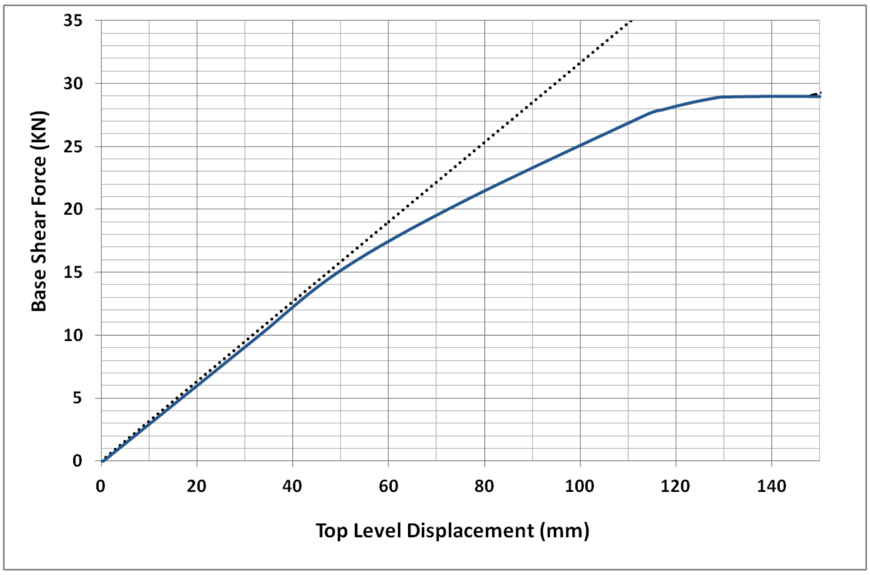

Figure 7.28: Capacity curve and the linear push curve

Step 2.

- *Dynamic Analysis*: Linear dynamic modal analysis was performed in SPACE GASS software package and the fundamental period of vibration was obtained:

  T = 0.7 Sec.

Step 3.

- *Elastic top storey displacement* (Δ_{eTop}): First the elastic displacement spectrum was depicted for 1940 El Centro earthquake with equivalent viscous damping ratio of 8 percent of critical ($\xi = 8\%$).

  $\alpha = 0.8$

$\varDelta_e(T,\xi) = \varDelta_e(0.7, 8\%)$ = 68.2 mm (See Figure 7.29)

$$\varDelta_{e\,Top}(0.7, 8\%) = \frac{\alpha\, \varDelta_e(0.7, 8\%)}{\lambda} = \frac{0.8\ \times 68.2}{0.9} = 60.62$$

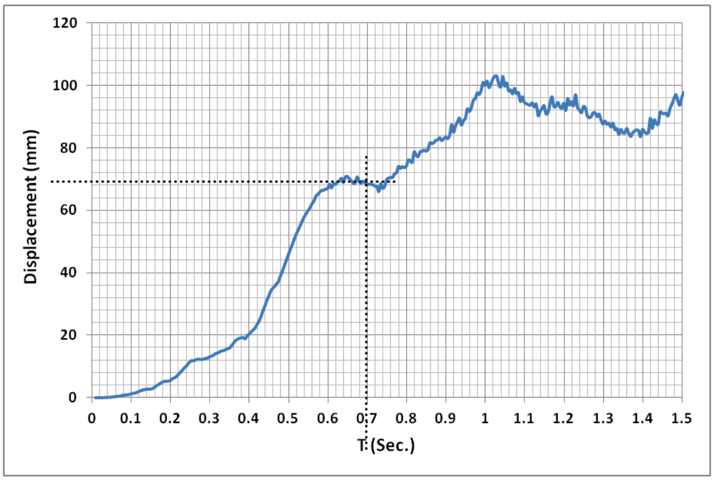

Figure 7.29: Reading the elastic top level displacement from displacement response spectrum

Step 4.

- Find the inelastic top level displacement of the structure ($\varDelta_{pTop}$): the plastic (inelastic) top level displacement can be found by taking the horizontal projection point of the elastic top level displacement ($\varDelta_{eTop}$) of the linear push over line to the capacity curve. (See Figure 7.30)

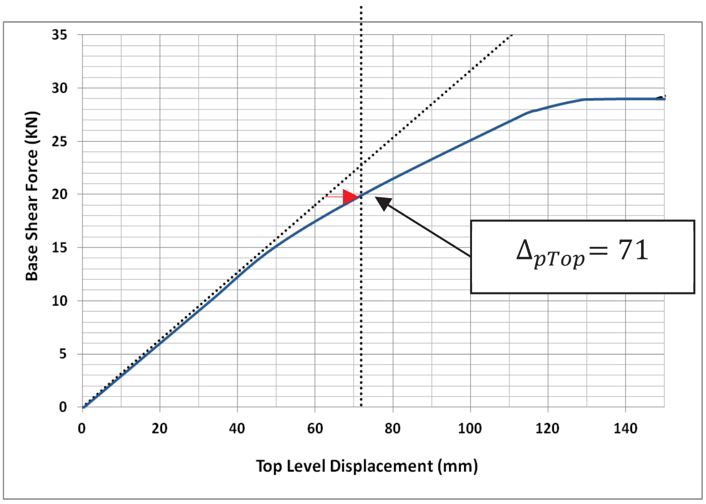

Figure 7.30: Reading Δ_{pTop}

Δ_{pTop}= 74.9 mm

Step 5.

- *Stability check:* Allowable stability drift will be calculated from 7.8, as follows:

$$p_{cr} = \frac{4\,[N_c f_c(\theta)+N_{bp} f_{bp}(\theta)]}{N_c h\,(C+1)\,\sin\varphi} = \frac{4\,[N_c f_c(\theta)+N_{bp} f_{bp}(\theta)]}{N_c h\,(C+1)\,h\,\Delta_S}$$

Then,

$$\Delta_S = \frac{4\,[N_c f_c(\theta)+N_{bp} f_{bp}(\theta)]}{N_c h\,(C+1)\,h\,p_{cr}} \qquad (7\text{-}15)$$

h = 1.320 m

P_{cr} = 1 tonne = 10 kN

Nc = 8, *Nbp* = 6, C = 2

fc at maximum allowable drift = 2.4 kN.m

fbp = 0 kN.m

Substituting the above values into Equation 7-5, Δ_S can be calculated:

Δ_S = 189.4 mm

then, $\Delta_{pTop} \leq \Delta_S$ OK

Steps 6.

- *Structural Analysis:* Analyze the structure based on the lateral seismic displacement obtained from Δ_{pTop} (See Figure 7.31)

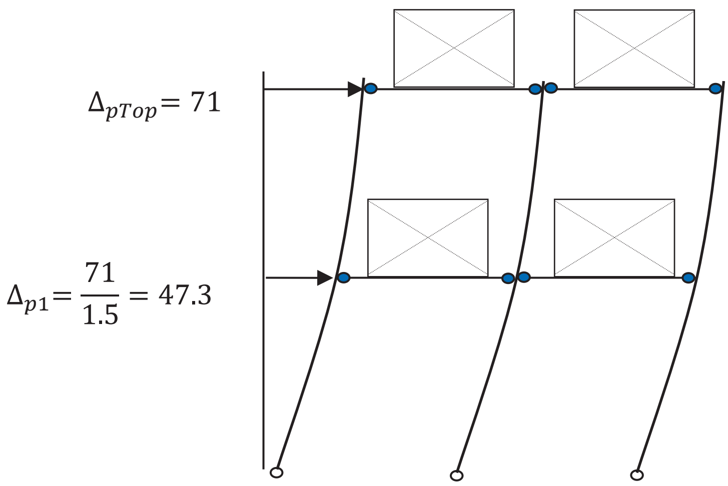

Figure 7.31: Displacement loading for structural analysis

In order to compare the accuracy of this method with the seismic design methods of the current seismic codes the same structure was also analyzed based on the RMI (2012) and FEM 10.2.08 (2010).

To focus only on the effect of ductility of the structure, the same elastic spectral acceleration was used for both analyses and also the pallet weight modification factor[39] of 0.8 due to the effect of sliding of pallets on the beams was used in both analyses methods.

The analysis parameters are shown in Table 7-1 and the results of different analysis approaches are illustrated in Table 7-2.

[39] This factor is equal to 0.67 in RMI : 2012 and FEM 10. 2. 08 : 2011 proposes a variable modification factor of ED2 which is related to the severity of the earthquake as well as the friction factor between the timber pallet and the beams.

Table 7-1. Seismic Analysis Assumptions

	FEM 10. 2. 08 : 2011	RMI 2012
Spectral Acceleration (a) (m/s/s)	6.05	6.05
Ductility factor (q or R)	2.0	6
Pallet weight modification factor (λ)	0.8	0.8
Elastic Base Shear ($=\frac{\lambda a}{q\ or\ R}$)	9680 N	3226 N

Table 7-2. Comparison of different analysis methods

	Δ_e 2nd Level	Δ_e 1st Level	Δ_p 2nd Level	Δ_p 1st Level	F1	F2	F3
FEM	14.39 mm	17.54 mm	28.78 mm	17.54 mm	6014 N	9301 N	3184 N
RMI	5.1 mm	3.07 mm	27.05 mm	16.89 mm	5070 N	9316 N	4122 N
Proposed Design Method	-	-	71 mm	47.3 mm	11005N	9931 N	-892 N*
FE Time History	-	-	73.2 mm	46.71 mm	11027N	9990 N	-1014N*
Shake Table tests	-	-	76.2 mm	58 mm	-	-	-

* *the negative sign shows the uplift force*

Table 7-2 shows the inaccuracy of the current Equivalent Static Lateral Force method (ELSF) for seismic analysis and design of the rack structures. This proves that the current force based design methods should be urgently modified.

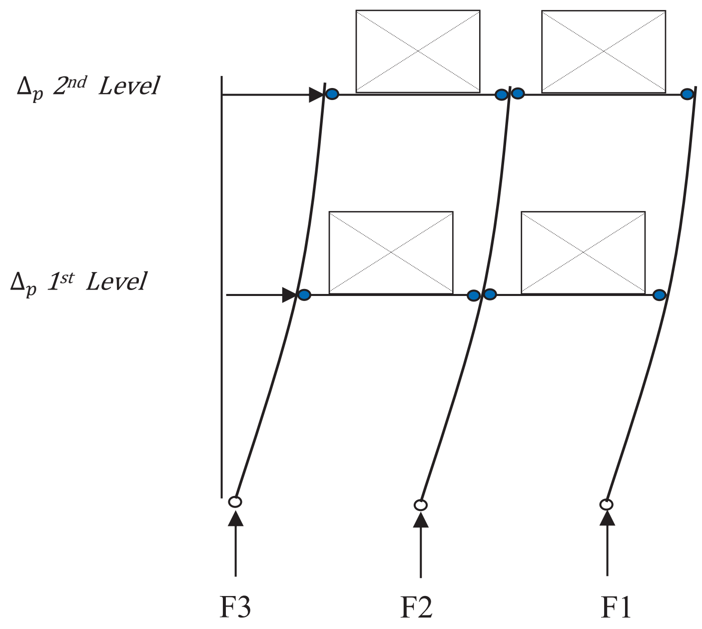

Figure 7.32: Deformed shape of the system after analysis

7.4 Conclusions

This chapter presents the experimental full scaled cyclic tests (Push - Pull) of a 2-storey, 2-bay rack under cyclic loads. The tests were conducted based on displacement control method and the distribution pattern along the height of the frame was adopted from the failure mode monitored from the shake table tests presented in Chapter 5. The test was terminated at top beam level displacement amplitude of 165 mm when the structure was in stable condition.

The hysteresis curves were then derived and the following observations are made:

1. System shows good ductility with relatively high top level displacement.
2. Significant strength deterioration and stiffness degradation were observed in the hysteresis curves of the consecutive cycles.

3. Hysteresis curves show almost identical behaviour of the frame under both push and pull forces.
4. The structure could satisfy stability criterion.

The hysteresis cyclic back bone curve (envelope) was drawn and compared by the Incremental Dynamic Analysis curves from the dynamic shake table tests. The good agreement between the static cyclic test results and dynamic shake table tests verifies the test method of conducting the cyclic tests based on displacement control loading technique and also the displacement loading pattern along the height of the frame.

The proposed moment – rotation backbone for the beam to upright connection was used to run the push over analysis and the results were compared to the experimental full scaled cyclic tests backbone. Good agreement between the experimental and numerical results was considered as further proof of suitability of the proposed moment rotation backbone curves of the beam – upright connections.

A displacement based method for seismic analysis and design of the structures was also proposed and the results were compared against the dynamic time history analysis results which show much more accurate results in comparison to the current design methods.

8. CHAPTER 8: CONCLUSIONS AND RECOMMENDATIONS FOR FURTHER STUDIES

8.1 Summary and Conclusion

Racking systems are cold formed steel structures for the storage of goods in warehouses. These structures present a different behavior compared with traditional steel frames. Lack of sufficient design rules and specifications provides an urgent need to better understand their performance under seismic loads by developing finite element models to simulate the behavior of rack structures and to verify them against extensive experimental investigations. Prior to commencement of this research project, a set of 108 beam end connector monotonic bending tests, a number of beam end connector shear test, braced frame shear test have been conducted on the different configurations of beam to upright connections. 24 monotonic tests were conducted in order to determine the stiffness and load carrying capacity of base plate connections. The experimental results were expressed in form of nonlinear moment-rotation curves of the base plate connections as a function of different parameters like axial force on the upright and base plate type. The results of these tests were made available for this research program courtesy of DEXION Australia[40]. After preliminary analysis of the test results the urgency of more detailed investigations has been highlighted. For this reason about 60 monotonic beam to upright bending tests followed by 7 beam to upright cyclic bending tests have been designed and tested (August-September 2012, UTS). An accurate monotonic and cyclic finite element model of the beam to upright connections has been developed later and was verified against the test results. The effect of different geometrical parameters of beam to upright connections such as beam depth and width on the strength and rigidity of the connections has been investigated (See Chapter 2 of this thesis).

Upright base plate connections as very important components in providing stability

[40] An International rack manufacturer company

of the whole frame have also been investigated in this study. For this reason, a detailed finite element model was later developed and verification against experimental data showed good agreement whereby the reported errors were less than 10%. The finite element method was also applied to investigate the performance of base plate connections subjected to monotonic and cyclic loads.

Braced frame systems used in cross aisle directions were also investigated using Finite Element simulations and verified against existing experimental results. Moreover the behaviour of braced frame was analytically modeled using simple structural element like springs and beam element.

After having modeled and carefully studied the monotonic and cyclic behaviors of different connection components, such as the beam connector, the bolt connection of bracing members and the base plate connection, a complete racking frame that incorporate a realistic simulation of those connections can be modelled.

Full scale shake table tests and cyclic push over tests were conducted in the second half of this PhD program to confirm the results of the analytical and numerical investigations of the beam to upright connections. Performing either a full scale shake table test or cyclic push over test requires consideration of many practical, technical and safety issues which are addressed in chapter 5 and 7.

Shake table tests were simulated by the SAP 2000 finite element software package and were verified against the experimental tests results. Details of the FE model and their results comparison are presented in chapter 6.

Results of shake table tests and cyclic push over tests were compared and as a result a performance based design method was proposed in chapter 7.

Summary of important achievements and findings of this PhD thesis is listed below;

Chapter 2, Beam to upright connections:

- An experimental study was carried out to investigate the behaviour of boltless beam to upright connections under monotonic as well as cyclic loads.

- A yield rotation[41] (θ_y) of around 0.02 was observed for all of the connections.

- The connections for deeper boxed beams showed less non-dimensional initial stiffness and moment capacity despite their higher actual moment capacity and initial stiffness.

- Although the thickness of the uprights was not significantly effective on the monotonic moment – rotation behaviour of the connections, it can remarkably change the cyclic performance of those connections.

- FE models were developed and were able to simulate the behaviour of beam to upright connections under monotonic and cyclic actions.

- An analytical method was developed and verified by experimental results to determine the moment - rotation behaviour of the connections.

- An analytical method was proposed to determine the hysteresis curve of the connections under a given cyclic load by using an existing hysteresis model.

Chapter 3, Base plate connections:

- Experimental results of the base plate connection tests were thoroughly investigated and the effect of anchoring arrangement and compression force of the upright on the moment – rotation behaviour of the base plate connections were explained in chapter 3.

- The moment rotation behaviour of the base plate connections was found to be very sensitive to the second order effect due to the axial

[41] The rotation at which the connections start to yield

compression forces of the uprights. For these reason the moment – rotation curves showed that under displacement control the moment in the base plate never drops even when the shear force of the connections drops.

- Experimental test results showed that almost all the connections lose their capacity at rotations approximately 0.02 Rad. This limitation should be considered for seismic design of the rack structures when they are subjected to heavy lateral forces.

- An analytical model was also developed to determine the ultimate rotation of base plate connections based on a stability analysis.

- The current method of determining the moment rotation behaviour of the base plate connections was found to be unsafe.

- Finite Element models of base plate connections were developed in order to investigate the effect of different anchoring arrangements on the moment – rotation characteristics of the connections.

- An analytical method was proposed to determine the stiffness of the base plate connections under a given axial compression force.

- FE models were used to investigate the moment – rotation behaviour of different types of base plate connections under cyclic loads.

- Significant stiffness deterioration was observed in hysteresis moment – rotation curves of the connections. For this reason a rational method was proposed to model the behaviour of the base plate connections for the seismic design of rack structures.

- An analytical method was proposed to determine the hysteresis curve of the base plate connections under a given cyclic load by using an existing hysteresis algorithm.

Chapter 4, Braced frame systems:

- Experimental results of the braced frame tests were analysed and the failure modes and force – deformation curves were explained.

- The behaviour of the shear frames were numerically and theoretically modeled in order to obtain the transverse stiffness of the frames.

- A stability analysis was presented in chapter 4 to calculate the load carrying capacity of the upright frames under seismic actions.

Chapter 5, Full scale shake table test:

- A full scaled shake table test program was conducted in two stages and the actual behaviour of a full scale 2-story, 2-bay frame was investigated under the El Centro earthquake record. The results of the shake table tests are presented in chapter 5.

- The bottom storey of the rack was the most severely affected (soft story mechanism)

- Dynamic features of the frame such as fundamental period of vibration and damping ratio were calculated from sine sweep tests results.

- Damping ratios higher than 5% (current design assumption) were observed.

Chapter 6, Finite Element simulation of full scaled shake table tests:

- The Sap 2000 finite element software package was used to develop 3-D full scale models of rack structures focusing on the beam to upright connections.

- Base plate connections were modeled as hinged connections since they showed very low rotational stiffness under a low axial compression force. This resulted in a soft story mechanism which was in line with the test observation.

- The calculation of natural modes of vibration for use in seismic analysis methods for steel storage racks (e.g. ESLF, NLTH, mode superposition, etc) should consider the P-Δ effect, as for high rise racks with heavy pallet loads it significantly elongates the periods of vibration.

- Three different hysteresis models of, Kinematic, Takeda and Pivot models were used to simulate the behaviour of beam to upright connections under seismic actions and the overall response of the rack frame under different earthquake records of Northridge and El Centro were investigated.

- Numerical investigations showed that the responses of rack structures with typical boltless beam to upright connections are very different under the far field earthquake record of El Centro and near field earthquake record of Northridge and hence rack structures show different ductility under different seismic actions.

- In addition to the time history dynamic analysis, a full frame push over analysis was also performed with rectangular and triangular lateral load pattern distributions over the structure height. The Non-Linear Push Over (NLPO) curve of the structure with rectangular lateral load pattern was shown to have a closer correlation with the Incremental Dynamic Analysis (IDA) curve of the structure under both El Centro and Northridge earthquakes.

- The Equivalent Static Lateral Force (ELSF) method is not capable of modelling the dynamic effects of near-fault earthquakes.

- The seismic load reduction factor of ‘R = 4.0’ and the over strength factor ‘Ω = 1.33’ were calculated from the El Centro earthquake Incremental Dynamic Analysis (IDA) curves using the PGA ratio with respect to the first significant yield point.

- A Seismic load reduction factor ‘R’ of around ‘2.0’ and an over strength factor ‘Ω’ of around ‘1.2’ were calculated based on the Non Linear Push Over (NLPO) Analysis curves.

- Based on a comparison with the Equivalent Static Lateral Force (ELSF) method, the values R = 1.8, $R\mu$ = 1.5 and Ω = 1.2 were recommended.

- FE models were used to simulate the shake table tests with the following assumptions:

    - Beam to upright connections were modelled using the proposed pivot hysteresis model.
    - Upright base connections were modelled as hinged connections.
    - An equivalent viscous damping of 8 percent was used.

- An acceptable agreement was reached between the FE analysis results and actual experimental test results which confirmed the accuracy of the proposed modelling approach and consequently all of it's results.

Chapter 7, Full frame cyclic test:

- A 2-story, 2-bay rack frame similar to the one tested on the shake table was tested under cyclic reversal loads in its down aisle direction. The tests were performed based on a displacement control method. The applied displacement pattern along the height was adopted from the failure mode observed from the actual shake table test results.

- A hysteresis curve and its cap curve (envelop curve) were established and compared against the incremental Dynamic Analysis (IDA) curve of the actual shake table test series. Good agreement between the two curves confirmed the accuracy of the loading pattern which was applied along the heights of the frame.

- A seismic displacement based method was proposed to analyse and design the rack structures. The accuracy of the proposed method was assessed by comparing that method with the current seismic design methods based on RMI (2012) and FEM 10.2.08 (2010).

8.2 Recommendations for future research

- Thorough investigations of combined bolted/hooked connections under monotonic and cyclic actions.

- Investigating the behaviour of the base plate connections in cross aisle directions under combined uplift/bending actions.

- Studying ductile 'V' bracing systems in cross aisle direction of the rack structures.

- More shake table tests on different rack structures including spine braced rack structures.

- Replacing the current ELSF seismic design method by more rational displacement based seismic design methods in both cross aisle and down aisle directions.

APPENDICES

Appendix A: Experimental beam to upright Connection bending test results

Table A-1 shows the different beam to upright connections bending test results. It can be seen that the common failure modes are hook failure and upright slot indentation. The ultimate moment is also between 2 kNm to 4 kNm.

Table A-1. Beam End Connector Test Results

Specimen Label	Failure mode
Box-80x40/2.5mm Upt	Weld Failure + Hook Failure
Box-80x40/2.5mm Upt.	Weld Failure + Hook Failure
Box-80x40/2.5mm Upt.	Weld Failure + Hook Failure
Box-80x40/2.5mm Upt	Weld Failure + Hook Failure
Box-80x40/1.6mm Upt.	Hook Failure + Upright Indentation
Box-80x40/1.6mm Upt.	Hook Failure + Upright Indentation
Box-80x40/1.6mm Upt.	Hook Failure + Upright Indentation
Box-80x40/1.6mm Upt.	Hook Failure + Upright Indentation
Box-85x50/2.5mm Upt.	Weld Failure + Hook Failure
Box-85x50/2.5mm Upt.	Weld Failure + Hook Failure

Box-85x50/2.5mm Upt.	Weld Failure + Hook Failure
Box-85x50/2.5mm Upt.	Weld Failure + Hook Failure
Box-85x50/1.6mm Upt.	Hook Failure + Upright Indentation
Box-85x50/1.6mm Upt.	Hook Failure + Upright Indentation
Box-85x50/1.6mm Upt.	Hook Failure + Upright Indentation
Box-85x50/1.6mm Upt.	Hook Failure + Upright Indentation
Box-90x40/2.5mm Upt.	Hook Failure
Box-90x40/2.5mm Upt.	Hook Failure
Box-90x40/2.5mm Upt.	Hook Failure
Box-90x40/2.5mm Upt.	Hook Failure
Box-90x40/1.6mm Upt.	Shear failure in Hooks + Upright Indentation
Box-90x40/1.6mm Upt.	Shear failure in Hooks + Upright Indentation
Box-90x40/1.6mm Upt.	Shear failure in Hooks + Upright Indentation
Box-90x40/1.6mm Upt.	Shear failure in Hooks + Upright Indentation
Box-100x40/2.5mm Upt.	Hook Failure
Box-100x40/2.5mm Upt.	Hook Failure
Box-100x40/2.5mm Upt.	Hook Failure
Box-100x40/2.5mm Upt.	Hook Failure + Upright Indentation

Box-100x40/1.6mm Upt.	Hook Failure + Upright Indentation
Box-100x40/1.6mm Upt.	Hook Failure + Upright Indentation
Box-100x40/1.6mm Upt.	Hook Failure + Upright Indentation
Box-100x40/1.6mm Upt.	Hook Failure + Upright Indentation
Box-105x50/2.5mm Upt.	Hook Failure
Box-105x50/2.5mm Upt.	Hook Failure
Box-105x50/2.5mm Upt.	Hook Failure
Box-105x50/2.5mm Upt.	Hook Failure
Box-105x50/1.6mm Upt.	Hook Failure + Upright slot Indentation
Box-105x50/1.6mm Upt.	Hook Failure + Upright Indentation
Box-105x50/1.6mm Upt.	Hook Failure + Upright Indentation
Box-105x50/1.6mm Upt.	Hook Failure + Upright Indentation
Box-130x40/2.5mm Upt.	Hook Failure
Box-130x40/2.5mm Upt.	Hook Failure
Box-130x40/2.5mm Upt.	Hook Failure
Box-130x40/2.5mm Upt.	Hook Failure

Box-130x40/1.6mm Upt.	Hook Failure + Upright slot Indentation + upright local damage (Squash)
Box-130x40/1.6mm Upt.	Hook Failure + Upright slot Indentation + upright local damage (Squash)
Box-130x40/1.6mm Upt.	Hook Failure + Upright slot Indentation+ upright local damage (Squash)
Box-130x40/1.6mm Upt.	Hook Failure + Upright slot Indentation+ upright local damage (Squash)
Box-140x50/2.5mm Upt.	Hook Failure + upright local damage (Squash)
Box-140x50/2.5mm Upt.	Hook Failure + upright local damage (Squash)
Box-140x50/2.5mm Upt.	Hook Failure + upright local damage (Squash)
Box-140x50/2.5mm Upt.	Hook Failure + upright local damage (Squash)
Box-140x50/1.6mm Upt.	Hook Failure + Upright slot Indentation
Box-140x50/1.6mm Upt.	Hook Failure + Upright slot Indentation + upright local damage (Squash)
Box-140x50/1.6mm Upt.	Hook Failure + Upright slot Indentation + upright local damage (Squash)
Box-140x50/1.6mm Upt.	Hook Failure + Upright slot Indentation + upright local damage (Squash)

Box = Beam Type

Upt = Upright

The Experimental moment rotation curves of the tested connections are shown below (See Figure A.1 to Figure A.21).

The specimen label has the following ID:

C-BT-B- ‘ Beam Dimentions’ - ‘Upright’

C: Specimen Group Code

BT: Bending Test

B = Beam Type (BOX BEAM)

Upright type is also shown by putting the upright width and it’s thickness next to it:

G: 1.5 mm R:1.6 mm H:2.5 mm

The moment values in the vertical axis of the moment rotation curves are not shown as the test results are confidential.

C-BT-B-80x40x1.5-90G

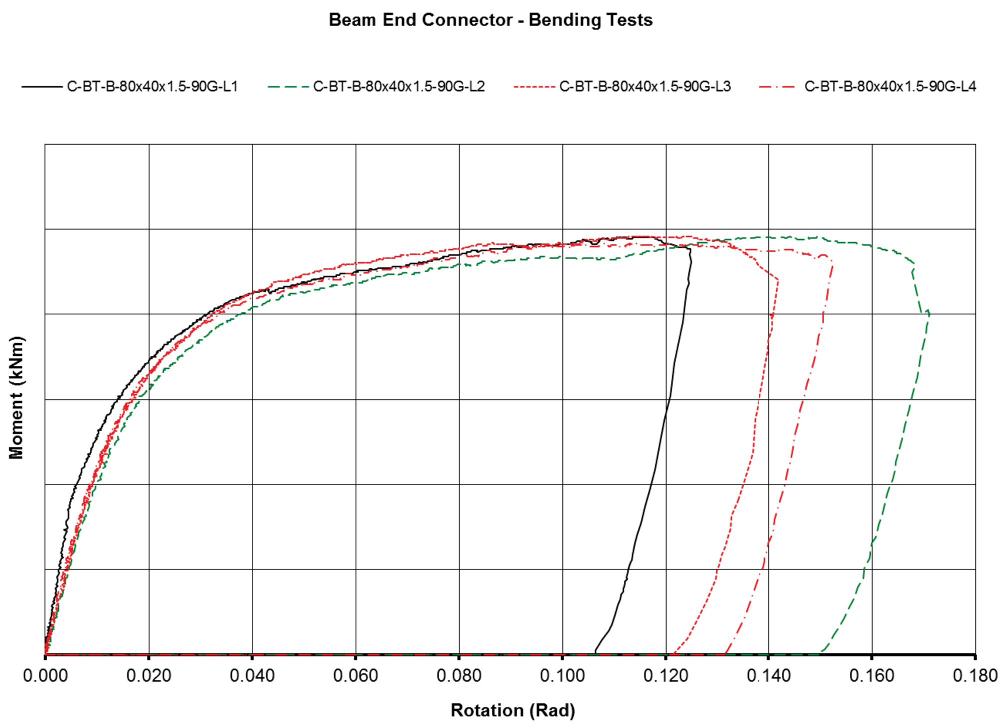

Figure A.1. Moment rotation curves for C-BT-B-80x40x1.5-90G beam end connectors

C-BT-B-80x40x1.5-90H

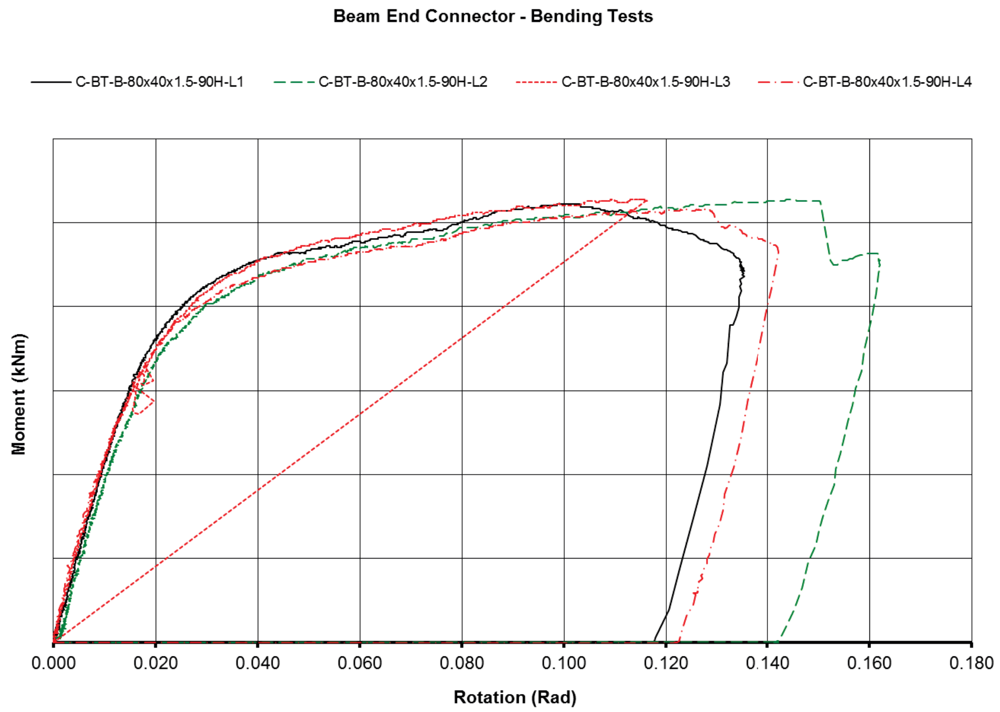

Figure A.2. Moment rotation curves for C-BT-B-80x40x1.5-90H beam end connectors

C-BT-B-80x40x1.5-100R

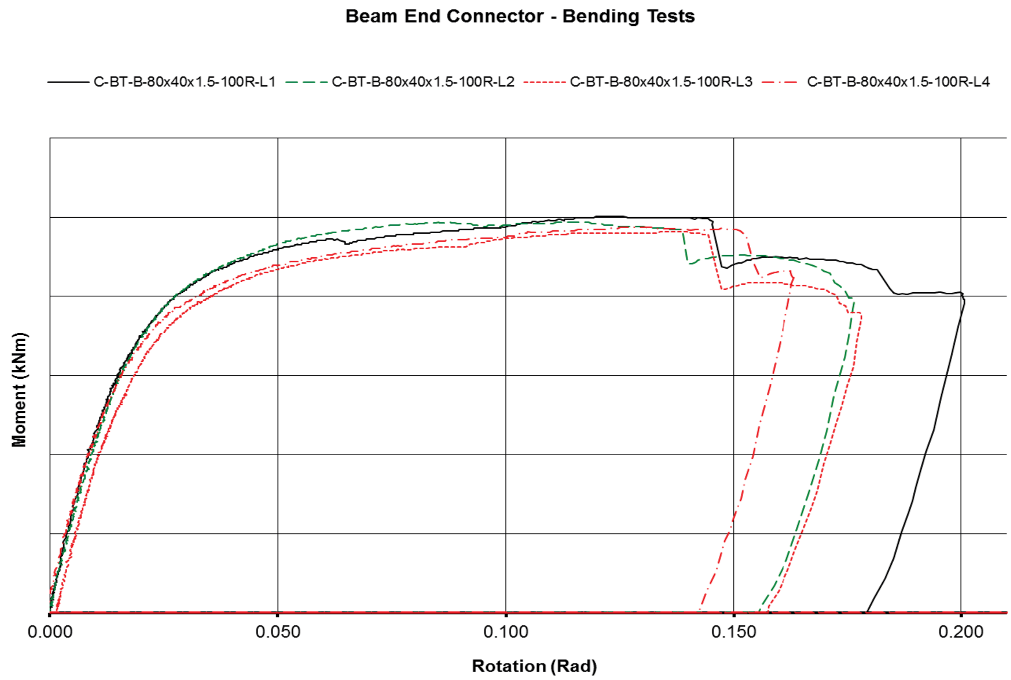

Figure A.3. Moment rotation curves for C-BT-B-80x40x1.5-100R beam end connectors

C-BT-B-85x50x1.5-90G

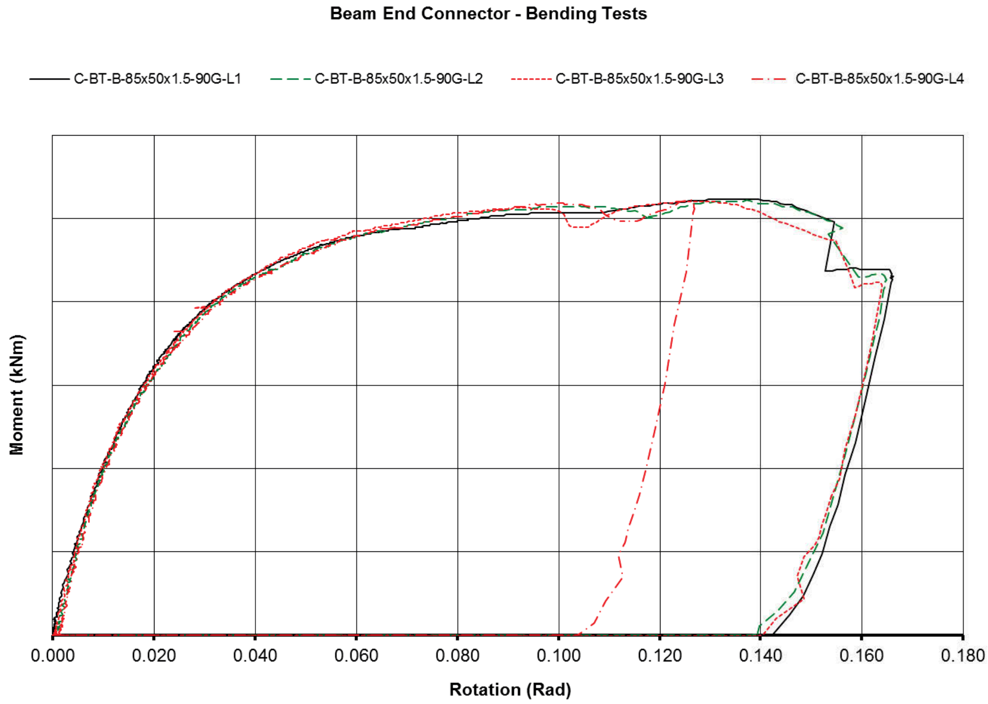

Figure A.4. Moment rotation curves for C-BT-B-85x50x1.5-90G beam end connectors

C-BT-B-85x50x1.5-90H

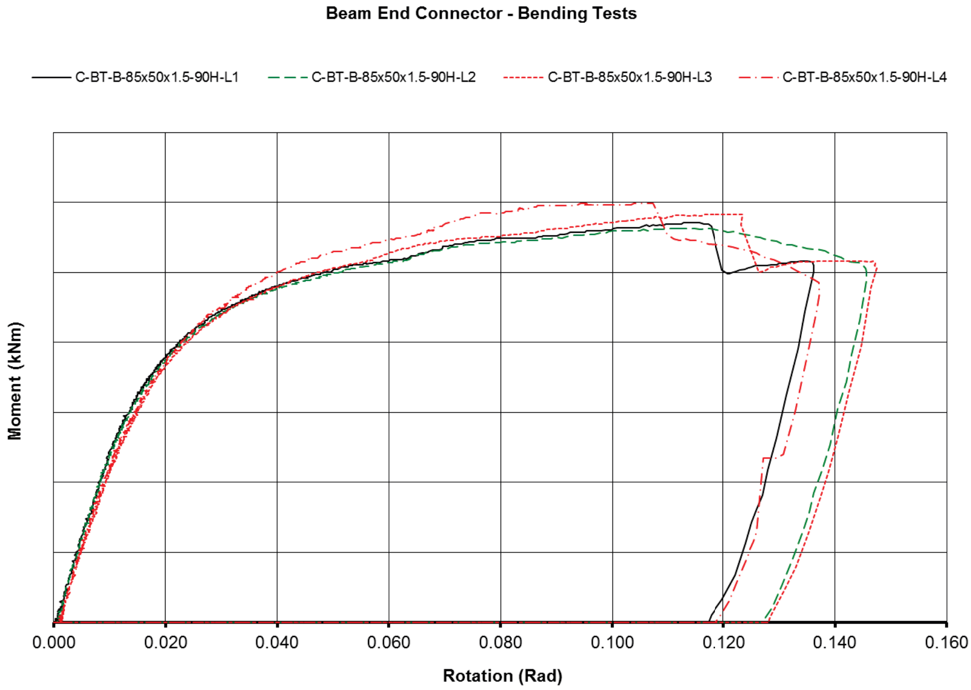

Figure A.5. Moment rotation curves for C-BT-B-85x50x1.5-90H beam end connectors

C-BT-B-85x50x1.5-100R

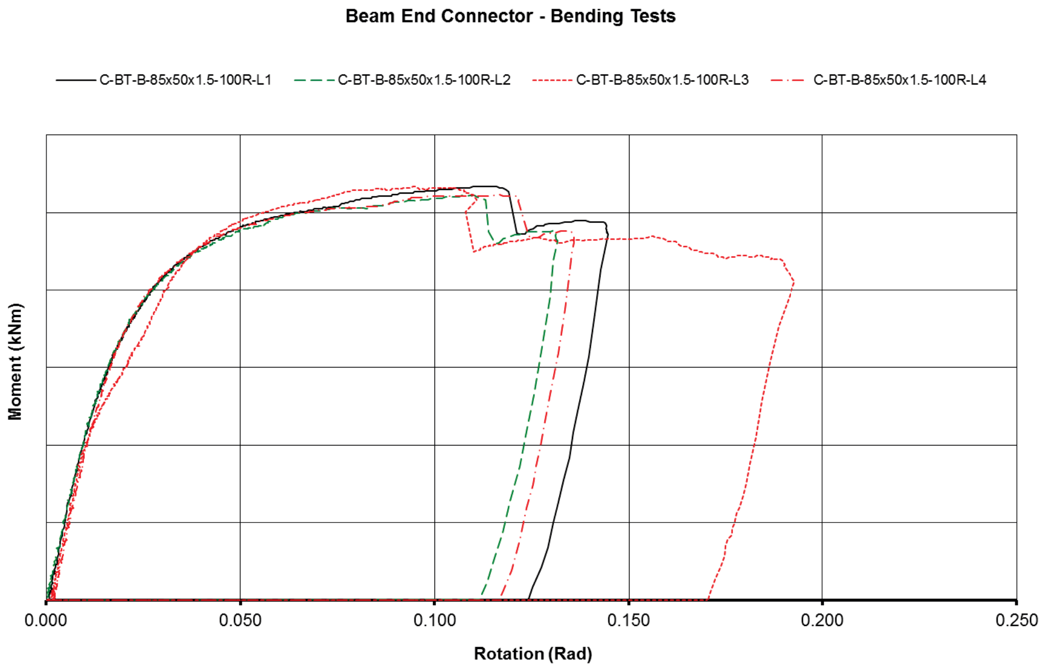

Figure A.6. Moment rotation curves for C-BT-B-85x50x1.5-100R beam end connectors

C-BT-B-90x40x1.5-90G

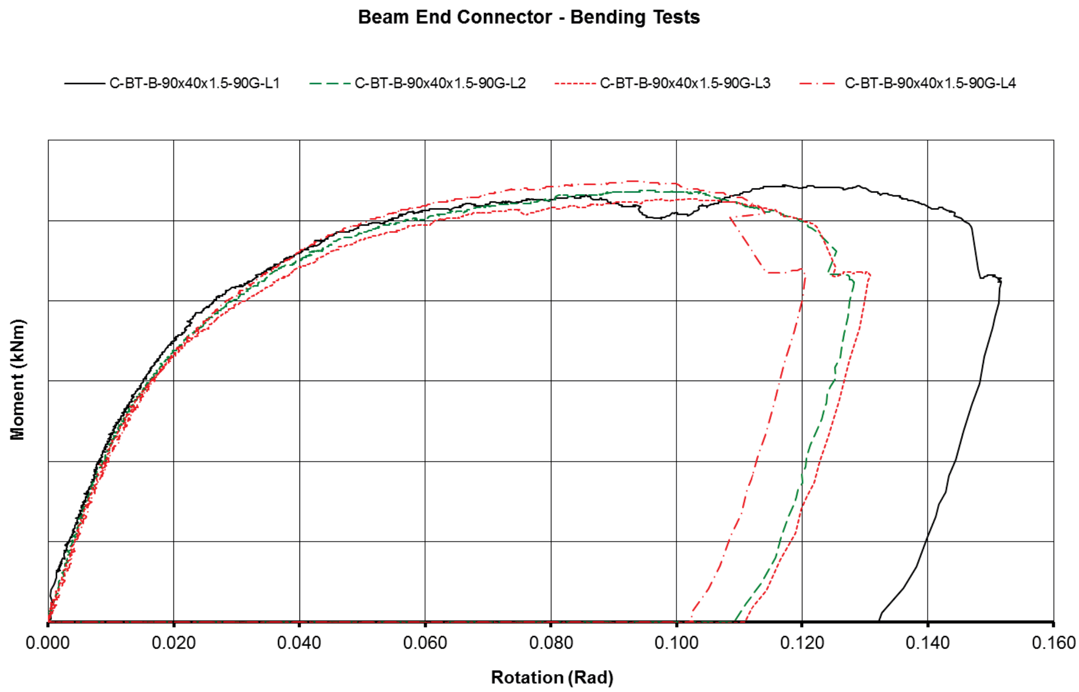

Figure A.7. Moment rotation curves for C-BT-B-90x40x1.5-90G beam end connectors

C-BT-B-90x40x1.5-90H

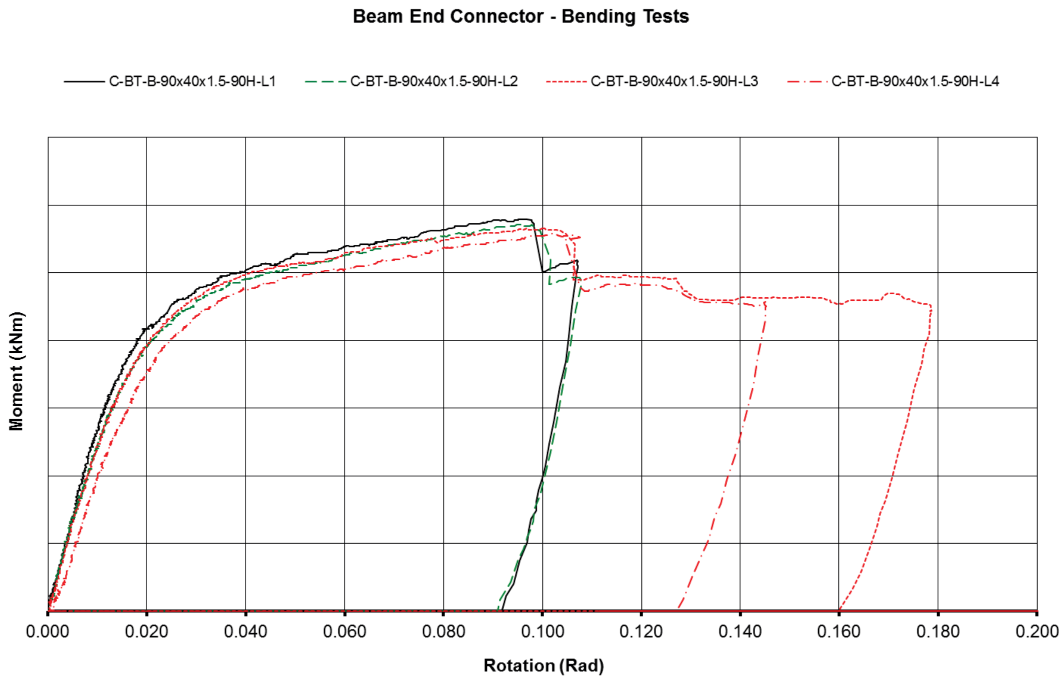

Figure A.8. Moment rotation curves for C-BT-B-90x40x1.5-90H beam end connectors

C-BT-B-90x40x1.5-100R

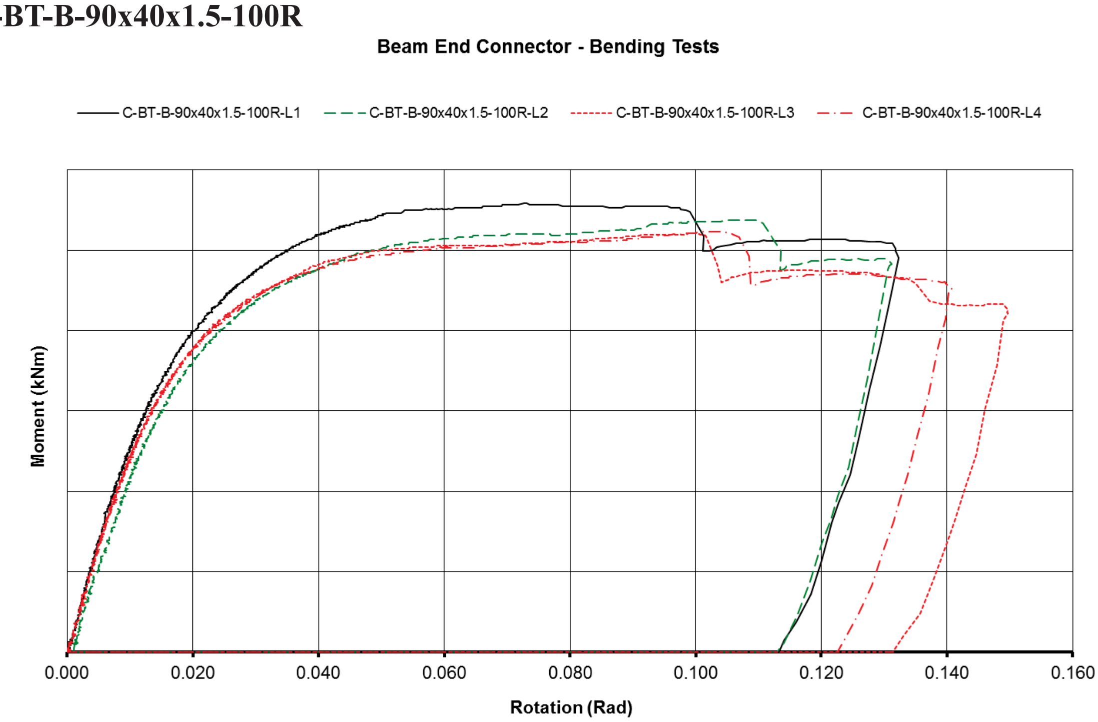

Figure A.9. Moment rotation curves for C-BT-B-90x40x1.5-100R beam end connectors

C-BT-B-100x40x1.5-90G

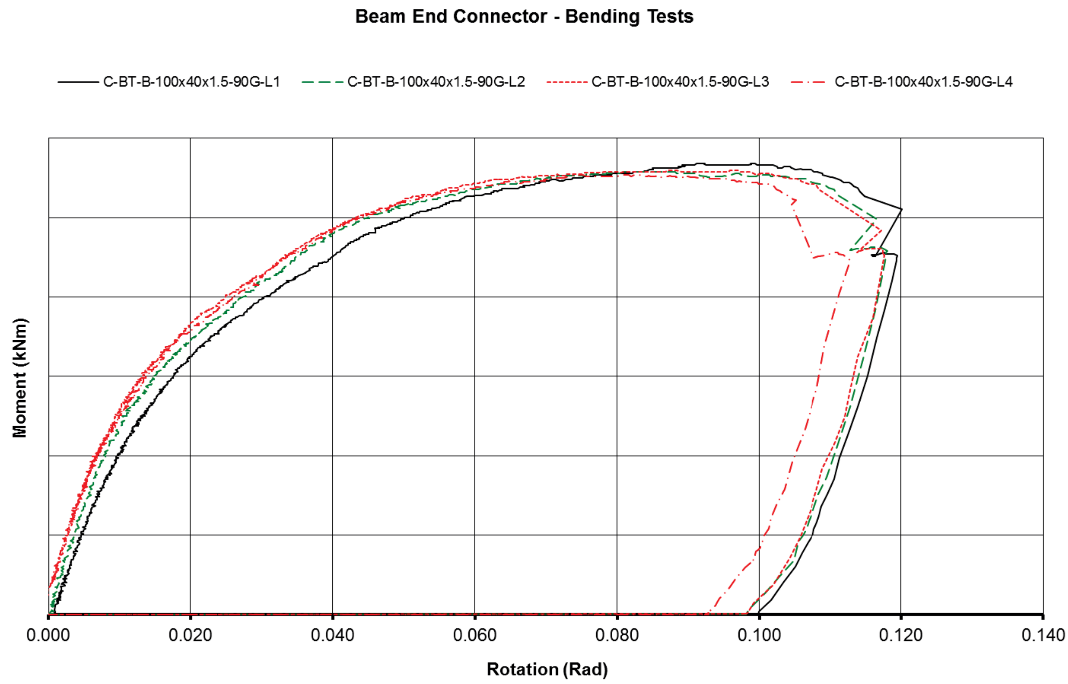

Figure A.10. Moment rotation curves for C-BT-B-100x40x1.5-90G beam end connectors

C-BT-B-100x40x1.5-90H

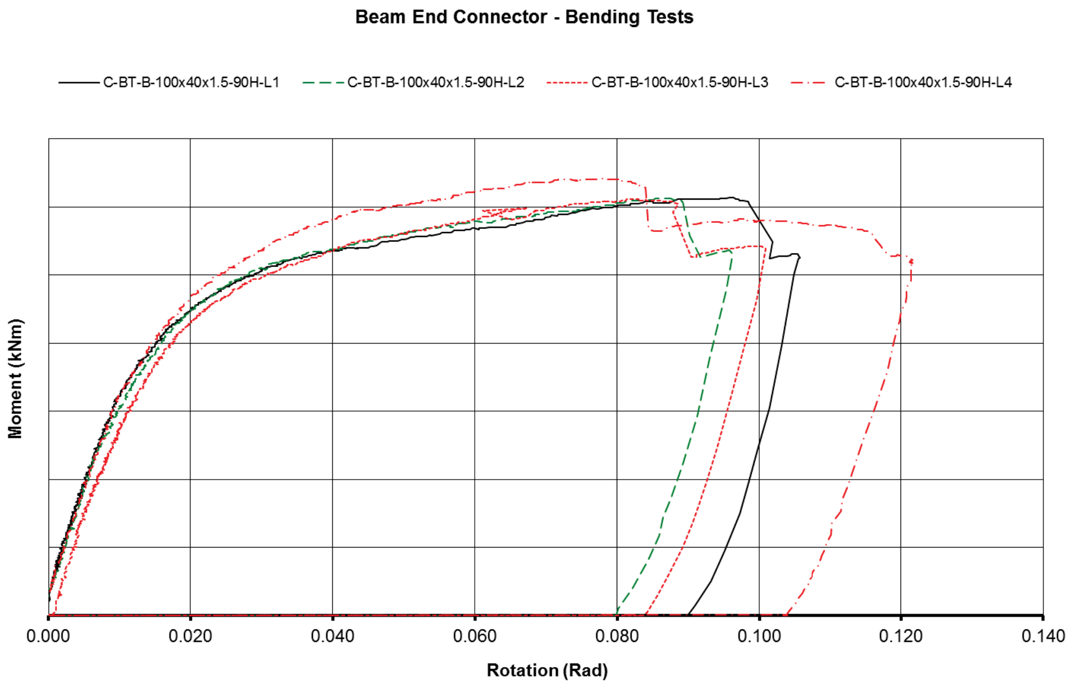

Figure A.11. Moment rotation curves for C-BT-B-100x40x1.5-90H beam end connectors

C-BT-B-100x40x1.5-100R

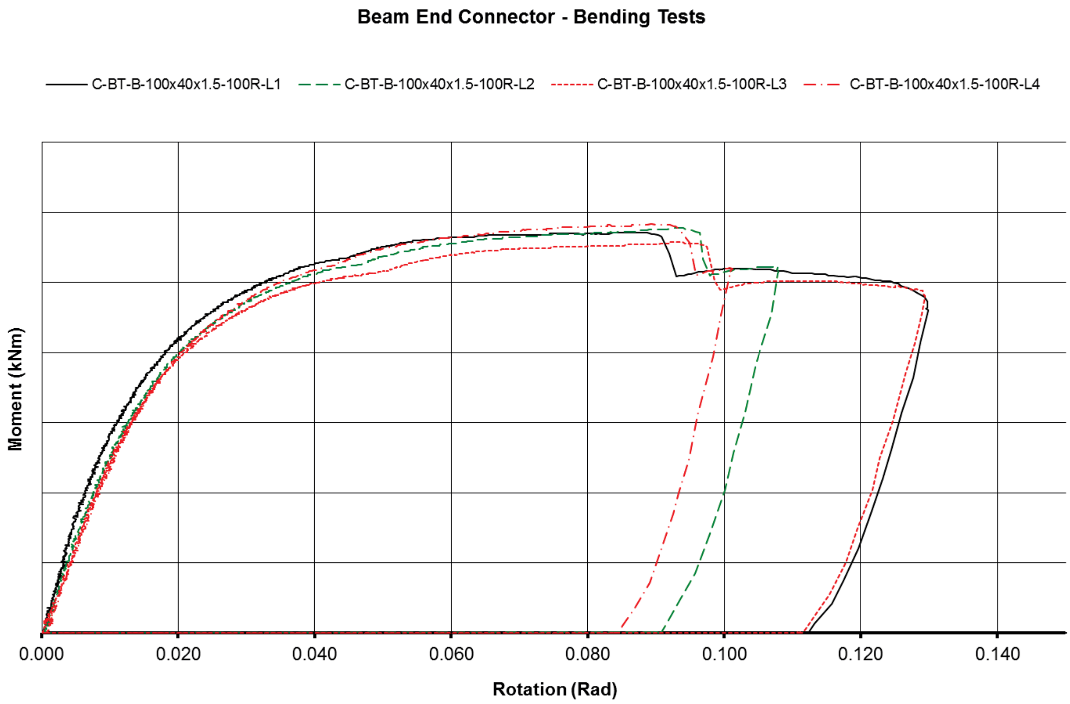

Figure A.12. Moment rotation curves for C-BT-B-100x40x1.5-100R beam end connectors

C-BT-B-105x50x1.5-90G

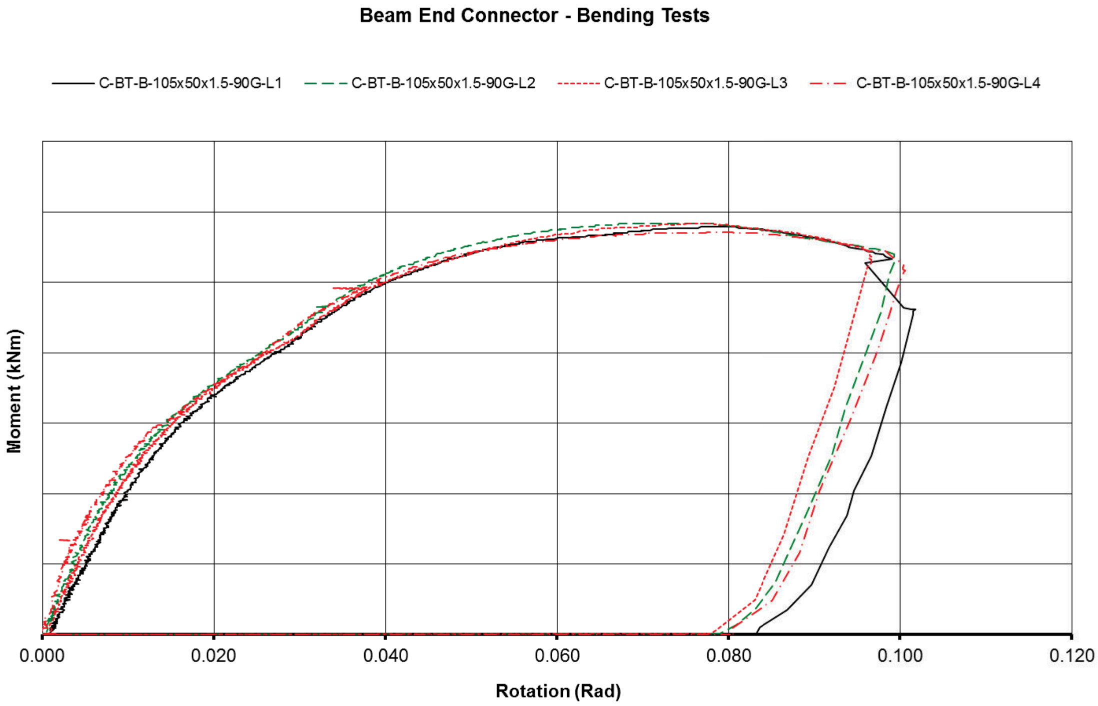

Figure A.13. Moment rotation curves for C-BT-B-105x50x1.5-90G beam end connectors

C-BT-B-105x50x1.5-90H

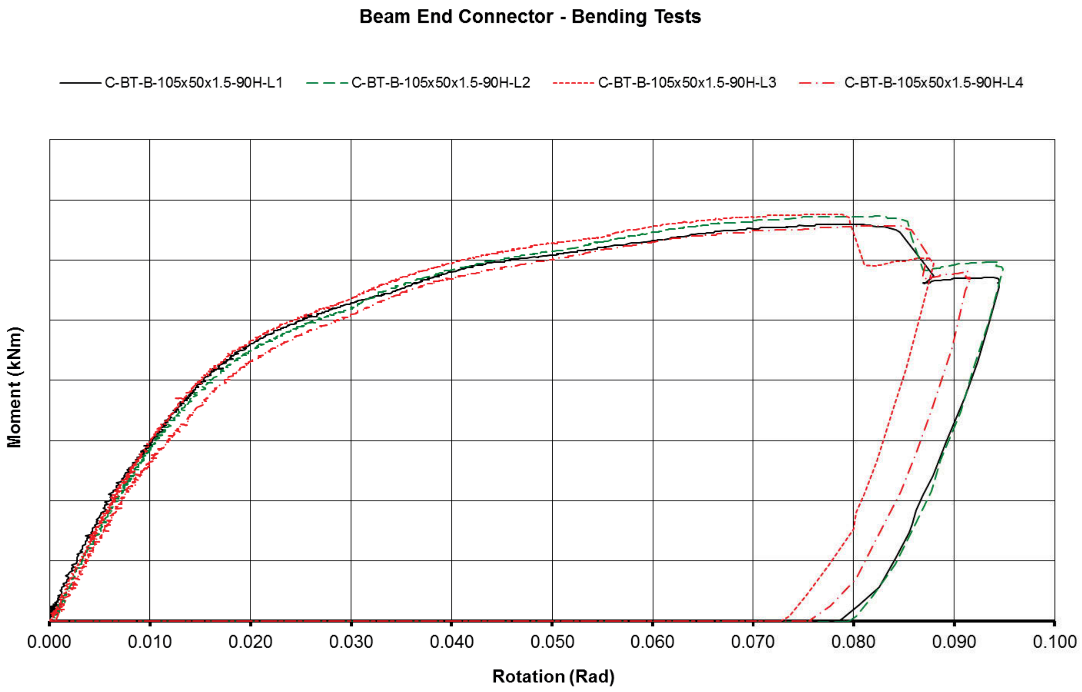

Figure A.14. Moment rotation curves for C-BT-B-105x50x1.5-90H beam end connectors

C-BT-B-105x50x1.5-100R

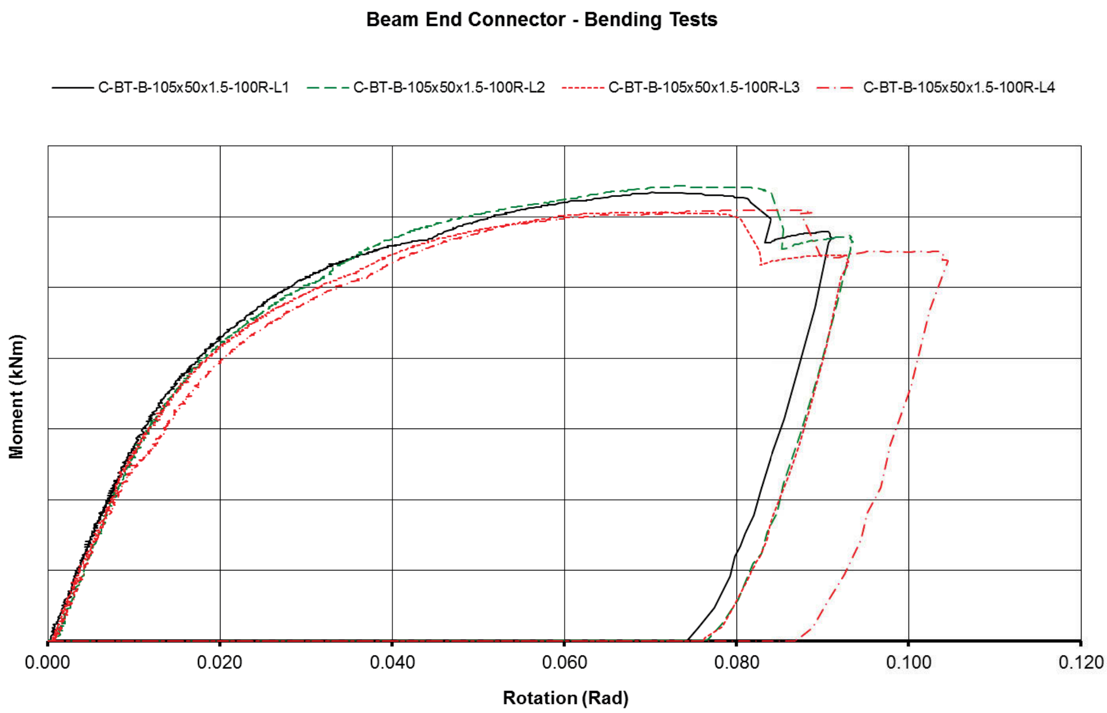

Figure A.15. Moment rotation curves for C-BT-B-105x50x1.5-100R beam end connectors

C-BT-B-130x40x1.5-90G

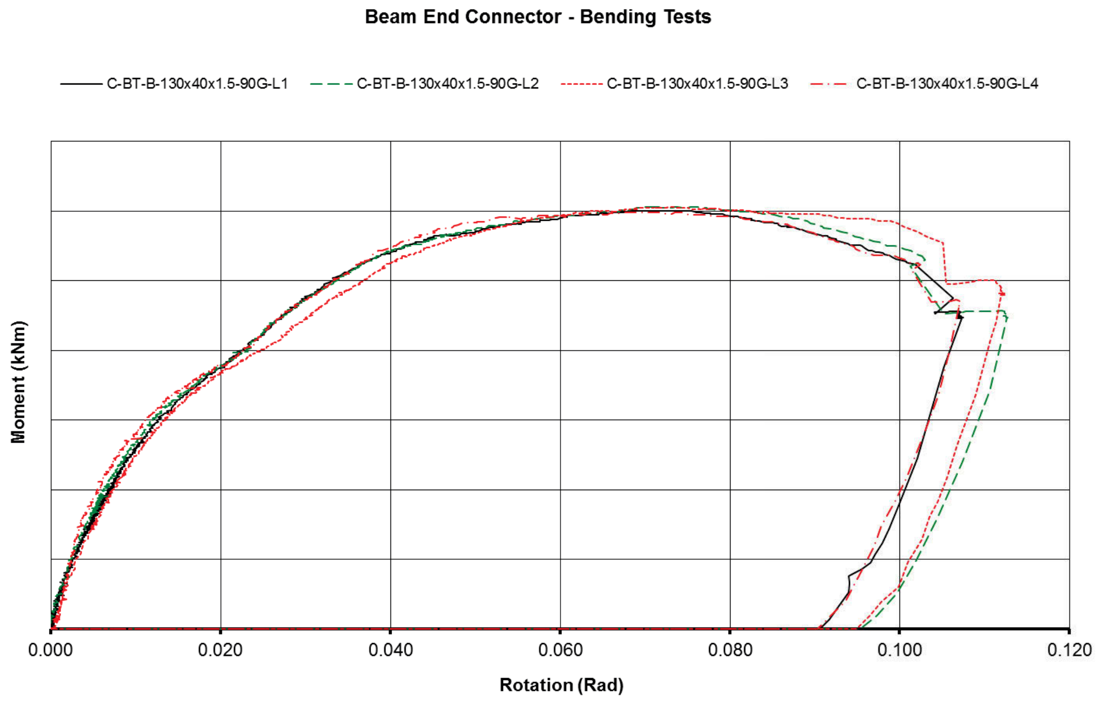

Figure A.16. Moment rotation curves for C-BT-B-130x40x1.5-90G beam end connectors

C-BT-B-130x40x1.5-90H

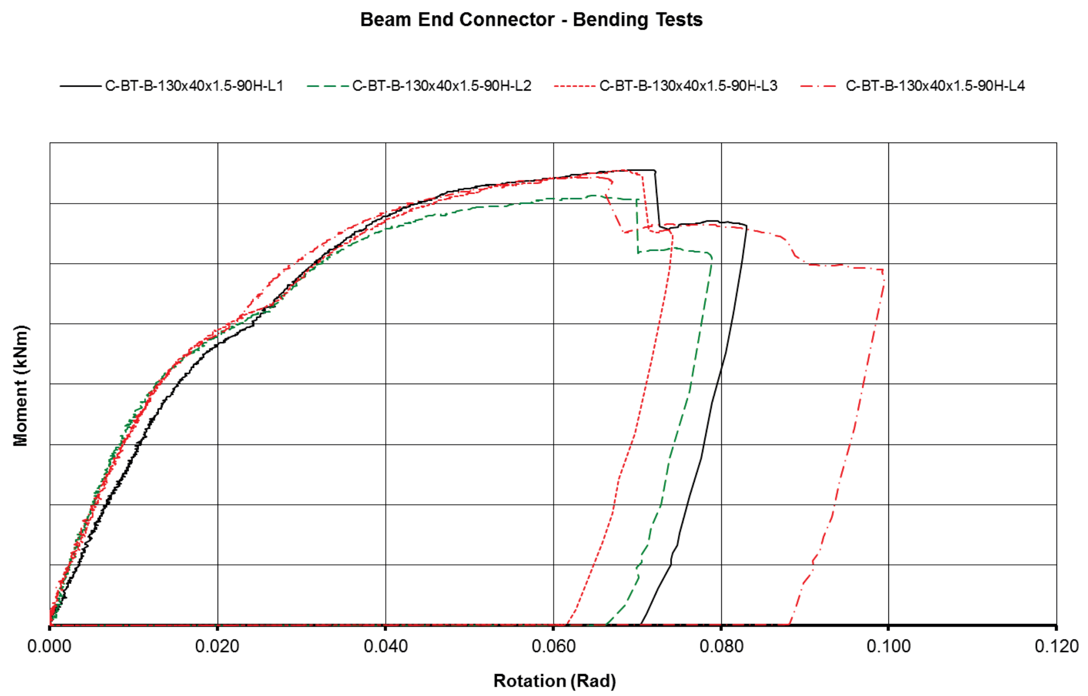

Figure A.17. Moment rotation curves for C-BT-B-130x40x1.5-90H beam end connectors

C-BT-B-130x40x1.5-100R

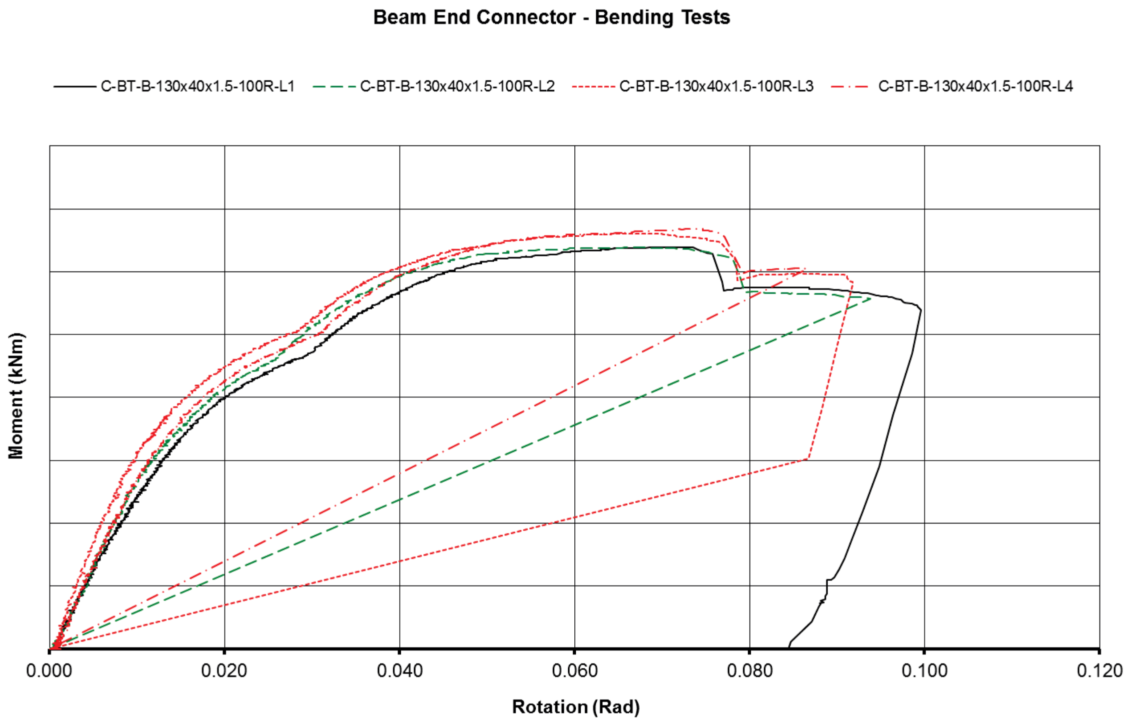

Figure A.18. Moment rotation curves for C-BT-B-130x40x1.5-100R beam end connectors

C-BT-B-140x50x1.6-90G

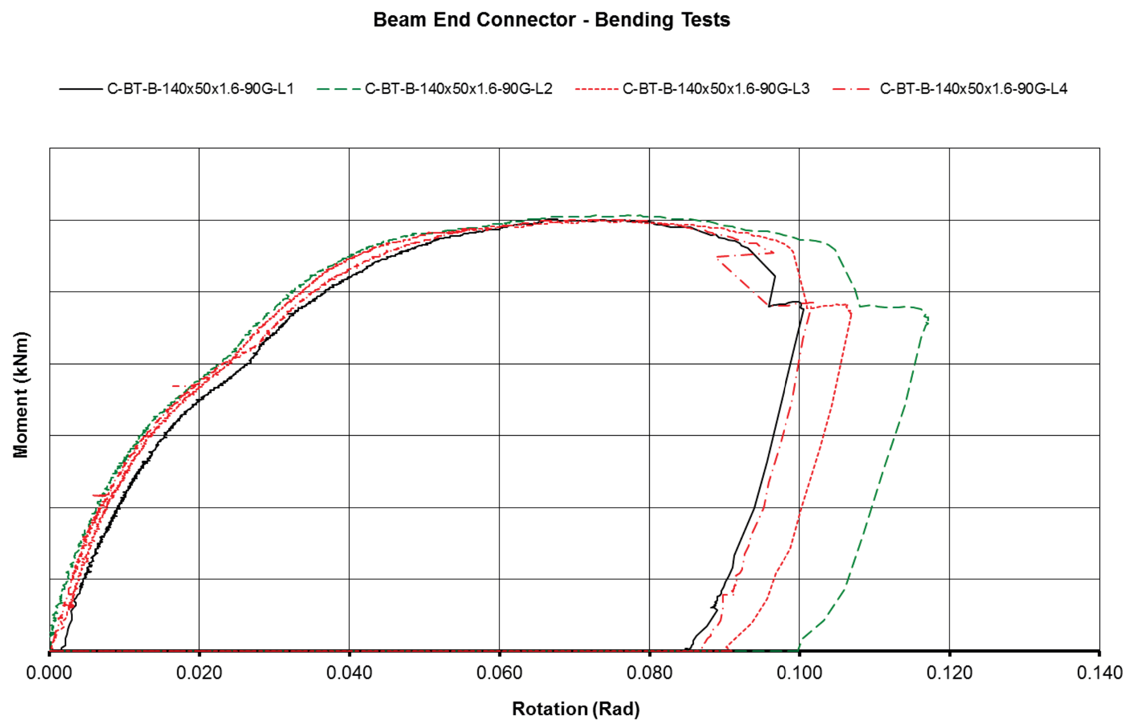

Figure A.19. Moment rotation curves for C-BT-B-140x50x1.6-90G beam end connectors

C-BT-B-140x50x1.6-90H

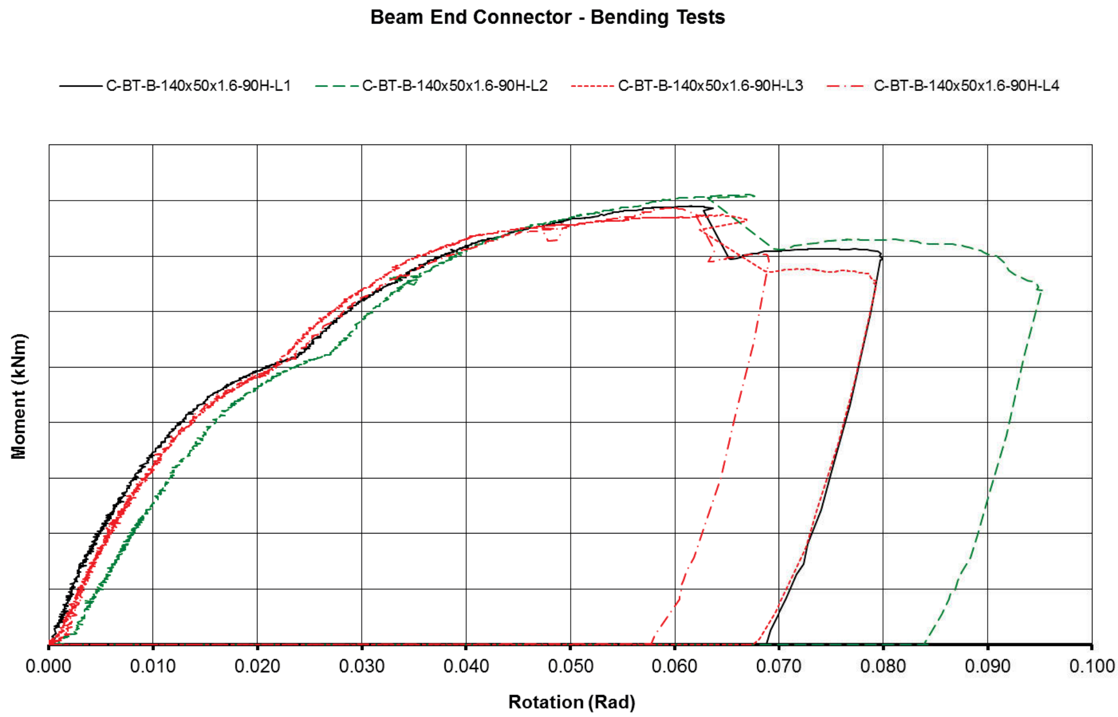

Figure A.20. Moment rotation curves for C-BT-B-140x50x1.6-90H beam end connectors

C-BT-B-140x50x1.6-100R

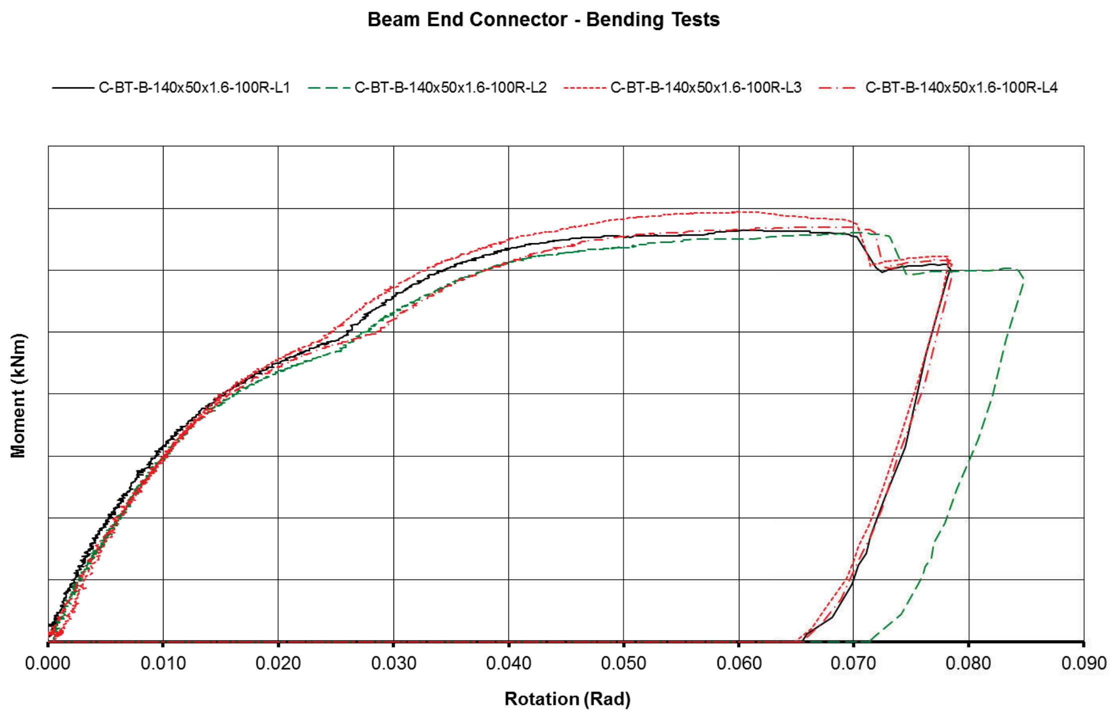

Figure A.21. Moment rotation curves for C-BT-B-140x50x1.6-100R beam end connectors

Table A-2. Yield and Ultimate rotations of the connections

Test No	Connection Type	Yield Rotation ‘θ_y’ (Rad)	Ultimate Rotation ‘θ_u’ (Rad)
1	B-80x40-Upt 1.5mm	0.02	0.11
2	B-80x40-Upt 1.5mm	0.021	0.11
3	B-80x40-Upt 1.5mm	0.021	0.14
4	B-80x40-Upt 2.5mm	0.022	0.1
5	B-80x40-Upt 2.5mm	0.022	0.11
6	B-80x40-Upt 2.5mm	0.021	0.125
7	B-80x40-Upt 2.5mm	0.022	0.143
8	B-85x50-Upt 1.5mm	0.023	0.122
9	B-85x50-Upt 1.5mm	0.023	0.122
10	B-85x50-Upt 1.5mm	0.023	0.13
11	B-85x50-Upt 1.5mm	0.023	0.135
12	B-85x50-Upt 2.5mm	0.022	0.105
13	B-85x50-Upt 2.5mm	0.022	0.115
14	B-85x50-Upt 2.5mm	0.022	0.115
15	B-85x50-Upt 2.5mm	0.023	0.115
16	B-90x40-Upt 1.5mm	0.021	0.095
17	B-90x40-Upt 1.5mm	0.021	0.1
18	B-90x40-Upt 1.5mm	0.021	0.1
19	B-90x40-Upt 1.5mm	0.021	0.115
20	B-90x40-Upt 2.5mm	0.021	0.1
21	B-90x40-Upt 2.5mm	0.021	0.1
22	B-90x40-Upt 2.5mm	0.021	0.1
23	B-90x40-Upt	0.022	0.095

	2.5mm		
24	B-100x40-Upt 1.5mm	0.02	0.08
25	B-100x40-Upt 1.5mm	0.02	0.08
26	B-100x40-Upt 1.5mm	0.02	0.085
27	B-100x40-Upt 1.5mm	0.023	0.1
28	B-100x40-Upt 2.5mm	0.02	0.08
29	B-100x40-Upt 2.5mm	0.02	0.08
30	B-100x40-Upt 2.5mm	0.02	0.08
31	B-100x40-Upt 2.5mm	0.02	0.095
32	B-105x50-Upt 1.5mm	0.018	0.075
33	B-105x50-Upt 1.5mm	0.021	0.07
34	B-105x50-Upt 1.5mm	0.022	0.075
35	B-105x50-Upt 1.5mm	0.023	0.077
36	B-105x50-Upt 2.5mm	0.021	0.077
37	B-105x50-Upt 2.5mm	0.021	0.077
38	B-105x50-Upt 2.5mm	0.022	0.082
39	B-105x50-Upt 2.5mm	0.022	0.082
	Avg.	***0.021 Rad***	***0.099 Rad***
	Std (Standard Deviation)	***0.00114 Rad***	***0.0199 Rad***
	COV(Coefficient of Variation)	***0.0667***	***0.2***

Appendix B: Theoretical analysis of beam to upright connections

B.1 Example of using mathematical equations of ultimate and yield moment

Application of the proposed model for the connector plate failure mode is presented below and compared with experimental results.

Details of the connection's geometrical properties are shown in Table B-1 and the theoretical Bi-Linear moment rotation curves are shown in Figure B.1Figure to Figure B.3. In these figures, the change in the bi-linear moment-rotation expression, as a result of factor 'α' in equation (2-4) is shown for the limiting values of 0.3 and 0.4.

- Connection Type 1: Box beam 105 – 50 to 2.5 mm thick upright
- Connection Type 2: Box beam 80 – 40 to 2.5 mm thick upright
- Connection Type 2: Box beam 85 – 50 to 2.5 mm thick upright

Table B-1. Geometrical characteristics of the connections

Geometrical characteristics	*Connection type 1*	*Connection type 2*	*Connection type 3*
t_c (mm)	4	4	4
l (mm)	6.55	6.55	6.55
c_1 (mm)	7	7	7
c_2 (mm)	11	11	11
h_1 (mm)	134	109	114
h_2 (mm)	91	66	71
h_3 (mm)	34	9	14
σ_{yc} (Mpa)	350	350	350
M_y(kN.m)	2.4	1.7	1.8
M_u(kN.m)	3.2	2.4	2.6
θ_y(Rad)	0.021	0.021	0.021
θ_u(Rad)	0.1	0.1	0.1

Connection Type 1: Box beam 150 – 50 to 2.5 mm thick upright (Mode 1)

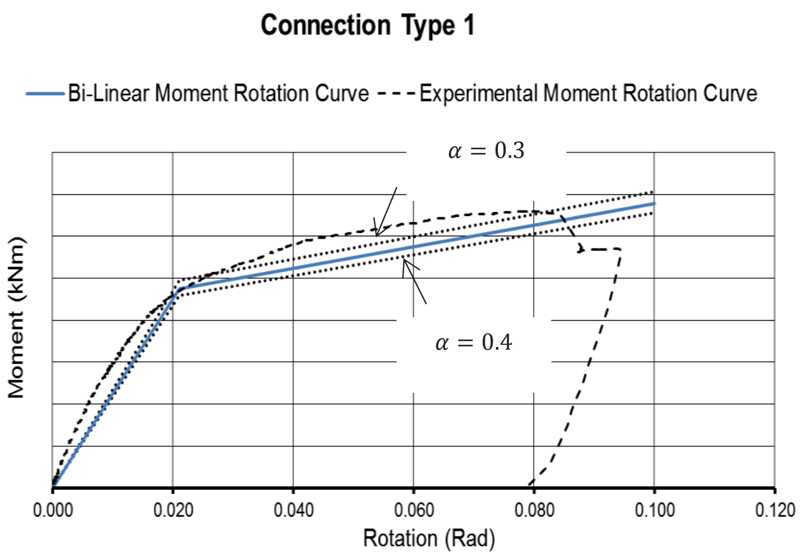

Figure B.1. Analytical result vs. Test result

Connection Type 2: Box beam 80 – 40 to 2.5 mm thick upright (Mode 1)

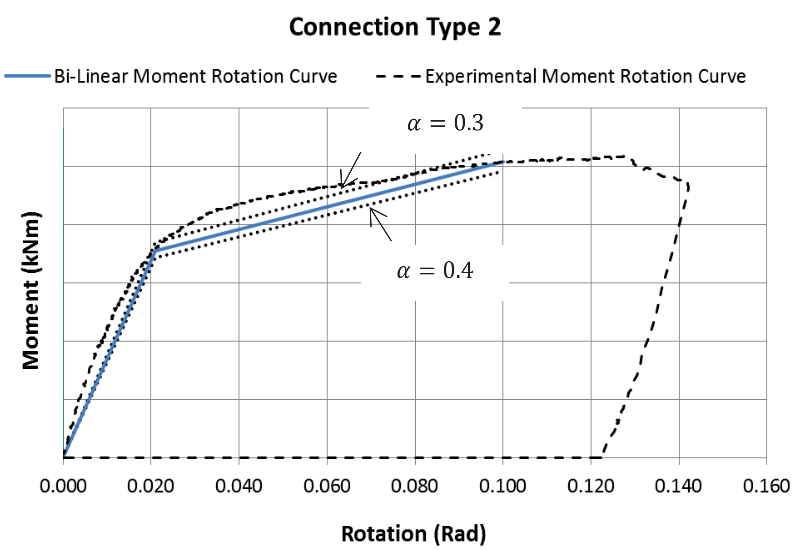

Figure B.2. Analytical result vs. Test result

Connection Type 3: Box beam 85 – 50 to 2.5 mm thick upright (Mode 1)

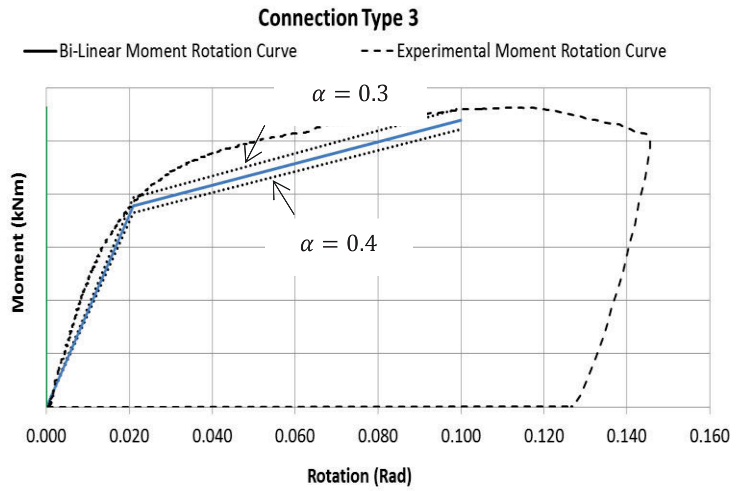

Figure B.3. Analytical result vs. Test result

Appendix C: Response of different connection models

This part is adopted from the report prepared by Reyes (2013) as part of the concurrent work on this project. It should be noted that an elastic Single Degree of Freedom model was also programmed in OFFICE EXCEL software by Reyes (2013) using Duhamel Integration method and the results were compared with the dynamic time history analysis results (See Figure C.Figure C.1 to Figure C.11).

1. Rack's base shear.

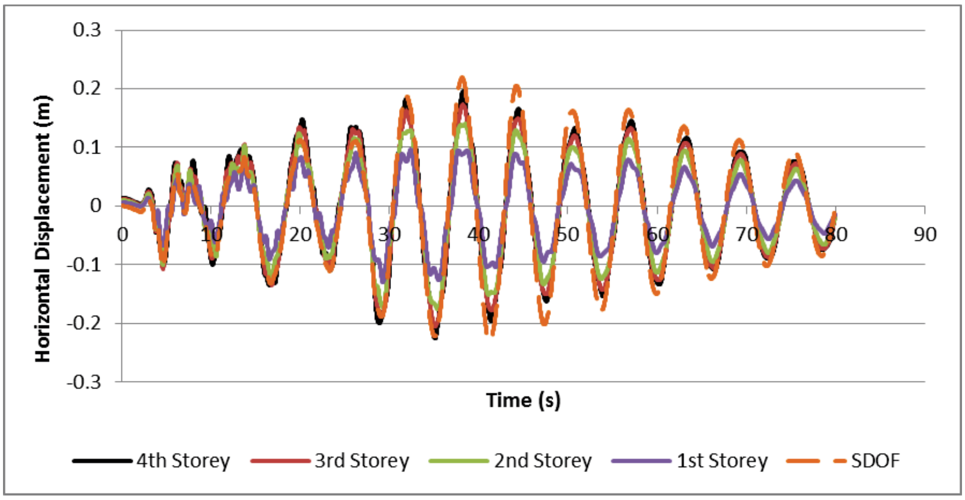

Figure C.1. Response of KIN-MON to 60% 1940 El-Centro earthquake.

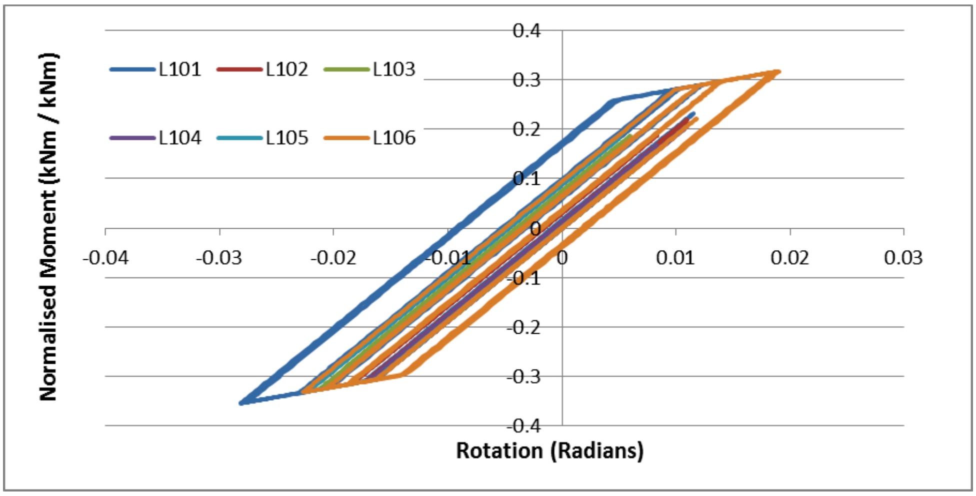

Figure C.2. First Storey KIN-MON Link response to 60% 1940 El-Centro earthquake. Upper storey links remain linear[42].

[42] Link Numbers are illustrated in Figure 6.5

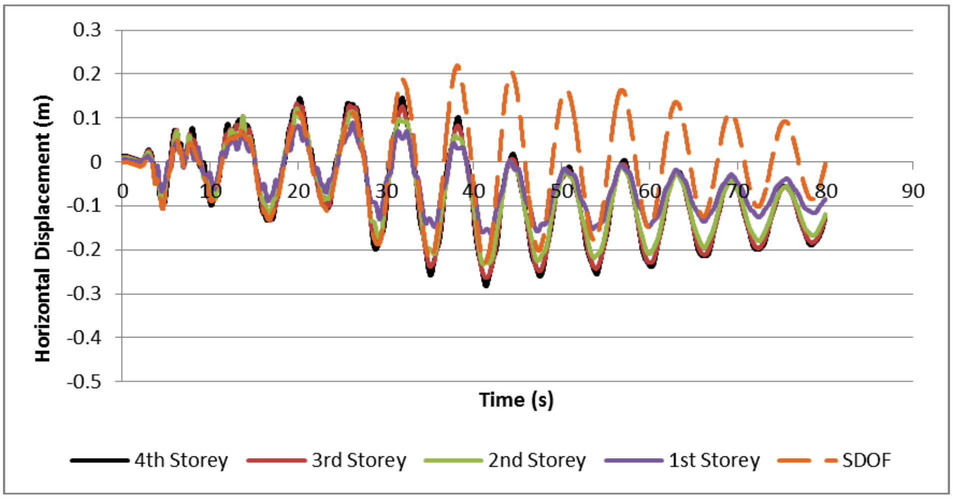

Figure C.3. Deflection Response of KIN-EQV to 60% 1940 El-Centro earthquake.

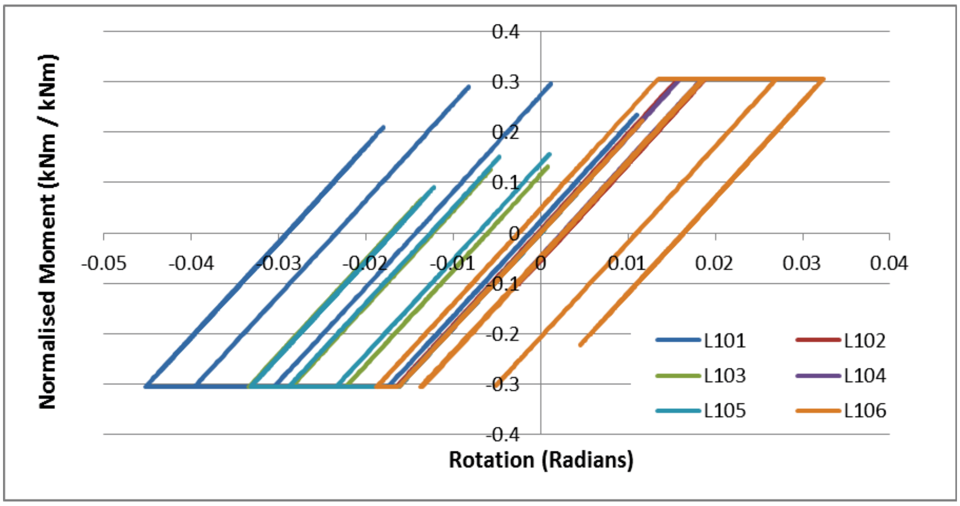

Figure C.4. First Storey KIN-EQV Link response to 1940 60% El-Centro earthquake. Upper storey links remain linear.

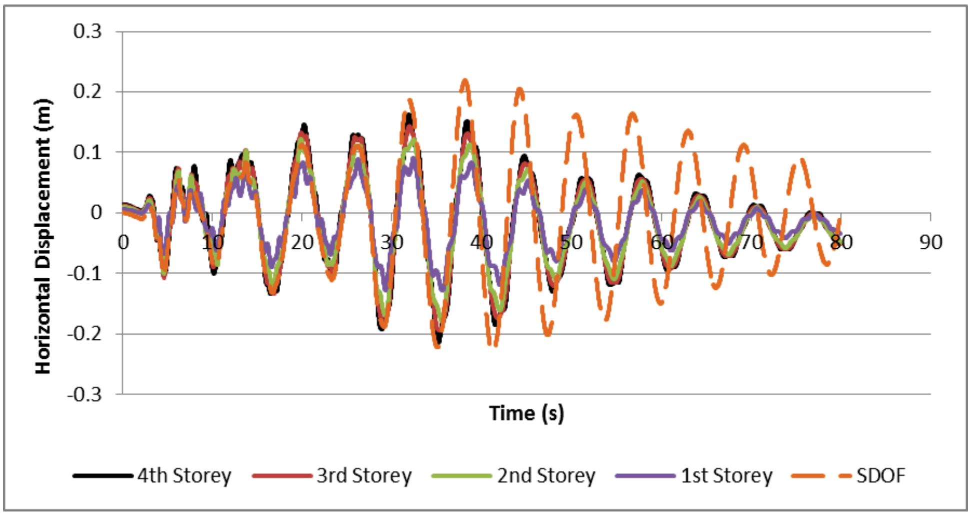

Figure C.5. Deflection Response of TAK-EQV to 60% 1940 El-Centro earthquake.

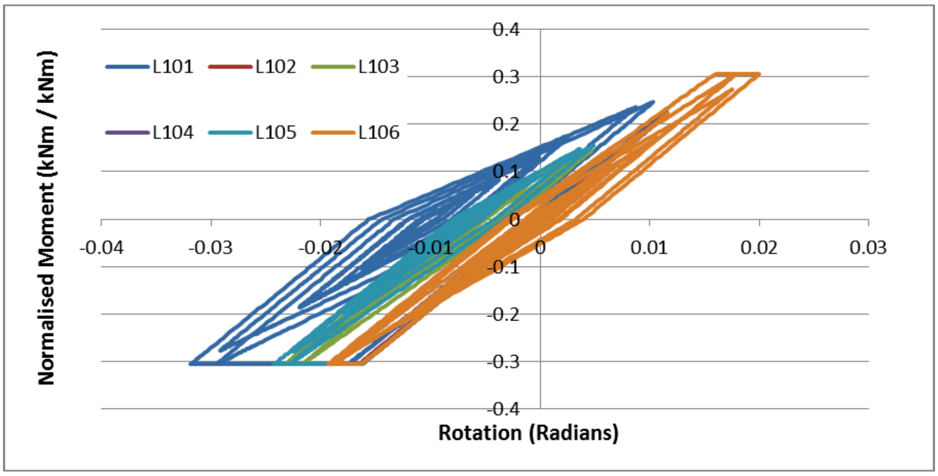

Figure C.6. First Storey TAK-EQV Link response to 60% 1940 El-Centro. Upper storey links remain linear.

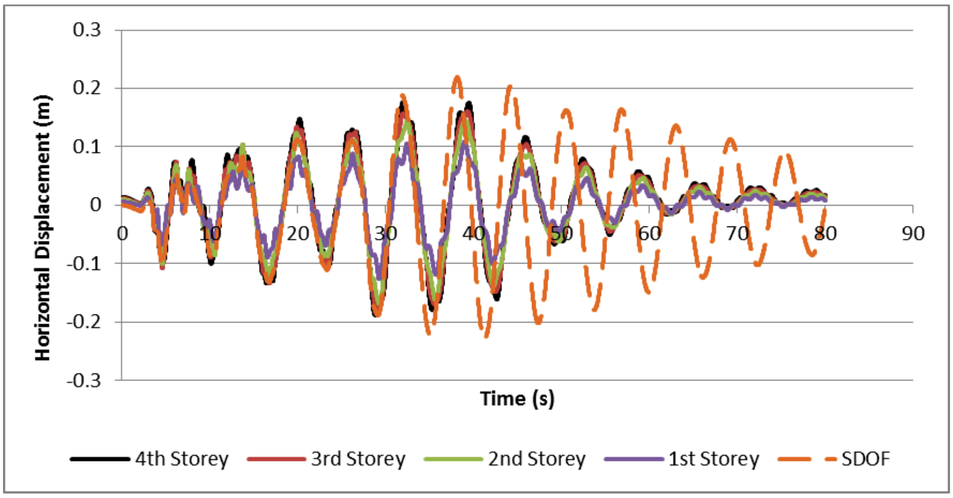

Figure C.7. Deflection Response of PIV-EQV to 60% 1940 El-Centro earthquake.

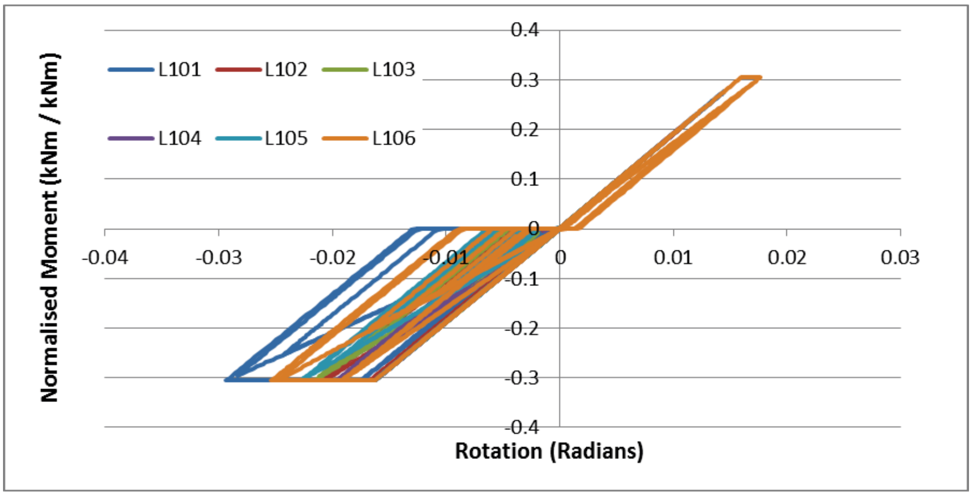

Figure C.8. First Storey PIV-EQV Link response to 60% 1940 El-Centro earthquake. Upper storey links remain linear.

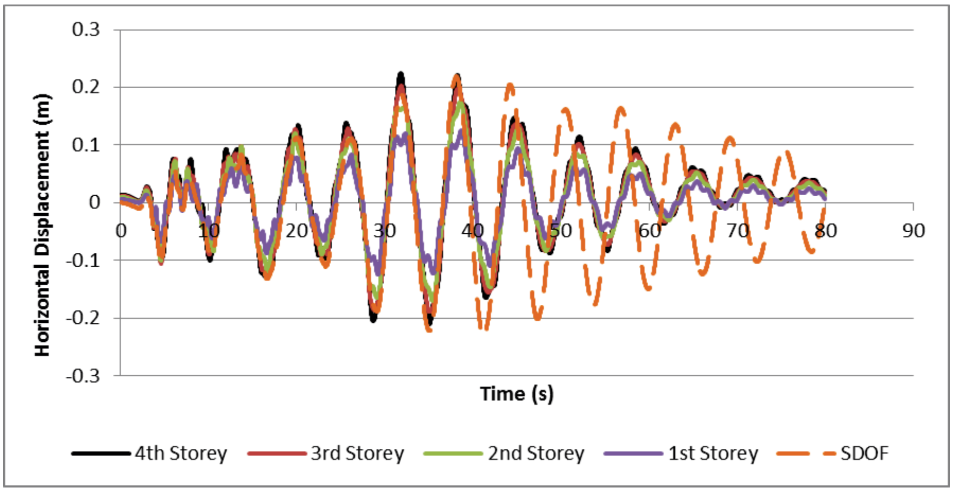

Figure C.9. Deflection Response of PIV-CYC to 60% 1940 El-Centro earthquake.

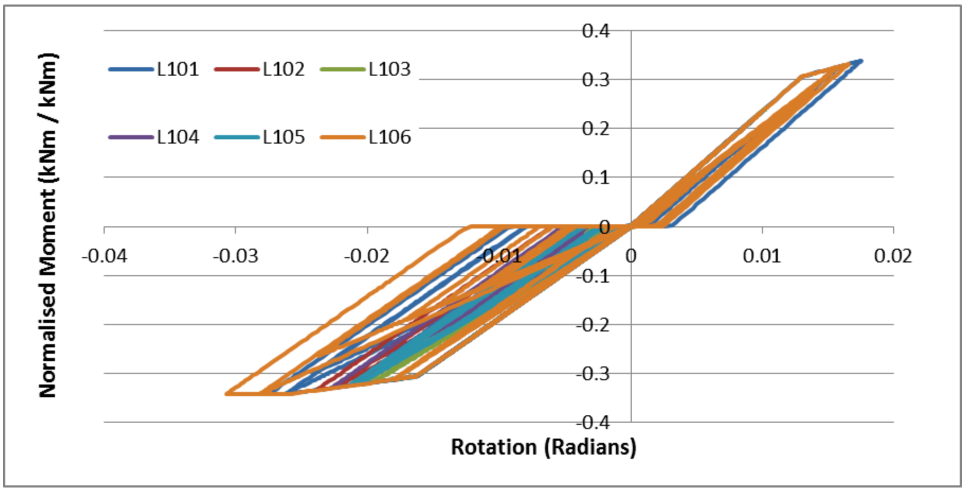

Figure C.10. First Storey PIV-CYC Link response to 60% 1940 El-Centro earthquake.

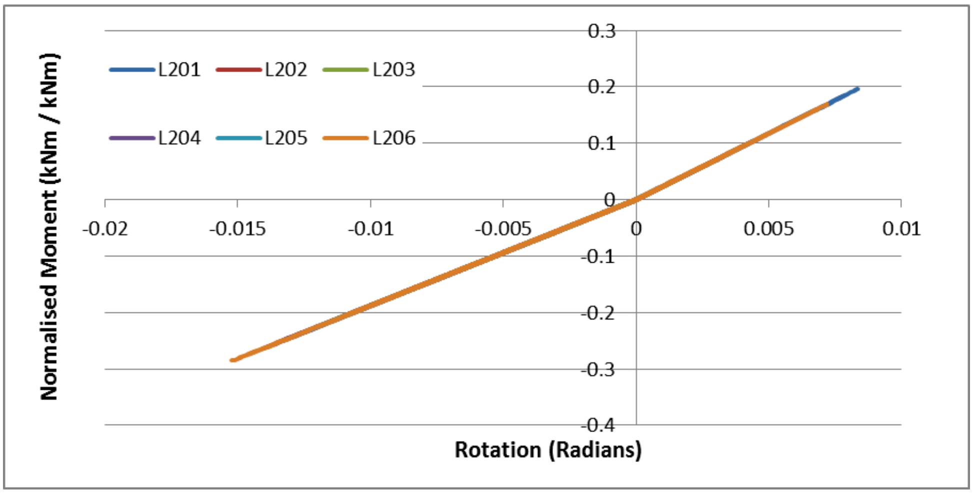

Figure C.11. Second Storey PIV-CYC Link response to 60% 1940 El-Centro. Third and fourth storey links also remain linear.

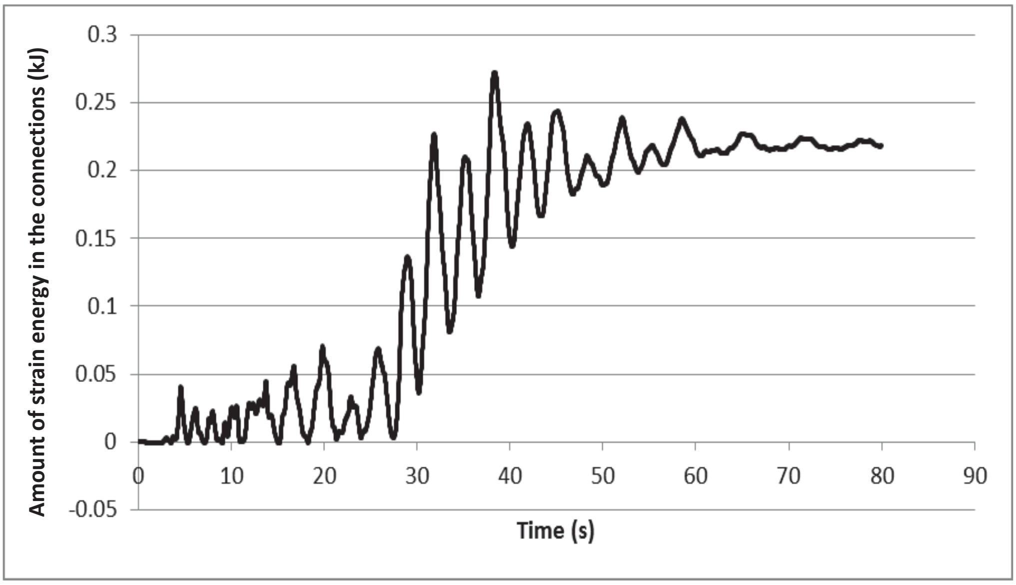

Figure C.12. Energy Dissipated by PIV-EQV when Subjected to 60% 1940 El-Centro earthquake.

Appendix D: Proposing the appropriate response modification factor (R factor)

The R factor values presented in literature ranges from approximately 2 to 6. It was hoped that the IDA and NLPO results calculated in Section 6.1.5.4 and 6.1.5.5 would narrow this range so as to clarify what R factor is indeed most suitable. However, the 'scatter' in results presented thus far has not contributed to narrowing this range of approximately 4 > R > 2.

D.1 NLTH and ESLF comparison

The results of the unscaled and half-scaled (i.e. 100% and 50%) 1940 El-Centro earthquake NLTH will be compared with a range of ESLF method calculations in this section. Four values of R, (i.e. R = 1.8, 2, 3, and 4) and two lateral loading distributions (i.e. triangular and uniform) are investigated.

To assess the most appropriate R value, and to generally evaluate the ESLF method, the following response parameters are compared between the NLTH and ESLF results:

i. Maximum moment in first storey uprights, $M_{max\text{-}ups}$.
ii. Maximum first storey inter-storey drift ratio, θ_1.
iii. Maximum top storey drift ratio, $\theta_{top\ storey}$.

Note that the ratio of NLTH moment and ESLF moment calculates the over-strength factor, Ω. Considering this 'in reverse', if ESLF was used for design, the calculated moment should be multiplied by Ω to determine the actual internal demand on force controlled members.

Additional parameters and assumptions are as follows:

- P-Δ is switched on in both NLTH and ESLF.
- The NLTH connection is LabCyc-PIV. The ESLF connection is 'linear'.
- For T_1 = 6.18 seconds and ξ = 3%, the elastic base shear coefficient (C_e) of the unscaled and half scaled 1940 El-Centro record is 0.04 and 0.02, respectively. The spectral acceleration ordinate of the 1940 El-Centro response spectrum is the basis of this calculation.
- W = 88.3 kN (weight of the rack)

- V_e = Ce x W
- $V_{base\ shear}$ = Ve / R
- ESLF multiplies calculated 'linear' displacements by $C_d = \mu\ \Omega = R_\mu\ \Omega = R$, to obtain 'inelastic' displacements.

D.1.1 Results

Comparison results are shown in Table D-1 to Table D-4.

Table D-1. 100% 1940 El-Centro NLTH vs. ESLF comparison for different R factors. Triangular load pattern.

100% El Centro	ElC	Triangular ESLF			
Ve = 3.53 kN	NLTH	**R = 1.8**	R = 2	R = 3	R = 4
Vb (kN)	2.48	1.96	1.77	1.18	0.88
Mmax-ups (kNm)	5.26	4.66	4.22	2.86	2.17
Ω	-	1.13	1.25	1.84	2.42
θ_1 (%)	8.0%	13.2%	13.3%	13.6%	13.9%
θroof (%)	2.9%	6.1%	6.2%	6.4%	6.5%

Table D-2. 100% 1940 El-Centro NLTH vs. ESLF comparison for different R factors. Rectangular load pattern.

100% El Centro	ElC	Rectangular ESLF			
Ve = 3.53 kN	NLTH	**R = 1.8**	R = 2	R = 3	R = 4
Vb (kN)	2.48	1.96	1.77	1.18	0.88
Mmax-ups (kNm)	5.26	4.48	4.06	2.76	2.10
Ω	-	1.17	1.30	1.91	2.50
θ_1 (%)	8.0%	12.7%	12.8%	13.1%	13.3%
θroof (%)	2.9%	5.6%	5.6%	5.8%	5.9%

Table D-3. 50% 1940 El-Centro NLTH vs. ESLF comparison for different R factors. Triangular load pattern.

50% El C	El C NLTH	Triangular ESLF			
Ve = 1.76 kN		**R = 1.8**	R = 2	R = 3	R = 4
Vb (kN)	1.87	0.98	0.88	0.59	0.44
Mmax-ups (kNm)	3.63	2.40	2.17	1.51	1.16
Ω	-	1.51	1.67	2.40	3.13
θ1 (%)	5.7%	6.9%	6.9%	7.3%	7.5%
θroof (%)	2.7%	3.2%	3.3%	3.4%	3.6%

Table D-4. 50% 1940 El-Centro NLTH vs. ESLF comparison for different R factors. Rectangular load pattern.

50% El C	El C NLTH	Rectangular ESLF			
Ve = 1.76 kN		**R = 1.8**	R = 2	R = 3	R = 4
Vb (kN)	1.87	0.98	0.88	0.59	0.44
Mmax-ups (kNm)	3.63	2.32	2.10	1.45	1.12
Ω	-	1.56	1.73	2.50	3.24
θ1 (%)	5.7%	6.6%	6.6%	7.0%	7.2%
θroof (%)	2.7%	2.9%	3.0%	3.2%	3.3%

Comparison of calculated parameters tabulated in this section indicates the case of R = 1.8 providing the best results. When R = 1.8 is used with a rectangular load pattern, a more accurate yet still a conservative estimation of drifts is provided relative to the triangular pattern. However, use of R =1.8 and the triangular pattern provides a more accurate estimate of internal action value, i.e. in this case the maximum bending moment in the second upright on the first storey. Multiplying this ESLF calculated internal action by the over-strength factor provides the designer with the required force level he/she must design his or her section for. For the triangular pattern, R = 1.8 case, Ω must be greater or equal to 1.13 for the unscaled record, or 1.51 for the half-scaled record. For higher R factors, i.e. 2, 3 or 4, the over-strength factor must also be increased accordingly so as to amplify calculated internal actions to their 'actual' level.

In light of the range of over-strength factors calculated in Section 6.1.5.4 and Section 6.1.5.5, the rack does not seem to demonstrate significant over-strength. This is supported by literature, which states it is well known that thin-walled steel sections do not possess a significant post-elastic strength (Dubina, 2008). Ungureanu, Kotełko, Mania and Dubina (2010) discussed the failure mechanisms of thin walled steel sections as resulting from a combination of local buckling and local plastic mechanisms, and point out such structure types have a limited post-elastic strength.

Calculated results and the aforementioned literature, therefore, suggest it is inappropriate to specify a high over-strength factor of, say, ≥ 1.5.

Note however, that if an 'inappropriately high' R factor was to be specified, safe design requires that members be designed for a correspondingly higher over-strength, as indicated in the tabulated results of Section 6.1.5.5. This is because over-strength plays a very important role "in the survival of buildings during severe earthquake shaking." (Uang, 1991, p. 24)

REFERENCES:

Abaqus, A. V. (2005). 6.5-4-User manual, ABAQUS. *Inc., Providence, USA*.

Abdel-Jaber, M. Beale, R. G., & Godley, M. H. R. (2005). A theoretical and experimental investigation of pallet rack structures under sway. *Journal of Constructional Steel Research*, *62*, 68-80.

Aguirre, C.(2005). Seismic behavior of rack structures. *Journal of Constructional Steel Research*, *61*(5), 607-624.

Analysis reference manual for SAP2000, ETABS, and SAFE. (2009). California, USA: Computers and Structures, Inc.

Asgarian, B., & Shokrgozar, H. R. (2009). BRBF response modification factor. *Journal of constructional steel research*, *65*(2), 290-298.

Bajoria, K. M., & Talikoti, R. S. (2006). Determination of flexibility of beam-to-column connectors used in thin walled cold-formed steel pallet racking systems. *Thin-Walled structures*, *44*, 372-380.

Baldassino, N., & Bernuzzi, C. (2000). Analysis and behaviour of steel storage pallet racks. *Thin Walled Structures Journal, 37*, 277-304.

Beale, R. G., & Godley, M. H. R. (2002). The design of the pallet program. In R. A. LaBoule, & W. W. Yu, (Eds.), *16th International Specialty Conference on Cold-Formed Steel Structures* (pp. 353-368). Florida, U.S.A.

Beg, D., Zupančič, E., & Vayas, I. (2004). On the rotation capacity of moment connections. *Journal of Constructional Steel Research*, *60*(3), 601-620.

Bernuzzi, C., & Castiglioni, C. A. (2001). Experimental analysis on the cyclic behaviour of beam-to-column joints in steel storage pallet racks. *Thin-Walled Structures*, *39*(10), 841-859.

Bernuzzi, C., Chesi, C., & Parisi, M. A. (2004). *Seismic Behavior and Design of Steel Storage Racks*. Paper presented at the 13th World Conference on Earthquake

Engineering, Vancouver, Canada.

Blume, J. A., & Associates. (1973). *Seismic investigation of steel industrial storage racks* (Report prepared for the Rack Manufacturer Institute). California, USA.

Blume, J. A., & Associates. (1987). *Application of Eccentric Bracing to Rack Structures* (Report prepared for the Rack Manufacturer's Institute). California, USA.

Borzi, B., & Elnashai, A. (2000). Refined force reduction factors for seismic design. *Engineering Structures*, *22*(10), 1244-1260.

Bruneau, M. I. C. H. E. L., Clifton, C., MacRae, G., Leon, R., & Fussell, A. (2011). Steel Building Damage from the Christchurch earthquake of February 22, 2011. *Preliminary Reconnaissance Report, as yet published only on the mceer. buffalo. edu website*.

Carneiro, J. O., Jalali, S., Teixeira, V., & Tomás, M. (2006). The use of pseudo-dynamic method in the evaluation of damping characteristics in reinforced concrete beams having variable bending stiffness. *Mechanics Research Communications*, *33*(5), 601-613.

Castiglioni, C., Carydis, P., Negro, P., Calado, L., Degée, H., & Rosin, I.(2009). Seismic behaviour of steel storage racking systems. *Proceedings of the STESSA Conference* (pp. 757-764). Pennsylvania, USA.

EN (2004). 1998-1-8. *Design of structures for earthquake resistance- Part 1: General rules, seismic actions and rules for buildings.* European Committee for Standardization (CEN).

EN (2005). 1993-1-8. *Design of steel structures—Part 1. 8 Design for joints, joints in building frames.* European Committee for Standardization (CEN).

EN (2009). 15512. *Steel static storage systems–adjustable pallet racking systems–principles for structural design.* European Committee for Standardization (CEN).

Chen, C. K., Scholl, R. E., & Blume, J. A. (1980). Earthquake Simulation Tests of Industrial Steel Storage Racks. *Proceedings of the Seventh World Conference on*

Earthquake Engineering (pp. 379-386). Istanbul, Turkey.

Chen, C. K., Scholl, R. E., & Blume, J. A. (1980). *Seismic Study of Industrial Storage Racks* (Report prepared for the National Science Foundation and for the Rack Manufacturers Institute and Automated Storage and Retrieval Systems). San Francisco, CA: URS/John A. Blume & Associates.

Chen, C. K., Scholl, R. E., & Blume, J. A. (1981). Seismic-Resistant Design of Industrial Storage Racks. *Proceedings of the Second Specialty Conference on Dynamic Response of Structures: Experimentation, Observation and Control* (pp. 745-759) Atlanta, USA.

Chen, W. F., Kishi, N., Matsuoka, K. G., & Nomachi. S. G. (1988). Moment–rotation relation of single double web angle connections (pp. 121-134). Proceeding of the state of the art workshop on Connections and behaviour, strength and design of steel structures, France.

Chen, W. F., Lui, E. M. (1991). *Stability deign of steel frames*, CRC Press.

Chopra, A. K. (1995). *Dynamics of structures: theory and applications to earthquake engineering*. New Jersey, USA: Prentice Hall.

Clough, R.W., & Penzien, J. (1993). *Dynamics of structures* (2nd ed.). New York, USA: McGraw-Hill.

Code, U. B. (1997). UBC. 1997. In *International Conference of Building Officials, Uniform Building Code, Whittier, California*.

Computers and Structures, Inc. (2009). *Analysis reference manual for SAP2000, ETABS, and SAFE*. California, USA: CSI.

Davies, J. M. (1980). Stability of unbraced pallet racks. Paper presented at the *Fifth Int. Specialty Conference on Cold Formed Steel Structures*. University of Missouri-Rolla.

Davies, J. M. (1992). Down-aisle stability of rack structures. *Eleventh Int. Specialty Conference on Cold-Formed Steel Structures* (pp417-435). St. Louis, Missouri, USA.

de la Manutention, F. E. (1998). *Section X – Recommendations for the design of steel static pallet racking and shelving*. FEM.

de la Manutention, F. E. (2010). *Recommendations for the Design of Static Steel Pallet Racking in Seismic Conditions.* FEM 10.2.08.

Diaz, C., Marti, P., Victoria, M., & Querin, O. M. (2011). Review on the modelling of joint behavior in steel frames. *Journal of Constructional Steel Research, 67*, 741-758.

del Coz Díaz, J. J., Nieto, P. G., Biempica, C. B., & Rougeot, G. F. (2006). Non-linear analysis of unbolted base plates by the FEM and experimental validation. *Thin-Walled Structures*, *44*(5), 529-541.

Dowell, R. K., Seible, F., & Wilson, E. L. (1998), Pivot hysteresis model for reinforced concrete members, *ACI Structural Journal*, *95*(5), 607-617.

Dubina, D. (2008). Behavior and performance of cold-formed steel-framed houses under seismic action. *Journal of Constructional Steel Research*, *64*(7), 896-913.

Fathi, M., Daneshjoo, F., & Melchers, R. E. (2006). A method for determining the behaviour factor of moment-resisting steel frames with semi-rigid connections. *Engineering structures*, *28*(4), 514-531.

FEMA. (2005). Seismic Considerations for Steel Storage Racks Located in Areas Accessible to the Public (FEMA 460). *Federal Emergency Management Agency*.

Feng, X. (1994). *The influence of semi-rigid connections on the behaviour of slender structures* (Doctoral dissertation, Oxford Brookes University).

Feng, X., Godley, M. H. R., & Beale, R.G. (1993). Elastic buckling analysis of pallet rack structures. *Proceedings of Civil-Comp, Fifth International Conference Civil and Structural Engineering Computing* 93 (pp. 297-305). Edinburgh, 207-305.

Filiatrault, A., & Wanitkorkul, A. (2004). *Shake-Table Testing of Frazier Industrial Storage Racks* (Report No. CSEE-SEESL-2005-02). New York, USA: University at Buffalo, State University of New York, Structural Engineering and Earthquake

Simulation Laboratory, Departmental of Civil, Structural and Environmental Engineering.

Filiatrault, A., Higgins, P. S., & Wanitkorkul, A. (2006), Experimental stiffness and seismic response of pallet-type steel storage rack connectors. *Practice Periodical on Structural Design and Construction*, *11*(3), 161-170.

Firouzianhaji, A. Saleh, A., & Samali, B. (2012, December). *Finite Element modelling of a beam-column connection in industrial storage racking structures*. Paper presented at 22nd Australian conference on the mechanics of structures and materials, Sydney, Australia.

Firouzianhaji, A., Saleh, A., & Samali, B. (2014, December). *Stability Analysis of steel storage rack structures*. Paper presented at the 23rd Australasian Conference on the Mechanics of Structures and Materials (ACMSM23), Byron Bay, Australia.

Firouzianhaji, A., Saleh, A., & Samali. (2014). *Non-Linear Analysis of base Plate Connections used in Industrial Pallet rack Structures*. Paper presented at the Australasian Structural Engineering Conference, Auckland, New Zealand.

Frye, M. J., & Morris, G. A. (1975). Analysis of flexibly connected steel frames. *Canadian Journal of Civil Engineering*, *2*(3), 280-91.

Gilbert, B. P. (2010). *The behaviour of steel drive-in racks under static and forklift truck impact forces* (Doctoral dissertation, University of Sydney).

Gilbert, B. P., & Rasmussen, K. J. (2009). *Experimental test on steel storage rack components*. Sydney, Australia: The University of Sydney, School of Civil Engineering.

Gilbert, B. P., & Rasmussen, K. (2011). Determination of the base plate stiffness and strength of steel storage racks. *Journal of Constructional Steel Research*, *67*, 1031-1042.

Gilbert, B. P., Rasmussen, K. J. R., Baldassino, N., Cudini, Y., & Rovere, L. (2012). Determining the transverse shear stiffness of steel storage rack upright frames. *Journal of Constructional Steel Research*, *78*,107-116.

Godley, M. H. R. (1997). Plastic design of pallet rack beams. *Thin-Walled Structures*, *29*(1), 175-188.

Godley, M. H. R. (2007). The behaviour of storage racking baseplates. In Beale R. G. (Ed.), *Proceedings of 6th international conference on steel and aluminium structures* (pp. 433-440). Oxford, UK.

Godley, M. H. R., Beale, R. G., & Feng, X. (2000). Analysis and design of down-aisle pallet rack structures. *Computers & Structures*, *77*(4), 391-401.

Godley, M. H. R., & Beale, R. G. (2008). Investigation of the effects of looseness of bracing components in the cross-aisle direction on the ultimate load-carrying capacity of pallet rack frames. *Thin walled structures*, *46*(7),848-854.

Hamburger, R. O. (2009). *Facts for Steel Buildings - Earthquakes and Seismic designs*. USA: American Institute of Steel Construction (AISC).

Horne, M. R. (1975). An approximate method for calculating the elastic critical loads of multi storey plane frames. *The Structural Engineer*, *53*(6) 242-248.

Ibarra, L.F., Medina, R. A., & Krawinkler, H. (2005). Hysteretic models that incorporate strength and stiffness deterioration. *Earthquake Engineering & Structural Dynamics*, *34*(12), 1489-1512.

IBC, I. (2006). International building code. *International Code Council, Inc.(formerly BOCA, ICBO and SBCCI)*, *4051*, 60478-5795.

Khodaie, S., Mohamadi-Shooreh, M. R., & Mofid, M. (2012). Parametric analyses on the initial stiffness of the SHS column base plate connections using FEM. *Engineering structures*, *34*, 363-370.

Kim, J., & Choi, H. (2005). Response modification factors of chevron-braced frames. *Engineering Structures*, *27*(2), 285-300.

Kishi, N., & Chen, W. P. (1987). Moment–rotation relations of semi-rigid connections with angles. *Journal of Structural Engineering*, *116*(7), 1813–1834.

Kosteski, N., & Packer, J. A. (2003). Welded Tee-to-HSS connections. *Journal of*

Structural Engineering, *129*(2), 151-159.

Krawinkler, H., Cofie, N. G., & Astiz, M. A., & Kircher, C. A. (1979). *Experimental Study on the seismic behaviour of storage racks*.(Report Number 41). Stanford, USA: Stanford University, The John A. Blume Earthquake Engineering Center, Department of Civil and Environmental Engineering.

Krishnamurthy, N. (1978). Fresh look at bolted end-plate behaviour and design. *Engineering Journal*, *15*(2), 39-49.

Lewis, G.M. (1991). Stability of Rack Structures. *Thin-Walled Structures, 12*(2),163-174.

Markezi, F. D., Beale, R. G., & Godley. M. H. R. (1997). Experimental analysis of semi-rigid boltless connectors. *Thin-Walled Structures*, *28*, 344-347.

Medina, R.,A., & Krawlinker, H. (2003), *Seismic Demands for Nondeteriorating Frame Structures and their dependence on Ground Motions* (Report No. 144). Stanford, USA: Stanford University, Blume Earthquake Engineering Center.

Medina, R. A., & Krawinkler, H. (2004). *Seismic demands for nondeteriorating frame structures and their dependence on ground motions* (Doctoral dissertation, Pacific Earthquake Engineering Research Center).

Mofid, M., Mohammadi, M. R. S., & McCabe, S. L. (2005). Analytical approach on endplate connection: Ultimate and Yielding Moment. *Journal of structural engineering (ASCE), 131*, 449-456.

Mwafy, A. M., & Elnashai, A. S. (2001). Static pushover versus dynamic collapse analysis of RC buildings. *Engineering structures*, *23*(5), 407-424.

Baldassino, N., & Zandonini, R. (2008). Performance of base-plate connections of steel storage pallet racks. *Proceedings of the 5th international colloquium on coupled instabilities in metal structures. The University of Sydney* (pp. 119-30), Sydney, Australia.

Newmark, N. M. (1959). A Method of Computation for Structural Dynamics. *ASCE*

Journal of the Engineering Mechanics Division, *85*(3), 67-94.

Prabha, P., Marimuthu, V., Saravanan, M. & Jayachandran, S. A. (2010). Evaluation of connection flexibility in cold formed steel racks. *Journal of Constructional Steel Research*,*66*(7), 863-872.

Rao, S. S., Beale, R. G., & Godley, M. H. R. (2004). Shear stiffness of pallet rack upright frames. *Proceedings of 7th International specialty Conference on Cold-Formed Steel Structuresa* (pp. 295-311). Florida, USA.

Reyes, J. R. A. (2013). *Seismic Analysis of Storage Racks with Geometric and Connection Non-Linearity* (Bachelor dissertation, University of Technology, Sydney).

RMI, M. (1997). Specification for the Design, Testing and Utilization of Industrial Steel Storage Racks. *RMI–Rack Manufacturers Institute*.

RMI, M. (2008). Specification for the Design, Testing and Utilization of Industrial Steel Storage Racks. *RMI–Rack Manufacturers Institute*.

RMI, M. (2012). Specification for the Design, Testing and Utilization of Industrial Steel Storage Racks. *RMI–Rack Manufacturers Institute*.

Rosin, I., Calado, L., Proença, J., Carydis, P., Mouzakis, H., Castiglioni, C., … & Molina, F. J. (2009). Storage racks in seismic areas. *Report EUR,23744EN*. Luxembourg: European Commission.

Sajja, S. R., Beale, R. G., & Godley, M. H. R. (2006). Factors affecting the shear stiffness of pallet rack uprights. In Camotim, D. et al. (Eds.). *Proceedings of the Stability and Ductility of Steel Structures* (pp. 365-372). Lisbon, Portugal.

Sajja, S. R., Beale, R. G., & Godley, M. H. R. (2008). Shear stiffness of pallet rack upright frames. *Journal of Constructional Steel Research*, *64*(7), 867-874.

Saleh, A. (2012). *Base Plate Tests – Components manufactured in China*, Report prepared on behalf of AccessUTS Pty. Ltd. For Dexion Australia. Sydney, Australia: University of Technology, Sydney.

Saleh, A. (2012). *Bending Tests on Beam End Connectors - Components manufactured in China and Australia*, Report prepared on behalf of AccessUTS Pty. Ltd. For Dexion Australia. Sydney, Australia: University of Technology, Sydney.

Saleh, A. (2012). *Cyclic Bending Tests on Beam End Connectors - Components manufactured in China and Australia*, Report prepared on behalf of AccessUTS Pty. Ltd. For Dexion Australia. Sydney, Australia: University of Technology, Sydney.

Saleh, A. (2012). *Looseness Tests on Beam End Connectors – Components manufactured in Australia*, Report prepared on behalf of AccessUTS Pty. Ltd. For Dexion Australia. Sydney, Australia: University of Technology, Sydney.

Saleh, A. (2011). *Shear Stiffness of Upright Frames tests - Components manufactured in Australia* (Project 201100070). Sydney, Australia: University of Technology, Sydney, Report prepared on behalf of AccessUTS Pty. Ltd. For Dexion Australia.

Sangle, K. K., Bajoria, K. M., & Talicotti, R. S. (2011). Elastic stability analysis of cold-formed pallet rack structures with semi-rigid connections. *Journal of Constructional Steel Research*, *71*, 245-262.

Standards Australia. (1993). *Steel storage racking (AS 4084).* Standards Australia.

Standards Australia. (2012). *Steel storage racking (AS 4084).* Standards Australia.

Standards Australia. (2007). *Cold formed steel structures (AS 4600).* Standards Australia.

Standards Australia. (2007). *Earthquake actions in Australia* (AS 1170.4). Standards Australia.

Stark, J. W. B., & Tilburgs, C. J. (1979). Frame instability of unbraced pallet racks. Paper presented at the *Int. Conference on Thin-Walled Structures*, (pp. 160-185) University of Strathclyde.

Takeda, T., Sozen, M. A., & Nielsen, N. N. (1970). Reinforced Concrete Response to Simulated Earthquakes, *Journal of the Structural Division, ASCE*, *96*(12), 2557-

2573.

Taucer, F., Spacone, E. & Filippou, F.C. (1991). *A fiber beam-column element for seismic response analysis of reinforced concrete structures* (Vol. 91, No. 17)(Report No. UBC/EERC-91/17). Berkeley, USA: Earthquake Engineering Research Center, University of California, Berkeley.

Teh, L. H., Hancock, G. J., & Clarke, M. J. (2004). Analysis and design of double-sided high-rise steel pallet rack frames. *Journal of Structural Engineering*, *130*(7), 1011-1021.

Timoshenko, S. P., & Gere J. M. (1961). *Theory of elastic stability*. Tokyo, Japan: McGrow-Hill.

Timoshenko, S., & Woinowsky-Krieger, S. (1959). *Theory of plates and shells.* New York, US: McGraw-hill.

Uang, C. (1991). Establishing R (or R w) and C d factors for building seismic provisions. *Journal of Structural Engineering,117*(1), 19-28.

Ungureanu, V., Kotełko, M., Mania, R. J., & Dubina, D. (2010). Plastic mechanisms database for thin-walled cold-formed steel members in compression and bending. *Thin-walled structures*, *48*(10), 818-826.

Vamvatsikos, D., & Cornell, C. A. (2002). Incremental dynamic analysis. *Earthquake Engineering & Structural Dynamics*, *31*(3), 491-514.

Wang, M., Shi, Y., Wang, Y., & Shi, G. (2013). Numerical study on seismic behaviors of steel frame end-plate connections. *Journal of Constructional Steel Research*, *90*, 140-152.

Yura, J. A., Zettlemoyer, N., & Edwards. I. F. (1980). Ultimate capacity equations for tubular joints. *Proceedings of 12th annual offshore technology conference* (pp. 113-125). Houston, USA.

Zaharia, R., & Dubina, D. (2006). Stiffness of joints in bolted connected cold-formed steel trusses. *Journal of Constructional Steel Research*, *62*(3), 240-249.